HESSELØ OFFSHORE WIND FARM
INTEGRATED GEOLOGICAL MODEL

REPORT

COWI

MARCH 2022
ENERGINET

HESSELØ OFFSHORE WIND FARM
INTEGRATED GEOLOGICAL MODEL

REPORT

CONTENTS

1   Executive Summery

This report describes the work and outcome of the integrated 3D model for Hesselø Offshore Wind Farm based on 2021 preliminary geotechnical site investigation (by Gardline) and 2020 geophysical investigations (by Fugro). The established integrated 3D model comprises deposits from the Holocene, Pleistocene and Early Cretaceous/Jurassic time periods.

Energinet is developing the Hesselø Offshore Wind Farm area on behalf of the Danish Energy Agency to be tendered out during 2022. The area of investigation is found approximately 30 km offshore the Northern coast of Zealand in the inner waters of Kattegat and covers 247 km².

The 3D geological model is established using the model and interpretation software Kingdom™ by IHS Markit® applying 2D Ultra-High-Resolution Seismic data with 1000 m between north-south lines and 250 m between east-west lines, Sub-bottom profiler data, bathymetry and two small 3D cubes (each 550 m x 1700 m) of Ultra-High-Resolution Seismic data for the proposed substation locations. Interpretation integrates geotechnical investigations at 40 locations including cone penetration testing (CPT's) and boreholes. Additionally, 25 shallow CPTs are imported into the Kingdom™ project. Major soil units are assessed and described for the combined data set. Factual report summarizing the results from geotechnical field tests and laboratory testing is used to evaluate the geotechnical properties for the soil units.

The integrated geological model has 11 layers for which geological descriptions are provided. The descriptions include stratigraphic, lithological and geotechnical characteristics. The 11 layers include 3 Holocene marine to deltaic layers ranging from clay to sand, 5 Late Weichselian, late glacial, glaciomarine layers mostly consisting of clay, 2 Weichselian and earlier Pleistocene glacial layers consisting of mixed sediment, 1 Early Cretaceous/Jurassic Mudstone/Siltstone. Geotechnical samples and tests have made it clear that both Holocene and Late Weichselian layers should be regarded as low strength soils. A glacial advance in Late Weichselian has overridden the 3 deepest Late Weichselian layers in part of the investigated area, however, this event does not seem to have had significant impact on the soil strength of these layers. These 11 layers have been further subdivided based on their geotechnical soil behaviour type. The soil properties of

all soil units have been evaluated and the soil properties for the main soil units are visualized in the appendices and enclosures.

A soil zonation encircles the geological model and structures evaluated to have a potentially significant impact on the foundation design: low strength layers, glaciated layers and channel structures. The soil zonation is simplified into one single map dividing the entire site into four different soil provinces. These four different soil provinces are defined based on the cumulated thickness of soil with low strength, which is considered the most important parameter with respect to foundation design.

Enclosures provided with the digital model present the new layers with respect to depth below seabed, thickness and lateral extent. The enclosures also visualize cumulated thickness of low strength soils. Furthermore 13 cross-sections distributed over the entire area show the layering in the model together with borehole information.

All enclosures are provided digitally as shapefiles. The integrated geological model is delivered as a digital 3D model in a Kingdom suite project.

2   Introduction

Energinet and the Danish Energy Agency are investigating the Hesselø Offshore Wind Farm (OWF) area to identify a developer for the project by 2022.

To enable evaluation of subsurface soil conditions and related constraints, Energinet has procured a geophysical 2D Ultra-High Resolution Seismic (2D-UHRS) survey and 2 small 3D seismic (3D-UHRS) cubes from Fugro in 2020, and preliminary geotechnical investigations from Gardline in 2021. These surveys have provided the basis for an integrated geological model of the OWF area.

This report presents the results of the integrated geological modelling of the Hesselø OWF area of investigation as carried out by COWI June 2021 - January 2022.

2.1   Area of Investigation

The area of investigation (AOI) is situated ~30 km offshore the Northern coast of Sealand in the inner waters of Kattegat and covers 247 km² (Figure 2.1-1)
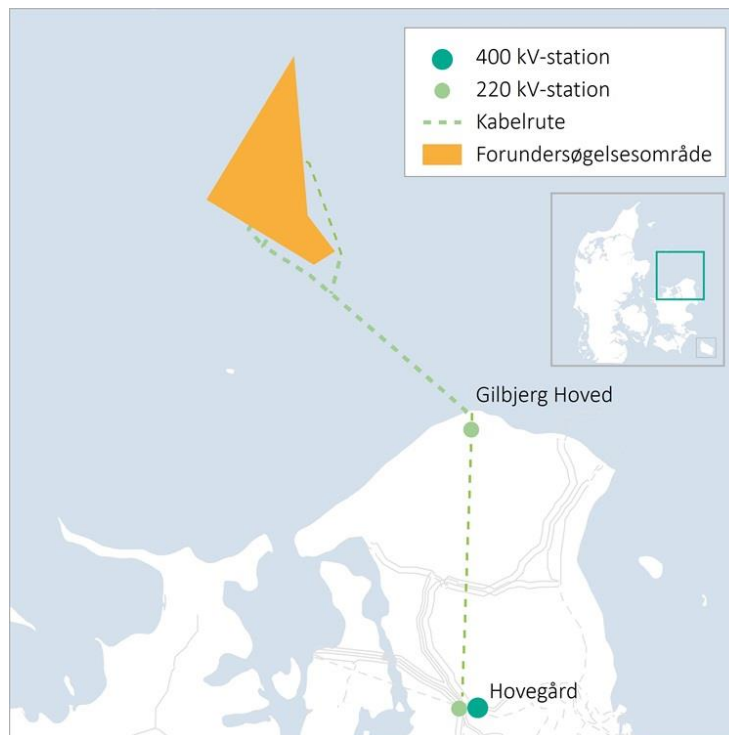
*Figure 2.1-1   Location of Hesselø area of investigation. Figure
                   from Scope of work.*

POINTID	EASTING [meter]	NORTHING [meter]	LATITUDE [DD mm.mmm]	LONGITUDE [DD mm.mmm]
1	680 433	6 247 210	56° 20,110' N	11° 55,130' E
2	664 326	6 256 983	56° 25,724' N	11° 39,884' E
3	675 002	6 274 480	56° 34,914' N	11° 50,963' E
4	677 460	6 278 554	56° 37,052' N	11° 53,528' E
5	679 510	6 254 602	56° 24,111' N	11° 54,539' E
6	683 606	6 249 200	56° 21,108' N	11° 58,289' E

2.2   Scope of Work

The purpose of the assignment is to establish an Integrated Geological Model for the Hesselø project to inform Tenderers, that are applying for the licence to develop and construct the OWF, about the geology, the associated geotechnical properties and potential geo-hazards.

The output of the assignment must be applied for

> Sub-selection of specific OWF area within the area of investigation.

> Initial determination of foundation concept and design.

> Assessment of the soil-related risks for installation of foundations.

> Initial planning of the layout for turbines.

These applications are relevant for both the license tender process and the subsequent development performed by the nominated developer.

The integrated geological model comprises a conceptual geological model, a digital, spatial geological model and a geotechnical characterization of the soil units in the model. Further a soil province map is provided.

The technical work was carried out in three phases addressing the geotechnical stream of data into the model and structured in three aligned work packages, see Table 2-1.

Table 2-1   *Overview of the workflow and phases of the technical work*

Phases	Phase 1- Geophysical data and CPT	Phase 2 – Geophysical data, CPT and boreholes	Phase 3 – Factual report with laboratory results
WP1 – **3D spatial geological model and integrated interpretation**	-Adopt Kingdom Model and import CPT data -Assess and assign major soil units combined from CPT and seismic data in the Kingdom model -Integrated interpretation of horizons	-Consider Geohazards in relation to geotechnical results -Import boreholes and assess correlation -Adjust interpretations and continue integrated interpretation	-Final adjustments of interpretations -Further interpretations of 3D cube -Produce grids and cross - sections -Preparation of deliverables
WP2 – **Conceptual geological model and soil provinces**	-Conceptualization of the geological model for the site -Regional geological setting -Initial subdivision of soil units	-Establish subdivision of soil units and zonation -Conceptualization of geological model(s) -Establish a description of the geology and soil units -Initial soil provinces	-Final adjustments of the conceptual model(s) and zonation -Establishment of soil provinces -Preparation of deliverables
WP3 - **Geotechnical characterization of soil units**	-Initial soil unit framework from CPT data -Initial soil description -Initial soil classification and strength/stiffness properties	-Final soil unit framework from CPT and borehole data. -Soil suitability considerations and risk assessments -Adjust soil descriptions and soil classification	-Summarize geotechnical parameters for the soil units -Establish typical values and variance -Final soil classification and strength/stiffness properties

A separate work package for reporting assured the content of the Integrated Geological Model Report as well as drawings and digital deliverables.

A full list of deliverables can be found in section 9.

3   Basis

Data packages have been received successively from Energinet. An overview of the data received as basis from Energinet is listed below, divided into the geotechnical and geophysical data packages including reports.

Project datum is ETRS89 (EPSG:25832) using the GRS80 Spheroid. The coordinate system is the UTM projection in Zone 32 N. Units are in meters. Vertical reference is MSL, height model DTU18.

Geotechnical data packages	
Datatype	Year
Gardline: Final AGS for Factual Report - Issue sequence 6 (File: "*11596 Final AGS_rev4.ags"*) AGS data providing results from offshore and onshore works of the Geotechnical site investigation	2021
Rambøll: Gilleleje Wind Farm AGS's (CPTs imported in Kingdom and used for integrated interpretation)	2020

Geophysical data packages	
Datatype	Year
Fugro: Kingdom Project with › 3D Ultra-High Resolution Seismic (3D-UHRS) – grid inline 1 m * crossline 0.5 m › Multi-channel Ultra-High Resolution Seismic (2D-UHRS) – grid 250 * 1000 m (SEGY linked in Seismic Direct) › Sub-bottom profiler data (SBP) – grid ~50 * 1000 m (SEGY linked in Seismic Direct)	2021
Fugro: Raster and Vector Database from Geophysical suvey. ESRI and geoDB › Multibeam (MBES) and Side Scan Sonar data (SSS) › Results from Sub-bottom Profiler (SBES): Blanking area, potential peat, glacial anomalies, postglacial anomalies	2021

Reports		
Author	Title	Year
GEUS	General geology of southern Kattegat, the Hesselø wind farm area, Desk Study	2020
Fugro	Geophysical Results Report v2 FINAL	2021

Fugro	3D-UHR Survey results Report WPD FINAL	2021
Gardline	Volume ll: Measured and Derived Geotechnical Parameters Report – Revision 2, Final	2021
Rambøll	Geotechnical Data Report. Hesselø OWF Supplementary VC – Gilleleje	2021

3.1   Geotechnical basis

The geotechnical basis for the project can generally be divided into two categories:

> Offshore sampling and testing

> Onshore description and testing

The offshore works have been divided into a seabed CPT campaign and a composite borehole campaign (composite downhole CPT and borehole sampling).

The onshore works consist of soil description and classification as well as a comprehensive laboratory test programme.

The offshore and onshore works have been performed by Gardline Ltd (some of the onshore laboratory tests have been performed at RINA, i2 Analytical, Geolabs and Geotechnical Engineering), and the outcome of the works has been documented in Ref. /1/.

3.1.1   Offshore works

The offshore works consist of in-situ testing (seabed, downhole and seismic CPTs), P-S logging and borehole drilling and sampling. The acquired samples are used for testing in the onshore works (laboratory testing programme).

An overview of the positions for CPT – seabed (CPT), downhole (dCPT) and seismic (SCPT) – and boreholes (with sampling) is shown Table 3-1 and on Enclosure 1.02.

Several locations across the site have multiple CPTs due to premature CPT refusal, which means that the total number of unique locations surveyed is 40. Of these 40 locations, 14 locations have been surveyed with minimum one (1) CPT and one (1) borehole, while the remaining 26 have been surveyed with minimum one (1) CPT but no borehole. Seven of the these have been performed as seismic cone penetration tests, i.e. including measurement of the shear wave velocity. For both boreholes and CPTs a target depth of 70 m was considered. However, it is noted that the seabed CPTs have not reached the target depth due to CPT refusal.

The distance between CPT's and boreholes performed at the same location and the distance between extra repeated CPTs performed at the same location is maximum 12 m.

The offshore works furthermore include geological description, strength testing (pocket penetrometer and Torvane tests), classification testing (water content, bulk and dry density), chemical testing (carbonate content) and P-S logging. A summary of the offshore laboratory works is presented in Table 3-2.

Table 3-1   Summary of offshore geotechnical works.

Test type	Quantity
Seabed Cone Penetration Test (CPT)	52 (incl. 12 retests)
Composite Cone Penetration Test and sampling boreholes (BH)	14 (incl. 2 bump overs)
Seismic Cone Penetration Test (SCPT)	7
P-S logging	At 5 BHs
Dissipation Tests	23

Table 3-2   Summary of performed offshore laboratory tests.

Test type	Quantity
Water content	1388
Bulk and dry density	85
Bulk density	499
Pocket penetrometer	1483
Torvane	1398
Carbonate content	36

3.1.2 Onshore works

The onshore works consist of classification testing, advanced laboratory testing and chemical testing. The performed onshore laboratory tests are summarized in Table 3-3.

All onshore works are performed using samples acquired from the geotechnical composite downhole CPT and boreholes.

The detailed test reports are enclosed in Ref. /1/ and will not be repeated in this report.

Table 3-3   Summary of performed onshore laboratory tests.

Test type	Laboratory at which tests are performed	Quantity
Water content	Gardline	31
Bulk and dry density	Gardline	25
Particle density	Gardline	123
Atterberg limits	Gardline	107
Particle size distribution (wet sieve)	Gardline	128
Particle size distribution (Hydrometer)	Gardline	119
Angularity	Gardline	22
Maximum and minimum dry density	RINA	13
Carbonate content	Gardline	42
Acid soluble Sulphate	Geolabs	42
Loss on ignition	Gardline	36
Thermal conductivity	Gardline	23
Acid soluble Chloride	i2 Analytical	42
Oedometer (incremental load)	Gardline	50
Torvane	Gardline	19
Unconsolidated Undrained (UU) triaxial test	Geotechnical Engineering and Gardline	172
Unconfined compressive strength (UCS)	RINA	1
Consolidated Isotropically Undrained (CIU) triaxial tests	RINA	12
Consolidated Isotropically Drained (CID) triaxial tests	RINA	20
Consolidated Anisotropically Undrained (CAU) triaxial tests	RINA	28
Cyclic Consolidated Anisotropically Undrained (CAUcyc) triaxial tests	RINA	9
Direct simple shear (DSS) tests	RINA	14

3.2   Geophysical and hydrographical basis

The geophysical basis for this report is a geophysical survey including SBP, 2D-UHRS and 3D-UHRS data, acquired in 2020.

The main objectives from this survey were:

> Initial marine archaeological site assessment;

> Planning of environmental investigations;

> Planning of initial geotechnical investigations;

> Decision of foundation concept and preliminary foundation design;

> Assessment of subsea inter-array cable burial design;

> Assessment of installation conditions for foundations and subsea cables;

> Site information enclosed in the tender for the offshore wind farm concession

The work described above and below has been performed by FUGRO, and the outcome of the SI's has been documented in Ref. /3/

3.2.1   Bathymetry

MBES data were acquired resulting in a bathymetry dataset fully covering the survey area. A bathymetry grid is available in both 0.25 m and 1.00 m resolution.

3.2.2   Subsurface data

The 2D-UHRS data were acquired with N-S oriented survey lines with a 1000 m line spacing and E-W oriented cross lines with 250 m line spacing. The SBP data was also acquired with N-S orientated survey lines with a line spacing of 1000 m, but with E-W oriented lines approximately 50 m apart (Figure 3.2-1).

The initial seismostratigraphic interpretation resulted in mapping of 9 horizons. The mapped horizons correspond to the either top or base of the seismic units of geological significance. The relationship between the seismic units and their horizons are summarized in Table 7-1.

Seismic reflectors were selected based on their geological and geotechnical significance and spatial continuity across the site. The individual horizons were picked using a combination of the physical characteristics of the seismic reflectors, seismic facies analysis and reflector terminations. The relevance of the horizons from a sequence stratigraphic standpoint was also a prime consideration.

Furthermore, shallow gas, organic rich sediments and sub-surface boulders were mapped where these were observed (7.6).

All interpretations are included in a Kingdom Suite project together with processed seismic profiles in both time and depth domain.
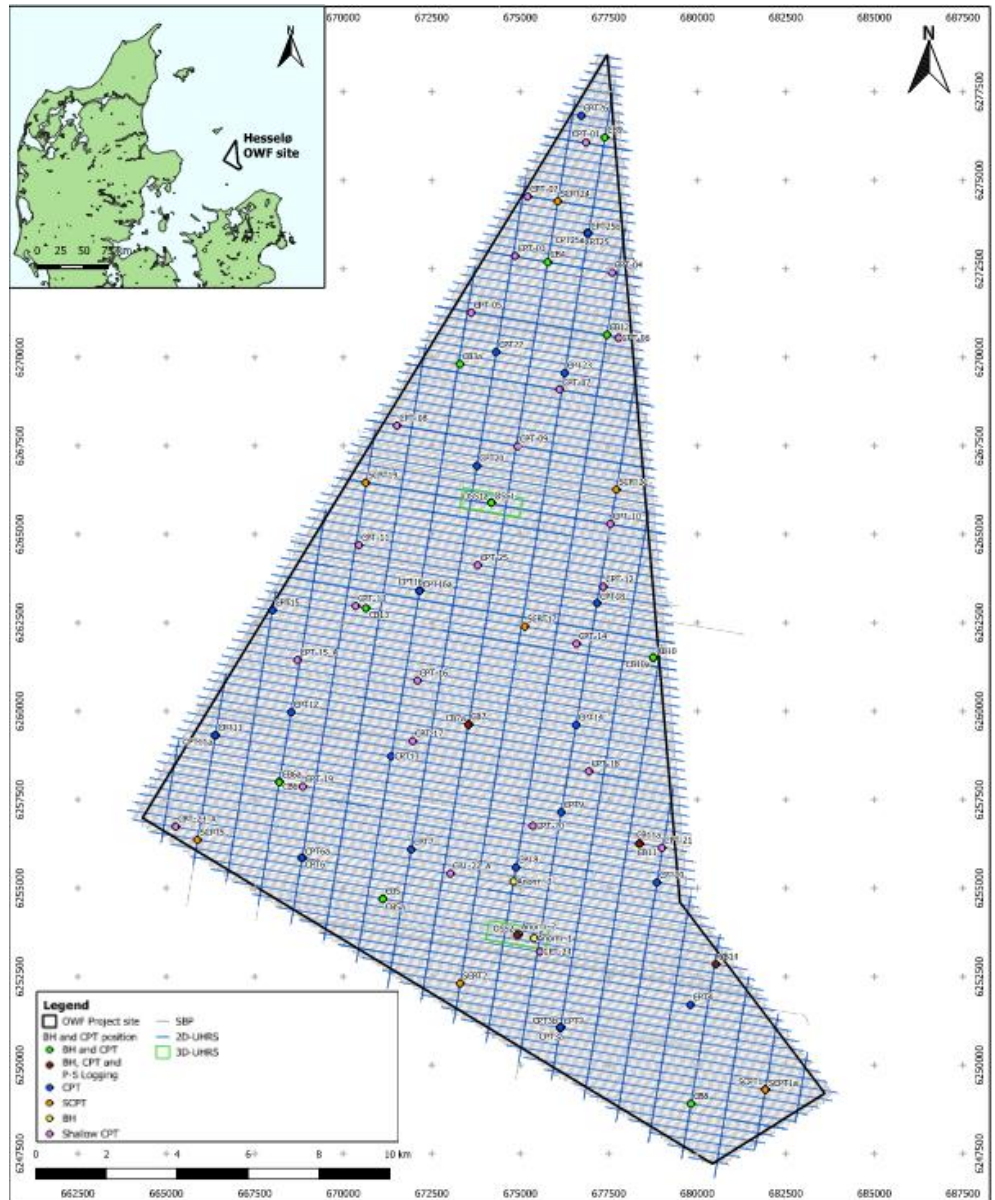
Figure 3.2-1   Lineplan for the 2D-UHRS survey and the SBP survey. Ref. /3/. Refer to enclosure 1.02A for full resolution and legend.

4 Geotechnical interpretation

In this section it is described how the geotechnical data has been evaluated to characterize the soils at the site and the layering of soil units at each geotechnical location (Note that borehole logs and CPT logs that are performed in near vicinity of each other, i.e. up to 12 m, is considered as one geotechnical location in total). The layering and soil characterization interpreted at geotechnical locations have supported the assessment of the stratigraphy across the entire site, cf. section 7.

For each geotechnical location, a geotechnical interpretation of the stratigraphy has been carried out. This interpretation has considered input from borehole logs, CPT logs (using CPT correlations as presented in section 0) and geophysical data (in order to link geotechnical soil units across the site). One geotechnical interpretation of the stratigraphy has been prepared for each geotechnical location. This also implies that at geotechnical locations where both borehole and CPT data are available, the information from these has been combined into one interpreted stratigraphy. A total of 40 unique geotechnical interpretations of stratigraphy have been developed, cf. Appendix A. All these interpretations have been applied as input to the integrated geological model.

The following sections describe the procedure for the geotechnical stratigraphic interpretation in further detail.

4.1 Geotechnical soil unit overview

The development of the soil stratigraphy can generally be divided into two parts:

> based on borehole log descriptions.

> based on CPT classification and correlation.

The work documented in Ref. /1/ can be considered the basis. The soil descriptions provided in the borehole log provide descriptions of soil type/class as well as estimates of soil age and depositional environment. In addition, the seismic horizons interpreted from the geophysical data also serves as input into the definition of geotechnical soil units. To ensure compliance between the interpretation of the geophysical data and the geotechnical data minimum one soil unit is defined per geophysical unit, cf. section 7.6.5. An overview of the defined geotechnical soil units is presented in Table 4-1. The following is noted in regard to the defined geotechnical soil units:

> The units A, B and C are relatively thin layers located at shallow depth. The unit A is at many geotechnical locations less than 1 m thick and hence, interpretation of soil properties based on CPT are uncertain. The soil units A and B generally classify as clay, whilst unit C classifies as sand.

> The main geophysical units D, E, F and H all consist of layers of sand, layers of mixed material (Silty material or heavily layered material of mixed behaviour) and layers of clay. These geophysical units are therefore

subdivided into subunits considering their geotechnical behaviour from borehole logs and CPT. The geophysical units D and F consists mainly of clay and only at a limited number of geotechnical locations and depth ranges, mixed material and/or sand is identified for these units. The geophysical unit E also consist mainly of clay. However, at several geotechnical locations and depth ranges, the material has been classified as sand. This is mainly the case at the area of the site which has experienced glacial impact during late Weichselian, cf. section 7.7.5 and Enclosure 1.07.

> In the top part of the geophysical unit H, a lower strength clay is identified at some geotechnical locations. The clayey material identified in unit H is therefore classified into two geotechnical subunits: the lower strength clay Hclaysoft and the main clay unit Hclay. The latter, Hclay, shows evidence of being overconsolidated.

> At each geotechnical location, a stratigraphic interpretation is performed considering the geotechnical soil units presented in Table 4-1. It is noted that geotechnical properties presented in section 5.4 are only included for the main geotechnical soil units present across the majority of the site.

> The assessment of the geophysical data has identified a Unit G, cf. section 7.7.7. This unit is however not included in the list of geotechnical soil units given in Table 4-1, as no geotechnical data (CPT or borehole data) is available for the soil unit.

Table 4-1   Overview of identified geotechnical soil units.

Soil unit ID	Soil age group	Soil type class group	Comments
A	Holocene	Clay	
B	Holocene	Clay	Generally, has lower CPT friction ratio than unit A
C	Holocene	Sand	
D1clay	Late Weichselian	Clay	Main geotechnical unit within D1
D1sand	Late Weichselian	Sand	Limited presence across the site
D1mix	Late Weichselian	Silt, sandy, clayey	Limited presence across the site
D2clay	Late Weichselian	Clay	Main geotechnical unit within D2
D2sand	Late Weichselian	Sand	Limited presence across the site
D2mix	Late Weichselian	Silt, sandy, clayey	Limited presence across the site

Soil unit ID	Soil age group	Soil type class group	Comments
E1clay	Late Weichselian	Clay	Main geotechnical unit within E1
E1sand	Late Weichselian	Sand	Mainly located in the zone of the site where unit E has been glacially impacted
E1mix	Late Weichselian	Silt, sandy, clayey	Limited presence across the site
E2clay	Late Weichselian	Clay	Main geotechnical unit within E2
E2sand	Late Weichselian	Sand	Mainly located in the zone of the site where unit E has been glacially impacted
E2mix	Late Weichselian	Silt, sandy, clayey	Limited presence across the site
Fclay	Late Weichselian	Clay	Main geotechnical unit within F
Fmix	Late Weichselian	Silt, sandy, clayey	Limited presence across the site
Hclaysoft	Pleistocene	Clay	Clayey material within H having a lower strength. Generally located in top of H.
Hclay	Pleistocene	Clay	Main geotechnical unit within H
Hsand	Pleistocene	Sand	Main geotechnical unit within H
Hmix	Pleistocene	Silt, sandy, clayey	Limited presence across the site
I	Pre-Quaternary	Siltstone, Mudstone	Geotechnical investigation has limited penetration into this unit

4.2   Stratigraphic interpretation based on CPT

The process of estimating the stratigraphy for all geotechnical locations based on the CPT trace is described in the following steps:

1   Load raw CPT data from AGS-file into CPT classification script.

2   Calculate additional parameters for soil interpretation and classification.

3   Determine soil behaviour type index for each depth with available CPT data.

4   Select stratigraphy based on calculated parameters and soil behaviour type index related to depth.

5   Define geotechnical soil unit for all defined layers.

Initially, the raw CPT data is loaded into a script designed to classify the soils encountered in the CPT (Step 1). Some post-processing of the raw data is performed to derive additional parameters required for classifying the soil using the Robertson-method (Step 2). These parameters are shown below.

Corrected cone resistance: $q_t = q_c + u_2 \cdot (1-a)$

Friction ratio: $R_f = \frac{f_s}{q_t}$

Normalised cone resistance: $Q_{tn} = \left(\frac{q_t - \sigma_{v0}}{P_a}\right) \cdot \left(\frac{P_a}{\sigma'_{v0}}\right)^n$

Stress exponent: $n = 0.381 I_c + 0.05\left(\frac{\sigma'_{v0}}{P_a}\right) - 0.15$

Normalised pore pressure: $B_q = \frac{u_2 - u_0}{q_t - \sigma_{v0}}$

Normalised friction ratio: $F_r = \left(\frac{f_s}{q_t - \sigma_{v0}}\right)$

Soil behaviour type index: $I_c = [(3.47 - \log Q_{tn})^2 + (\log F_r + 1.22)^2]^{0.5}$

Where:

f_s is the measured CPT sleeve friction

q_c is the measured CPT cone tip resistance

u_2 is the measured pore pressure

u_0 is the hydrostatic pore pressure

σ_{v0} is the total vertical in situ stress

σ'_{v0} is the effective vertical in situ stress

a is the area ratio of the adopted CPT cone

P_a is the atmospheric pressure

From the available parameters, an initial estimation of the soil behaviour type for each layer is made based on different classification methods (Step 3). Three different classification methods are used for evaluating the variation in the soil behaviour type (SBT):

> Using soil behaviour type index

> Using normalised cone resistance and friction ratio

> Using normalised cone resistance and pore pressure

Based on the measurements in the CPT (cone resistance, sleeve friction and pore pressure) and the estimated SBT, the soil layering can be determined, and the geotechnical soil units can be defined (Step 4 and 5).

Once the soil stratigraphy and the associated geotechnical soil units have been defined, layer specific information can be determined in the post-processing. For each soil layer, the associated CPT data can be used to estimate the strength and stiffness parameters for that specific soil layer. The methods adopted for defining strength and stiffness properties can be found in section 5.

4.2.1   Soil behaviour type index

The estimation of the SBT is based on the soil behaviour type index I_c value using Table 4-2 as seen below. It shall be noted that the correlation between the soil behaviour type index and SBT only applies for SBT zones 2-7, i.e. zones 1, 8 and 9 are not considered here.

This method considers both the normalised cone resistance and the normalised friction ratio, whilst pore pressure is not accounted for.

Table 4-2   Soil behaviour types (SBT) based on I_c.

Zone	Soil Behaviour type	I_c
1	Sensitive, fine grained	N/A
2	Organic soils – clay	> 3.6
3	Clays – silty clay to clay	2.95 - 3.6
4	Silt mixtures – clayey silt to silty clay	2.6 - 2.95
5	Sand mixtures – silty sand to sandy silt	2.05 - 2.60
6	Sands – clean sand to silty sand	1.31 - 2.05
7	Gravelly sand to dense sand	< 1.31
8	Very stiff sand to clayey sand	N/A
9	Very stiff, fine grained	N/A

4.2.2   Normalised cone resistance and friction ratio

SBT is estimated from Ref. /2/ where normalised cone penetration resistance, Q_{tn}, and normalised friction ratio, F_r, are used as basis, cf. Figure 4.2-1.

As seen from Figure 4.2-1, information about OCR/age and sensitivity can also be deduced from the plot. However, this type of information shall be treated with some caution, and it has not been used actively to establish geological age or degree of pre-consolidation for the soils.
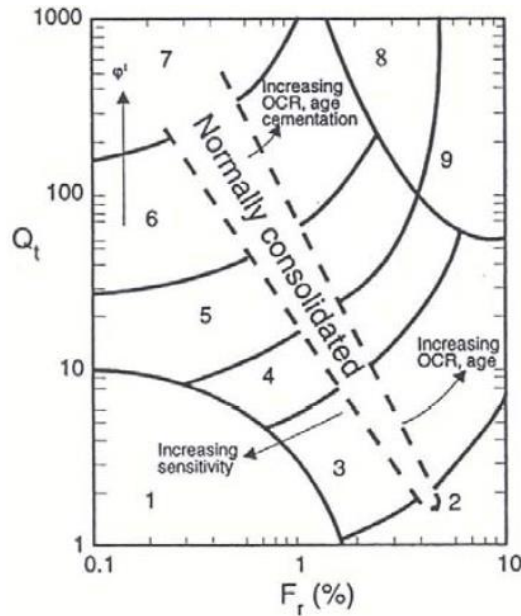
Figure 4.2-1 Robertson Q_t – F_r classification chart for soil behaviour type, cf. Ref. /2/. As recommended in Ref. /2/ the normalised cone resistance (Q_{tn}) is considered instead of Q_t when evaluating the soil behaviour type.

4.2.3 Normalised cone resistance and pore pressure

SBT is estimated based on Ref. /2/ were normalised cone penetration resistance, Q_{tn}, and normalised pore pressure, B_q, are used as basis, cf. Figure 4.2-2.
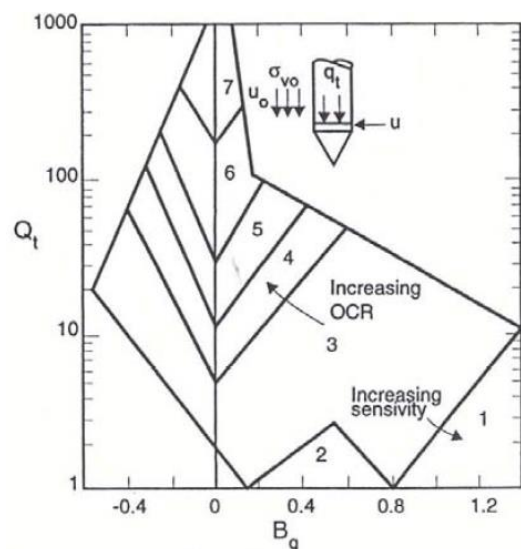
Figure 4.2-2 Robertson Q_t – B_q classification chart for soil behaviour type, cf. Ref. /2/. As recommended in Ref. /2/ the normalised cone resistance (Q_{tn}) is considered instead of Q_t when evaluating the soil behaviour type.

4.3   Classification of soils using CPT, borehole logs and geophysical horizons

For the classification of soils used for the definition of the stratigraphy and the geotechnical soil units, the following is noted:

› In the borehole logs, the soil types given are evaluated based on classification tests (particle size distribution, Atterberg limits, etc.) and based on geological evaluation.

› Classification based on CPT interpretation, cf. Section 0, generally takes into consideration the mechanical behaviour of the soil.

Hence, the source of the interpreted stratigraphy from borehole log and CPT is different and each geotechnical investigation type is valuable for a detailed understanding of the soil characteristics and behaviour.

At the geotechnical locations with both borehole and CPT, the distance between borehole and CPT is maximum 11 m, cf. Ref. /1/. At geotechnical locations for which repeated seabed CPTs have been performed the maximum distance between these is 12 m, cf. Ref. /1/. Some lateral variation of the stratigraphy may be present between the locations for borehole and CPT. However, given the short distance between borehole and CPT, such lateral variation is expected to be insignificant.

When defining the stratigraphy, it is noted that some of the geophysical horizons are difficult to identify in the borehole logs and CPTs. This is particularly the case for horizons between the fine-grained materials within unit D to F. An example of this is shown in Figure 4.3-1 for which the geophysical horizon between soil unit D2 and E1, and the horizon between soil units E1 and F are difficult to identify. A similar finding has generally been observed across the site.
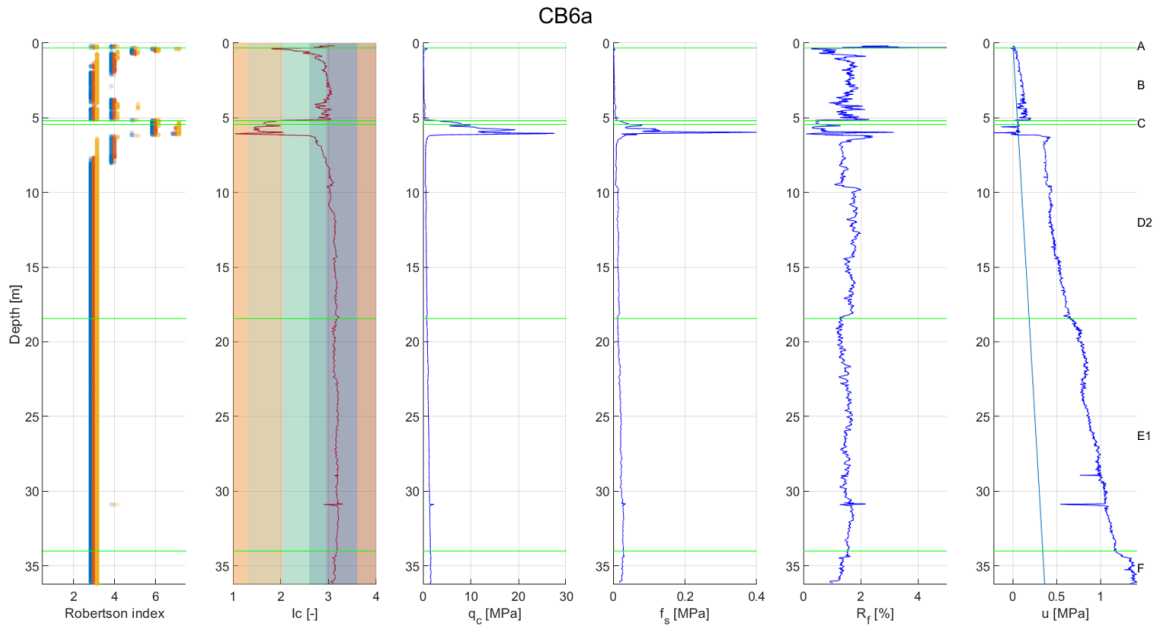
Figure 4.3-1   CPT trace and CPT classification for CPT6a. Example of difficulty in noticing geophysical horizons (green lines) in fine-grained materials of soil unit D to F.

The variation in soil behaviour type (Based on normalised cone resistance and friction ratio, cf. section 4.2.2) interpreted from CPT of selected soil units is presented in Figure 4.3-2 to Figure 4.3-5. It is observed that the clay units D1clay, D2clay, E1clay, E2clay and Fclay all plot in soil behaviour type zone 3 and 4 representing "Clay – silty clay to clay" and "Silt mixtures – clayey silt to silty clay", respectively, cf. Figure 4.3-3. The rather small area in the soil behaviour type plot covered by these clay units highlights the similarity in behaviour of these clay units.

The clay unit Hclay generally plot within soil behaviour type zone 4 representing "Silt mixtures – clayey silt to silty clay", cf. Figure 4.3-5. This is as expected given the presence of silt, sand and gravel particles within the soil unit. Further, it is noted that Hclay in the soil behaviour type plot shows a tendency to have experienced some overconsolidation.

Both C and E1sand fall within the soil behaviour zone 6 representing "Sands – clean sand to silty sand", cf. Figure 4.3-2 and Figure 4.3-4.
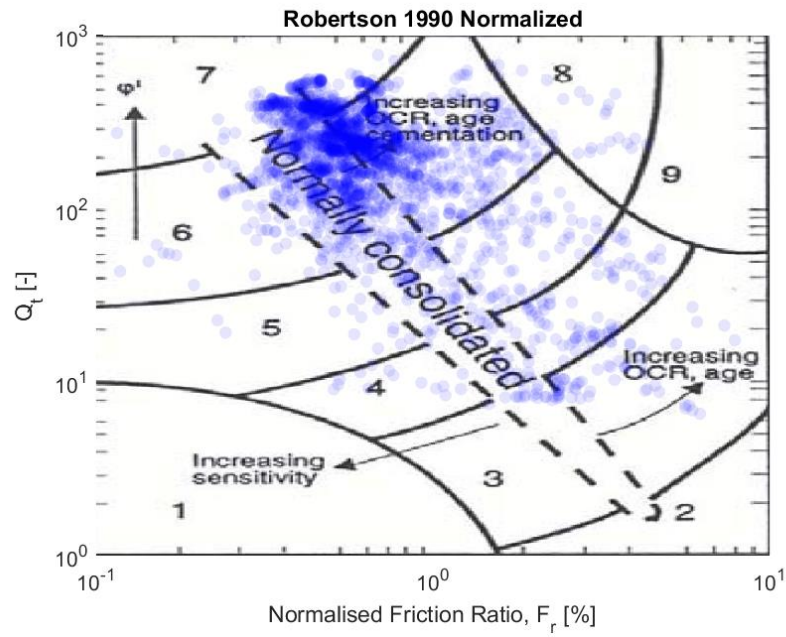
Figure 4.3-2   Robertson $Q_{tn} - F_r$ classification chart for soil behaviour type plotted for all CPT locations for soil unit C.
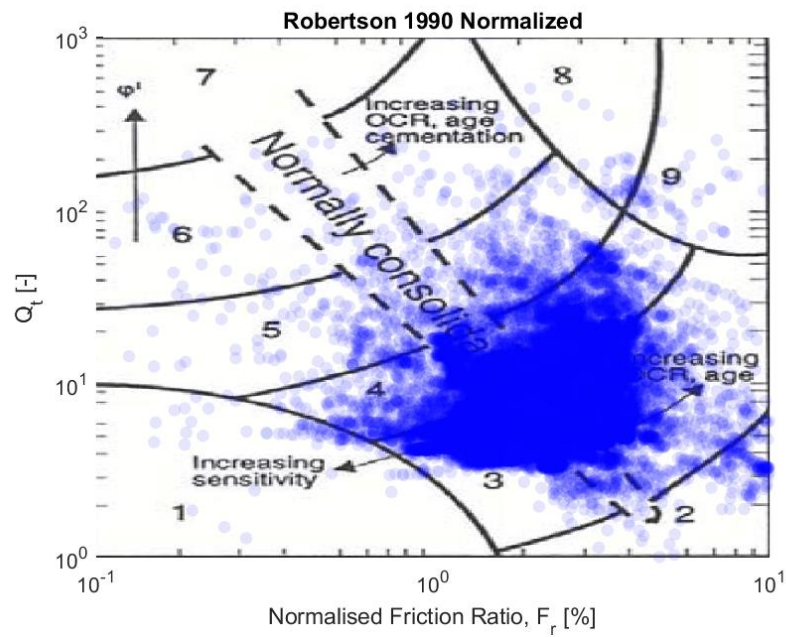
Figure 4.3-3   Robertson $Q_{tn} - F_r$ classification chart for soil behaviour type plotted for all CPT locations for soil units D1clay, D2clay, E1clay, E2clay and Fclay.
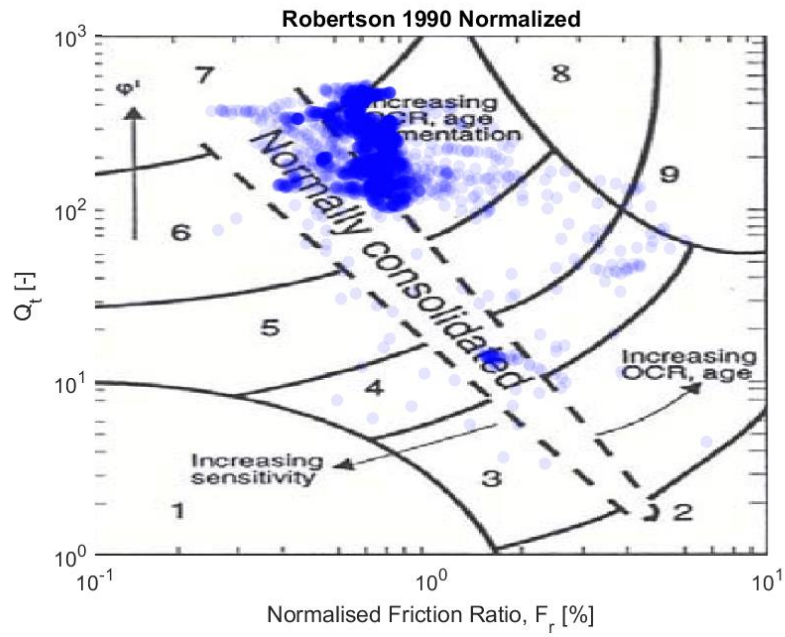
Figure 4.3-4   Robertson $Q_{tn} - F_r$ classification chart for soil behaviour type plotted for all CPT locations for soil unit E1sand.
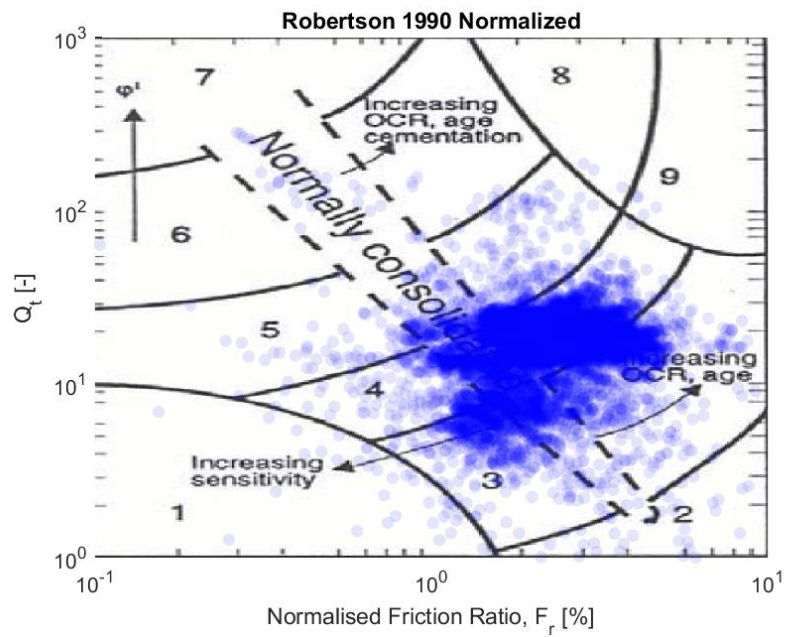
Figure 4.3-5   Robertson $Q_{tn} - F_r$ classification chart for soil behaviour type plotted for all CPT locations for soil unit Hclay.

4.4   Weichselian glacial impact on unit E properties

According to assessment of the geology and the geophysical data available at the site, it has been evaluated that unit E for parts of the site has experienced glacial impact from glacial advance in late Weichselian, cf. section 7.7.5 and Enclosure 1.06. To explore the impact of this Glacial advance on the soil behaviour type and soil properties of unit E, the CPT behaviour and the interpreted strength properties have been compared, cf. Appendix E, between the zones of no, moderate and high impact from the glacial advance during late Weichselian. The following observations are made:

> Unit E in the zone having experienced high glacial impact shows at several geotechnical locations a sandy or mixed behaviour. This is also the case in the zone having experienced moderate glacial impact. In contrast, unit E generally behaves as a clay material at geotechnical locations where the material has not experienced glacial impact.

> Within the zones having experienced moderate to high glacial impact during late Weichselian, more clean clays are encountered at some geotechnical locations and for some depth ranges. It is observed that for these clay layers, the undrained shear strength is in the same order of magnitude as the clay layer of unit E in the zone with no impact by glaciation.

> The above findings indicate that the glacial advance during late Weichselian primarily has transported material from older soil units into unit E, whilst the glacial advance has implied limited to no overconsolidation of the clay material in unit E.

5 Geotechnical properties and variation

Following the definition of soil layers and stratigraphy based on CPT and borehole data outlined in section 4, this section addresses the determination of geotechnical properties and associated variation including the assignment of these properties to the geotechnical soil units.

The determination of geotechnical properties is based on both CPT correlations, cf. Ref. /2/, and onshore laboratory test data, cf. Ref. /1/. For the CPT data, the geotechnical properties are determined based on established correlations, while the properties derived on the basis of onshore laboratory testing are taken as-is from the outcome of the testing – no additional interpretation has been imposed on the laboratory testing.

The use of CPT correlations to derive soil parameters is an efficient way of assessing the soil characteristics without the need for soil sampling and subsequent onshore laboratory testing. It must, however, be emphasized that these correlations shall ideally be benchmarked using results from testing of soil specimens under controlled laboratory conditions. The assessed soil properties based on the CPT correlations are shown for all CPT locations in Appendix B.

The relevant geotechnical properties assessed in the following are divided into three categories:

> State properties

> Strength properties

> Stiffness properties

Table 5-1 provides an overview of the parameters that will be determined including the data sources considered for each of these. The focus is to provide estimates for traditional soil parameters including the expected ranges of variation for the different soil units. These parameters provide an estimate of the soils' ability to withstand loads and a general understanding of the deformation characteristics of the soil.

In addition, an overview of the ranges of classification, strength and stiffness properties per soil unit are presented in section 5.4.

Table 5-1   Overview of geotechnical properties.

Category	Soil property	Data source
State	Over-consolidation ratio	CPT correlation
	Relative density	CPT correlation
Strength	Undrained shear strength	CPT correlation Triaxial testing (CAU, CIU, UU) Direct Simple Shear (DSS) Pocket penetrometer (PP) Torvane
	Friction angle	CPT correlation Triaxial testing (CID)
Stiffness	Small-strain shear modulus	CPT correlation Seismic CPT (SCPT) P-S logging (PS)

5.1   Presentation of CPT properties

As outlined in section 5, the soil parameters are derived partly using CPT correlations and partly using results from onshore laboratory testing.

This section presents the data from the CPTs across the site. The results are presented per geotechnical soil unit.

Figure 5.1-1 shows an example of range of variation of basic parameters such as CPT cone resistance and CPT friction ratio for D1clay, D2clay, E1clay, E2clay and Fclay (all assembled into one plot). The figure shows that the CPT measurements in these fine-grained materials generally plots within a narrow range and that they have a consistent trend with depth. In Appendix C.1, the variation of CPT cone resistance and CPT friction ratio is presented for further geotechnical soil units.
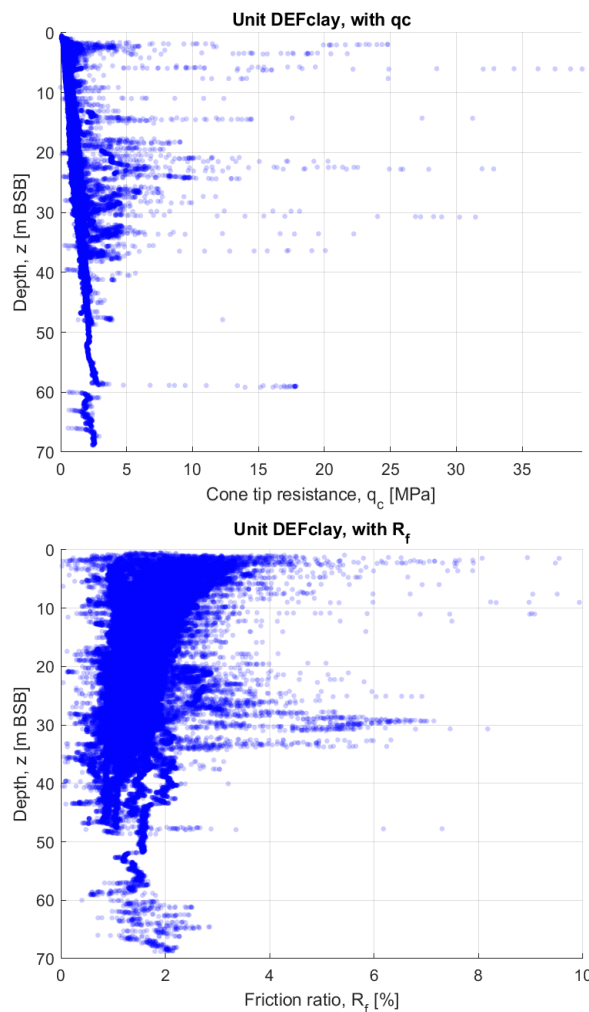
Figure 5.1-1   Range of q_c (upper) and R_f (lower) for geotechnical soil units D1clay, D2clay, E1clay, E2clay and Fclay.

5.2   Presentation of state properties

As outlined in section 5, state parameters such as over-consolidation ratio (for cohesive soils) and relative density (for non-cohesive soils) have been determined from CPT correlations.

The assessment of these parameters serves as input to the overall understanding of the in-situ soil state, which is a crucial parameter for assessing the general soil behaviour. This section presents the method adopted for the analyses of these parameters as well as the outcome.

The over-consolidation ratio, OCR, is determined for cohesive soils as:

$$OCR = k \left(\frac{q_t - \sigma_{v0}}{\sigma'_{v0}} \right)$$

where q_t is the corrected cone resistance, σ_{v0} is the total in situ vertical stress, σ'_{v0} is the effective in situ vertical stress and k is a dimensionless constant, which in accordance with Ref. /2/ is set to 0.33.

For the non-cohesive soils, the relative density, I_D, is calculated as:

$$I_D = \frac{100}{2.91} \ln\left(\frac{q_t}{205\,(\sigma'_m)^{0.51}} \right)$$

where q_t is the corrected cone resistance and σ'_m is the in situ mean effective stress.

Figure 5.2-1 shows the variation of OCR (interpreted based on CPT) with depth for the geotechnical soil units D1clay, D2clay, E1clay, E2clay and Fclay (all assembled into one plot). It is observed that all these layers generally have an OCR between 1 and 2 unity, i.e. they are in a slightly overconsolidated state. In Appendix C.2, the variation of OCR with depth is presented for the individual geotechnical soil units.
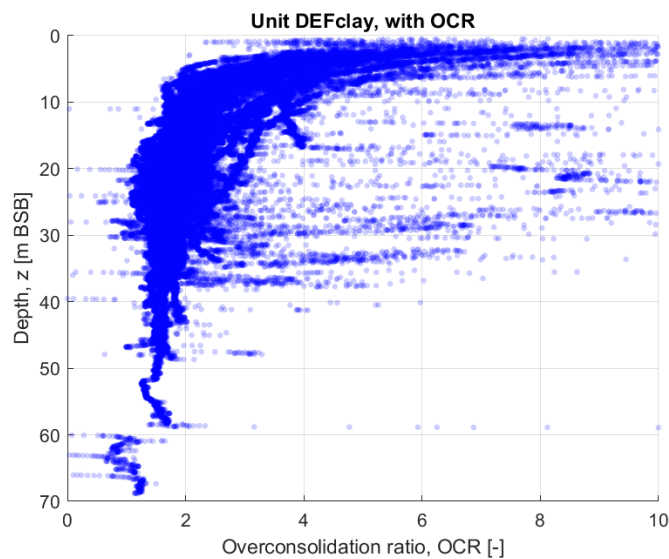
Figure 5.2-1   Range of OCR for geotechnical soil units D1clay, D2clay, E1clay, E2clay and Fclay.

In Figure 5.2-2, an example of the variation of relative density (interpreted based on CPT) with depth is presented. It is observed that the relative density of the geotechnical soil unit E1sand is in the range 60% to 100%. In Appendix C.3, the variation of relative density with depth is presented for the further geotechnical soil units.
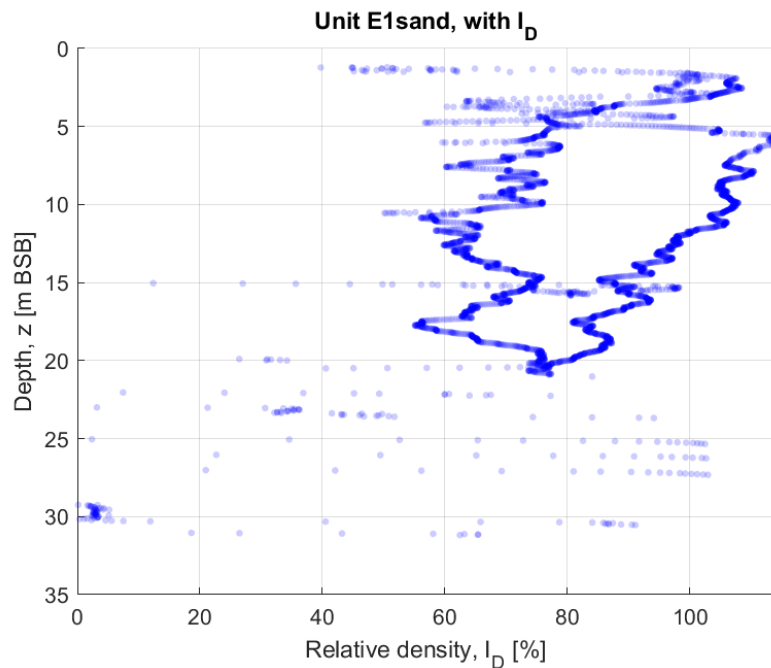
Figure 5.2-2   Range of I_D for geotechnical soil unit E1sand.

5.3   Presentation of strength and stiffness properties

Following the state parameters described in section 5.2, strength and stiffness parameters such as undrained shear strength (for cohesive soils), friction angle (for non-cohesive soils) and small-strain shear modulus (all soils) have been determined from CPT correlations, cf. Ref. /2/, supplemented by onshore laboratory testing, cf. Ref. /1/. In addition, the small-strain shear modulus has also been evaluated based on SCPT and P-S logging.

The assessment of these parameters serves as input to the overall understanding of the soil behaviour during loading, e.g. in relation to placement of wind turbine foundations or jack-up operations on the site. This section presents the method adopted for the analyses of these parameters as well as the outcome.

The results originating from CPT analyses have been used to visualize the variation of soil strength and stiffness for selected soil units across the site. This method adopts local CPT data correlated to soil strength and stiffness properties to indicate the variation of the specific parameter throughout the site by determining local values for each geotechnical location. This is shown in Enclosures 2.01 to 2.12. For the visualisation of soil strength and stiffness variation across the site, the following is noted:

> Due to the limited thickness of geotechnical soil units A, B and C, the spatial variation of the properties of these units has not been visualized.

› The geotechnical soil units D1clay, D2clay, E1clay, E2clay and Fclay all show an approximately linear increase in undrained shear strength with depth. Hence, the spatial variation in strength for these soil units is visualized through the ratio between undrained shear strength and depth.

› For the geotechnical soil unit Hsand, several CPT refusals have been encountered. Hence, interpretation of friction angle based on CPT measurements are uncertain and the spatial variation in strength for this soil unit is not visualized.

› The geotechnical soil units D1sand, D1mix, D2sand, D2mix, E1mix, E1sand, E2mix, E2sand, Fmix and Hmix are only present at few survey points. Hence, the variation across the site of the soil properties of these soil units is not visualised.

To determine just one representative value (soil strength/stiffness) per soil unit per geotechnical location, the average value for each soil unit is determined. When deriving the average value for the soil layer, the peaks and troughs in the CPT trace (usually found close to the layer boundaries) are removed to reduce the impact of this data on the average value, i.e. to obtain the most representative value.

5.3.1   Friction angle

The peak friction angle, φ_p', is calculated for non-cohesive soils according to the method of Schmertmann (Presented in Ref. /4/) assuming that the sand is "uniform medium sand" to "Well-graded fine sand":

$$\varphi_p' = 31.5 + 12\, I_D$$

where I_D is the relative density.

Further to the CPT correlation, the friction angle is obtained through triaxial testing, CID. The CID triaxial tests have been performed as single tests, i.e. tests have not been performed at varying confining pressure. The confining pressure adopted for the tests have generally been set to approximately the in-situ mean effective stress of the sample. The peak friction angle, φ_p', has been derived from the CID tests through the following equations:

$$M = q/p'$$

$$\varphi_p' = \operatorname{asin}\left(\frac{3M}{6 + M}\right)$$

where q is the deviatoric stress at failure and p' is the effective mean stress at failure. Hereby it is assumed that the effective cohesion is zero.

Using CPT data for all geotechnical locations as well as the available laboratory test data, the range of friction angle for soil unit E1sand is shown in Figure 5.3-1. It is observed that the friction angle interpreted based on CPT matches

reasonably well to those measured in the CID tests. In Appendix C.4, the variation of relative density with depth is presented for the further geotechnical soil units.
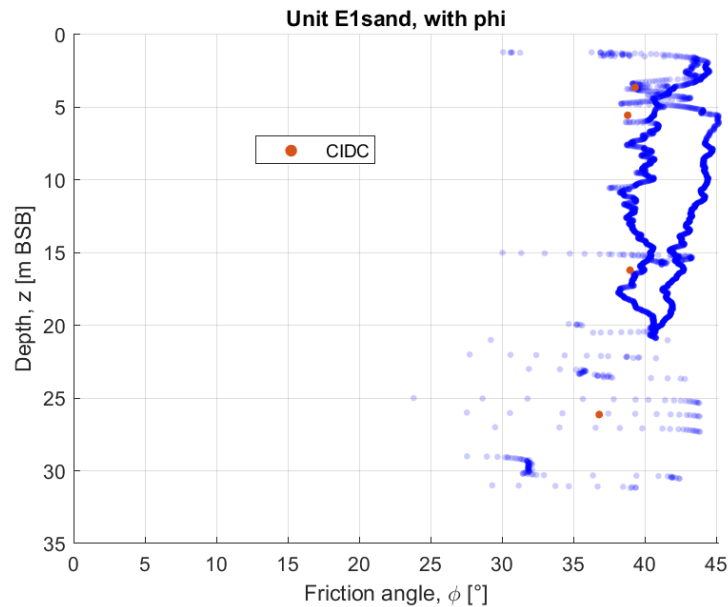
Figure 5.3-1   Range of φ for soil unit E1sand using CPT correlation and laboratory test results (CD – Consolidated Drained triaxial test).

5.3.2   Undrained shear strength

The undrained shear strength, c_u, is determined for cohesive soils according to Ref. /2/ as:

$$c_u = \frac{q_t - \sigma'_{v0}}{N_{kt}} = \frac{q_{net}}{N_{kt}}$$

For determination of undrained shear strength, a cone factor of $N_{kt} = 15$ has been applied fine-grained materials in soil unit A to F, whilst $N_{kt} = 20$ has been applied for fine-grained materials in unit H. These values are in agreement with the recommendations of N_{kt} ranges in Ref. /1/, and they are found to ensure a proper match between the undrained shear strength determined based on CPT and the undrained shear strength from the consolidated undrained triaxial tests (CIU and CAU).

Further to the CPT correlation, the undrained shear strength is obtained through triaxial testing, namely consolidated anisotropically undrained (CAU) tests, consolidated isotropically undrained (CIU) tests and unconsolidated undrained (UU) tests, from direct simple shear (DSS) tests, Torvane tests and Pocket penetrometer tests. Using CPT data for all geotechnical locations as well as the available laboratory test data, the range of undrained shear strength is shown in Figure 5.3-2 for the geotechnical soil units D1clay, D2clay, E1clay, E2clay and Fclay (all assembled into one plot). It is observed that these fine-grained materials show similar strength profile and that the undrained shear strength

generally increases linearly with depth. Further, it is observed that the CPT predicted strength matches well the strength derived from consolidated triaxial tests and DSS tests. In contrast the Torvane tests, pocket penetrometer tests and unconsolidated undrained triaxial tests generally yield lower strength than the CPT predictions. In this regards it is emphasized that consolidated triaxial tests and DSS tests are considerably more reliable than the other laboratory tests.

In Appendix C.5, the variation of undrained shear strength with depth is presented for the individual geotechnical soil units. In Appendix C.6, the depth variation of the ratio between undrained shear strength and depth is presented for the individual geotechnical soil units.
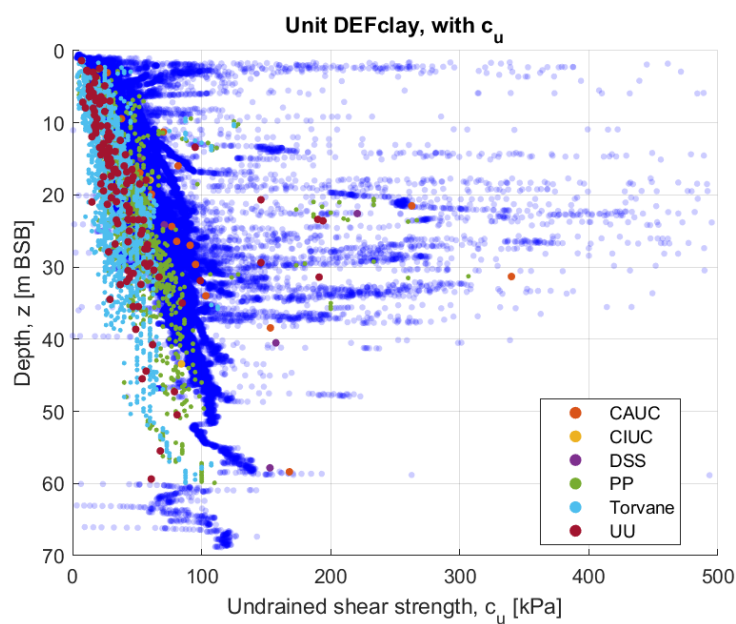
Figure 5.3-2   Range of c_u for the geotechnical soil units D1clay, D2clay, E1clay, E2clay, Fclay using CPT correlation (blue) and laboratory test results. (CU denotes consolidated [Isotropically or Anisotropically] undrained triaxial tests).

5.3.3   Small-strain shear modulus

The small-strain shear modulus, G_{max}, is determined in all soils as:

> $G_{max} = \rho\, V_s^2$

where ρ is the bulk density of the material and V_s is the shear wave velocity.

The shear wave-velocity, V_s, is for non-cohesive soils estimated from CPT using the following equation, cf. Ref. /2/:

> $V_s = 277\, q_c^{0.13}\, \sigma'_{v0}{}^{0.27}$

where q_c is the measured CPT cone tip resistance and σ'_{v0} is the effective in situ vertical stress.

For cohesive soils, the shear wave velocity, V_s, is estimated from CPT using the following equation, cf. Ref. /2/:

> $V_s = (10.1 \log q_c - 11.4)^{1.67} \left(\frac{f_s}{q_c}\right)^{0.3}$

where q_c is the measured CPT cone tip resistance, and f_s is the measured CPT sleeve friction.

Further to the CPT correlation, the small-strain shear modulus is obtained through seismic CPT (SCPT) and P-S logging. It is noted that the shear wave velocity from SCPT provided in AGS format (version 4) deviates from that documented in latest version received of Ref. /1/. In the assessment presented herein it is assumed that the shear wave velocity presented in AGS format is correct.

Using CPT data for all geotechnical locations as well as the available SCPT data and P-S logging data, the range of small-strain shear modulus for selected soil units is shown in Figure 5.3-3. It is noted that the small-strain shear modulus predicted based on P-S logging is significantly higher than the small-strain shear modulus predicted from CPT data and SCPT data. The small-strain shear modulus from SCPT on the other hand fits well with the values interpreted from CPT. Considering the OCR and undrained shear strength of units D1clay, D2clay, E1clay, E2clay and Fclay, the small-strain shear modulus values from P-S logging appear unexpectedly high.

In Appendix C.7, the variation of small-strain shear modulus with depth is presented for the individual geotechnical soil units.
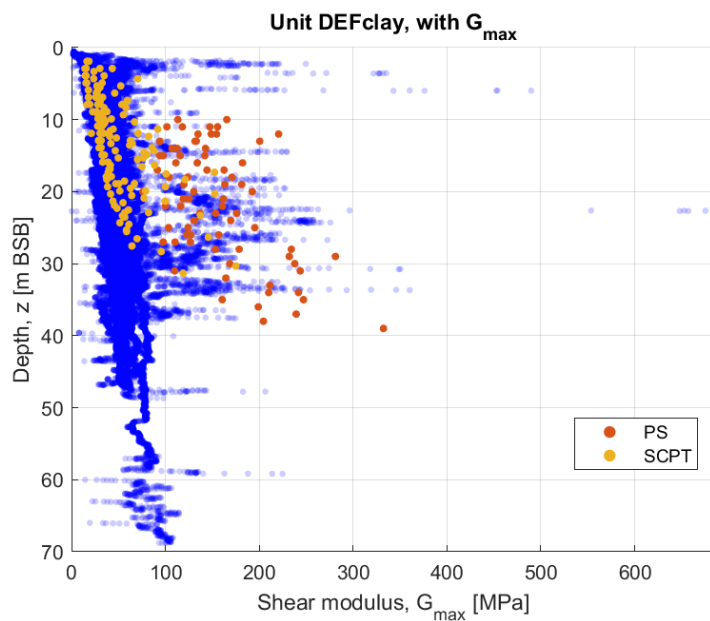
Figure 5.3-3   Range of G_{max} for the geotechnical soil units D1clay, D2clay, E1clay, E2clay, Fclay using CPT correlation, SCPT and P-S logging.

5.4   Range of soil parameters per soil unit

In Appendix D the range and average values (covering the full site) of classification, strength and stiffness parameters are presented for the main geotechnical soil units.

6   Geological Setting

In this section the geological setting for the Hesselø OFW is presented.

6.1   Pre-Quaternary Geology

The Hesselø OWF is located near the south-western boundary of the Baltic Shield between the southern part of Sweden, the Kattegat and the northern part of Jutland (Figure 2.1-1). The area is strongly influenced by the Sorgenfrei Tornquist zone, a south-east to north-west oriented fault system where one of the major faults, the Børglum Fault, transcends the northern part of the Hesselø OWF (Figure 6.1-1).
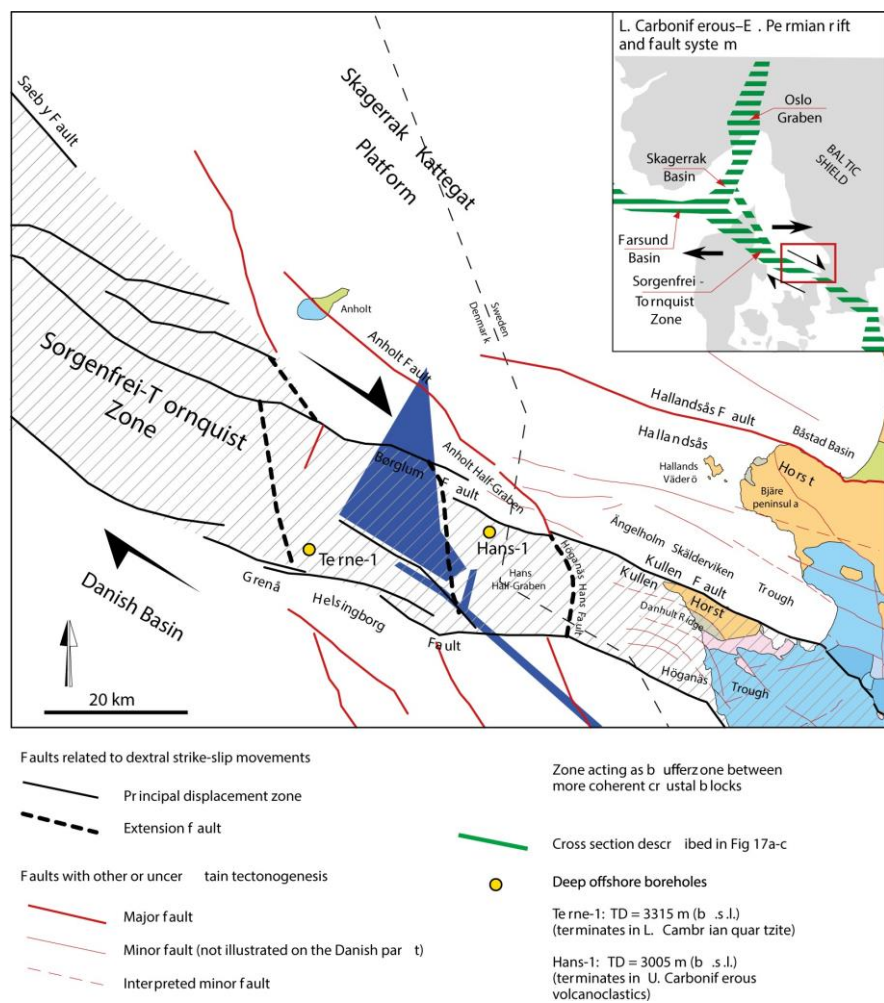
Figure 6.1-1.   Regional structures as reported by GEUS in the southern part of the Kattegat and the location of the Hesselø OWF (Ref. /5/).

In the late Cretaceous – early Paleogene, the previous subsiding depocenter became inverted, primarily along pre-existing faults, due to a change in the regional stress orientation dominated by compression associated with the Alpine Orogeny and the opening of the north Atlantic.

The bedrock of the Hesselø OWF is expected to consist of Jurassic to Lower Cretaceous mudstone or siltstone and Precambrian crystalline may be found in the northern part (Ref. /5/).

6.2   Quaternary Geology

During the Quaternary period several glacial events have been identified the northern Danish area. The different glacial events are separated by interglacial or interstadial marine or glaciolacustrine conditions. Till from Last Weichselian glaciation is found south of Anholt along with late glacial and Holocene deposits. The Scandinavian Ice Sheet reached its maximum extent in Denmark about 22 ka BP followed by stepwise retreat. Around 18 ka BP the sea began to inundate northern Denmark which led to rapid deglaciation. At ca. 17 ka BP the ice margin had retreated to the Halland coastal moraines along the Swedish west coast (Ref. /5/).

In the Danish area the ice cap steadily retreated, which caused the opening of the Kattegat depression and transgression of the area. A glaciomarine environment was established where the glacier was in direct contact to the sea. Therefore discharge of meltwater borne sediments could be dispersed from the glacier to the sea and drop stones rafted by calving icebergs should be expected (Figure 6.2-1). Thick glaciomarine deposits related to late glacial are reported from the area (Ref. /5/).

The interplay between eustatic sea-level rise caused by global melting of ice caps and glacio-isostatic rebound (regional reaction to the relief of the glacier burden) causes the sea-level to fluctuate in late glacial and Holocene. In early Holocene the sea level dropped and may have caused the area to become terrestrial for a short time before a new transgression from which marine conditions continued through the rest of the Holocene (Ref. /5/).
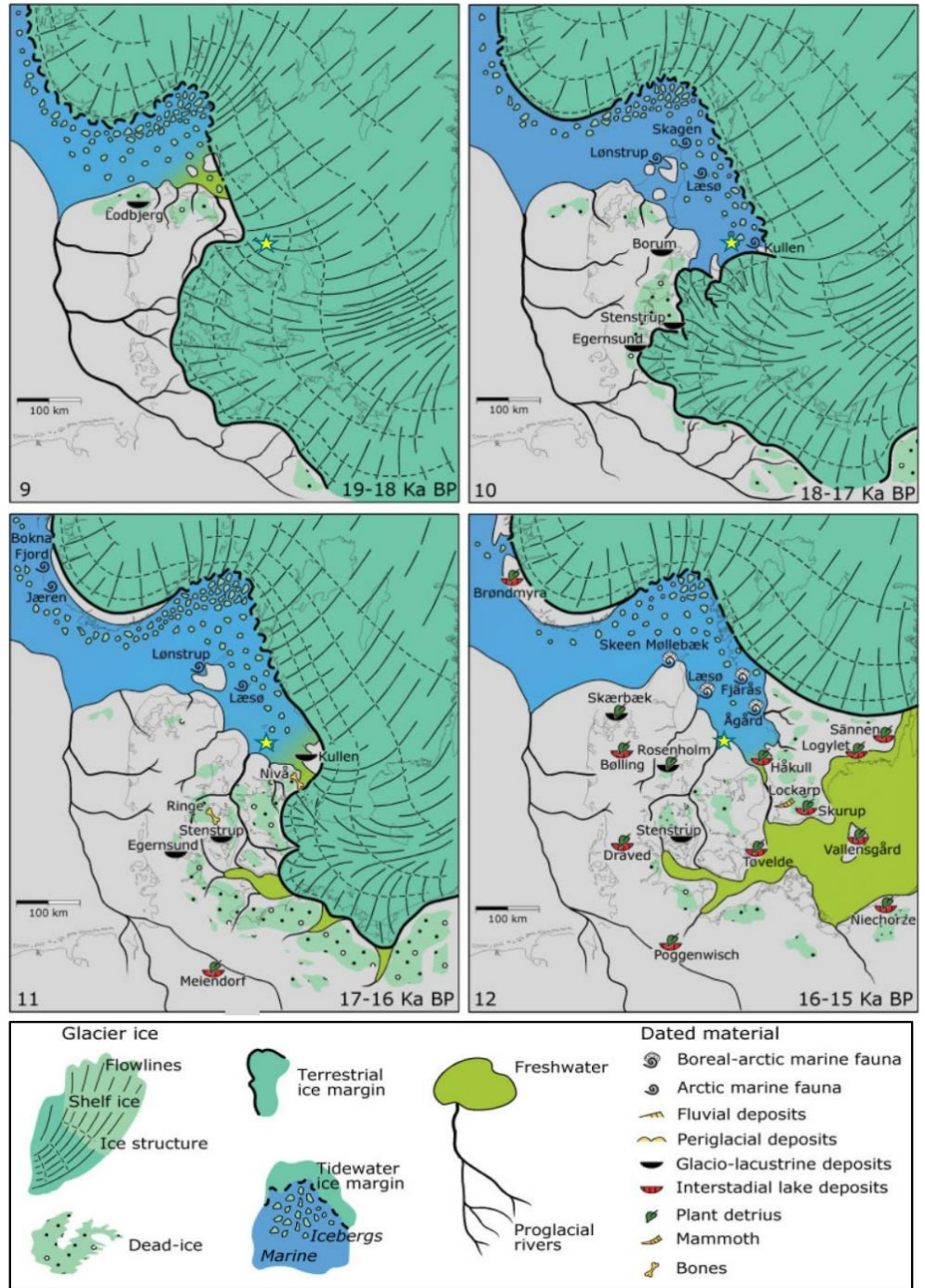
Figure 6.2-1   Palaeogeographical reconstructions of the last deglaciation of southern Scandinavia (Ref. /5/).

7 Integrated Geological Model

In this section it is described how the integrated geological model has been developed using the geotechnical results from Ref. /1/, Ref. /10/ and geotechnical interpretations in this study along with the geophysical results from Ref. /3/ and Ref. /11/.

7.1 Datum, coordinate system and software

The model is set up with datum ETRS89 (EPSG:4936) and the GRS80 Spheroid. The coordinate system used is the UTM projection in Zone 32 N. Units are in meters. Vertical reference is MSL, height model DTU18.

The software used for interpretations was the IHS Markit Kingdom suite 2021. Seismic data was delivered in three data packages: 2D-UHRS, 3D-UHRS and SBP data. The 2D-UHRS seismic data was imported both in time and depth domain, and the delivered velocity model was imported as RMS velocity. The data was delivered and imported in the SEG-Y format. The SBP data was imported in both time and depth domain, however, no velocity model was delivered with this dataset. The 3D-UHRS datasets covered an area of 0.935 km^2 (550 m x 1700 m) around each of two potential offshore substation locations, in the north and south of the site. Geotechnical data and borehole information was imported into the software from the delivered AGS files.

Horizons (geological layer boundaries) have been interpreted directly along clear reflectors in the seismic data. Finally, results have been exported as grids for visualization. The grids include layer boundaries as well as grid calculations such as depth below seabed and vertical thickness of layers.

7.2 Assessment of existing geophysical model

A geophysical model created by Fugro based on solely geophysical data forms the basis for integrated geological model together with the geotechnical data from Gardline (Ref. /1/). The received geophysical model (Ref. /3/) was based on the two seismic datasets, 2D-UHRS and SBP data. The upper most units have only been identified on the SBP data, while the intermediate and deep units only can be recognised on the 2D-UHRS data. Table 7-1 gives an overview of the received units and which seismic data type set they have been identified on, as well as the top and base horizon boundaries for each unit. The 3D-UHRS data (Ref. /11/) have not been used to identify individual seismic units, but many of the interpreted units, have been recognised on the 3D-UHRS dataset. The 3D-UHRS data has been applied for assessment of geohazards in the areas designated for two OSS locations.

*Table 7-1   Units, horizons and their relation in geological model received from Fugro
(Ref. /3/).*

Data type	Unit name	Unit boundary (Horizons) Top	Base
SBP	A	H00 /Seafloor	H01, H05, H10
	B	H01	H05, H10
	C	H05	H10
2D-UHRS	D	H10	H20
	E	H10, H11, H20	H25
	F	H20, H25	H30
	G	H25, H30	H35
	H	H20, H25, H30, 35	H50
	I	H30, H35, H50	N/A

The interpreted unit boundaries in the existing SBP and 2D-UHRS-based geophysical model, were generally interpreted along some of the most clear and continuous reflectors identified in the seismic dataset. Horizons have then been drawn on these, as unit boundaries. However, especially in areas interpreted as having been glacially overridden, the impact of glacial deformation made it necessary to make the interpretation more detailed. In these areas, some of the delivered horizons was not fully interpreted but was left as unfinished unit bases.

7.2.1 Incorporation of RMS-Velocity SEG-Y data

The Kingdom project received from Fugro contains seismic data in both two-way-time and depth. Interpretations in two-way-time were by Fugro converted to depth using a velocity model applied in external software and reimported into Kingdom. The applied model was an RMS velocity model based stacking velocities setup in SEG-Y format.

The only way we would be able to apply this RMS velocity model was if it could be loaded onto the same lines in Kingdom as two-way-time and depth data. The

received Kingdom project from Fugro did not originally include the RMS velocity. SEG-Y data and the setup for 2D-UHRS SEG-Y files (two-way-time and depth) were loaded on individual lines. Therefore, all 2D-UHRS data and interpretations had to be reimported – SEG-Ys through Seismic Direct placing the different SEG-Y types (two-way-time, depth, RMS velocities) on the same line, and interpretations with renamed line names in the file, to fit the reimported line names from Seismic Direct. For 3D-UHRS the RMS velocity SEG-Ys were loaded directly (not Seismic Direct) into Kingdom, with the same setup as the two-way-time and depth data already in place.

7.3   Interpolation and adjustment of surfaces

Geotechnical data (Ref. /1/, Ref. /10/) were imported in the Kingdom Model and integrated interpretation performed establishing correlation between seismic reflectors and the stratigraphy established based on CPT and borehole logs (Section 4). The geotechnical data were imported in depth and converted to TWT ms for interpretation of horizons.

An overview of the resulting model layers in the integrated geological model is presented in Ref. /3/. Original layer names (unit numbers) have been kept in the updated model to allow easier comparison to the existing geophysical model.

Table 7-2   Summary of updates to the horizon based geological model.

Data type	Previous Units	Updated Units	Unit boundary (Horizons) Top	Base	Comments to updates
SBP	A	A	H00 /Seabed	H01, H05, H10	No changes to H01, H05, H10
	B	B	H01	H05, H10	No changes to H05, H10
	C	C	H05	H10	No changes to H10
2D UHRS	D	D1	H10	H11	No changes to H11
		D2	H10, H11	H20	H20 changed – interpretation finalised
	E	E1	H10, H11, H20	H25	H25 changed
		E2	H10, H20, H25	H26	New H26
	F	F	H20, H25, H26	H30	No changes to H30
	G	G	H25, H26, H30	H35	No changes to H35
	H	H	H20, H25, H26, H30, 35	H50	H50 updated to match BH descriptions
	I	I	H30, H35, H50	N/A	

Unit D has been divided into Subunits D1 and D2, where H11 mapped by Fugro is the bounding surface. D1 and D2 show significant different acoustic signature, which is also reflected in different lithological geotechnical properties. Subunits D1 and D2 can also be correlated to different late glacial stratigraphic units defined by Ref. /5/.

The base of Subunit D2 is marked by horizon H20. This horizon was not fully interpreted upon delivery but was lacking it the south-western corner of the site. This was partly due to a limited understanding of the complex glacial and geological history of the site. With added information from CPT data and a more thorough investigation of the glacially deposited units, H20 could be interpreted in more detail and finished in the missing areas. H20 have therefore been mapped in the entire site and serves as a unit boundary between the glacially impacted Unit E and the marine/lacustrine Unit D.

A new horizon has been added to the existing model: H26. However, H26 consist primarily of some of the original interpretations in H25. Since H25 has

been changed to represent base of Subunit E1 (previously it was placed at base Unit E) the remaining part the original H25 were then renamed to H26 to represent the base of Subunit E2. H26 represent base of Unit E where a glacial advance has pushed up material from the layers below Unit E and mixed it into Unit E. The boundary between Subunit E1 and Subunit E2 is represented by H25 which thereby marks the upper boundary of a mixing zone for sediments incorporated from layers below Unit E.

Updates have been made to H50 to make a better match with the levels in the boreholes where mudstone or siltstone has been described.

Minor updates to horizons between H10 and H50 have been carried out to fill gaps where the layers are partly or fully obscured by blanking, mostly to remove errors when calculating thickness grids and grids representing unit tops. To keep indicating uncertainty of these areas a blanking polygon has been introduced.

7.4   Uncertainty in the grid

According to Ref. /3/, the vertical resolution of the SBP data is better than 0,3 meter within the first 10 meter below seabed. For the 2D-UHRS data, vertical resolution is between 0.3 m to 1,0 m within the first 100 m below seabed. In reality, the resolution gradually decreases with depth. From the vertical resolution, the lateral resolution can be estimated to generally better than 2 m in the upper 10 m below seabed assuming a dominant frequency of 1000 Hz and velocities of 1800 m/s or smaller.

The grid cell size of 10x10 m is chosen to accommodate; file size, accuracy of the data and lateral resolution of the seismic data. For grids to be continuous across gaps between survey lines, interpolation was needed. The distance between UHRS survey lines is 250 meters, so an interpolation distance of 125 meters was chosen. For grids based on the SBP data, the interpolation distance was 40 meters. The cell size of the grid fits well along the seismic lines where the uncertainty is low. However, in areas far from the closest seismic line (maximum distance is 125 meters) the cell size is relatively small and may indicate a higher certainty than the actual seismic data density provides. The uncertainty becomes larger as the distance to the seismic lines increases independent of cell size and it is therefore important to note the location of the seismic lines when working with the grids in detail.

7.5   Depth conversion

The seismic data was converted from two-way-time (TWT) to depth in the processing and interpretation process. For the SBP dataset, a two-layer model was used, separating water column and subsurface, with sound velocities of 1470 m/s up to 1495 m/s for the water column (varying between lines) and 1500 m/s for the shallow soils, respectively (Ref. /3/). For the 2D-UHRS data, RMS velocities was calculated and delivered with the segy files.

All interpretation carried out on the data after the delivery, was performed in time domain. RMS velocities were then extracted for the given seismic layer, which was then converted to depth in the extended math calculator in the Kingdom software, using time and RMS velocity. This was done in order to ensure that interpretations were available both in time and depth domain, should any further work be needed. For the shallow interpretations on the SBP data, no new horizons were interpreted, so the delivered two-layer model made by Fugro was used.

7.6   Geological features

Table 7-3 summarizes the identified geological features and their expected geohazard potential. Further descriptions of the different geological features can be found in the following sections.

Table 7-3 Summary of interpreted geological features and their expected geohazard potential.

Interpretation	Description	Associated units	Geohazard potential
Local enhanced amplitude anomalies	Buried features which are possibly related to methane-derived authigenic carbonates. No actual carbonate sandstones sampled.	Holocene, Unit A and Unit B (See section 7.7.1 and 7.7.2)	If buried local cemented sands exist, they are not expected to a have a strength comparable to crystalline boulders.
Shallow gas	Acoustic blanking found primarily at the top the of pre-Quaternary depression.	Irregular top surface mostly located in Holocene, Unit B. (Section 7.7.2)	The associated deposits are not expected to be able to confine considerable concentrations of gas. Higher uncertainty of the thickness of masked layers.
Peat pockets	Area on top of the pre-Quaternary depression contains abundant discontinuous negative high-amplitude reflectors interpreted to be peat pockets.	Identified in Holocene, Unit B. (Section 7.7.2)	Found in formations with low strength. Should possibly be considered for thermal conductivity issues for subsurface cables.

Interpretation	Description	Associated units	Geohazard potential
Boulders, cobbles, and patches of gravel	Appear as positive point anomalies and display diffraction hyperbolas in unmigrated data.	Appear in Holocene and Quaternary Units A to E and H (Section 7.7). Found abundant in Subunit D2.	Possible boulders pose a potential geohazard for installation of WTG foundation.
Faults	Small faults related to mass transport deposits.	Seen in Late Weichselian Subunit D2 (Section 7.7.4).	The identified features have low influence on the soil properties.
Glacial deformation	Late Weichselian glacial re-advance has deformed Unit E and Unit F in part of the site.	Late Weichselian Unit E and F in the central and eastern part of the site (Section 4.4, 7.7.5 and 7.7.6).	Some unpredictability in soil characterization. Unit E may in some areas consist of more competent layers than the low strength clay which is most common for the layer.
Mass transport deposits	Movement of sediments driven by instability caused mainly by tectonic activity and high sedimentation rates.	Late Weichselian Subunit D2 and Subunit E1 (Section 7.7.4 and 7.7.5).	Geotechnical properties do not vary significantly from the undisturbed parts of the units.
Areas of debris	Areas of irregular seabed corresponding to 'Areas of debris' mapped on the seafloor.	Holocene Unit A (Section 7.7.1).	The potential of geohazard is depending on the nature of the debris identified at the seafloor.

Shallow gas, pockets of peat and sub-surface boulders constitutes potential geohazards as interpreted in Ref. /3/. However, further geotechnical investigations are needed to establish the character of each hazard.

7.6.1   Local enhanced amplitude anomalies

Local enhanced amplitude anomalies were observed in the SBP, 2D-UUHR and 3D-UHR seismic datasets. They appear as laterally limited amplitude enhancements, which extent vertically through the seismic records.

The top of these anomalies has a high-amplitude negative reflector generally observed in the Holocene Units A and B. Locally these anomalies appear to extend into the underlying Late Weichselian Unit D. The features are considered to have geological origin, though the exact origin has not been determined.

To help the interpretation of these features data from the geotechnical campaign has been applied (Ref. /1/). Three dedicated sampling boreholes (Anorm_1, Anorm_2 and Anorm_3) and one geotechnical test location (CB13-BH) penetrate these features (See enclosure 1.02).

The following possible origins for these local enhanced amplitude anomalies have been considered by Fugro (Ref. /3/):

> Local accumulations of coarse sediments have been considered as an explanation, however, only three of the four sampling locations indicate sand in these features, CB13-BH indicate fine sediments.

> Small amounts of free gas may cause the acoustic blanking and signal distortion. At these shallow depths, sealing capacity of normally consolidated soils is expected to be low and possibly insufficient to contain gas accumulations. The natural buoyancy of the free gas bubbles may be in equilibrium with capillary forces in pores within the fine-grained sediments of Unit A.

> Methane-derived authigenic carbonates are known from the northern Kattegat where seeping methane precipitates carbonates as cement between sand particles in sandy deposits and develop carbonate cemented sandstone. Often these structures are accompanied by a diverse marine ecosystem. The geotechnical campaign did not find carbonate cemented sandstones in the samples from these features. Thereby it is concluded that the targeted anomalies do not resemble fully developed methane-derived authigenic carbonate features. In addition, these features are covered by recent sediment that may suggest that gas seepage activity has ceased in the past, effectively stopping authigenic carbonate formation. However, the carbonate content in the sampled sands varies and an early-stage form of methane-derived authigenic carbonates cannot be excluded.

In the SBP sections the mapped local enhanced amplitude anomalies appears to be erosional remnants of a thicker bed belonging to Unit B though the current interpretation mostly groups these formations together with Unit A (Figure

7.6-1). When the erosive event has eroded all the surrounding sediments and left these many tops behind it indicates that something has made these obstacles more resistant to erosion. Methane-derived authigenic carbonates seem like the best possible explanation and similar processes are described in the northern Kattegat area (e.g. Ref. /12/). Even though they may not have developed actual carbonate cemented sandstone as the samples indicate some cementation of the sand particle may be enough for the tops to withstand the erosion.

Since the features is buried below Unit A and nothing from these features seem to stick above seabed actual sandstone reefs are less like to be found.

Seeping methane can also explain the high amplitude negative reflectors in the UHRS data. The presence of gas in the tops can be explained if the deposits of Unit B are more gas permeable than those of Unit A. In that way the tops will act as funnels for seeping gas through the lower part of Unit A.
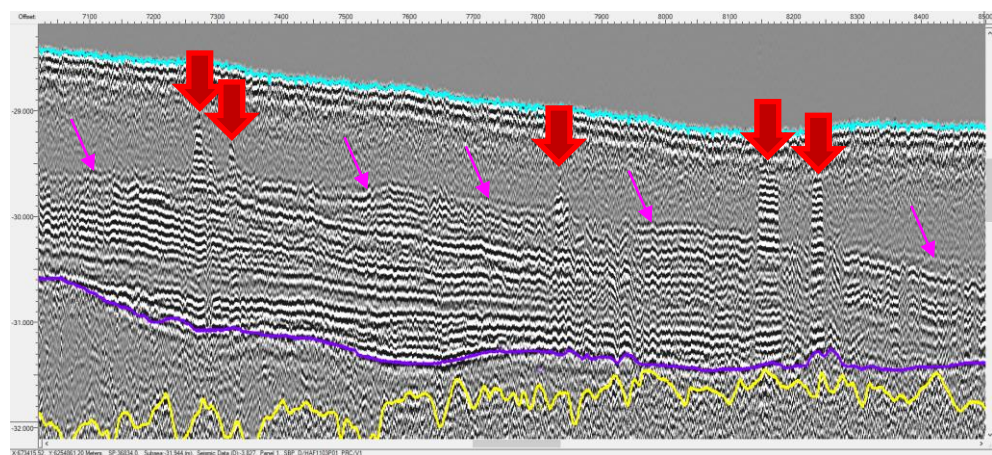
Figure 7.6-1   A closer look at some of the local enhanced amplitude anomalies. Thin pink arrows point at the boundary between Unit A and Unit B. Fat red arrows point at tops mapped as local enhanced amplitude anomalies (SBP line HAF2094P01_PRC).

7.6.2   Shallow gas

Acoustic blanking was observed locally both in the SBP data and 2D-UHRS data (Ref. /3/) and is assessed to indicate the presence of shallow gas in the soil. The main area of observed acoustic blanking is in the large pre-Quaternary depression to the north of the site. Occasionally, acoustic blanking is also observed in other parts of the site where it is associated with local enhanced amplitude anomalies and has a limited lateral extent (Figure 7.6-1). The blanking often obscures visibility of layered (clayey) deposits, primarily in Late Weichselian Unit D, suggesting that the blanking may be associated with (small quantities) of gas in the soil.
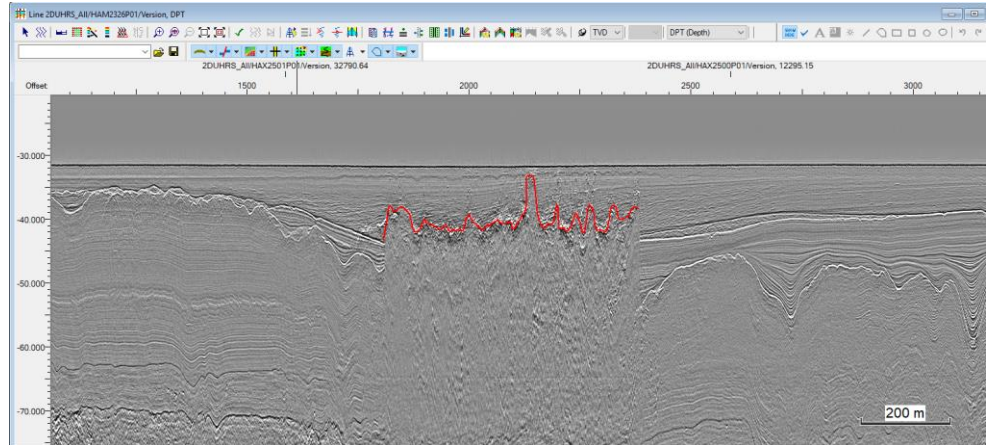
Figure 7.6-2   Acoustic blanking on 2D-UHRS seismic data (UHRS line HAM2326P01).

7.6.3   Peat pocket

High-amplitude reflectors, typically discontinuous and of limited extent, were observed in the SBP and 2D-UHRS data (Ref. /3/). In the 2D-UHRS data these seismic events show clear negative amplitudes. These negative amplitude events most likely represent small pockets of (reworked) peat or organic-rich clays. The high amplitude reflectors are very abundant within the Holocene Unit B in the large Quaternary depression. They are also sporadically present within Unit B outside of the large Quaternary depression.

7.6.4   Boulders, cobbles, and patches of gravel

Individual diffraction hyperbolas were observed in the SBP data (Ref. /3/) in all units within the penetration depth (i.e. Units A to D) (Figure 7.6-3). They are most abundant in the central part of the site and particularly within Unit A. Diffraction hyperbolas in the SBP data are indicative of coarse material; possibly gravel to cobble-sized shells and rock fragments.

In the 2D-UHRS data positive amplitude point anomalies were observed (Ref. /3/) as illustrated in Figure 7.6-3. They are mostly identified in Subunit D2 and are particularly abundant below Horizon H15. They also occur locally within Unit E and Unit H. They are most abundant in the centre and northern part of the site, which corresponds with the spatial distribution of Subunit D2.

In the 3D-UHRS data individual point diffractors are also observed. The same point diffractor are often visible on multiple in- and cross-lines due to the close line spacing (1 m for in-lines and 0.5 m for cross-lines) of the 3D data. Therefore, each point diffractor was picked at its highest point on one line only (Figure 7.6-3). Figure 7.6-4 show the point diffractors in a depth slice through the 3D-UHRS data at the OSS-1 location. Here, point diffractors are visible as circular objects. The picked diffractors across the two OSS locations can be seen in Figure 7.6-5 as depth below seabed.

The point anomalies observed in the 2D-UHRS and 3D-UHRS data may indicate the presence of individual cobbles and boulders or small patches of coarse material (e.g. gravel). Point anomalies in Subunit D2 may possibly represent ice-rafted debris.
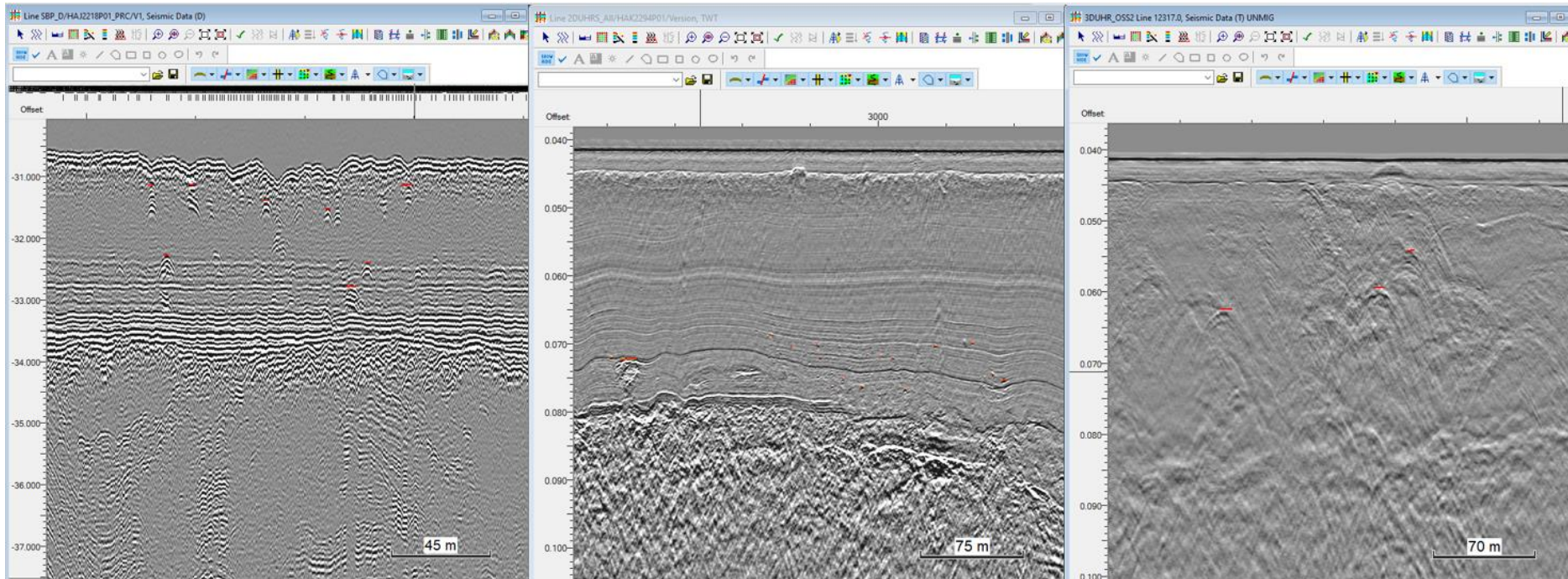
Figure 7.6-3   Examples of diffraction hyperbolas on the SBP data and individual point diffractors marked in red on the 2D-UHRS and 3D-UHRS data. These are indicative of patches of coarse-grained material, cobbles or boulders in the sediment.
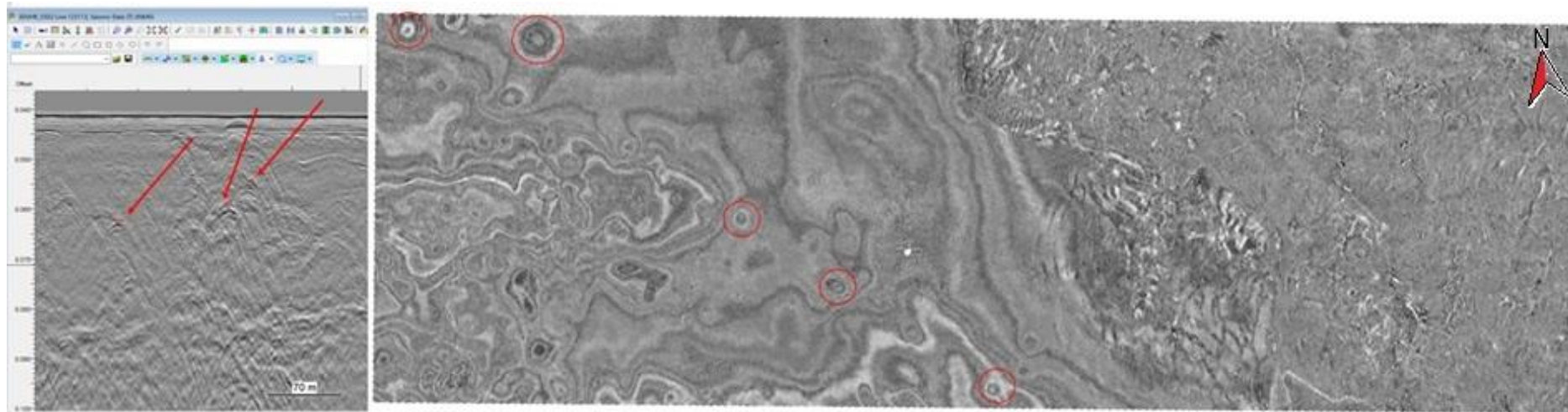
Figure 7.6-4 Example of point diffractors from the 3D-UHRS data. On the left, an example of the interpretation in 2D view. On the right, a depth slice through the 3D-UHRS data at OSS-1 at 50 meters below sea-level. Point diffractors show up as circular objects, here marked with red circles. The size of the depth slice is 550x1700 m, covering the whole 3D box at OSS1.
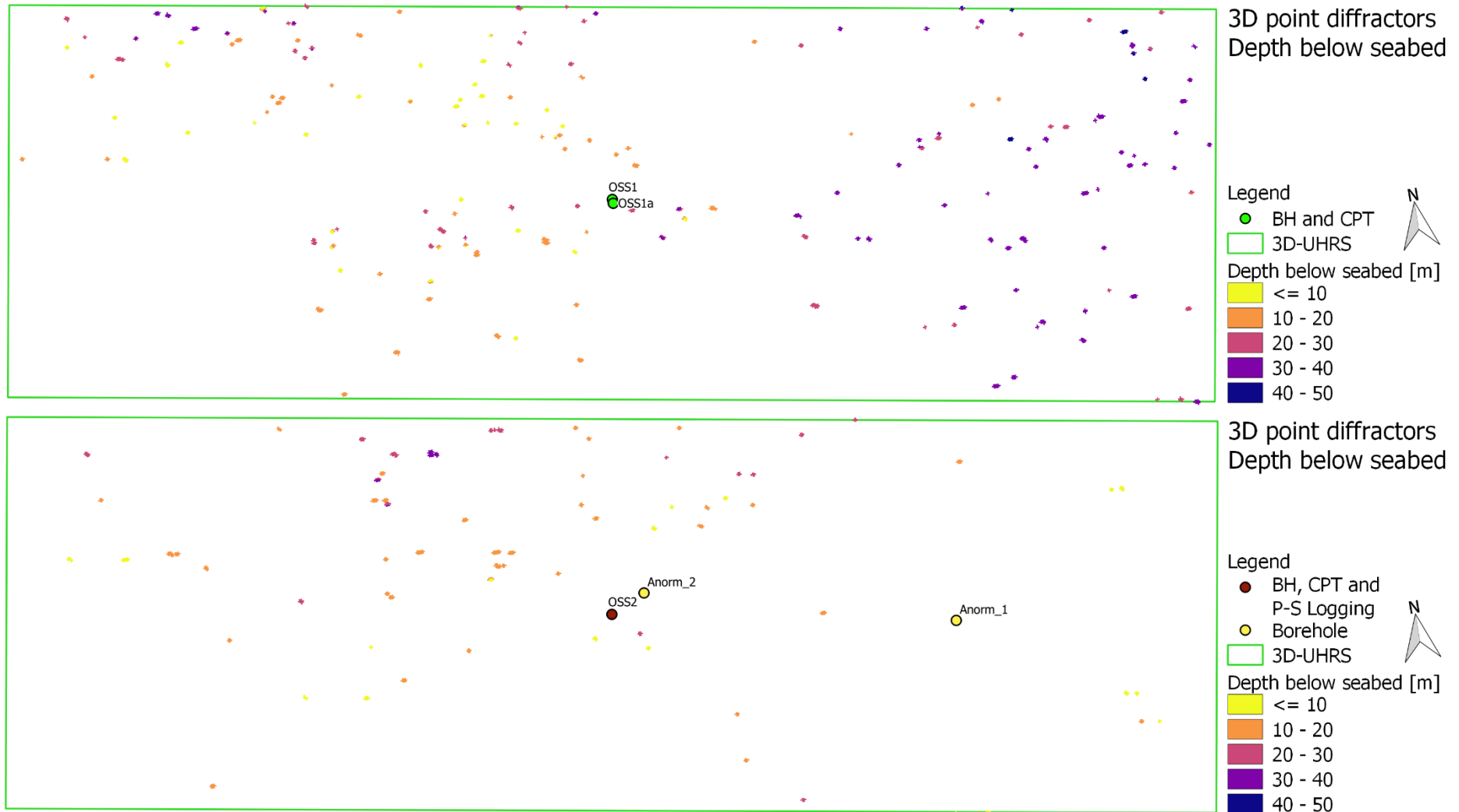
Figure 7.6-5 Picked point diffractors on the 3D-UHRS data set at the OSS1 (top) and OSS2 (bottom) locations, shown in Depth Below Seabed. The size of each area is 550x1700 meters, covering an area of 0.935 km².

7.6.5   Faults

Faults are expected to occur in the Hesselø site associated with the Sorgenfrei–Tornquist Zone. The sub-surface architecture, changes in unit thickness and erosive contact between units within the pre-Quaternary depression may imply tectonic activity during the Quaternary.

Large faults were not identified in the seismic data. They may occur at deeper levels, beyond the penetration depth of the seismic data. Faults are likely to be present in the bedrock (Unit I).

Small-scale faulting was observed in Late Weichselian Subunit D2 (See section 7.7.4), which is interpreted to be related to mass transport deposits (See section 7.6.7).

7.6.6   Glacial deformation

Glacial deformation is evident within Late Weichselian Units E and F (See sections 7.7.5 and 7.7.6). A Late Weichselian glacial readvance has terminated within the site. Which means that part of Unit E and F in the north and west is unaffected by glacial deformation whereas the eastern and central part of both units is impacted. The deformation has completely worked the thinner Unit F into Unit E and Unit F is therefore nearly absent as a separate layer in the deformed area. Material from deeper deposits has also been worked into Unit E. Subunit E2 shows the highest impact of incorporation material from the deeper layers. Enclosure 1.06 show areas where Units E and F have been impacted and highly impacted by glacial deformation.

7.6.7   Mass transport deposits

Evidence for mass transport deposits was observed at multiple levels within Late Weichselian Subunit D2 (See section 7.7.4). The interpreted mass transport deposits within Subunit D2 range from channel-like features with a transparent and locally chaotic seismic facies to fault separated blocks of intact stratification that change laterally into undisturbed Subunit D2 (Ref. /3/) (See Figure 7.6-6). The faulted blocks are found adjacent to channel-like mass transport features and represent deposits less affected by the mass transport process. The small faults described here are also mentioned in section 7.6.5.
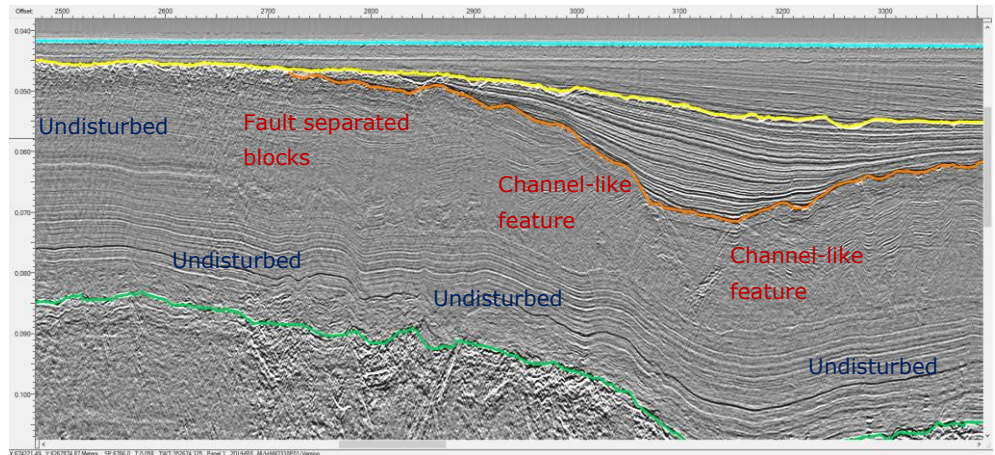
Figure 7.6-6 Example of Mass transport deposits in Subunit D2 (between the orange/yellow and the green horizons).

In Subunit E1 the seismic character of the area which has not been glacially impacted is dominated by semi-transparent to chaotic pattern and layered parts are only seen in small patches in the most western part of the site (See section 7.7.5). Comprehensive mass transport processes could explain the disturbed appearance. Post-depositional sedimentary processes such as slumping could also be part of the explanation.

Since the gradients generally are small across the Hesselø site the mass transport is interpreted mainly to be driven by instability posed by tectonic activity associated with the Sorgenfrei–Tornquist Zone, high sedimentation rates of fine-grained glaciomarine deposits and for Subunit E1 also glacial proximity.

7.6.8   Areas of debris

Seventeen small areas, 100 m to 200 m in diameter with clear irregular seafloor were observed in the SBP data (Figure 7.6-7). Just below the irregular seafloor, numerous diffraction hyperbolas were observed in Unit A.

These areas may have a man-made origin and could represent debris dropped on the seafloor. These areas correspond with the 'Area of Debris' as mapped on seafloor in Ref. /3/.
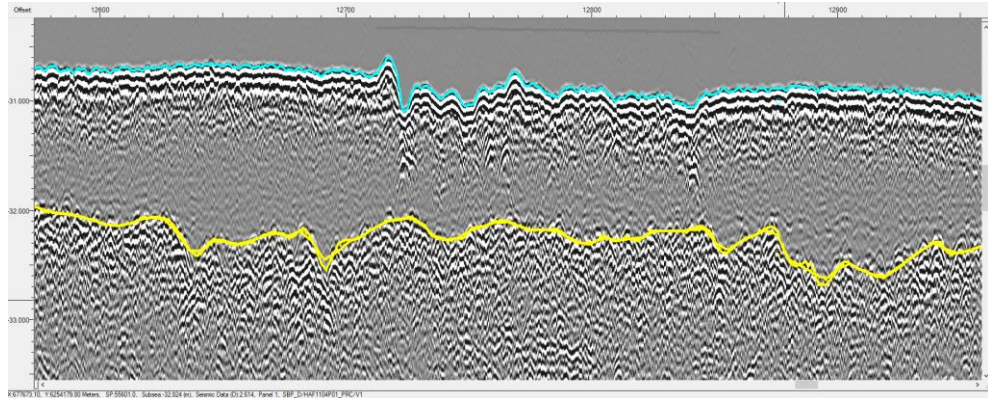
Figure 7.6-7 Irregularly shaped seabed as seen in this example indicate disturbed seabed and correspond to "Areas of Debris" mapped on the seafloor Ref. /3/. Unit A is found between the light blue and the yellow horizons (see section 7.7.1). (SBP line HAF1104P01_PRC).

7.7 Stratigraphy

The stratigraphy of Hesselø has been divided into nine main units. Two of these units (D and E) has been subdivided into D1 and D2, and E1 and E2 respectively. This gives the model a total of 11 model layers. A summarized description of the different units can be found in Table 7-4. Two profiles (Figure 7.7-1 and Figure 7.7-2), oriented north-south and east-west across the entirety of the site, gives an overview of the interpreted model layers and the stratigraphy across the site.

The stratigraphy interpreted in the data collected at the Hesselø OWF is guided by scientific papers and reports on the topic. Especially the desktop study completed by GEUS (Ref. /5/) give a good overview and frames the settings well. The timing and interplay of deglaciation and glaciomarine transgression in the final phase of the Weichselian are key elements in the interpretation of the stratigraphic setting in the Hesselø area.

Table 7-4 Summary of units in the integrated geological model.

Data type	Unit	Horizon		Seismic Character	Soil Type according to the borehole descriptions. (Ordered by frequency) Ref. /1/	Age	Depositional Environment	Correlation to units described by GEUS. Ref. /6/, Ref. /7/, Ref. /8/
		Top	Base					
SBP	A	H00/ Seabed	H01 H05 H10	Acoustically transparent with occasional vague internal reflector near the base	CLAY, Sandy CLAY, Silty sandy CLAY, Sandy gravelly CLAY, silty sandy gravelly CLAY	Holocene	Marine	PG III
	B	H01	H05 H10	Low to high amplitude horizontal and inclined stratified reflectors, locally chaotic	CLAY, Silty sandy CLAY, Silty SAND	Early Holocene	Deltaic	PG II
	C	H05	H10	Acoustically semi-transparent to chaotic	SAND, Silty SAND, Gravelly SAND, Sandy CLAY	Early Holocene	Shallow marine	PG I
2D-UHRS	D1	H10	H11	High amplitude parallel reflectors in channels/depressions.	Sandy CLAY to gravelly SAND	Late Weichselian	Glaciofluvial to glaciomarine	LG II
	D2	H10 H11	H20	Dominantly low to medium amplitude parallel reflectors, becoming increasingly distorted in the southern part of the site. In areas acoustically transparent or chaotic.	CLAY	Late Weichselian	Glaciomarine	LG I

	E1	H10 H11 H20	H25	Acoustically semi-transparent, in the central and eastern part often chaotic with locally steeply inclined internal reflectors	Sandy gravelly CLAY, CLAY, Silty CLAY, CLAY TILL, Sand, Silty SAND	Late Weichselian	Glaciomarine and glacial	LG I (or GL, WG I, WG II)
	E2	H10 H20 H25	H26	High amplitude chaotic with steeply inclined internal reflectors	Sandy gravelly CLAY, Gravelly CLAY, Silty CLAY, Silty SAND, SILT	Late Weichselian	Glaciomarine and glacial	LG I (or GL, WG I, WG II)
	F	H20 H25 H26	H30	Medium to high amplitude closely spaced parallel reflectors	CLAY, Silty CLAY, Gravelly CLAY,	Late Weichselian	Glaciomarine	LG I
	G	H20 H25 H26 H30	H35	Acoustically semi-transparent to chaotic. Locally inclined discontinuous reflectors are present within semi-transparent character.	-	Weichselian	Glacial, glaciofluvial, glaciomarine	GL, WG I, WG II
	H	H25 H26 H30 H35	H50	Variable, either medium amplitude parallel reflectors, acoustically semi-transparent with occasional inclined lateral discontinuous internal reflectors or a chaotic seismic character	Silty sandy gravelly CLAY, Sandy gravelly CLAY, CLAY TILL, CLAY, Silty CLAY, Gravelly CLAY, Silty sandy gravelly cobbly SAND, Clayey SAND, SAND, Silty SAND	Weichselian to earlier Pleistocene	Glacial, periglacial and/or glaciomarine	GL, WG I, WG II
	I	H35 H50	N/A	Low to medium amplitude low frequency parallel reflectors; Locally acoustically (semi-) transparent	MUDSTONE, SLITSTONE, CLAYSTONE,	Jurassic or Early Cretaceaous	Marine	BR
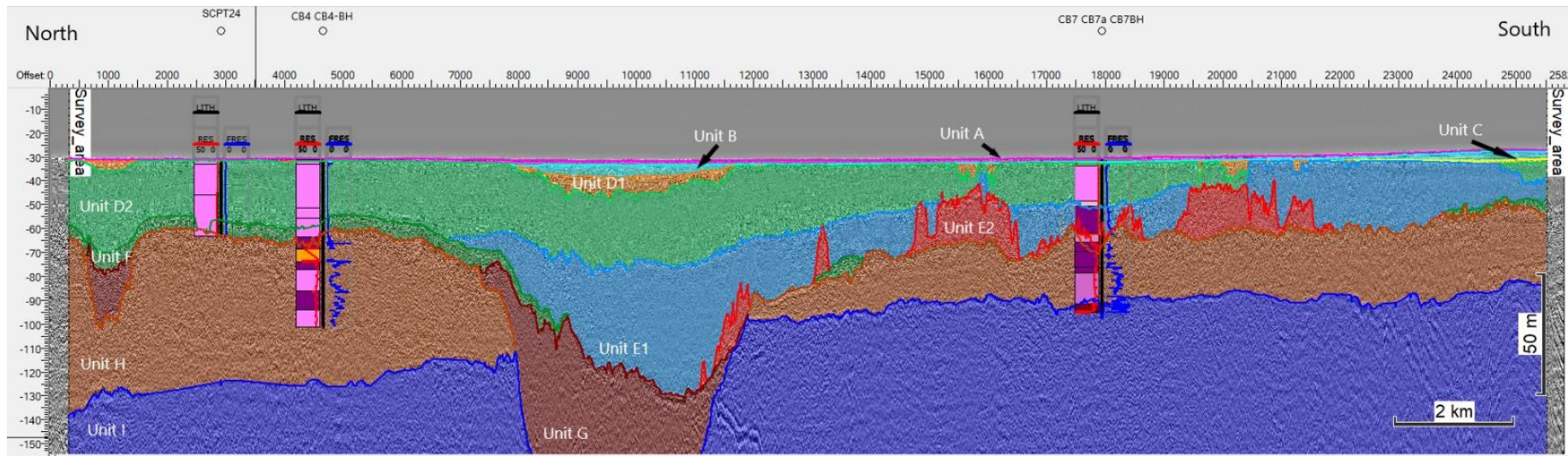
Figure 7.7-1 Profile oriented north to south, showing the interpreted units across the site with CPT and borehole information, supporting the interpretations.
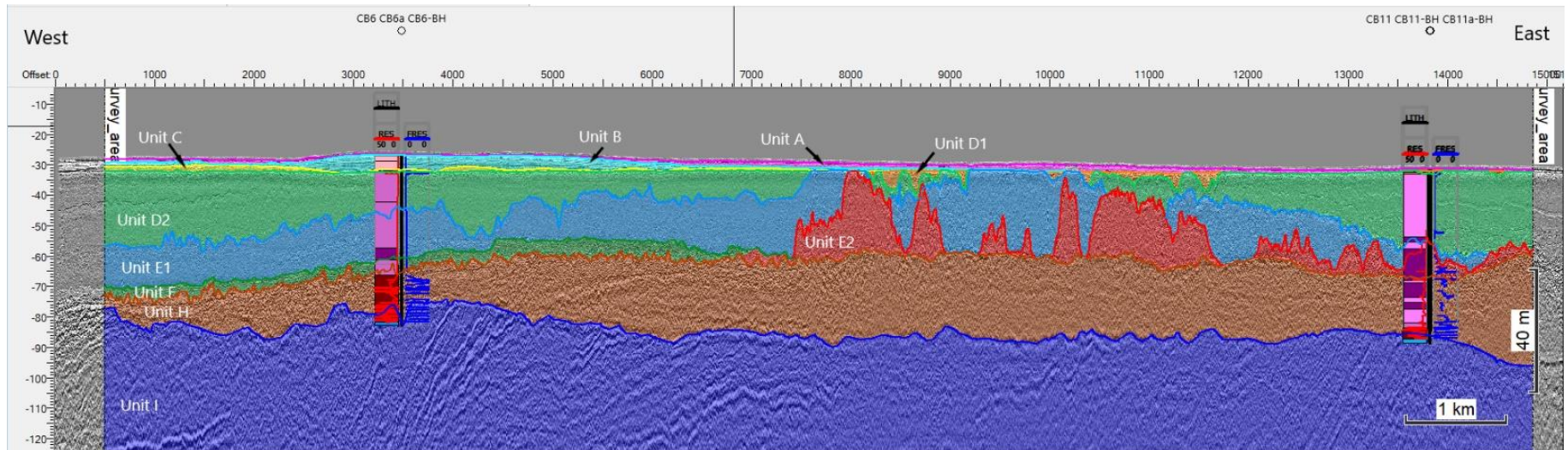
Figure 7.7-2 Profile oriented west to east, showing the interpreted units across the site with CPT and borehole information, supporting the interpretations.

7.7.1   Unit A – Holocene – Post glacial marine

Unit A is interpreted to be deposited during the Holocene in a marine environment.

Unit A, the uppermost interpreted unit, is present across the entire site, except for small areas within the eastern part of the site, where erosional escarpments are observed on the seafloor. The unit generally forms a thin layer, which drapes older units. The maximum thickness is observed in the centre of the site, where it reaches approximately 3 m and decreases to less than 1 m towards the eastern and western margins of the site. Internally the unit is acoustically transparent. Locally, vague internal reflector can be observed. Diffraction hyperbolas or enhanced amplitude reflections are present within this unit and are likely due to the presence of coarse material (i.e., gravel-sized shells, shell and rock fragments). Where the unit overlies Unit B (mostly in the west) the base is regular and varies from flat to undulating. Where the unit overlies Unit D (mostly in the east), the base has an irregular, rugose character. In the eastern part of the site, the unit overlies Unit C. In the western part of the site, Unit A is locally in erosional contact with the underlying Unit B, forming gullies 1 to 3 m deep and 80 to 200 m wide with a west–east orientation. As Unit A is thin and drapes Horizon H01, these gullies can still be observed in the present seafloor morphology (see enclosure 1.01). In the western part of the site, the base of Unit A forms the eastern margin of a wide channel with a north–south orientation. Potentially the gullies and the channel were formed by the Dana River (Great Belt palaeo-river; Ref. /7/, Ref. /8/). In the eastern part of the site, where the Holocene cover is generally thin, Unit A appears to fill in the depressional remnants of iceberg plough marks in the underlying Unit D. Table 7-4 provides the typical soil types for Unit A based borehole samples.
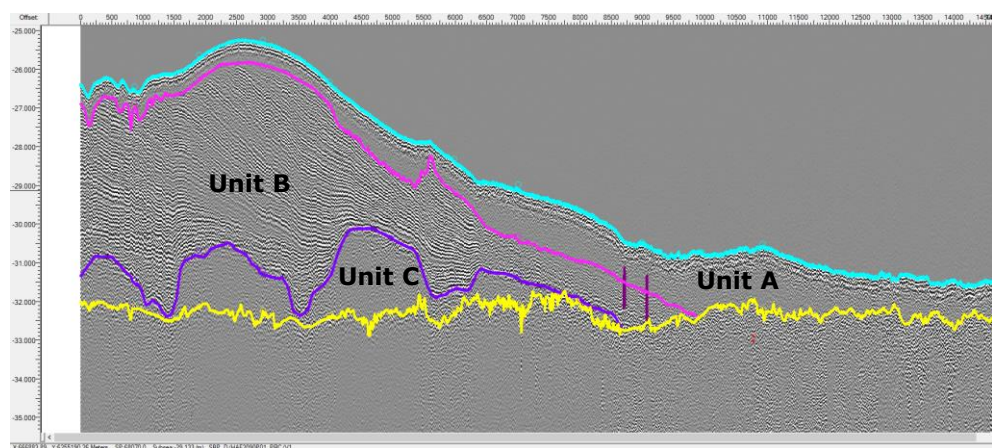
Figure 7.7-3   *Example of Units A, B, and C in seismic data from the southern part of the investigated area. Unit A between the light blue and the pink horizons is mostly relatively thin showing vague reflectors. Unit B between the pink and the purple horizons is stratified, comprising commonly medium to high-amplitude, parallel reflectors. Unit C between the purple and the yellow horizons is often acoustically semi-transparent to chaotic (SBP line HAF1707P01_PRC).*

7.7.2   Unit B – Holocene – post glacial marine

Unit B is interpreted to be deposited in a deltaic environment, at the mouth of the Dana River System (Great Belt palaeo-river) through which the Ancylus Lake drained into the Kattegat (Ref. /7/, Ref. /8/).

Unit B is present in the central and western part of the site. In general, the unit is thin, on average approximately 1 m thick. It reaches locally greater thicknesses of approximately 6 m in the shallower south-western part of the site and a maximum thickness of approximately 14 m in the large depression in the north-eastern part of the site. Internally, the unit is stratified, comprising of low to high-amplitude, parallel reflectors. Where Unit B is thickest in the south-western part of the site, the stratification has an eastward directed inclined orientation and high amplitudes. In the east where Unit B is thin, the stratification is sub-horizontal and is associated with low amplitudes. Locally, where Unit B overlies Unit C and becomes thinner, the low-amplitude stratification transitions into a more chaotic seismic character. Within the large Quaternary depression, the stratification in Unit B has a dominant westward orientation and shows abundant high-amplitude reflectors of variable lateral extent. These reflectors are interpreted as possible pockets of peat/organic clay. Acoustic blanking is observed in Unit B in the deepest parts of the large Quaternary depression. The character of the base of Unit B is either undulating (Horizon H05) or irregular (Horizon H10). Horizon H01 forms the top of this unit and marks a change in seismic characteristics between acoustically transparent (Unit A) above and a stratified character (Unit B) below. In the south-western part of the site, with shallower water depth, the internal stratification of Unit B shows an angular unconformity with the overlying Unit A. At the large Quaternary depression an internal angular unconformity can be observed (Figure 7.7-1). Table 7-4 provides the typical soil types for Unit B based borehole samples.
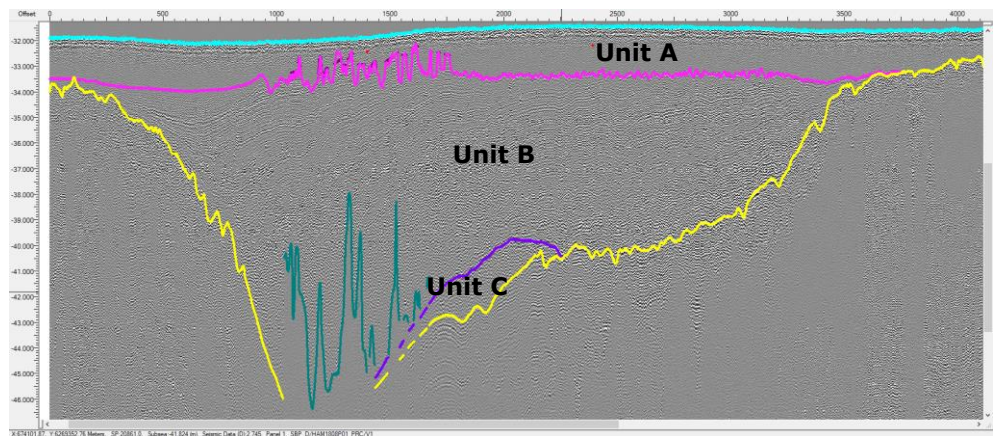
Figure 7.7-4   Example of Units A, B, and C in seismic data. This image shows an example above the deep Quaternary depression in the north. Unit A between the light blue and the pink horizons is mostly relatively thin showing vague reflectors. Unit B between the pink and the purple/yellow horizons is stratified with distorted high amplitude horizons possibly indicating peat pockets and areas of acoustic blanking (dark cyan). Unit C between the purple and the yellow horizons has a limited extent thickness in the depression area. (SBP line HAM1808P01_PRC).

7.7.3   Unit C – Holocene – post glacial marine

Unit C is interpreted to be deposited as coast-parallel spits or barrier islands during the marine transgression in the early Holocene.

Unit C is present in the south-western part of the site, where it forms hummocks/ridges with approximately a north–south orientation. The unit is also present in the Quaternary depression in the north of the site. Internally this unit is variable. Its seismic character is often acoustically (semi-)transparent to chaotic. However, where Unit C increases in thicknesses it can also show stratification, with low-amplitude parallel reflectors oriented in various directions. The base of Unit C has an irregular and erosional character. Table 7-4 provides the typical soil types for Unit C based borehole samples.

7.7.4   Unit D – Late Weichselian – Late glacial glaciomarine

Unit D consists of glaciomarine sediments and has been subdivided in Subunits D1 and D2.

Subunit D1 constitute a relatively small part in the top of Unit D and is limited downwards by horizon H11. D1 is restricted to depressions of varying sizes and is expected to correlate with late glacial sequence stratigraphic unit "LG II" described by GEUS (Ref. /5/). D1 is interpreted mainly to represent a transgressive system tract of the late glacial glaciomarine sea of Kattegat.

Thickness of D1 ranges from few metres to more than 20 m in the largest depressions in the northern part of the OWF site. The infill of these depressions is characterized by high-amplitude parallel reflectors, which contrasts to the underlying D1 which is showing low to medium-amplitude reflectors. Table 7-4 provides the typical soil types for Subunit D1 based borehole samples.
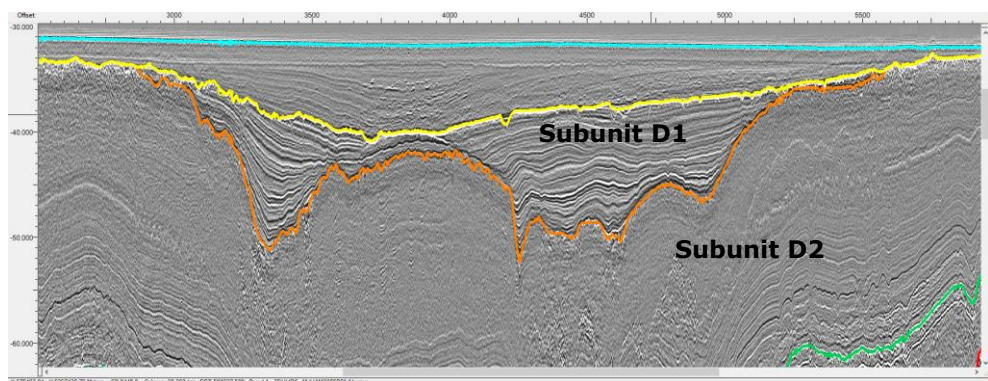
Figure 7.7-5 Subunit D1 between the yellow and the orange horizons. Here seen on top of the Quaternary depression in the north (2D-UHRS line HAM2306P01).

Subunit D2 constitute the main part of Unit D and is present in most of the site except for an area in the south where the underlying Unit E reaches the base of the Holocene. D2 is expected to correlate with late glacial sequence stratigraphic unit "LG I" described by GEUS (Ref. /5/). D2 is interpreted to represent a highstand system tract of the late glacial glaciomarine sea of Kattegat.

The unit has a typical thickness of 10 to 30 m and reaches a maximum thickness of more than 50 m in the area of the large Quaternary depression. It thins to less than 10 m in the south and becomes absent, where the underlying Unit E substantially increases in thickness. The internal seismic character of Subunit D2 is quite variable and varies mostly between low to medium-amplitude parallel reflectors or low amplitude chaotic or transparent reflectors. These changes in seismic character in D2 are marked by the internal horizons (H12 and H15). The differences to the reflection pattern are likely to reflect mass transport which is expected to have affected extensive parts of the subunit (See section 7.6.7). Where the reflectors are chaotic and transparent the mass transport is interpreted to have had high impact. Where the reflectors are parallel but discontinuous and shifted vertically the mass transport is interpreted to have some impact and where the reflectors are parallel and continuous the layers are interpreted to be unaffected. High-amplitude positive anomalies are common within Subunit D2 and are interpreted to represent drop stones. These are considered to be associated with coarse deposits (see section 7.6.4). Table 7-4 provides the typical soil types for Unit D2 based borehole samples.
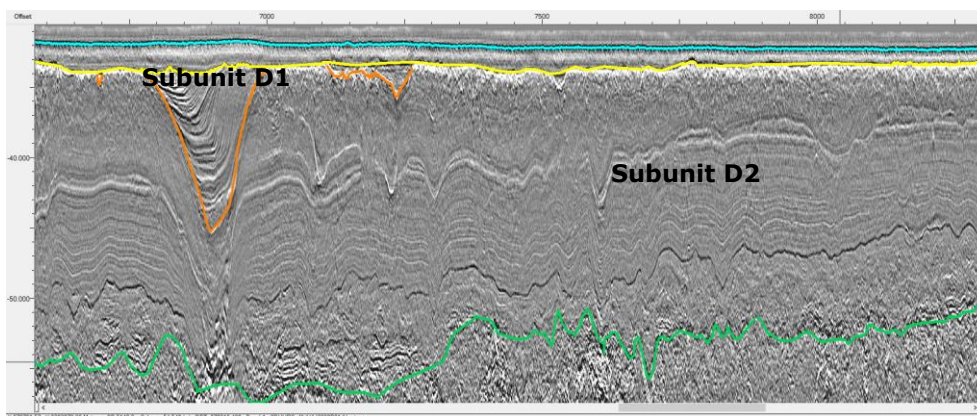
Figure 7.7-6   Subunit D2 between the orange/yellow and the green horizons. Reflection pattern varies between parallel reflectors and chaotic signature in different parts of the subunit (2D-UHRS line HAJ2238P01).

7.7.5   Unit E – Late Weichselian – Glacial/late glacial glaciomarine

Unit E is interpreted to be deposited in a glaciomarine environment similar that described for Subunit D2. What is interpreted to make Unit E different from Subunit D2 is that part of Unit E has been glacially overridden. Since the glacial advance which has overridden part of Unit E has reached its maximum within the investigated area, it is interpreted to be a Late Weichselian readvance. The readvance is interpreted to have taken place after the glacier has retreated from its maximum at the Main Stationary Line in Mid Jutland and opened Kattegat to marine conditions. From the mark that the glacier has imprinted in top of Unit E it's clear that the glacier has advanced from eastern direction.

Unit E may correlate with late glacial sequence stratigraphic "LG I" described by GEUS (Ref. /5/), the same as Subunit D2. However, in the glacier impacted areas glaciotectonics has changed and reworked part of the initial glaciomarine sediment. The glacier overridden area show great differences to the actual impact the unit has experienced. Therefore, Unit E has been subdivided into Subunits E1 and E2, where E2 is a basal layer displaying distinct reworking and incorporation of the layers below Unit E. However, E1 is also present in the glacier overridden area (see enclosure 1.06). The impact has been divided in two categories: Glacial impact and High glacial impact. E1 is dominating within the area of Glacial impact and E2 is dominating within the area of High glacial impact.

Subunit E1 constitute the biggest and most extensive part of Unit E and includes the part outside of the glacially overridden area and part of Unit E inside the glacially overridden area. Since the effect of the glacial overriding is seen as a gradual change there is no sharp boundary between these two parts of Subunit E1. E1 is present across a large part of the OWF site and shows a typical thickness of 10 m to 20 m. It reaches a maximum thickness of approximately 60 m within the deep Quaternary depression and approximately 40 m in the south. The unit is thinnest (< 10 m) along the western and eastern edge of the site. The internal seismic character of Subunit E1 is semi-transparent to chaotic. In the south-western part of the site, the top of the unit (Horizon H20) is fading out and it becomes difficult to properly differentiate this unit from the overlying Unit D. Table 7-4 provides the typical soil types for Unit E1 based borehole samples.
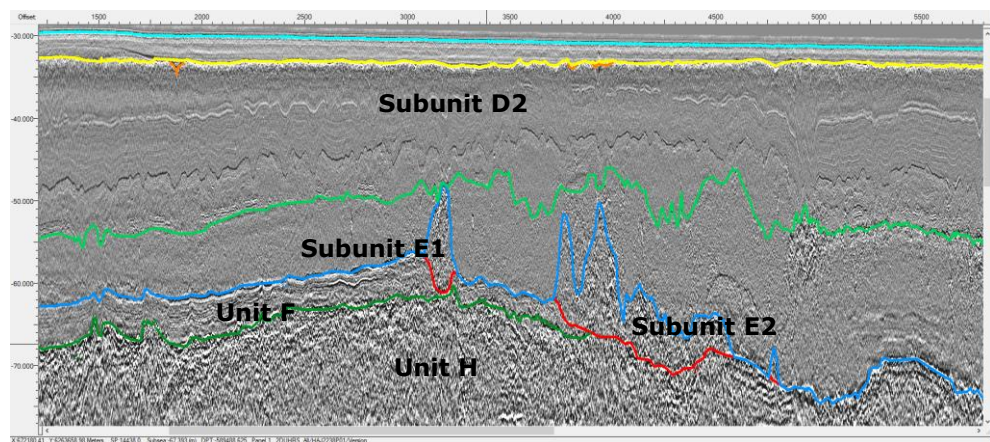
Figure 7.7-7   Subunit E1 between the light green and the blue horizons. Semi-transparent to chaotic seismic signature is common. The unit is glacially overridden in the right side of the image (2D-UHRS line HAJ2238P01).

The deposits of Subunit E1 outside of the glacier impacted area generally also appear disturbed and not layered as would be normal to marine fine-grained deposits. Only small undisturbed patches of layering can be identified furthest to west. This disturbance is interpreted to be related to mass transport processes like what has been identified for Subunit D2. But for Subunit E1 the process seems to have had a more intensive impact which may be explained by the proximity of the glacial readvance and the additional instability that might have applied to the area.

Subunit E2 is a basal layer of Unit E only located within the glacially overridden area (both within Glacial impact and High glacial impact) and represents a part which is highly impacted by mixing with underlying Units F and H. Within the glacially overridden area both E1 and E2 should be expected to be impacted by mixing both with the underlying Units F and H and with glaciofluvial sediments associated with the glacier advance. However, the impact of mixing especially with the of the underlying layers should be expected to be highest in E2. E2 has a patchy distribution in the central and eastern part of the OWF site. The subunit is characterized by chaotic high amplitude or laterally limited steeply sloping reflectors. The sloping reflectors reflect glaciotectonic thrust planes along which deep material has been mixed into the interior of both E2 and E1. Table 7-4 provides the typical soil types for Unit E2 based borehole samples.
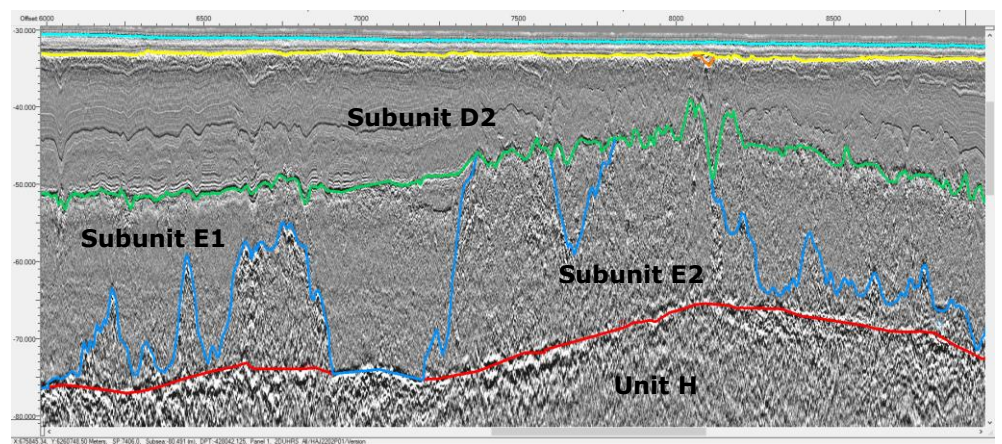
Figure 7.7-8   *Subunit E2 between the blue and the red horizons. High amplitude chaotic seismic signature with steeply sloping reflectors is common (2D-UHRS line HAJ2202P01).*

7.7.6 Unit F – Late Weichselian – Glacial/late glacial glaciomarine

Unit F is a relatively thin glaciomarine layer which has been deposited shortly after the Weichselian glacier has retreated from the Main Stationary Line and opened Kattegat to glaciomarine conditions. Unit F has been exposed to glacial deformation in part of area by the readvance that overrode Unit E in part of the site Late Weichselian. In the glacial overridden part Unit F has largely disappeared by reworking into Unit E.

Unit F is present locally, in the north and in the western part of the site. The unit is typically less than 10 m thick, but locally reaches thicknesses up to 39 m locally in the north eastern part of the site. The internal seismic character of Unit F shows closely spaced medium to high amplitude parallel reflectors. Unit F is overlain by Unit E in the centre and southern part of the site and by Unit D in the north. Unit F is interpreted as glaciomarine deposits due to its parallel seismic reflectors and similarity to the bedded facies of the overlying Unit D. Unit F is almost only present in the part of the area, which has not experienced glacial overriding in late Weichselian. In this area Unit F gently buries the marginal moraines in the surface of Unit H (see section 7.7.8). This indicates

that the glaciomarine sea in which Unit F was deposited stood direct in contact to the retreating glacier, so that no periglacial, fluvial or beach environments came between Unit H and Unit F to erode or change shape of the surface. Inside the glacially overridden area glaciotectonic processes seem to have squeezed and reworked Unit F into the overlying unit E. Unit F generally seem to be more susceptible to glacial deformation than the overlying Unit E. Table 7-4 provides the typical soil types for Unit F based on borehole samples.
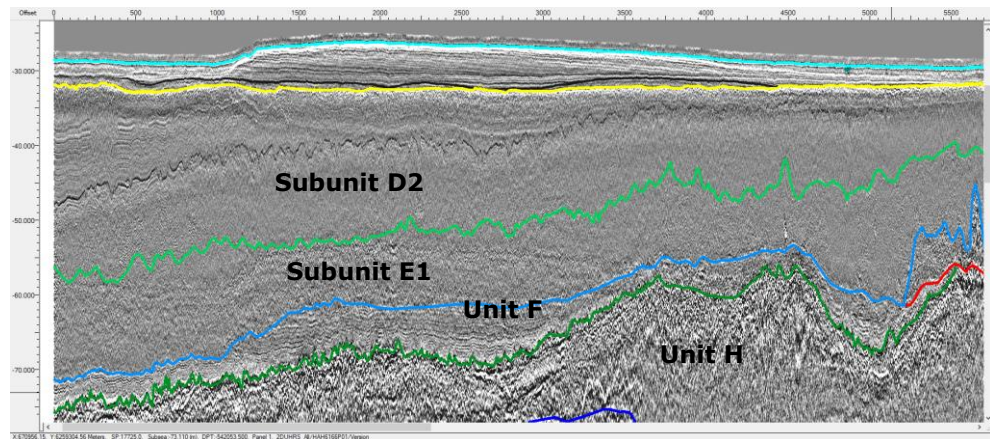
Figure 7.7-9   *Unit F between the red/blue and the dark green horizons. Mostly well-defined parallel and higher amplitudes than in E1 above. Unit F is almost only present outside the glacially overridden area (2D-UHRS line HAH6166P01).*

7.7.7   Unit G – Weichselian – Glacial mixed deposits

Unit G is mainly present in the large Quaternary depression and locally in other parts in the site. The depression Unit G is located in is interpreted to be a tunnel valley which is filled by glacial deposits.

The unit reaches a maximum thickness of approximately 94 m in the deepest parts of the depression and shows a typical thickness of approximately 10 m in the shallower parts. The base of Unit G is an erosional surface cutting deeply into the underlying Unit H and Unit I. The seismic character of Unit G varies from acoustically semi-transparent with occasional inclined discontinuous internal reflectors where Unit G is thick, to more chaotic where Unit G is thin.
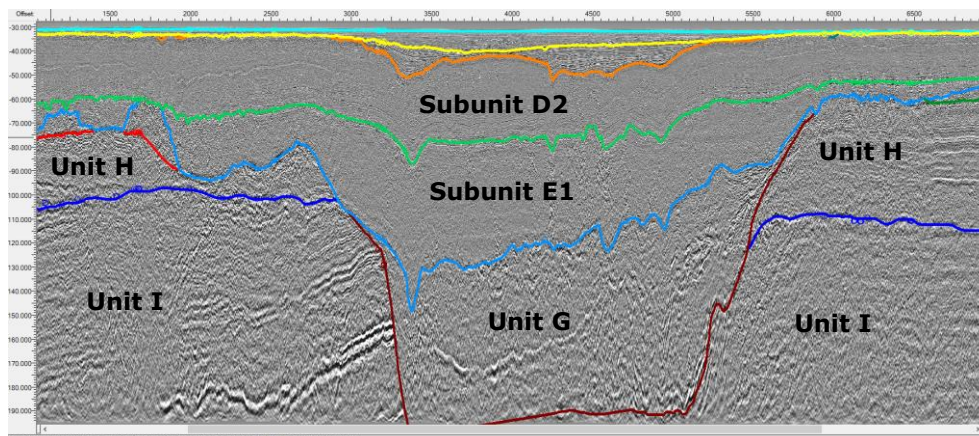
Figure 7.7-10   Unit G between the red and the brown horizons. Semi-transparent to chaotic seismic signature. Unit G is mostly restricted to a deep depression in the northern part of the site (2D-UHRS line HAM2306P01).

Unit G is interpreted as a complex Weichselian layer which has been overridden by glaciers. Based on extend and the morphological features of the base Unit G it is interpreted to be a buried tunnel valley carved out mainly by subglacial meltwater erosion. Unit G is expected to consist of sediments related to a glacial environment – probably till together with glaciofluvial and/or glaciolacustrine sediments. The chaotic appearance of Unit G, which may partly be induced by the glacial overriding, makes it difficult to see which type of sediment it was prior to glacial overriding. The location of a deep Quaternary tunnel valley on top of a fault zone is not interpreted to be coincidence. Tunnel valleys are often developed in weak zones in pre-Quaternary surface or in pre-existing depressions (Ref. /9/). Since there are no samples from the layers constituting Unit G (boreholes or CPTs) there are no confirmation of the nature of this layer. Unit G may very well be related to the same glacial advance as the top of Unit H was formed by (see 0).

7.7.8 Unit H - Pleistocene – Glacial mixed deposits

Unit H is interpreted to be glacial layer which may include deposited from many different glaciations. The latest event to have contributed to Unit H is the Weichselian glaciation and its retreat from the Main Stationary Line in central Jutland.

Unit H is present in the entire site, except where Unit G cuts through it and further into the pre-Quaternary layers and form the large depression in the north. Unit H shows typical thicknesses of 25 m to 35 m south of the depression and reaches a thickness beyond 80 m north of the depression. The internal seismic character of Unit H is very variable from medium-amplitude parallel reflectors, dominantly observed south of the large Quaternary depression to acoustically transparent and chaotic with short internal reflectors, observed north of the depression. The base of Unit H is a low to medium positive amplitude reflector and marks an angular unconformity, where the underlying bedrock (Unit I) is clearly folded. This is most prominently visible south of the depression. North of the depression, Horizon H50 is often obscured by the first seafloor multiple. As a result, the depth at which Horizon H50 occurs is subject

to uncertainty. Table 7-4 provides the typical soil types for Unit H based borehole samples.
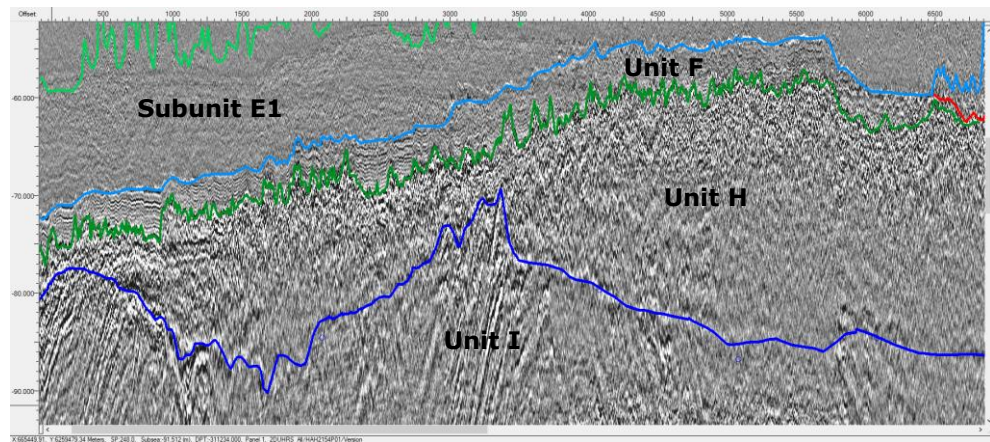
Figure 7.7-11   Unit H between the dark green and the dark blue horizons. Acoustically transparent and chaotic with short internal reflectors. De Geer moraines in the top where overlain by Unit F. In other areas the moraines have been eroded by the later glacial advance (2D-UHRS line HAH2154P01).

Unit H is interpreted as a Pleistocene layer and may include deposits from many events through Pleistocene. The sediments are expected to have been deposited in mainly glacial, periglacial and/or glaciomarine conditions. The main glacial advance of the Weichselian is expected to be responsible of depositing the upper part of Unit H and shaping the surface of it. The surface of Unit H below the undisturbed glaciomarine Unit F display numerous well preserved marginal moraines (De Geer moraines is expected to be the most precise term for this type of moraines) with the near-original shape which indicates that the deglaciation responsible for shaping and depositing the top of Unit H was succeeded by glaciomarine conditions leaving the moraines in near-original shape since they immediately were gently buried by glaciomarine sediments of Unit F. Where Unit F is eroded by a later glacial advance (see section 7.7.5) the De Geer moraines are also largely eroded.

7.7.9   Unit I – Pre-Quaternary – (Jurassic/Cretaceous siltstone/mudstone)

Unit I is present over the entire site. Within the deep Quaternary depression and locally north of this depression the top of Unit I was not observed as it lies below the penetration depth of the 2D-UHRS data. Unit I is interpreted as pre-Quaternary bedrock. The internal seismic character shows predominantly low to medium-amplitude, large wavelength parallel reflectors. Particularly north of the deep Quaternary depression, the seismic character of Unit I can be acoustically (semi-)transparent. Where Unit I shows parallel inclined (possibly folded) reflectors, the horizon marking the top of Unit I (Horizon H50) represents an angular unconformity with the overlying units. Due to the tectonic history of the general area, the presence of faults may be expected in Unit I. However, no faults were identified within Unit I in the 2D-UHRS data. The bedrock consists of Jurassic/Lower Cretaceous marine deposits. Samples from boreholes of this layer has been described as mudstone and siltstone (Ref. /1/). North of the deep

Pre-Quaternary depression the surface is not penetrated by any of the boreholes or CPTs. The depth of Unit I is 80-110 m below seabed here. GEUS indicate that the Pre-Quaternary surface may consist of Precambrian crystalline bedrock in this area (Ref. /5/). Since there are no boreholes to this depth here, we can't confirm this interpretation. GEUS describe the crystalline bedrock as without any true reflectors in the seismic section.
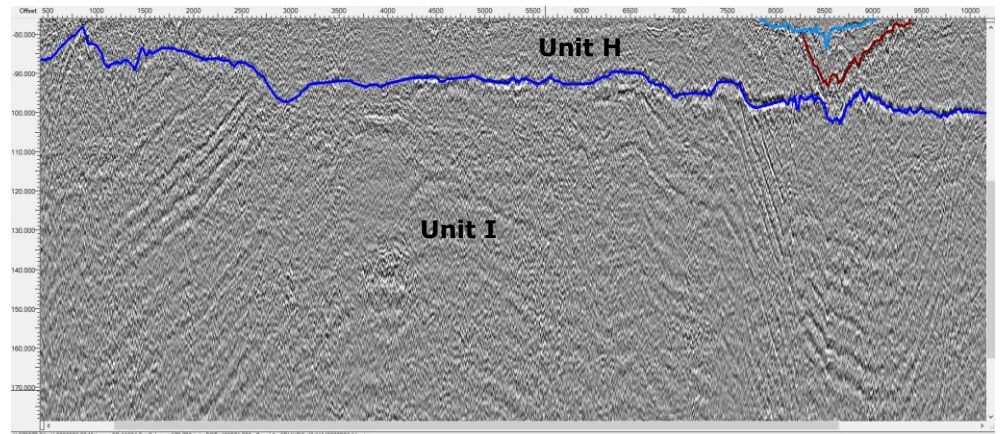
Figure 7.7-12   Unit I below the dark blue horizon. The seismic signature shows low to medium amplitudes in large wavelength parallel reflectors. The deep reflectors indicate a folding in deep reaching folds of the unit (2D-UHRS line HAJ2226P01).

At least 2-3 km north of the deep channel the Pre-Quaternary layer displays well-defined layering as seen in the southern part of the site and (see Figure 7.7-13) is expected to be similar layers as sampled in the boreholes (Ref. /1/). Further to the north the seismic show no layering and could potentially be something else, however, there is no clear boundary between these areas in the seismic, which would be expected if a high-density layer of crystalline type should be found in the north.
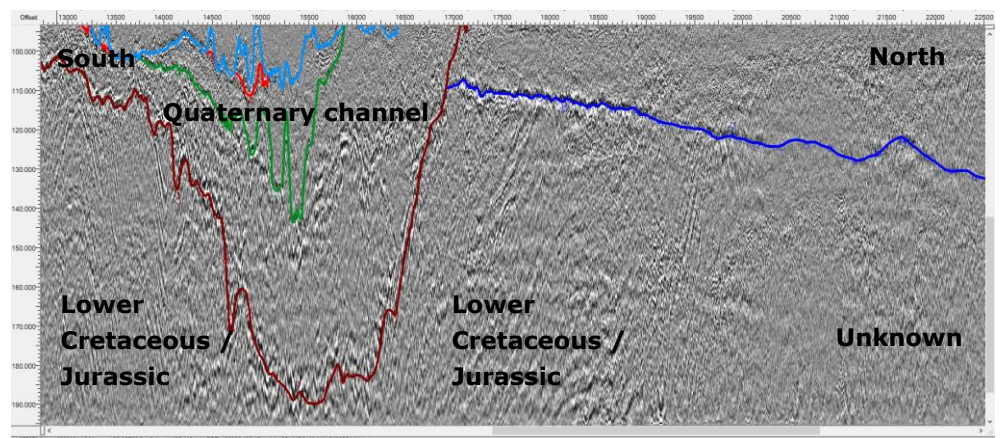
Figure 7.7-13   Unit I below the dark blue horizon in the northern part of the site. The seismic signature shows large wavelength parallel dipping reflectors towards the south and features signature towards the north (2D-UHRS line HAX2498P01).

8   Conceptual Geological Model

8.1   Presentation of Conceptual Geological Model

The Conceptual Geological Model is made as a hand-drawn geological profile that summarizes the geology across the entire Hesselø OWF area.

The purpose of the conceptual model is to provide:

> An overview of geological structures and overall layer thicknesses

> An understanding of the geology and the geological setting

The Conceptual Geological Model is shown in Figure 8.1-1. The model includes the layers in the Integrated Geological Model, c.f. Table 4-1 and is based on geological cross sections and layer thickness maps extracted from the 3D digital model.
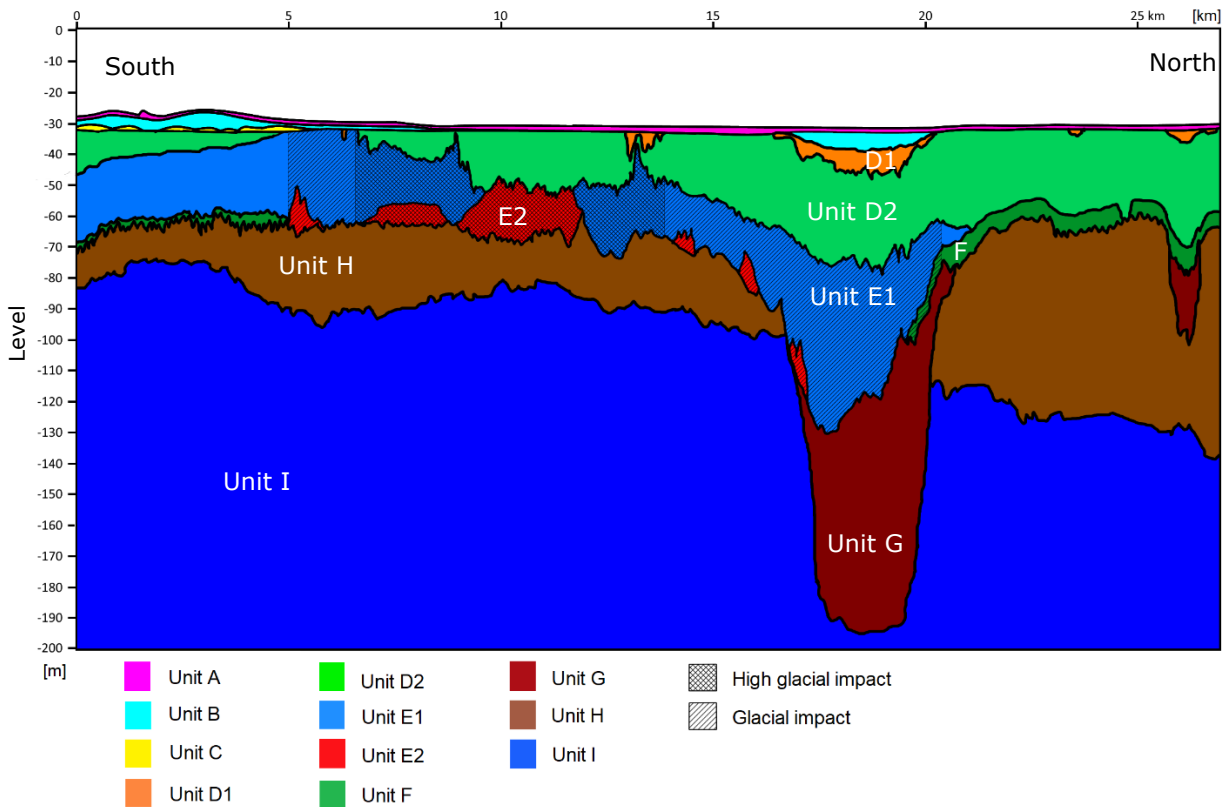
Figure 8.1-1   The Conceptual Geological Model of the Hesselø OWF.

The conceptual model shows the deep depression zone in the northern part of the site extending deep into the mudstone in Unit I. The deep depression zone has thick deposits of both Unit G and E1, but also the Subunits D2, D1 and Unit C are relatively thick in this area. Unit G is also seen in the more shallow channel structure furthest towards north.

All units above Unit H should be considered having relatively low strength. However, no geotechnical data is available from Unit G and the soil parameters

in this unit is thus unknown, see also section 7.7.7. Also, large variations in the soil strength parameters are seen in Subunits E1, E2 and Unit F, where these deposits have been glacially overridden (shaded/hatched in Figure 8.1-1), see also enclosure 1.06.

8.2 Soil Zonation and Soil Provinces

Based on the geotechnical data and the Integrated Geological Model a soil zonation has been made. The soil zonation provides the basis for clustering the main geological deposits and structures relevant for the foundation design.

The soil zonation is furthermore simplified into one single map dividing the entire site into four (4) different soil provinces. The simplification is made by selecting the most significant parameters in relation to foundation conditions.

The purpose of the Soil Provinces map is to provide a geological overview of the site with regards to foundation conditions. The map should ideally divide the site into a limited number of provinces with similar foundation conditions.

The workflow for the process is shown in Figure 8.2-1.

Figure 8.2-1   Workflow for dividing the area into geological soil provinces.

8.2.1 Map with Soil Zonation

The following parameters have been identified that could potentially have a significant impact on the foundation conditions within the Hesselø OWF site.

> Thickness of sediments with low strength

> Glaciated deposits (deposits glacially overridden)

> Deep channel structures

As the soil strength parameters of Unit G are unknown, two maps have been produced to show the cumulated thickness of sediments with low strength: One where Unit G is excluded (Enclosure 1.04) and one where Unit G is included as a soil with relatively low strength (Enclosure 1.05).

To include all the above parameters, the map of cumulated thickness of low-strength sediments (enclosure 1.05) has been combined with the areas of glaciated impact on Unit E-F (Enclosure 1.06). The result can be seen in Figure 8.2-2.

The map in Figure 8.2-2 outlines the deep depression zone that crosses the site in the area of the Børglum Fault (see Figure 6.1-1) as this depression zone has relatively thick deposits of the Units/Subunits C, D1, D2, E1 and G. This can also be seen from Enclosures 3.03-3.09. Also, areas where Units E-F have been glaciated are outlined on the map in hatched (high glacial impact) and oblique shading (glacial impact).
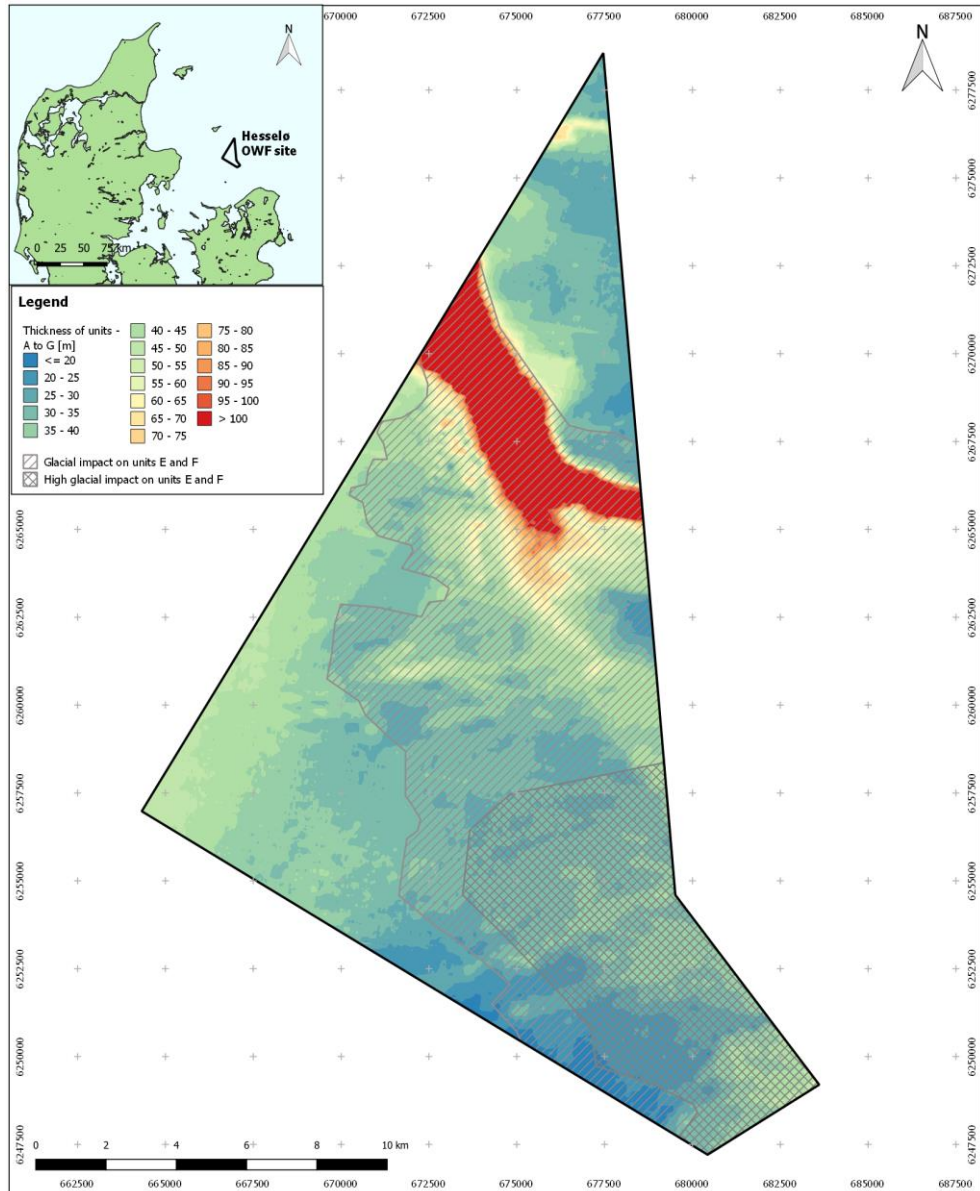
Figure 8.2-2   Map with Soil Zonations for Hesselø OWF.

8.2.2 Map of Soil Provinces

The map of the Soil Provinces is presented below in Figure 8.2-3 and on Enclosure 1.03. The map divides the site into four different provinces.

The division into four soil provinces is based on the most significant parameter in relation to foundation design which is evaluated to be the cumulated thickness of soil with low strength. It was also considered to include the areas of glaciated

deposits in Unit E-F, where higher strengths are seen. However, the data show large variations also with areas where low strength values dominate, and it is therefore uncertain whether these areas outline better foundation conditions.

The map of Soil Provinces shows that thick deposits (red color, more than 60 m) cover approx. 10% of the total site, whereas thin deposits (dark green, up to 20 m) cover only approx. 1%, see Table 8-1 for relative size of the four soil provinces.

The remaining 89% of the area has a cumulated thickness of low-strength sediments between 20 to 60 meters. The thickest deposits within this span are primarily seen in the south-western part of the site and in the area around the depression zone, but also the south-easternmost part show thicknesses between 35-60 m (yellow colour on the map).
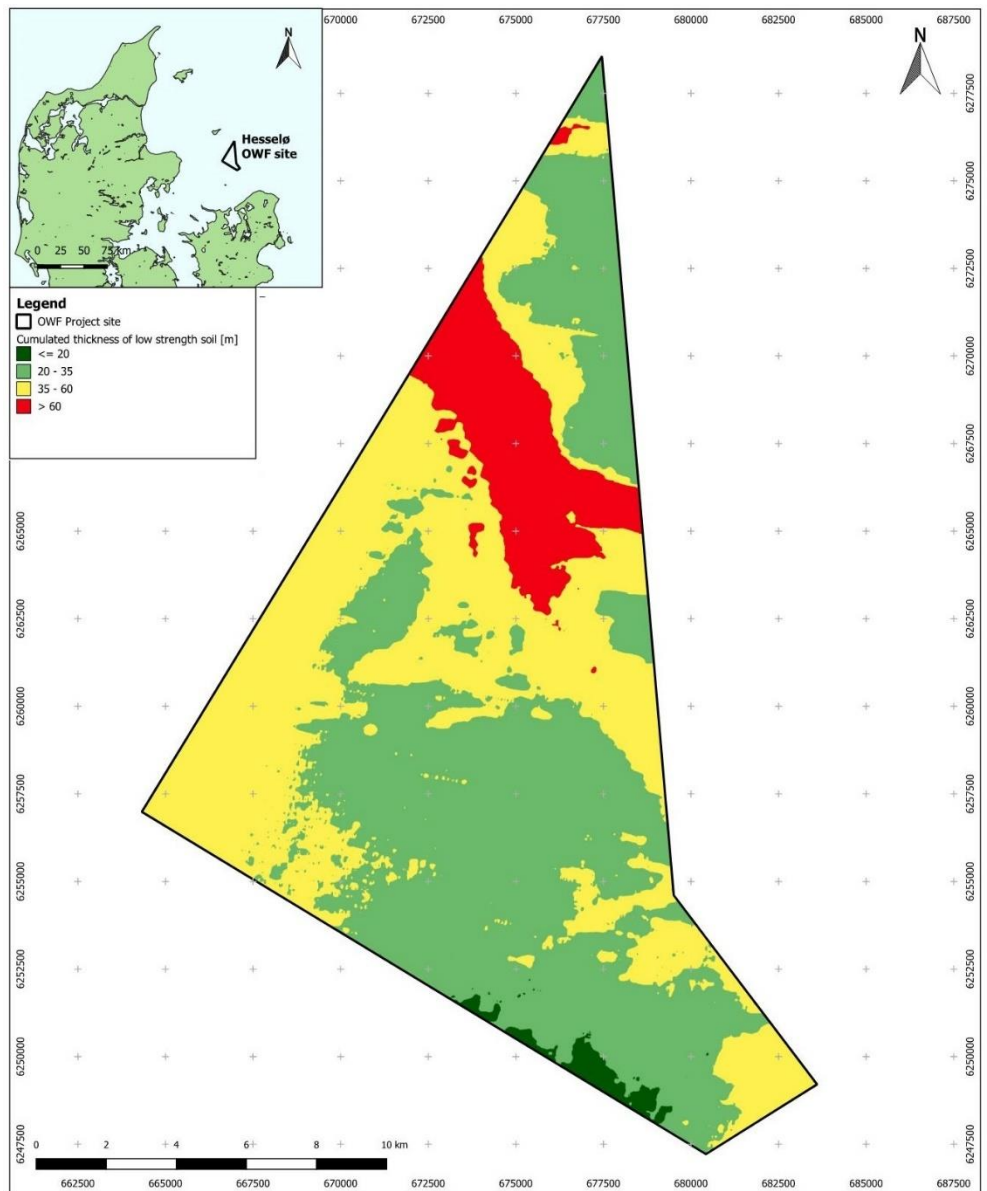
Figure 8.2-3   Soil Provinces map for Hesselø OWF, see also Enclosure 1.03.

Table 8-1   *Relative size of the four Soil Provinces in percentage of the total site area.*

Cumulated thickness of low-strength soil [m]	Area relative to site area [%]	Cumulated [%]
Up to 20	1	1
20 to 35	45	46
35 to 60	44	90
Above 60	10	100

9   List of deliverables

Below is a complete list of appendixes and enclosures delivered with this report.

All digital deliverables including the IHS Kingdom Suite project is provided on an external hard drive.

Appendixes	
Number	Title
Appendix A	Interpreted stratigraphy at CPT locations
Appendix B	CPT plots per geotechnical location including soil properties using CPT correlations
Appendix C	CPT plots per soil unit including properties from laboratory testing
Appendix D	Range of soil properties per soil unit
Appendix E	CPT measurements and soil properties in unit E – Effect of glaciation

Enclosures	
Number	Title
1.01	Overview map. Bathymetry
1.02	Overview of data
1.03	Soil Provinces
1.04	Thickness of low strength soils. Unit G excluded
1.05	Thickness of low strength soils. Unit G included
1.06	Glacial impact on units E and F
1.07	Overview of cross sections
2.01	Variation of ratio between undrained shear strength and depth in unit D1clay
2.02	Variation of ratio between undrained shear strength and depth in unit D2clay

Enclosures	
Number	Title
2.03	Variation of ratio between undrained shear strength and depth in unit E1clay
2.04	Variation of ratio between undrained shear strength and depth in unit E2clay
2.05	Variation of ratio between undrained shear strength and depth in unit Fclay
2.06	Variation of undrained shear strength in unit Hclay
2.07	Variation of small-strain shear modulus in unit D1clay
2.08	Variation of small-strain shear modulus in unit D2clay
2.09	Variation of small-strain shear modulus in unit E1clay
2.10	Variation of small-strain shear modulus in unit E2clay
2.11	Variation of small-strain shear modulus in unit Fclay
2.12	Variation of small-strain shear modulus in unit Hclay
3.01	Top of model layer Unit A. Depth below seabed
3.02	Top of model layer Unit B. Depth below seabed
3.03	Top of model layer Unit C. Depth below seabed
3.04	Top of model layer Unit D1. Depth below seabed
3.05	Top of model layer Unit D2. Depth below seabed
3.06	Top of model layer Unit E1. Depth below seabed
3.07	Top of model layer Unit E2. Depth below seabed
3.08	Top of model layer Unit F. Depth below seabed
3.09	Top of model layer Unit G. Depth below seabed
3.10	Top of model layer Unit H. Depth below seabed
3.11	Top of model layer Unit I. Depth below seabed

Enclosures	
Number	Title
4.01	Layer Unit A. Thickness
4.02	Layer Unit B. Thickness
4.03	Layer Unit C. Thickness
4.04	Layer Unit D1. Thickness
4.05	Layer Unit D2. Thickness
4.06	Layer Unit E1. Thickness
4.07	Layer Unit E2. Thickness
4.08	Layer Unit F. Thickness
4.09	Layer Unit G. Thickness
4.10	Layer Unit H. Thickness
5.01	Cross section HAX2491P01
5.02	Cross section HAX2496P01
5.03	Cross section HAX2498P01
5.04	Cross section HAX2499P01
5.05	Cross section HAX2503R01
5.06	Cross section HAE2038P01
5.07	Cross section HAF2090P01
5.08	Cross section HAF2094P01
5.09	Cross section HAG6138R01
5.10	Cross section HAJ6222P01
5.11	Cross section HAK6278P01
5.12	Cross section HAM2338P01

Enclosures

Enclosures	
Number	Title
5.13	Cross section HAN6362P01

Digital deliverables	
Item	Format
IHS Kingdom Suite Project including spatial geological model	Kingdom project
00.Basis	GIS files
01 Project area	Giles files
0.2 Bathymetry	Giles files
0.3 Soil provinces	GeoTIFF
0.4 Ground model: Top of model layers, elevation MSL (grids)	ASCII and GeoTIFF
0.4 Ground model: Top of model layers, depth below seabed (grids)	ASCII and GeoTIFF
0.4 Ground model: Model layers, isopach grids (vertical layer thickness)	ASCII and GeoTIFF
0.5 Cross section locations	ESRI Shapefile
0.6 Geotechnical parameters	ESRI Shapefile

10   Conclusions

A 3D integrated geological model has been made for the entire Hesselø OWF area. The new model comprises an updated and revised version of the existing geophysical model and is based on the newly gathered geotechnical data as well as the seismic data.

With respect to the purpose of the integrated geological model a new and better basis can now be provided for developers to evaluate the ground conditions in relation to foundation design and positioning of offshore wind turbines.

The integrated geological model has eleven (11) layers. Thus, the existing geophysical model has been revised with respect to both the number of layers as well as to the spatial distribution of the layers. The model comprises layers of Holocene, Pleistocene and Jurassic/Early Cretaceous deposits. These 11 layers have been further subdivided based on their geotechnical soil behaviour type. The soil properties of all soil units have been evaluated and the soil properties for the main soil units are visualized in the appendices and enclosures.

Together with the new model an updated geological description of the individual geological layers in the model is provided. The description includes stratigraphical, lithological and geotechnical characteristics.

The integrated geological model is delivered as a digital 3D model in a Kingdom suite project. Enclosures provided with the digital model present the layers with respect to depth below seabed, thickness and lateral extent. The enclosures also visualize cumulated thickness of Holocene layers, non-glaciated layers and glacial layers.

Thirteen (13) cross-sections distributed over the entire area show the layering in the model together with borehole information. The cross-sections follow the seismic survey lines and have been positioned so they comprise all boreholes.

A soil zonation has been made from the geological model with focus on the deposits and geological structures evaluated to have a potentially significant impact on the foundation design. This includes low strength layers, glaciated layers and deep channel structures. The soil zonation maps have been simplified into a single map showing four selected soil provinces which provides a geological overview of the entire site relevant for foundation conditions. The four different soil provinces are defined based on the cumulated thickness of soil with low strength.

11   References

Ref. /1/   Gardline 2021. Geotechnical Report, Preliminary Investigation, Hesselø
OWF. Volume II: Measured and Derived Geotechnical Parameters and
Final Results – Interim CPT Report. Project no. 11596. Client reference
20/07944, rev. 2, date 22.11.2021.

Ref. /2/   Robertson and Cabal, 2015: Guide to Cone Penetration Testing, 6th
Edition.

Ref. /3/   Fugro. Geophysical Results Report. Energinet Denmark Hesselø
Geophysical Survey | Denmark, Inner Danish Sea, Kattegat.
F172145-REP-GEOP-001 02 | 13 August 2021. Final

Ref. /4/   Lunne, T., Robertson, P. K., and Powell, J. J. M., 1997: Cone
Penetration Testing in Geotechnical Practice, 1st edition.

Ref. /5/   Jensen, J. B., Bennike, O., 2020; General geology of the southern
Kattegat, the Hesselø wind farm area, Desk Study. Report for
Energinet Eltransmission A/S. GEUS.

Ref. /6/   Jensen, J. B., Petersen, K. S., Konradi, P., Kuijpers, A., Bennike, O.,
Lemke, W. & Endler, R. 2002: Neotectonics, sea-level changes and
biological evolution in the Fennoscandian Border Zone of the southern
Kattegat Sea. Boreas, Vol. 31, pp. 133–150. Oslo.

Ref. /7/   Bendixen, C., Jensen, J.B. Boldreel, L. O., Claousen, O. R.,
Seidenkrantz, M.-S., Nyberg, J., Hübscher, C. 2015 - The Holocene
Great Belt connection to the southern Kattegat, Scandinavia: Ancylus
Lake drainage and Early Littorina Sea transgression. Boreas
10.1111/bor.12154.

Ref. /8/   Bendixen, C., Boldreel, L. O., Jensen, J. B., Bennike, O., Hübscher, C.,
Clausen, O. R. 2017: Early Holocene estuary development of the
Hesselø Bay area, southern Kattegat, Denmark and its implication for
Ancylus Lake drainage. Geo Mar Lett.

Ref. /9/   Lykke-Andersen, H, Seidenkrantz, M.-S. & Knudsen, K. L. 1993.
Quaternary sequences and their relations to the pre-Quaternary in the
vicinity of Anholt, Kattegat, Scandinavia. Boreas, bind 22, nr. 4, s.
291-298

Ref. /10/ Rambøll 2021. Geotechnical Data Report. Hesselø OWF Supplementary
VC – Gilleleje.

Ref. /11/ Fugro 2021. 3D-UHR Survey results Report WPD FINAL

Ref. /12/ Jensen, P., Aagaard, I., Burke, R. A., Dando, P. R., Jørgensen, N. O.,
Kuijpers, A., Laier, T., O'Hara, S. C. M., Schmaljohann, R. 1992.
'Bubbling reefs' in the Kattegat: submarine landcapes of carbonate-
cemented rocks support a diverse ecosystem at methane seeps. Marine
Ecology Progress Series Vol. 83 pp. 103-112-

Appendix A   Interpreted stratigraphy at CPT locations

Location	Layer	Top level	Bottom level	Unit	φ' - Avg	c_u - Avg	G_{max} - Avg
[-]	[No.]	[mBSB]	[mBSB]	[-]	[°]	[kPa]	[MPa]
CB3a	1	0	2.9	A	-	4.5	3.1
CB3a	2	2.9	12.4	B	-	107.5	46.7
CB3a	3	12.4	14	C	35.2	-	56.3
CB3a	4	14	25.9	D1clay	-	44.5	33.8
CB3a	5	25.9	58.5	D2clay	-	91.4	73.3
CB3a	6	58.5	59.2	E1clay	-	-	-
CB3a-BH	1	0	2.9	A	-	-	-
CB3a-BH	2	2.9	12.4	B	-	-	-
CB3a-BH	3	12.4	14	C	-	-	-
CB3a-BH	4	14	25.9	D1clay	-	-	-
CB3a-BH	5	25.9	58.5	D2clay	-	-	-
CB3a-BH	6	58.5	68.9	E1clay	-	92.3	83.2
CB4	1	0	1.3	A	-	6.3	3.8
CB4	2	1.3	1.9	B	-	43.7	21.0
CB4	3	1.9	2.5	C	38.8	-	21.1
CB4	4	2.5	24.8	D2clay	-	35.3	28.1
CB4	5	24.8	30.2	Fclay	-	62.7	41.3
CB4	6	30.2	32.6	Hclaysoft	-	47.4	37.4
CB4	7	32.6	35.9	Hclay	-	107.7	75.3
CB4-BH	1	0	1.3	A	-	-	-
CB4-BH	2	1.3	1.9	B	-	-	-
CB4-BH	3	1.9	2.5	C	-	-	-
CB4-BH	4	2.5	24.8	D2clay	-	-	-
CB4-BH	5	24.8	30.2	Fclay	-	-	-
CB4-BH	6	30.2	32.6	Hclaysoft	-	48.0	41.7
CB4-BH	7	32.6	37.5	Hclay	-	127.4	107.7
CB4-BH	8	37.5	43.2	Hsand	34.3	-	117.6
CB4-BH	9	43.2	69.7	Hclay	-	314.7	172.8
CB5	1	0	1	A	-	10.9	8.7
CB5	2	1	2.7	B	-	11.1	9.2
CB5	3	2.7	5.5	C	43.1	-	42.2
CB5a	1	0	1	A	-	9.1	6.7
CB5a	2	1	2.7	B	-	9.1	8.0
CB5a	3	2.7	5.9	C	41.6	-	39.3
CB5a	4	5.9	11.4	D2clay	-	47.0	46.4
CB5a	5	11.4	30.1	E1clay	-	69.8	57.6
CB5a	6	30.1	34.3	Fclay	-	102.9	70.7
CB5a	7	34.3	37	Hclaysoft	-	122.8	75.2
CB5a	8	37	37.3	Hsand	39.9	-	152.3
CB5-BH	1	0	1	A	-	-	-
CB5-BH	2	1	2.7	B	-	-	-
CB5-BH	3	2.7	5.9	C	-	-	-
CB5-BH	4	5.9	11.4	D2clay	-	-	-
CB5-BH	5	11.4	30.1	E1clay	-	-	-
CB5-BH	6	30.1	34.3	Fclay	-	-	-
CB5-BH	7	34.3	37	Hclaysoft	-	-	-
CB5-BH	8	37	39.3	Hsand	-	-	-
CB5-BH	9	39.3	55.9	Hmix	34.4	460.0	192.2
CB5-BH	10	55.9	63.9	Hsand	36.0	-	171.4
CB6	1	0	0.8	A	-	11.1	5.1
CB6	2	0.8	4.8	B	-	11.3	9.0
CB6	3	4.8	6.2	C	41.1	-	46.5
CB6	4	6.2	6.3	D2clay	-	-	-
CB6a	1	0	0.8	A	-	11.0	4.9
CB6a	2	0.8	4.8	B	-	11.4	9.5
CB6a	3	4.8	6.2	C	36.5	-	35.7
CB6a	4	6.2	18.3	D2clay	-	37.6	35.3
CB6a	5	18.3	34.3	E1clay	-	62.5	51.4
CB6a	6	34.3	36.3	Fclay	-	88.0	60.2

Location	Layer	Top level	Bottom level	Unit	φ' - Avg	c_u - Avg	G_{max} - Avg
[-]	[No.]	[mBSB]	[mBSB]	[-]	[°]	[kPa]	[MPa]
CB6-BH	1	0	0.8	A	-	-	-
CB6-BH	2	0.8	4.8	B	-	-	-
CB6-BH	3	4.8	6.2	C	-	-	-
CB6-BH	4	6.2	18.3	D2clay	-	-	-
CB6-BH	5	18.3	34.3	E1clay	-	-	-
CB6-BH	6	34.3	39.7	Fclay	-	84.0	63.0
CB6-BH	7	39.7	48.7	Hmix	35.1	465.2	250.8
CB6-BH	8	48.7	54.9	Hsand	38.4	-	174.3
CB6-BH	9	54.9	55.2	I	36.7	1082.9	241.0
CB7	1	0	1.9	A	-	6.2	5.4
CB7	2	1.9	2.4	C	30.4	-	12.4
CB7	3	2.4	20.2	D2clay	-	37.9	35.9
CB7	4	20.2	20.9	E1clay	-	58.7	64.8
CB7a	1	0	1.9	A	-	6.4	5.7
CB7a	2	1.9	2.4	C	32.1	-	14.4
CB7a	3	2.4	20.2	D2clay	-	37.6	36.4
CB7a	4	20.2	27.5	E1clay	-	64.3	72.8
CB7a	5	27.5	31	E2clay	-	54.0	99.2
CB7a	6	31	31.3	E2mix	35.2	701.9	150.6
CB7-BH	1	0	1.9	A	-	-	-
CB7-BH	2	1.9	2.4	C	-	-	-
CB7-BH	3	2.4	20.2	D2clay	-	-	
CB7-BH	4	20.2	27.5	E1clay	-	-	-
CB7-BH	5	27.5	31	E2clay	-	-	-
CB7-BH	6	31	36.3	E2mix	30.1	121.0	97.3
CB7-BH	7	36.3	45.1	Hclaysoft	-	113.6	89.2
CB7-BH	8	45.1	63.4	Hclay	-	366.1	213.3
CB7-BH	9	63.4	64.2	I	39.9	2370.4	338.7
CB8	1	0	1.2	A	-	4.2	2.8
CB8	2	1.2	20.5	E1sand	40.0	-	65.1
CB8	3	20.5	24.4	E2clay	-	355.9	166.6
CB8	4	24.4	24.6	Hsand	40.1	-	116.0
CB8-BH	1	0	1.2	A	-	-	-
CB8-BH	2	1.2	20.5	E1sand	40.0	-	84.4
CB8-BH	3	20.5	24.4	E2clay	-	-	-
CB8-BH	4	24.4	29.8	Hsand	40.0	-	123.8
CB8-BH	5	29.8	53.2	Hclay	-	326.8	198.1
CB8-BH	6	53.2	59.5	Hsand	37.4	-	170.9
CB8-BH	7	59.5	65.5	Hclay	-	395.6	175.2
CB8-BH	8	65.5	68.6	I	37.3	1580.4	166.5
CB9	1	0	1	A	-	5.9	3.5
CB9	2	1	2	D1clay	-	11.1	10.0
CB9	3	2	31.4	D2clay	-	39.7	32.5
CB9	4	31.4	38.2	Fclay	-	75.2	49.0
CB9	5	38.2	40.3	Hsand	35.4	-	118.8
CB9	6	40.3	41.9	Hclaysoft	-	105.8	65.8
CB9-BH	1	0	1	A	-	-	-
CB9-BH	2	1	2	D1clay	-	-	-
CB9-BH	3	2	31.4	D2clay	-	-	-
CB9-BH	4	31.4	38.2	Fclay	-	-	-
CB9-BH	5	38.2	40.3	Hsand	27.4	-	72.4
CB9-BH	6	40.3	56.3	Hclaysoft	-	84.6	62.8
CB9-BH	7	56.3	59.5	Hsand	38.9	-	190.7
CB9-BH	8	59.5	70.9	Hclay	-	454.5	206.3
CB10	1	0	1.8	A	-	12.4	16.4
CB10	2	1.8	24.1	D2clay	-	35.5	36.6
CB10	3	24.1	28.7	E1clay	-	84.6	61.3
CB10	4	28.7	29	E2clay	-	151.4	86.2
CB10a-BH	1	0	1.8	A	-	-	-

Location	Layer	Top level	Bottom level	Unit	φ' - Avg	c_u - Avg	G_{max} - Avg
[-]	[No.]	[mBSB]	[mBSB]	[-]	[°]	[kPa]	[MPa]
CB10a-BH	2	1.8	24.1	D2clay	-	-	-
CB10a-BH	3	24.1	28.7	E1clay	-	-	-
CB10a-BH	4	28.7	30.8	E2clay	-	-	-
CB10a-BH	5	30.8	37.3	Hsand	40.4	-	145.0
CB10a-BH	6	37.3	69.5	Hclay	-	374.1	185.3
CB11	1	0	1	A	-	4.6	2.4
CB11	2	1	1.3	D1clay	-	20.2	16.0
CB11	3	1.3	2.1	D1sand	40.2	-	19.6
CB11	4	2.1	22.3	D2clay	-	32.7	30.8
CB11a-BH	1	0	1	A	-	-	-
CB11a-BH	2	1	1.3	D1clay	-	-	-
CB11a-BH	3	1.3	2.1	D1sand	-	-	-
CB11a-BH	4	2.1	25	D2clay	-	-	-
CB11a-BH	5	25	35.3	E2clay	-	-	-
CB11a-BH	6	35.3	36.6	Hsand	-	-	-
CB11a-BH	7	36.6	52	Hclay	-	-	-
CB11a-BH	8	52	55.6	I	36.4	1176.5	230.8
CB11-BH	1	0	1	A	-	-	-
CB11-BH	2	1	1.3	D1clay	-	-	-
CB11-BH	3	1.3	2.1	D1sand	-	-	-
CB11-BH	4	2.1	25	D2clay	-	48.4	41.9
CB11-BH	5	25	35.3	E2clay	-	115.1	88.6
CB11-BH	6	35.3	36.6	Hsand	36.0	-	118.1
CB11-BH	7	36.6	52	Hclay	-	370.1	187.7
CB11-BH	8	52	53.1	I	36.3	937.5	271.4
CB12	1	0	1.7	A	-	8.1	7.9
CB12	2	1.7	23.9	D2clay	-	35.6	25.5
CB12	3	23.9	31.8	Fclay	-	63.9	43.1
CB12	4	31.8	35.1	Hclaysoft	-	89.5	66.8
CB12-BH	1	0	1.7	A	-	-	-
CB12-BH	2	1.7	23.9	D2clay	-	-	-
CB12-BH	3	23.9	31.8	Fclay	-	-	-
CB12-BH	4	31.8	38	Hclaysoft	-	-	-
CB12-BH	5	38	43.3	Hsand	39.3	-	158.7
CB12-BH	6	43.3	70.7	Hclay	-	322.0	156.6
CB13	1	0	1.8	A	-	7.1	4.2
CB13	2	1.8	3.6	B	-	13.5	7.6
CB13	3	3.6	4.7	C	36.4	-	27.6
CB13	4	4.7	19.9	D2clay	-	37.6	28.8
CB13	5	19.9	31	E1clay	-	66.2	41.7
CB13	6	31	33.8	Fclay	-	83.4	40.8
CB13	7	33.8	34.1	Hsand	33.8	-	99.6
CB13-BH	1	0	1.8	A	-	-	-
CB13-BH	2	1.8	3.6	B	-	-	-
CB13-BH	3	3.6	4.7	C	-	-	-
CB13-BH	4	4.7	19.9	D2clay	-	-	-
CB13-BH	5	19.9	31	E1clay	-	-	-
CB13-BH	6	31	33.8	Fclay	-	-	-
CB13-BH	7	33.8	39.4	Hsand	38.8	-	141.7
CB13-BH	8	39.4	57.9	Hclay	-	349.0	165.2
CB13-BH	9	57.9	64.3	Hsand	35.7	-	161.8
CB14	1	0	0.9	A	-	4.4	1.9
CB14	2	0.9	1.5	D1clay	-	8.3	7.0
CB14	3	1.5	4.8	D2mix	33.0	110.2	43.1
CB14	4	4.8	19.1	D2clay	-	42.1	37.1
CB14	5	19.1	21	E2mix	30.8	172.7	68.1
CB14	6	21	22.8	E2clay	-	159.3	94.2
CB14-BH	1	0	0.9	A	-	-	-
CB14-BH	2	0.9	1.5	D1clay	-	-	-

Location	Layer	Top level	Bottom level	Unit	φ' - Avg	c_u - Avg	G_{max} - Avg
[-]	[No.]	[mBSB]	[mBSB]	[-]	[°]	[kPa]	[MPa]
CB14-BH	3	1.5	4.8	D2mix	-	-	-
CB14-BH	4	4.8	19.1	D2clay	-	-	-
CB14-BH	5	19.1	21	E2mix	38.3	951.2	180.0
CB14-BH	6	21	29	E2clay	-	135.7	89.4
CB14-BH	7	29	30.8	E2sand	35.9	-	101.2
CB14-BH	8	30.8	37.6	E2clay	-	203.9	114.6
CB14-BH	9	37.6	58.6	Hclay	-	354.7	198.7
CB14-BH	10	58.6	62.2	Hsand	38.2	-	191.4
CPT3	1	0	1.1	A	-	4.8	3.1
CPT3	2	1.1	1.6	B	-	6.5	5.7
CPT3	3	1.6	7.7	E1clay	-	69.4	51.6
CPT3a	1	0	1.1	A	-	4.4	2.7
CPT3a	2	1.1	1.6	B	-	12.9	9.7
CPT3a	3	1.6	3.8	E1clay	-	160.8	117.2
CPT3b	1	0	1.1	A	-	5.1	4.0
CPT3b	2	1.1	1.6	B	-	8.5	6.1
CPT3b	3	1.6	2.1	E1clay	-	-	-
CPT4	1	0	0.9	A	-	4.4	2.5
CPT4	2	0.9	7.1	D1sand	38.9	-	30.1
CPT4	3	7.1	9.4	D1clay	-	46.4	39.3
CPT4	4	9.4	23.7	D2clay	-	52.1	48.3
CPT4	5	23.7	24.6	D2mix	31.3	157.7	43.5
CPT4	6	24.6	27	D2clay	-	75.7	51.4
CPT4	7	27	30.7	E2clay	-	82.1	60.2
CPT4	8	30.7	32.4	Hclay	-	181.3	117.2
CPT6	1	0	0.8	A	-	16.8	7.8
CPT6	2	0.8	4.2	B	-	13.1	11.4
CPT6	3	4.2	5.7	C	44.0	-	51.6
CPT6	4	5.7	6.1	D2clay	-	-	-
CPT6a	1	0	0.8	A	-	22.9	10.1
CPT6a	2	0.8	4.2	B	-	16.6	12.6
CPT6a	3	4.2	5.7	C	41.7	-	43.0
CPT6a	4	5.7	24.2	D2clay	-	47.3	45.7
CPT6a	5	24.2	32.3	E1clay	-	72.3	62.5
CPT6a	6	32.3	34.6	Fclay	-	82.9	63.9
CPT6a	7	34.6	37	Hclaysoft	-	87.6	68.5
CPT7	1	0	1.5	A	-	6.6	4.8
CPT7	2	1.5	2.1	B	-	16.1	15.0
CPT7	3	2.1	3.5	C	39.5	-	25.7
CPT7	4	3.5	6.2	D2clay	-	40.4	41.5
CPT7	5	6.2	31.5	E1clay	-	62.7	50.4
CPT7	6	31.5	35	Hclaysoft	-	89.8	72.6
CPT7	7	35	36.3	Hclay	-	374.2	211.7
CPT7	8	36.3	36.7	Hsand	40.1	-	151.8
CPT8	1	0	1.2	A	-	4.4	2.7
CPT8	2	1.2	1.5	B	-	132.2	40.9
CPT8	3	1.5	8.9	D2clay	-	39.1	40.1
CPT8	4	8.9	17.2	E1clay	-	70.2	48.9
CPT8	5	17.2	17.7	E2sand	37.9	-	82.1
CPT8	6	17.7	20.4	E2clay	-	240.0	111.8
CPT8	7	20.4	20.8	E2sand	42.3	-	118.3
CPT9	1	0	1.2	A	-	4.1	2.1
CPT9	2	1.2	4.8	E1sand	41.4	-	31.8
CPT9	3	4.8	20.9	E1sand	43.0	-	90.9
CPT9	4	20.9	26	E2sand	41.0	-	117.0
CPT9	5	26	29.8	E2clay	-	254.0	142.3
CPT9	6	29.8	32.3	Hclaysoft	-	73.4	60.2
CPT9	7	32.3	32.6	Hmix	34.6	329.3	166.4
CPT10	1	0	0.9	A	-	26.9	10.5

Location	Layer	Top level	Bottom level	Unit	φ' - Avg	c_u - Avg	G_{max} - Avg
[-]	[No.]	[mBSB]	[mBSB]	[-]	[°]	[kPa]	[MPa]
CPT10	2	0.9	25.7	D2clay	-	37.9	32.6
CPT10	3	25.7	32.6	E1clay	-	100.4	58.9
CPT10	4	32.6	34.3	E2clay	-	220.2	141.0
CPT10	5	34.3	36.5	Hclay	-	254.4	156.6
CPT10	6	36.5	37.3	Hmix	35.2	404.2	205.2
CPT11	1	0	1.8	A	-	7.0	3.5
CPT11	2	1.8	2.6	B	-	17.7	9.8
CPT11	3	2.6	4.2	C	44.1	-	39.4
CPT11a	1	0	1.8	A	-	7.4	4.9
CPT11a	2	1.8	2.6	B	-	15.1	9.6
CPT11a	3	2.6	4.2	C	43.1	-	37.1
CPT11a	4	4.2	28.3	D2clay	-	45.6	38.3
CPT11a	5	28.3	40.3	E1clay	-	88.6	57.4
CPT11a	6	40.3	43.7	Fclay	-	110.0	55.9
CPT12	1	0	0.5	A	-	17.0	9.4
CPT12	2	0.5	5.1	B	-	13.3	12.0
CPT12	3	5.1	5.5	C	37.4	-	35.3
CPT12	4	5.5	21	D2clay	-	42.1	42.1
CPT12	5	21	33.4	E1clay	-	72.3	62.4
CPT12	6	33.4	38.3	Fclay	-	91.8	61.2
CPT12	7	38.3	39.1	Hclay	-	127.0	81.9
CPT12	8	39.1	39.4	Hsand	38.1	-	143.6
CPT13	1	0	1.7	A	-	7.1	4.3
CPT13	2	1.7	2.3	B	-	12.2	7.7
CPT13	3	2.3	3.1	C	40.9	-	27.5
CPT13	4	3.1	11.9	D2clay	-	43.7	38.1
CPT13	5	11.9	29	E1clay	-	57.2	44.5
CPT13	6	29	31.9	Fclay	-	80.3	53.0
CPT13	7	31.9	34.8	Hclaysoft	-	71.6	41.3
CPT13	8	34.8	35.9	Hclay	-	426.1	114.0
CPT14	1	0	1.4	A	-	5.1	3.4
CPT14	2	1.4	21.7	D2clay	-	35.3	31.2
CPT14	3	21.7	27.7	E1clay	-	83.2	53.8
CPT15	1	0	1.5	A	-	4.1	2.5
CPT15	2	1.5	3	B	-	9.0	5.7
CPT15	3	3	6	C	43.0	-	44.9
CPT15	4	6	29.2	D2clay	-	41.5	37.2
CPT15	5	29.2	40.2	E1clay	-	72.6	59.8
CPT15	6	40.2	46.9	Fclay	-	93.2	65.8
CPT15	7	46.9	48.6	Hclaysoft	-	79.9	57.1
CPT15	8	48.6	49.8	Hmix	36.4	651.3	313.3
CPT16	1	0	1.7	A	-	5.6	4.0
CPT16	2	1.7	3.3	B	-	13.3	8.6
CPT16	3	3.3	15.9	D2clay	-	30.1	30.5
CPT16	4	15.9	25.9	E1clay	-	57.3	47.9
CPT16	5	25.9	29.8	Fmix	29.3	92.6	50.5
CPT16a	1	0	1.7	A	-	8.1	4.4
CPT16a	2	1.7	3.3	B	-	21.6	16.4
CPT16a	3	3.3	15.9	D2clay	-	30.6	29.7
CPT16a	4	15.9	25.9	E1clay	-	55.9	50.0
CPT16a	5	25.9	30	Fmix	30.1	128.7	63.1
CPT16a	6	30	33.3	Fclay	-	69.2	51.3
CPT16a	7	33.3	33.4	Hsand	39.9	-	141.0
CPT18	1	0	0.8	A	-	19.3	10.5
CPT18	2	0.8	19.1	D2clay	-	29.9	24.9
CPT18	3	19.1	36.3	E1clay	-	79.7	53.1
CPT18	4	36.3	37.4	Fclay	-	203.9	97.7
CPT18	5	37.4	37.8	Hsand	36.5	-	125.9
CPT20	1	0	1.7	A	-	4.7	3.5

Location	Layer	Top level	Bottom level	Unit	φ' - Avg	c_u - Avg	G_{max} - Avg
[-]	[No.]	[mBSB]	[mBSB]	[-]	[°]	[kPa]	[MPa]
CPT20	2	1.7	2.3	B	-	72.5	40.8
CPT20	3	2.3	31	D2clay	-	34.3	34.6
CPT20	4	31	48.7	E1clay	-	90.7	55.1
CPT20	5	48.7	49.8	Hclay	-	206.7	154.4
CPT22	1	0	4	A	-	8.2	4.4
CPT22	2	4	8	B	-	43.1	15.8
CPT22	3	8	9	D1clay	-	72.5	30.1
CPT22	4	9	9.8	D2clay	-	41.8	22.4
CPT22	5	9.8	10.8	D2sand	32.7	-	40.9
CPT22	6	10.8	40.6	D2clay	-	60.1	41.3
CPT22	7	40.6	46.2	E1clay	-	94.2	49.9
CPT23	1	0	1.5	A	-	4.9	3.2
CPT23	2	1.5	29.3	D2clay	-	39.4	38.8
CPT23	3	29.3	34.6	E1clay	-	71.3	56.6
CPT23	4	34.6	41.3	Fclay	-	83.9	57.2
CPT25	1	0	2.4	A	-	7.1	8.5
CPT25	2	2.4	22.1	D2clay	-	32.4	31.6
CPT25	3	22.1	29.7	Fclay	-	61.5	45.2
CPT25	4	29.7	30.6	Hmix	29.4	72.2	53.2
CPT25a	1	0	2.4	A	-	9.9	9.2
CPT25a	2	2.4	22.1	D2clay	-	35.3	31.4
CPT25a	3	22.1	29.7	Fclay	-	61.6	44.2
CPT25a	4	29.7	30.4	Hmix	28.9	58.0	45.8
CPT25b	1	0	2.4	A	-	8.0	9.1
CPT25b	2	2.4	22.1	D2clay	-	32.0	33.5
CPT25b	3	22.1	29.7	Fclay	-	57.9	46.6
CPT25b	4	29.7	31.1	Hmix	31.5	149.3	103.8
CPT26	1	0	0.7	A	-	6.3	3.7
CPT26	2	0.7	1.6	D1clay	-	15.8	12.4
CPT26	3	1.6	28.1	D2clay	-	38.4	36.9
CPT26	4	28.1	35	Fclay	-	70.1	55.5
CPT26	5	35	36.5	Hclaysoft	-	70.6	56.1
CPT26	6	36.5	37.3	Hmix	33.2	260.0	139.3
OSS_1	1	0	1.7	A	-	5.2	3.1
OSS_1	2	1.7	2.1	B	-	11.3	7.3
OSS_1	3	2.1	29.5	D2clay	-	36.1	29.4
OSS_1	4	29.5	48	E1clay	-	87.5	48.0
OSS_1a	1	0	1.7	A	-	22.9	8.7
OSS_1a	2	1.7	2.1	B	-	28.7	12.3
OSS_1a	3	2.1	18.8	D2clay	-	47.7	32.4
OSS_2	1	0	1.3	A	-	4.8	3.6
OSS_2	2	1.3	1.9	B	-	9.6	9.8
OSS_2	3	1.9	2.7	C	40.4	-	24.1
OSS_2	4	2.7	11.5	D2clay	-	37.5	35.4
OSS_2	5	11.5	15.1	E1clay	-	134.6	74.1
OSS_2	6	15.1	15.8	E1sand	42.2	-	97.1
OSS1-BH	1	0	1.7	A	-	-	-
OSS1-BH	2	1.7	2.1	B	-	-	-
OSS1-BH	3	2.1	29.5	D2clay	-	-	-
OSS1-BH	4	29.5	47.5	E1clay	-	-	-
OSS1-BH	5	47.5	70.1	Hclay	-	334.0	206.9
OSS2-BH	1	0	1.3	A	-	-	-
OSS2-BH	2	1.3	1.9	B	-	-	-
OSS2-BH	3	1.9	2.7	C	-	-	-
OSS2-BH	4	2.7	11.5	D2clay	-	-	-
OSS2-BH	5	11.5	15.1	E1clay	-	-	-
OSS2-BH	6	15.1	19.9	E1mix	38.4	906.4	209.8
OSS2-BH	7	19.9	31.2	E1sand	35.8	-	96.0
OSS2-BH	8	31.2	57.3	Hclay	-	324.6	179.4

Location	Layer	Top level	Bottom level	Unit	φ' - Avg	c_u - Avg	G_{max} - Avg
[-]	[No.]	[mBSB]	[mBSB]	[-]	[°]	[kPa]	[MPa]
OSS2-BH	9	57.3	60.7	Hclay	-	683.4	308.7
OSS2-BH	10	60.7	68.2	I	38.4	1955.5	244.2
SCPT1	1	0	0.5	A	-	2.2	1.0
SCPT1	2	0.5	2.6	D1clay	-	14.2	11.8
SCPT1a	1	0	0.5	A	-	3.3	1.7
SCPT1a	2	0.5	3.2	D1clay	-	13.1	11.4
SCPT1a	3	3.2	35.5	D2clay	-	57.3	44.9
SCPT1a	4	35.5	37.8	E2clay	-	127.3	52.1
SCPT2	1	0	1.1	A	-	5.3	4.1
SCPT2	2	1.1	2.2	B	-	7.9	7.5
SCPT2	3	2.2	3.9	C	40.9	-	30.0
SCPT2	4	3.9	23.9	E1clay	-	67.5	55.7
SCPT2	5	23.9	26.2	Fclay	-	89.6	61.0
SCPT2	6	26.2	26.5	Hsand	36.9	-	99.5
SCPT5	1	0	0.7	A	-	3.8	2.0
SCPT5	2	0.7	3.3	B	-	14.5	12.8
SCPT5	3	3.3	5.5	C	42.5	-	43.8
SCPT5	4	5.5	23.9	D2clay	-	46.0	45.1
SCPT5	5	23.9	30.1	E1clay	-	72.8	63.4
SCPT17	1	0	1.9	A	-	5.6	4.8
SCPT17	2	1.9	2.8	D1sand	38.8	-	22.5
SCPT17	3	2.8	3.8	D1clay	-	30.2	26.1
SCPT17	4	3.8	6	D1mix	32.4	114.1	44.8
SCPT17	5	6	15.4	D1clay	-	41.1	38.3
SCPT17	6	15.4	18.2	E1clay	-	63.1	54.8
SCPT17	7	18.2	18.7	E1mix	34.3	373.8	170.5
SCPT19	1	0	1.8	A	-	5.4	4.0
SCPT19	2	1.8	2.6	C	30.6	-	13.1
SCPT19	3	2.6	21.9	D2clay	-	40.7	32.9
SCPT21	1	0	1.1	A	-	7.2	3.4
SCPT21	2	1.1	1.5	D1clay	-	26.3	13.9
SCPT21	3	1.5	30	D2clay	-	43.7	34.7
SCPT21	4	30	31.7	E1clay	-	76.0	42.9
SCPT24	1	0	1	A	-	6.5	4.2
SCPT24	2	1	25.6	D2clay	-	35.5	33.8
SCPT24	3	25.6	32.8	Fclay	-	68.2	50.1
SCPT24	4	32.8	32.9	Hmix	30.6	138.2	79.1

Appendix B   Calculated soil properties per CPT location

For the figures in this appendix the horizontal red lines mark changes in geotechnical layer boundaries. These layer boundaries are defined based on the combined interpretation of available information from seismic horizons, CPT measurements and borehole logs.

CB3a /CB3a-BH
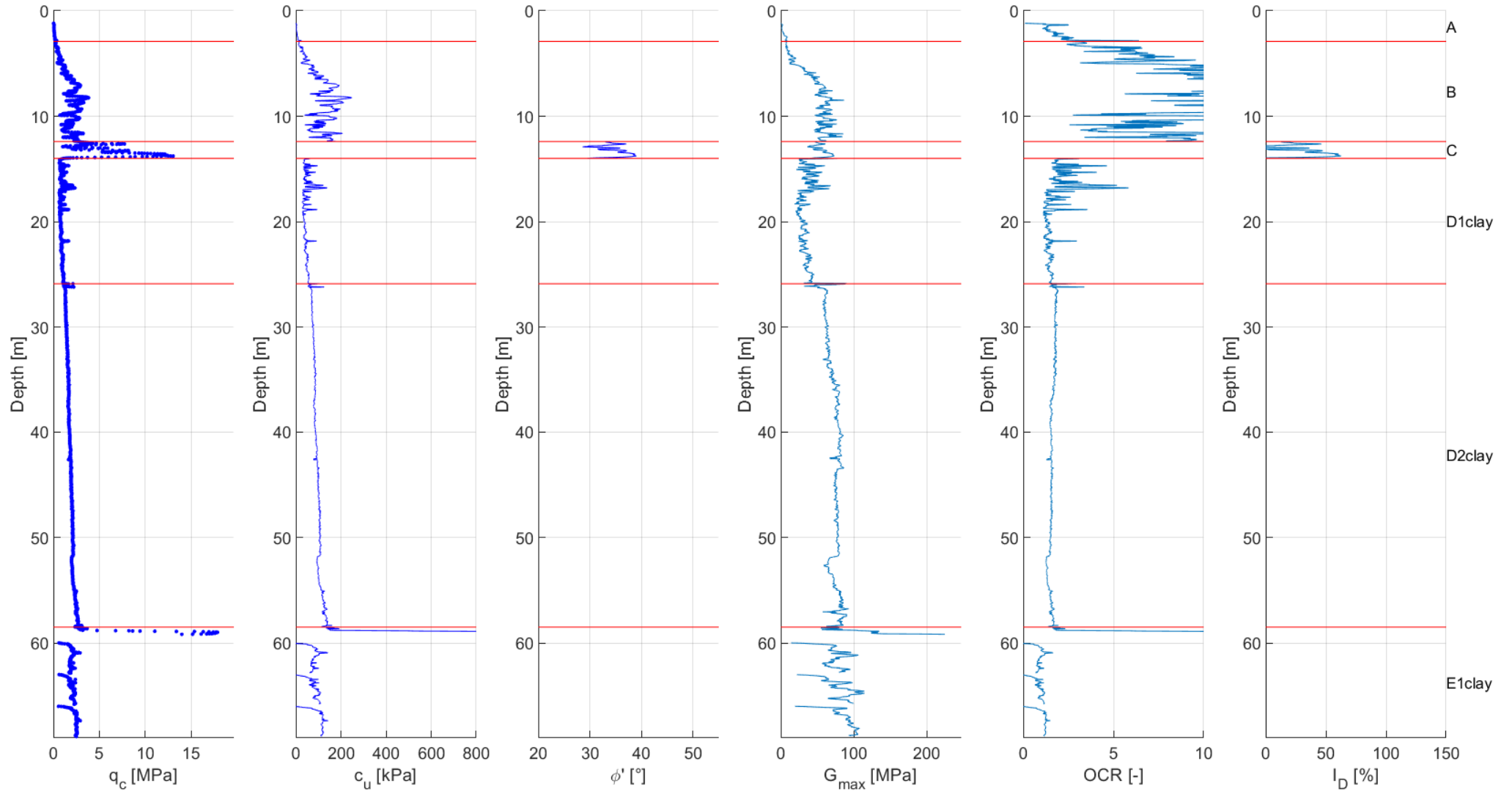
CB4 /CB4-BH
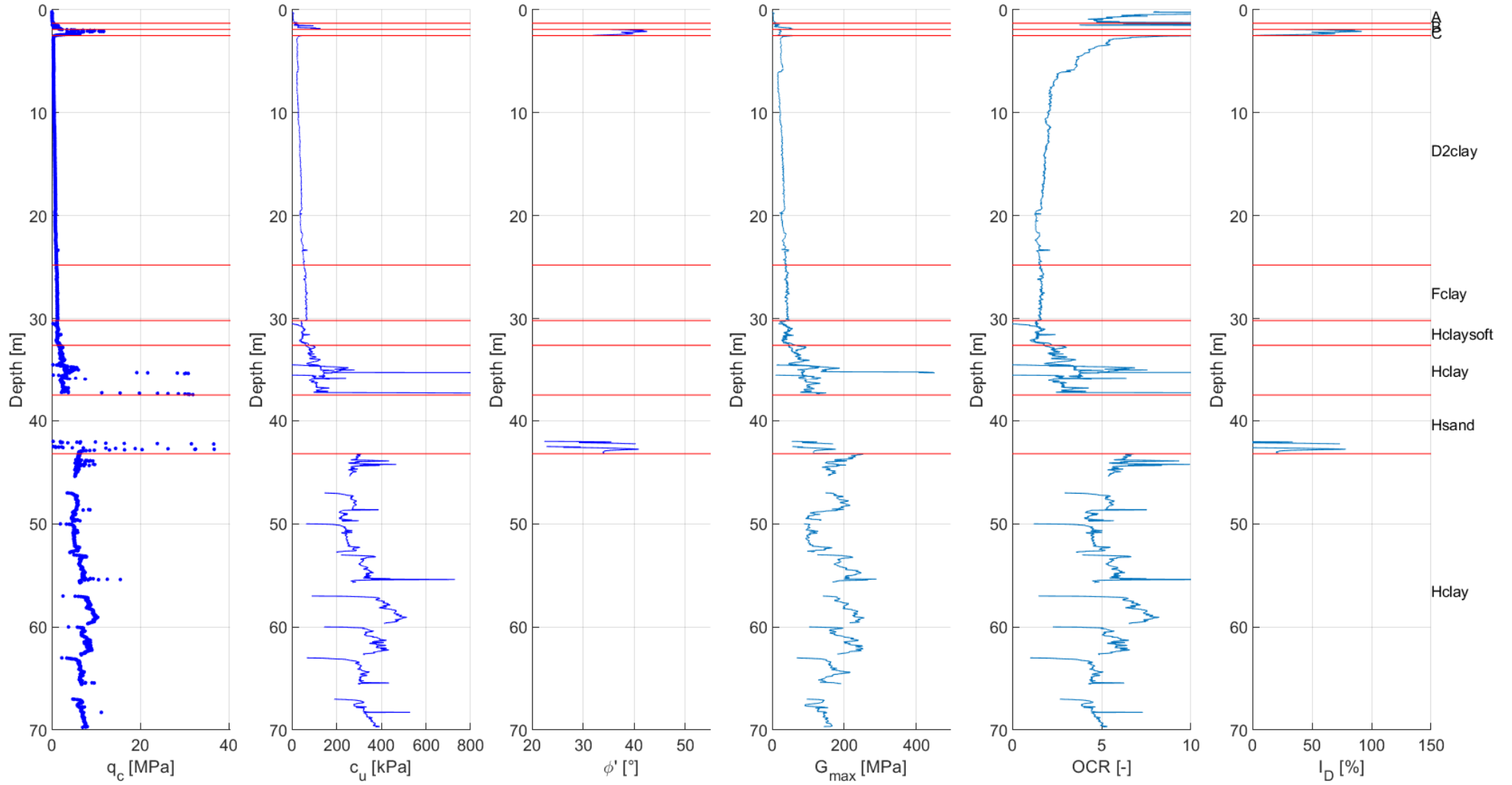
CB5 /CB5-BH /CB5a
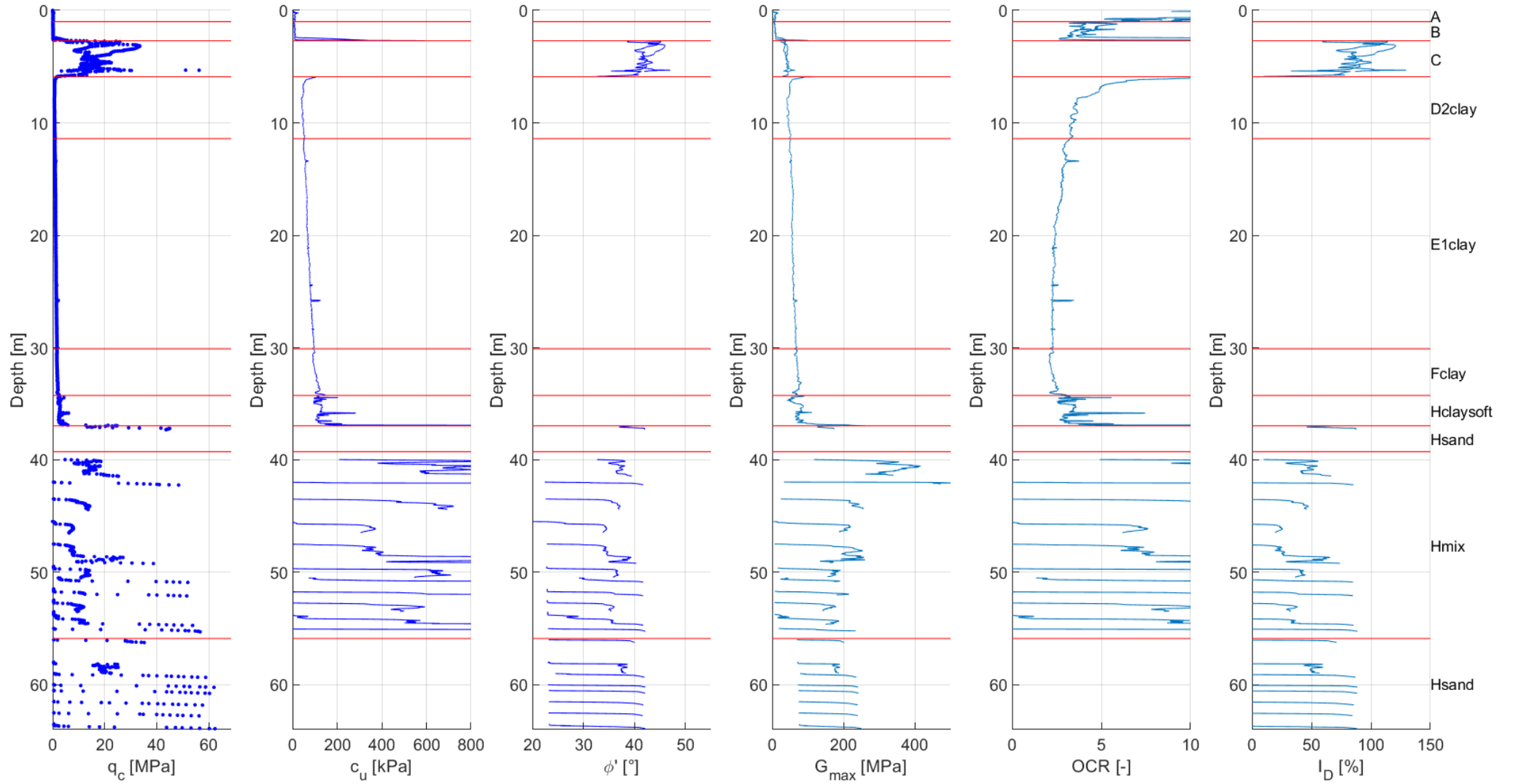
CB6 /CB6-BH /CB6a
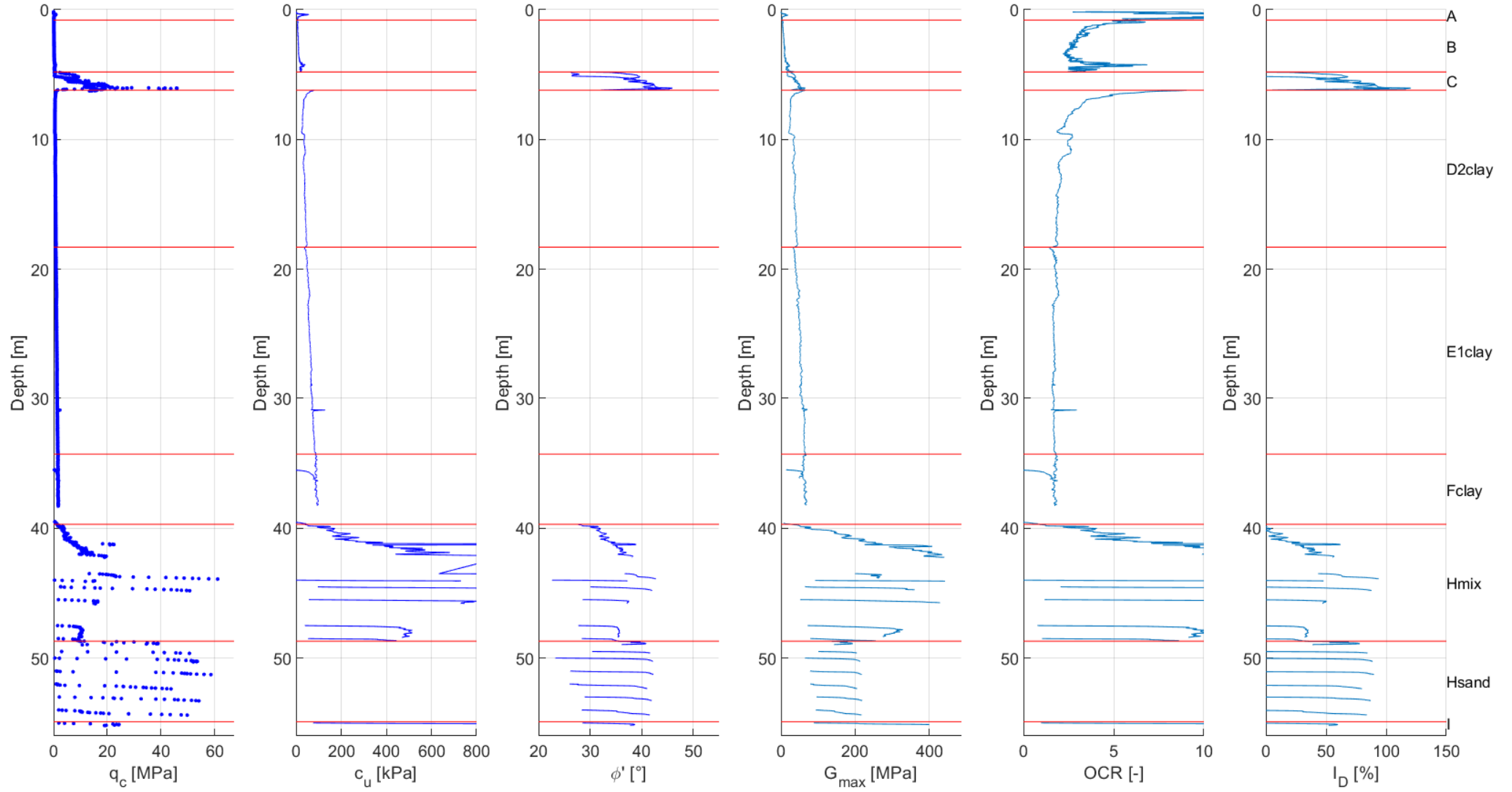
CB7 /CB7-BH /CB7a
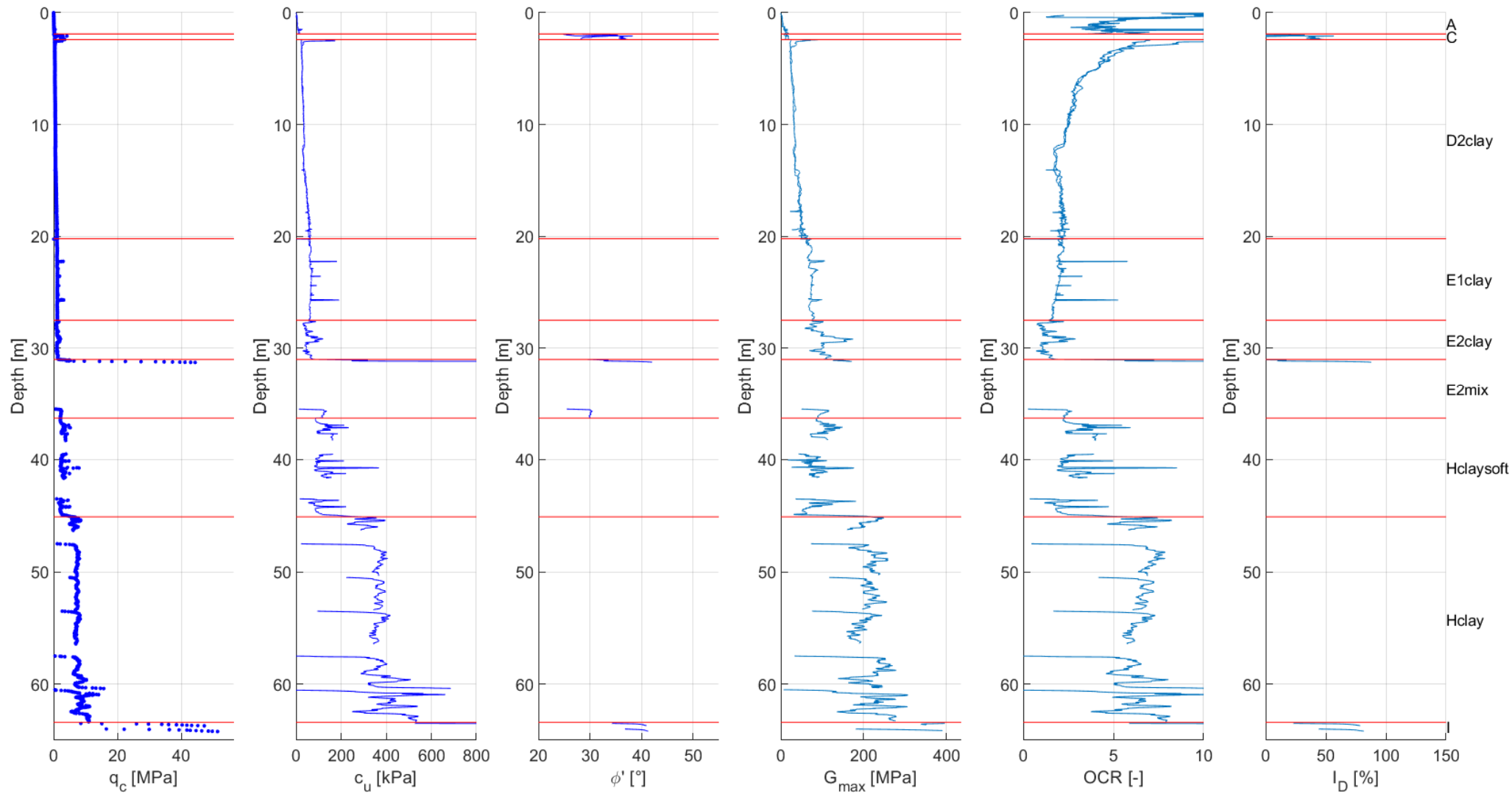
CB8 /CB8-BH
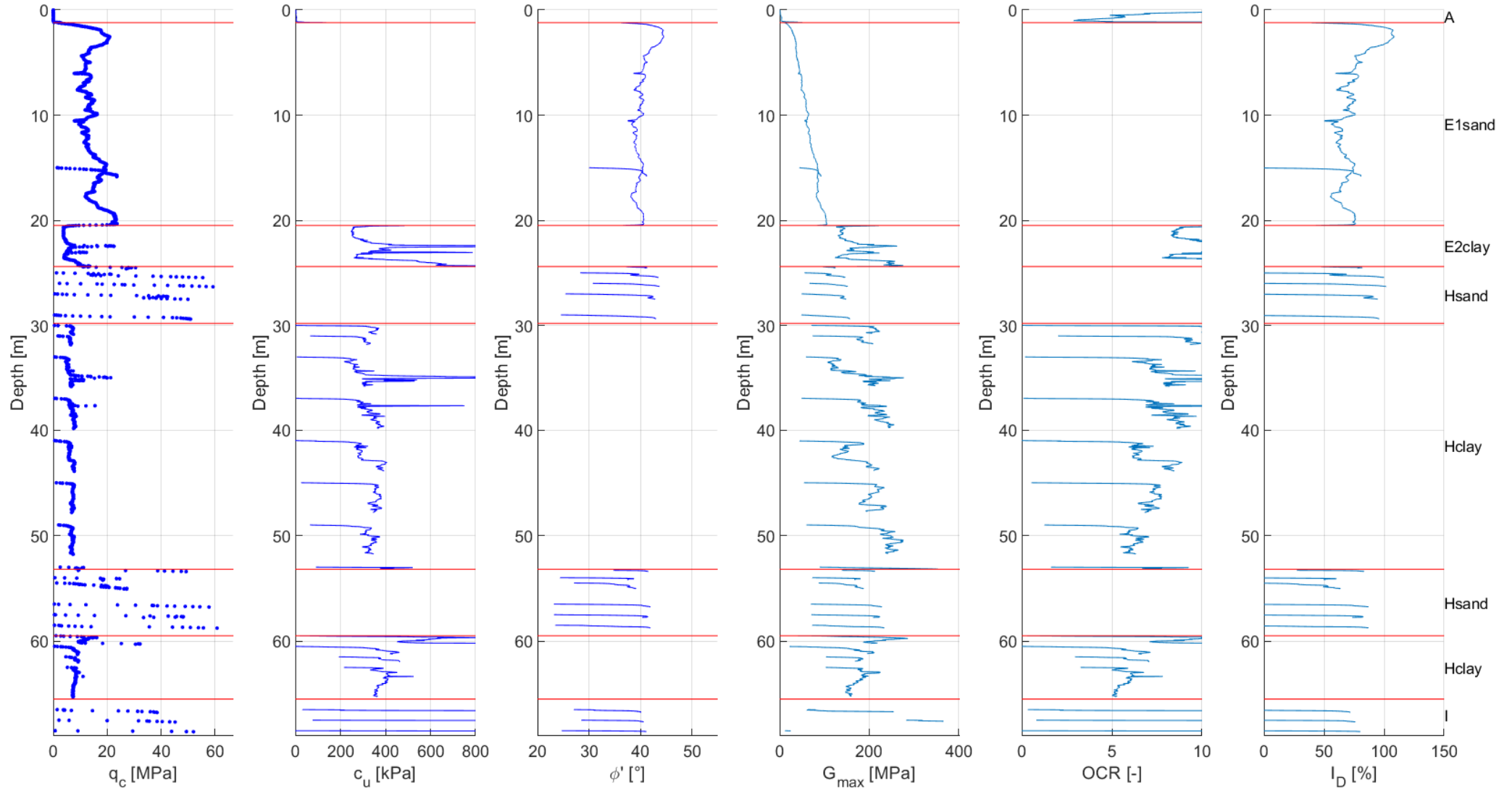
CB9 /CB9-BH
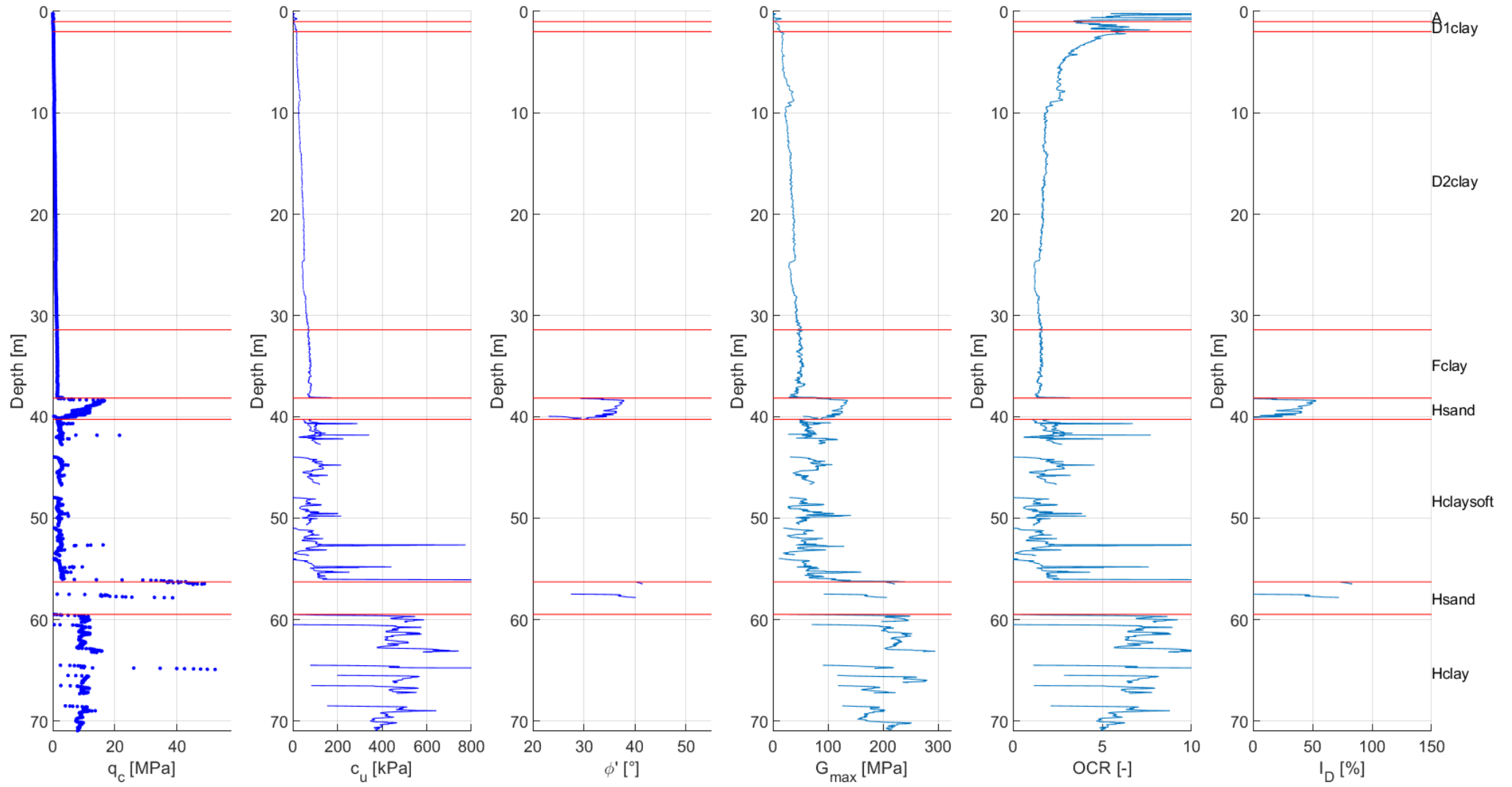
CB10 /CB10a-BH
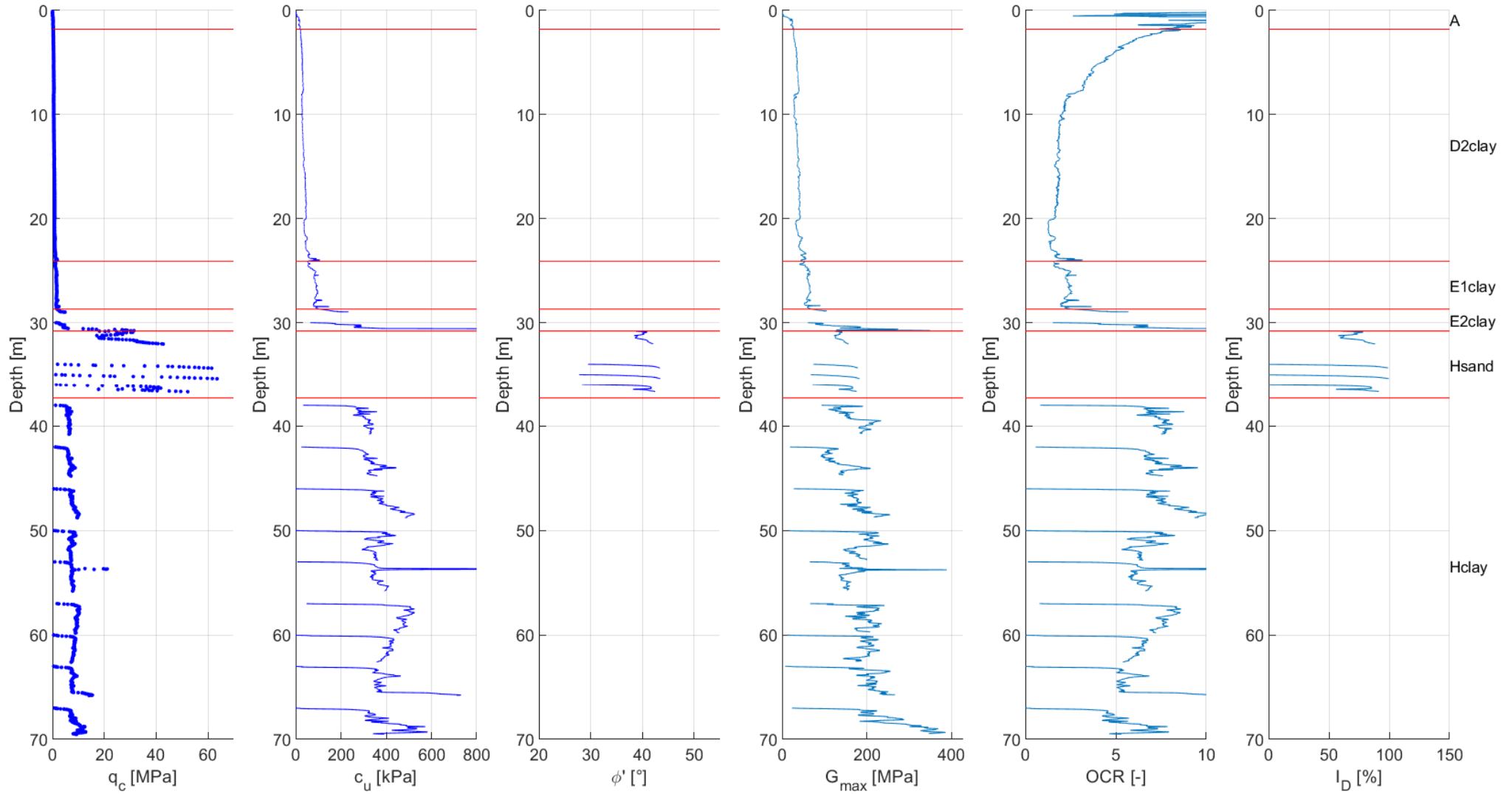
CB11 /CB11-BH /CB11a-BH
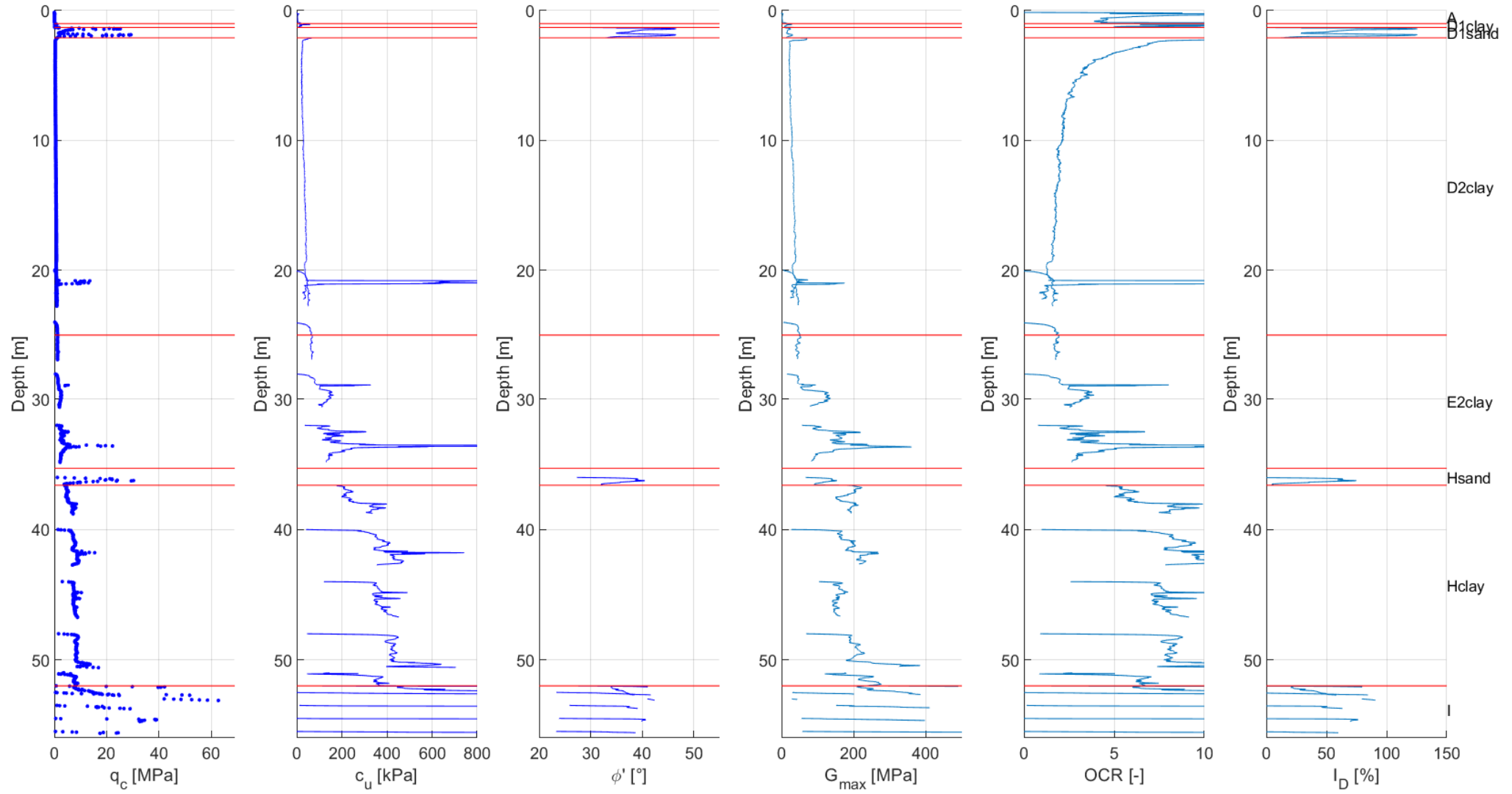
CB12 /CB12-BH
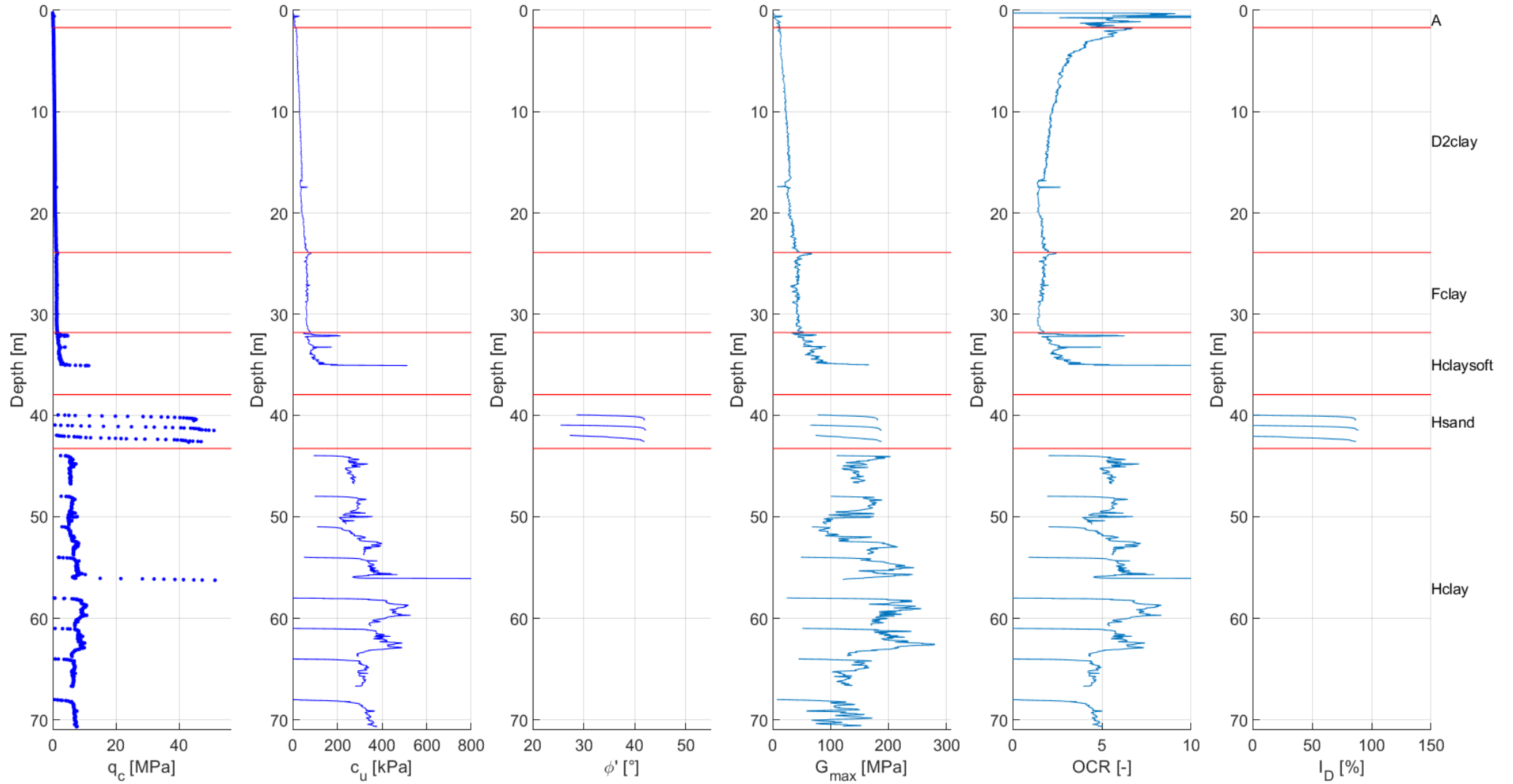
CB13 /CB13-BH
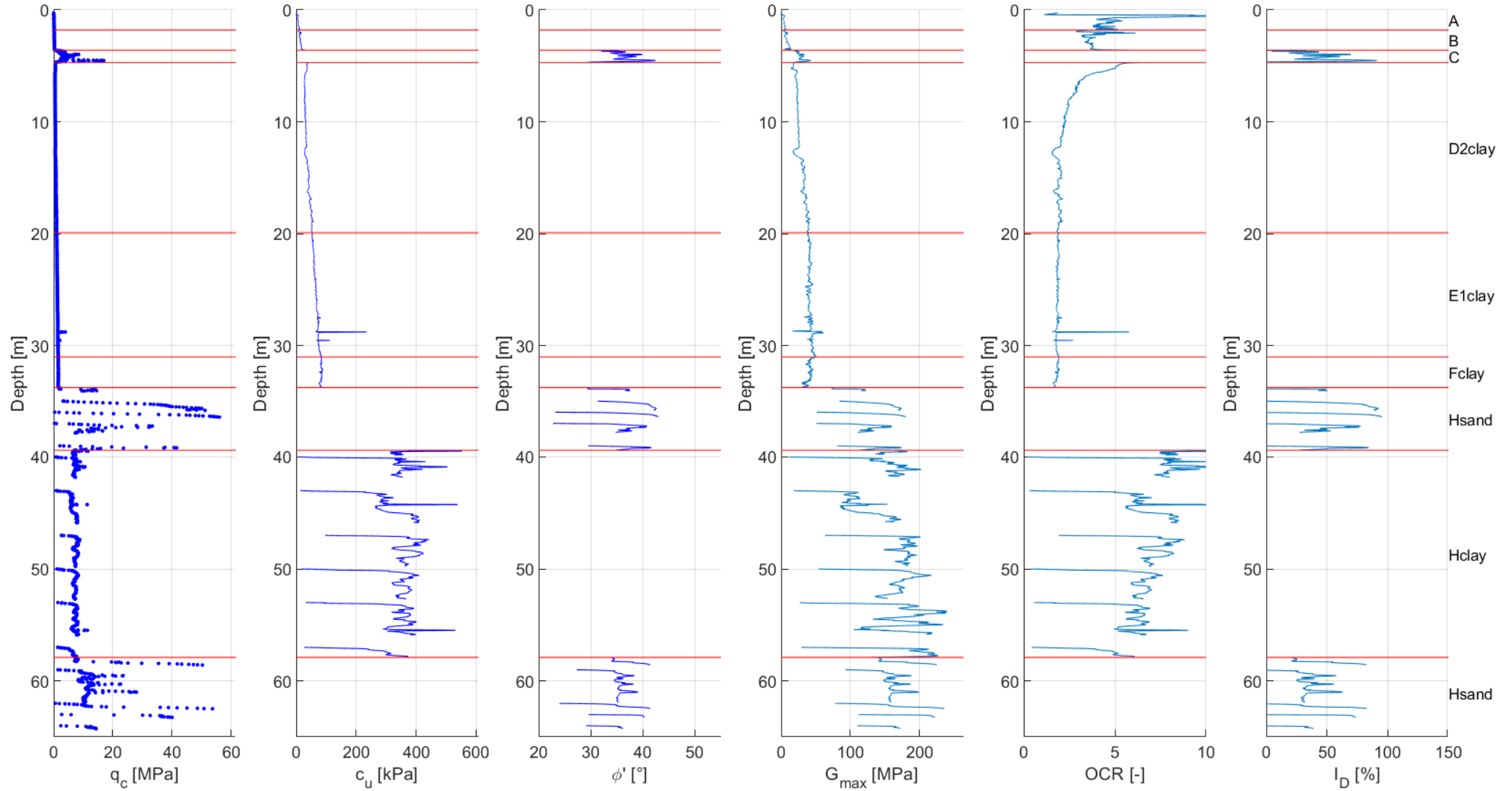
CB14 /CB14-BH
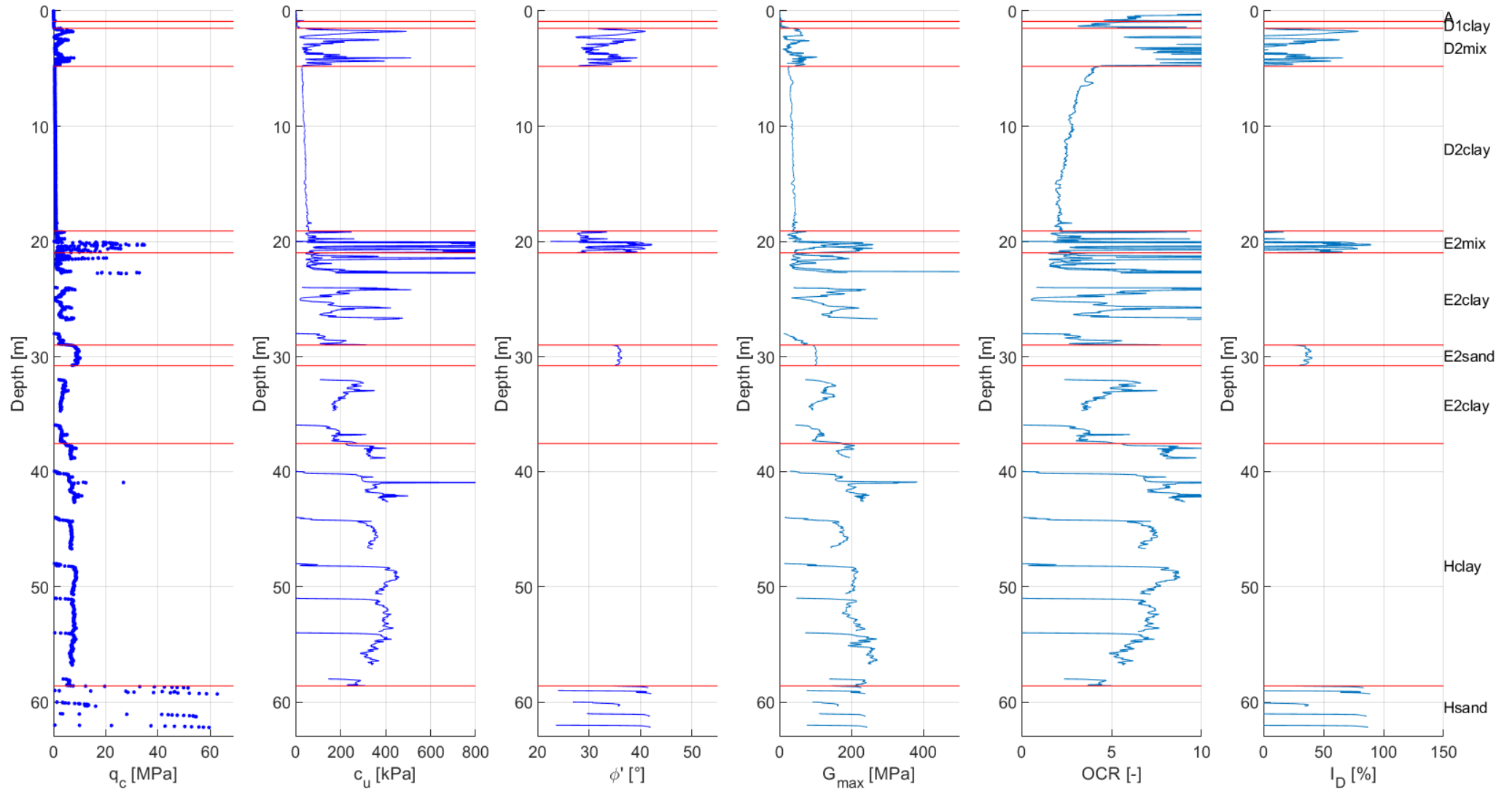
CPT3 /CPT3a /CPT3b
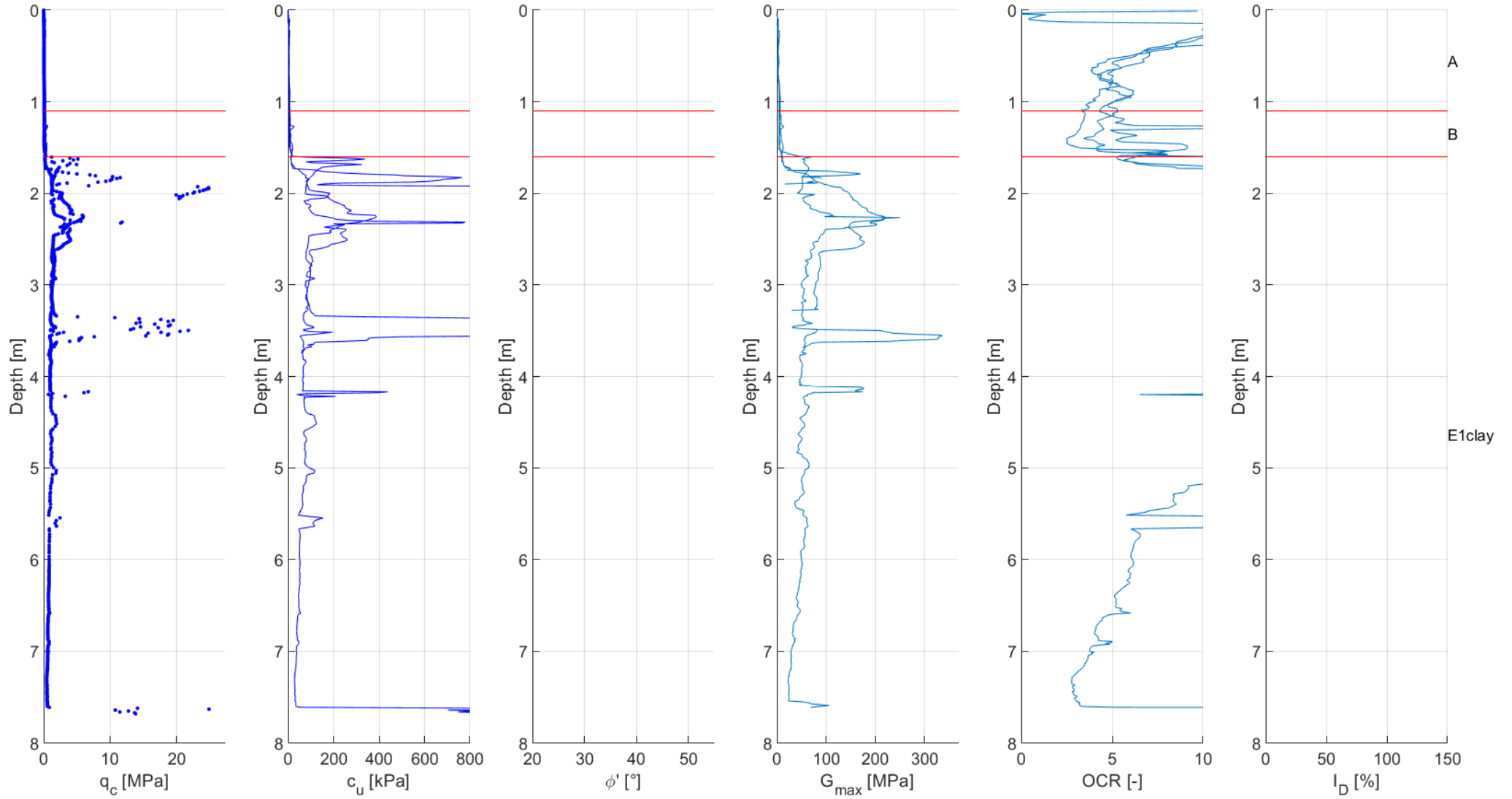
CPT4
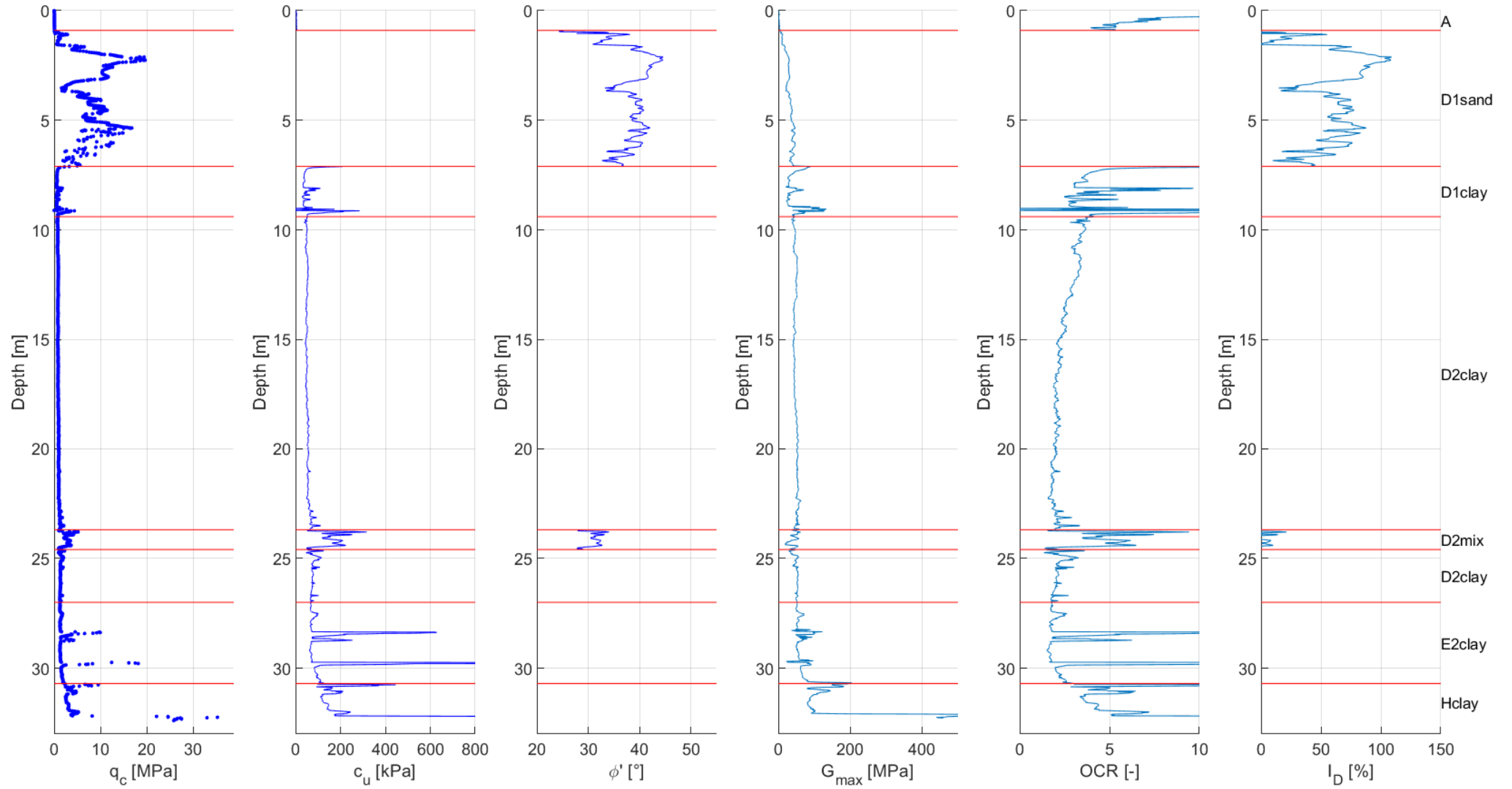
CPT6 /CPT6a
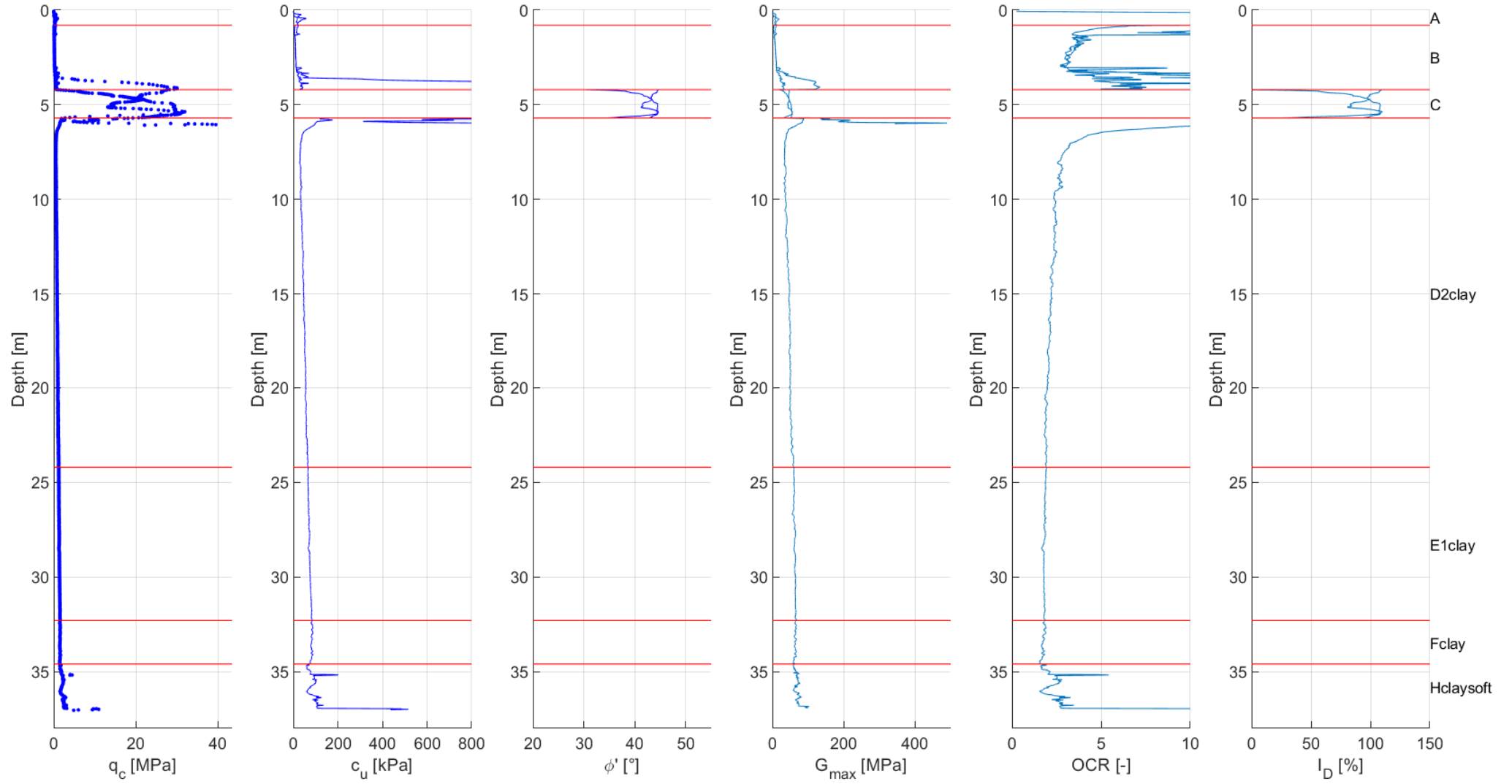
CPT7
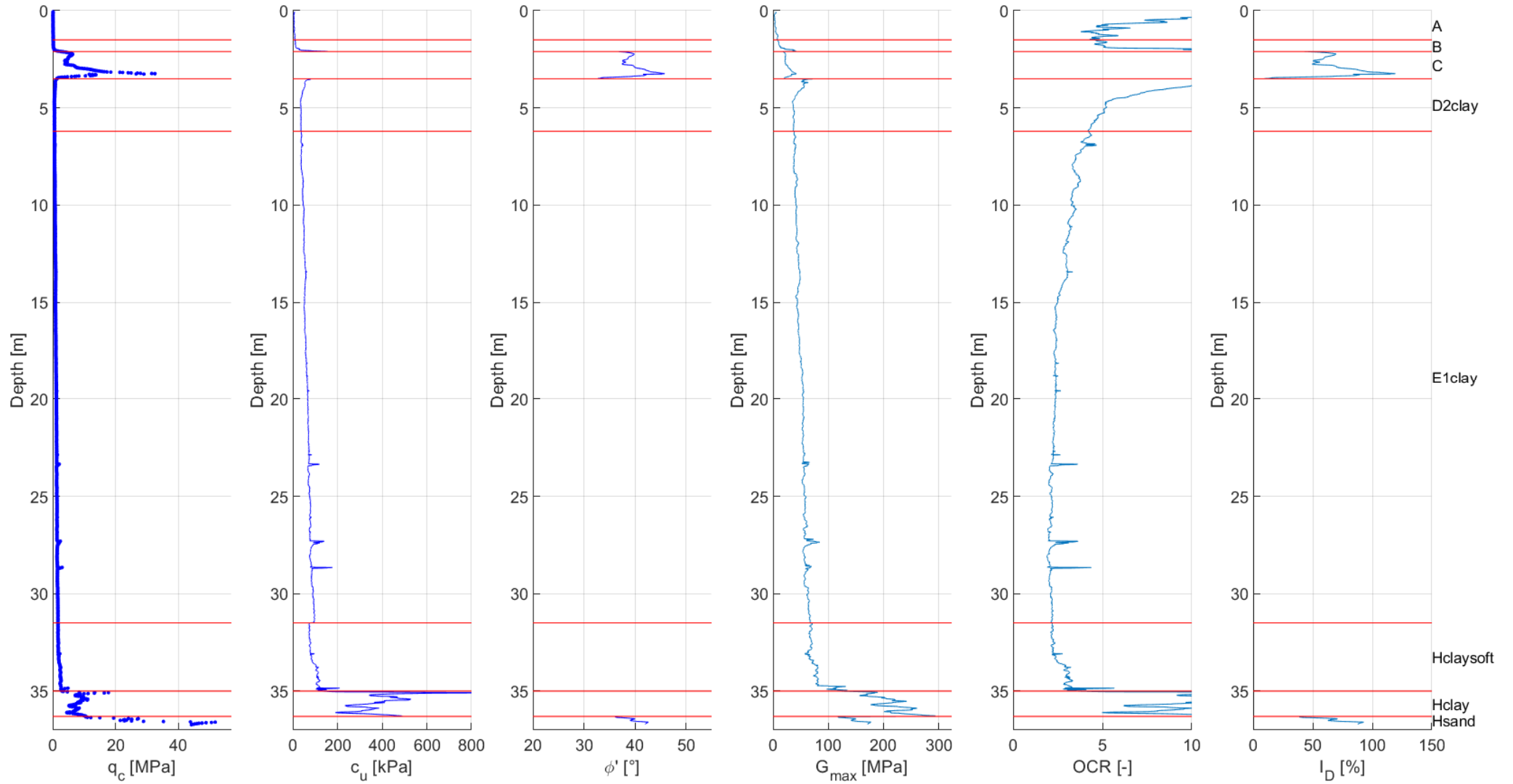
CPT8
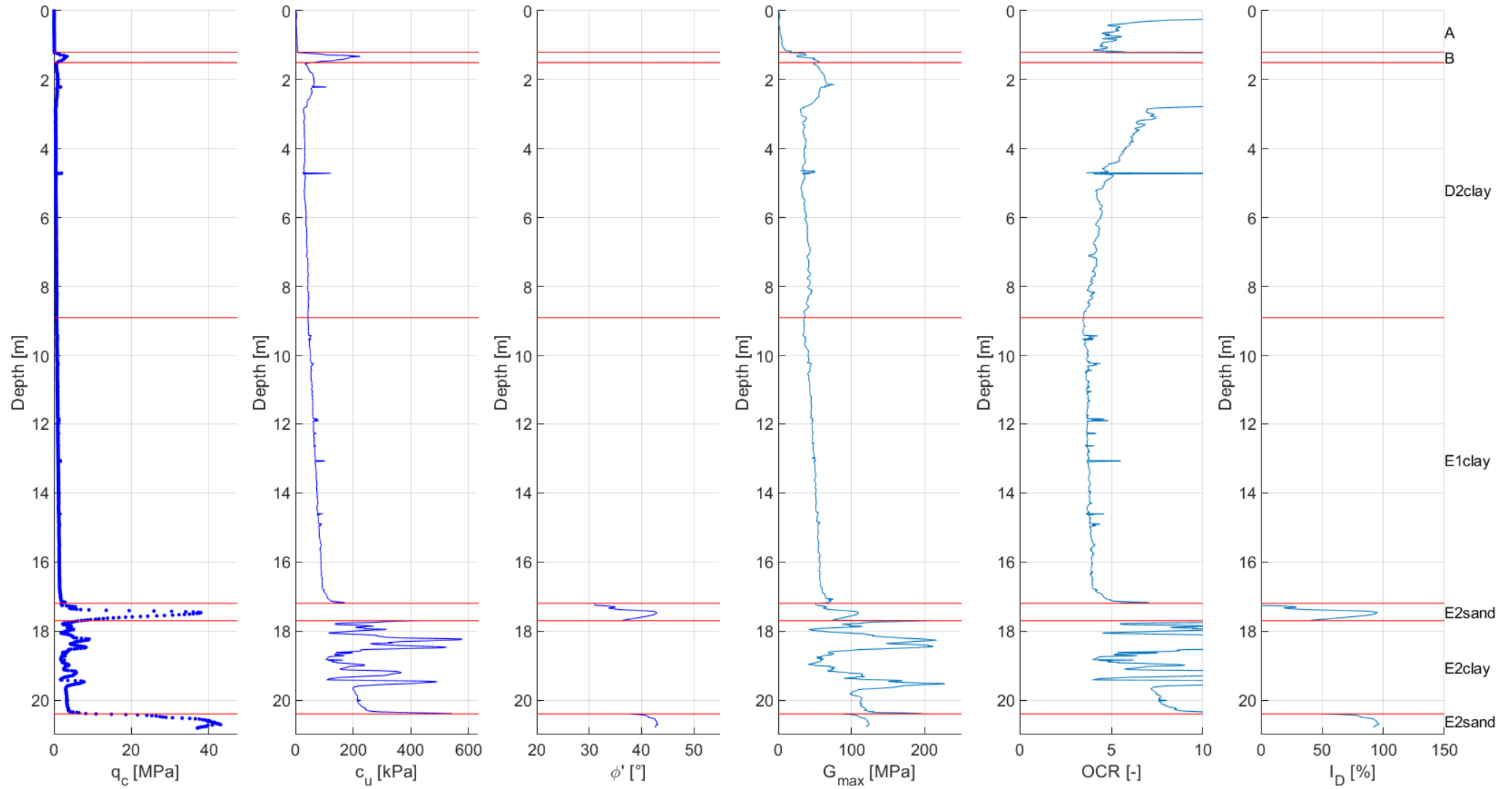
CPT9
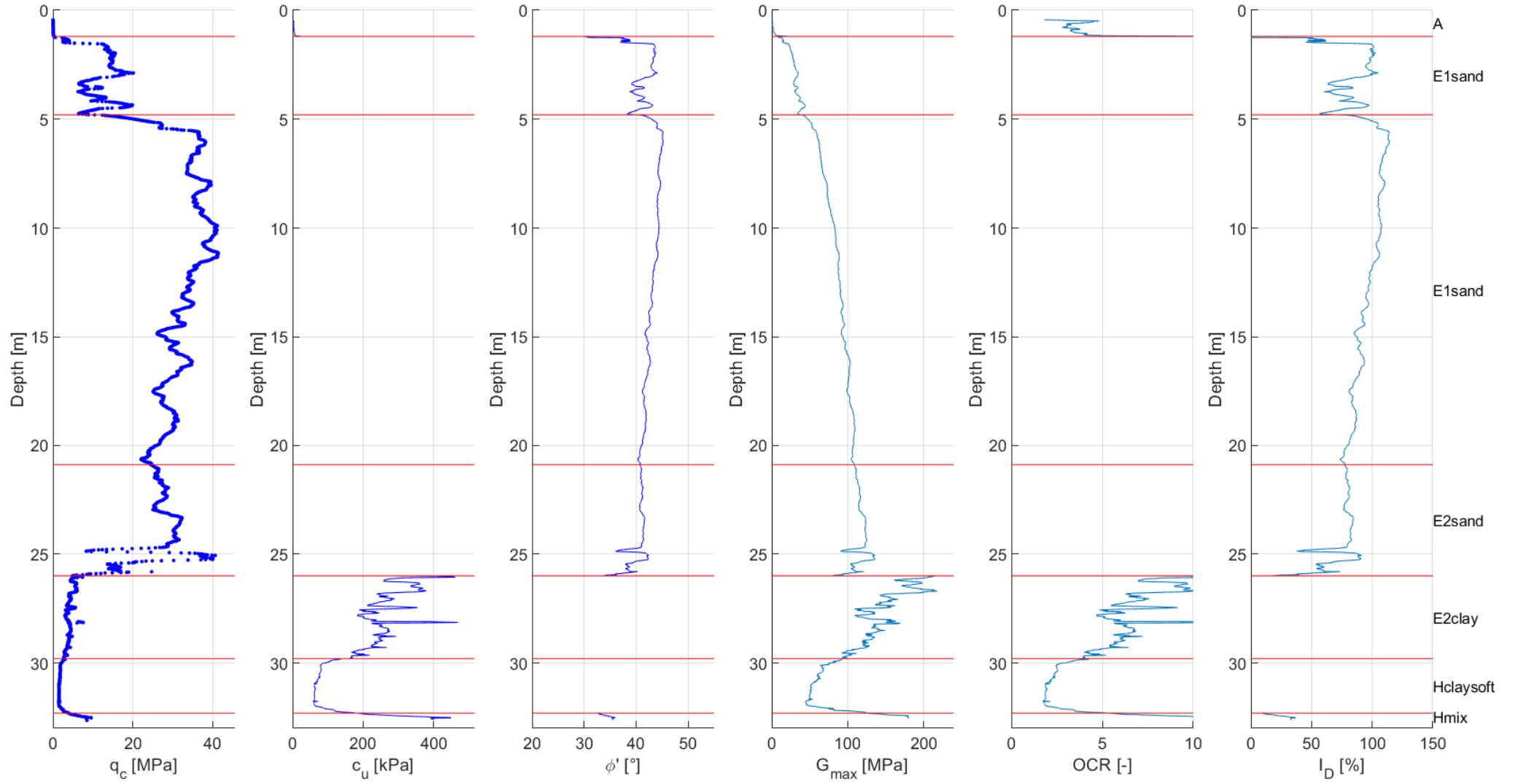
CPT10
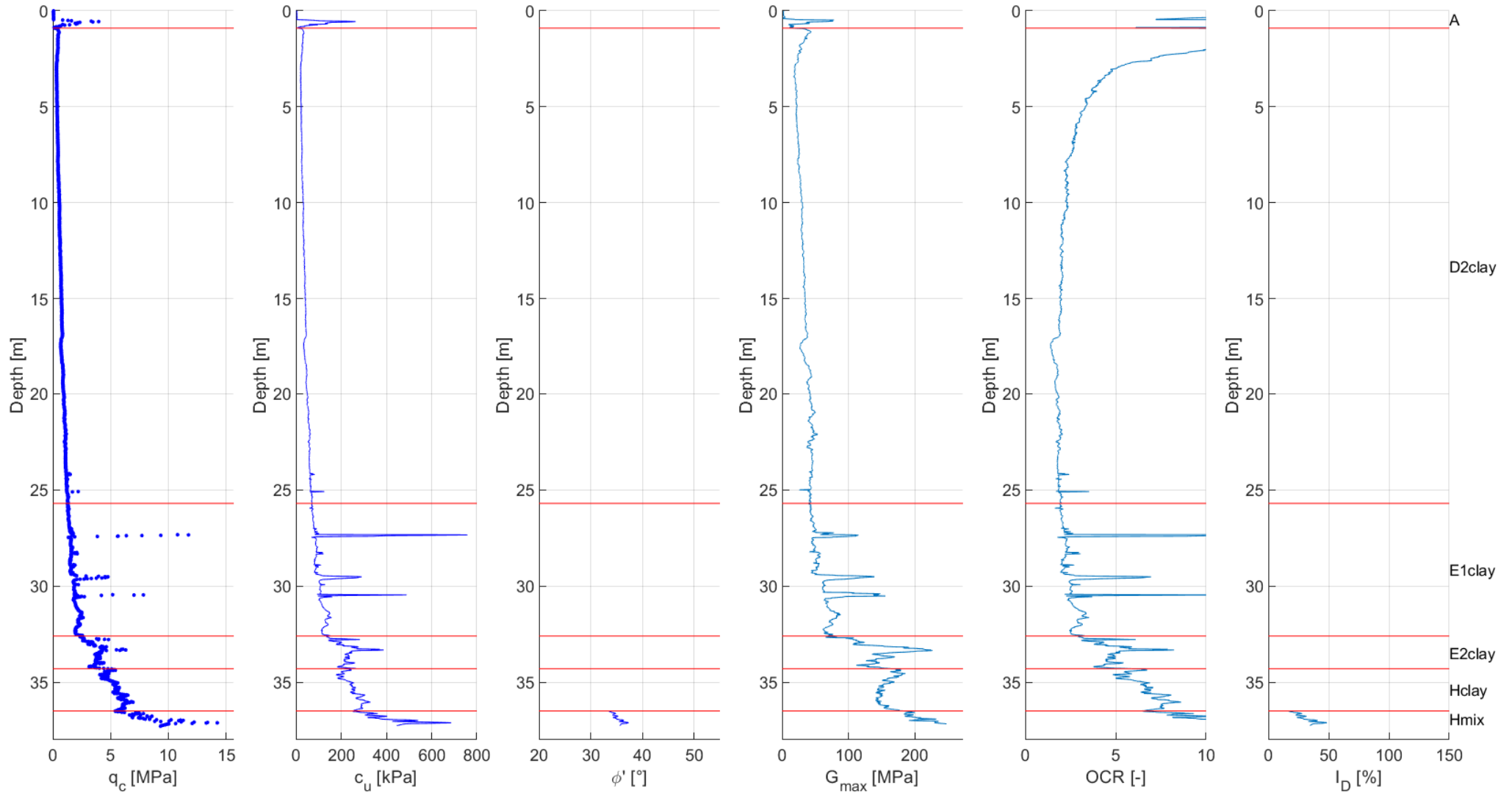
CPT11 /CPT11a
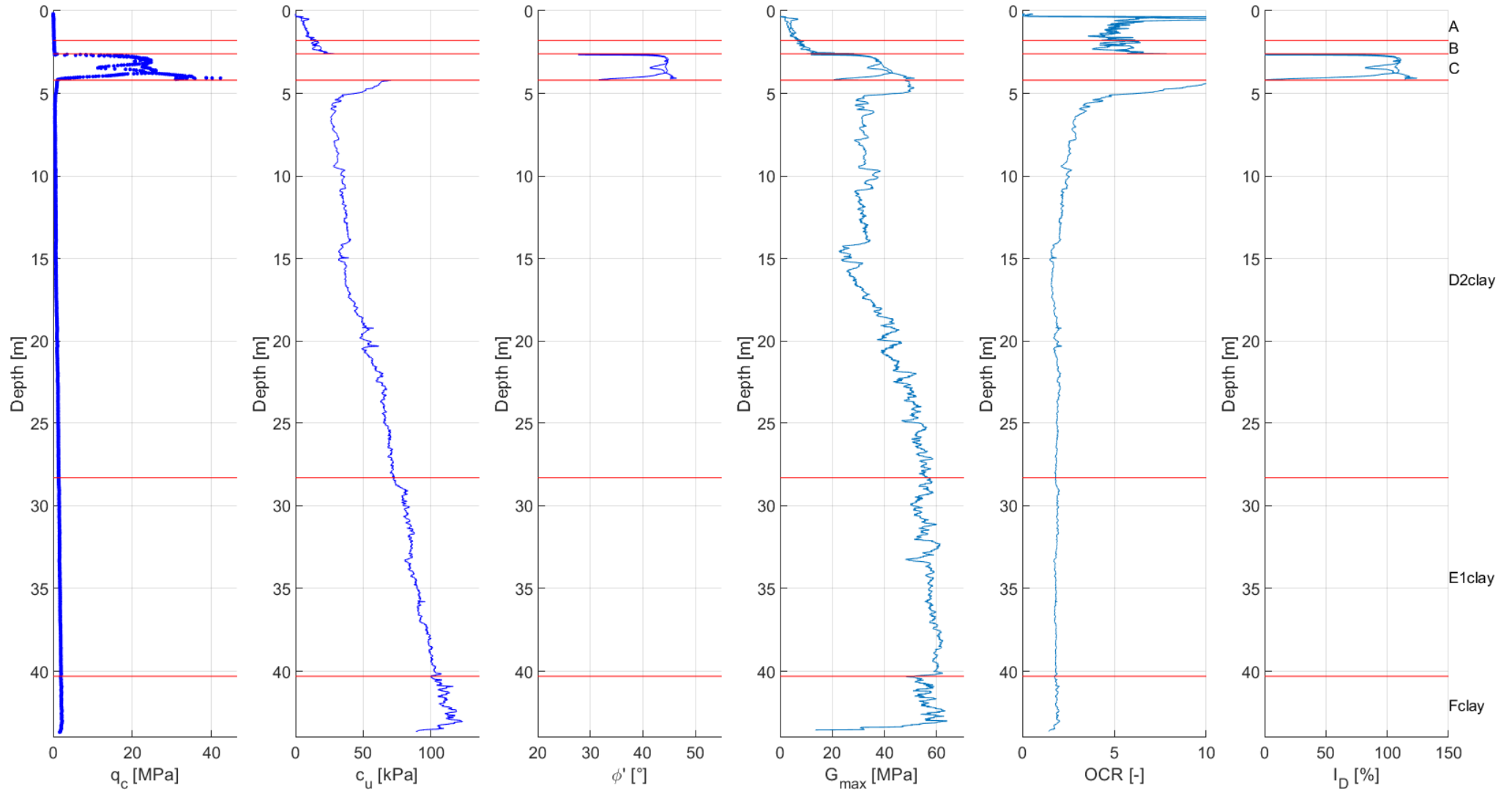
CPT12
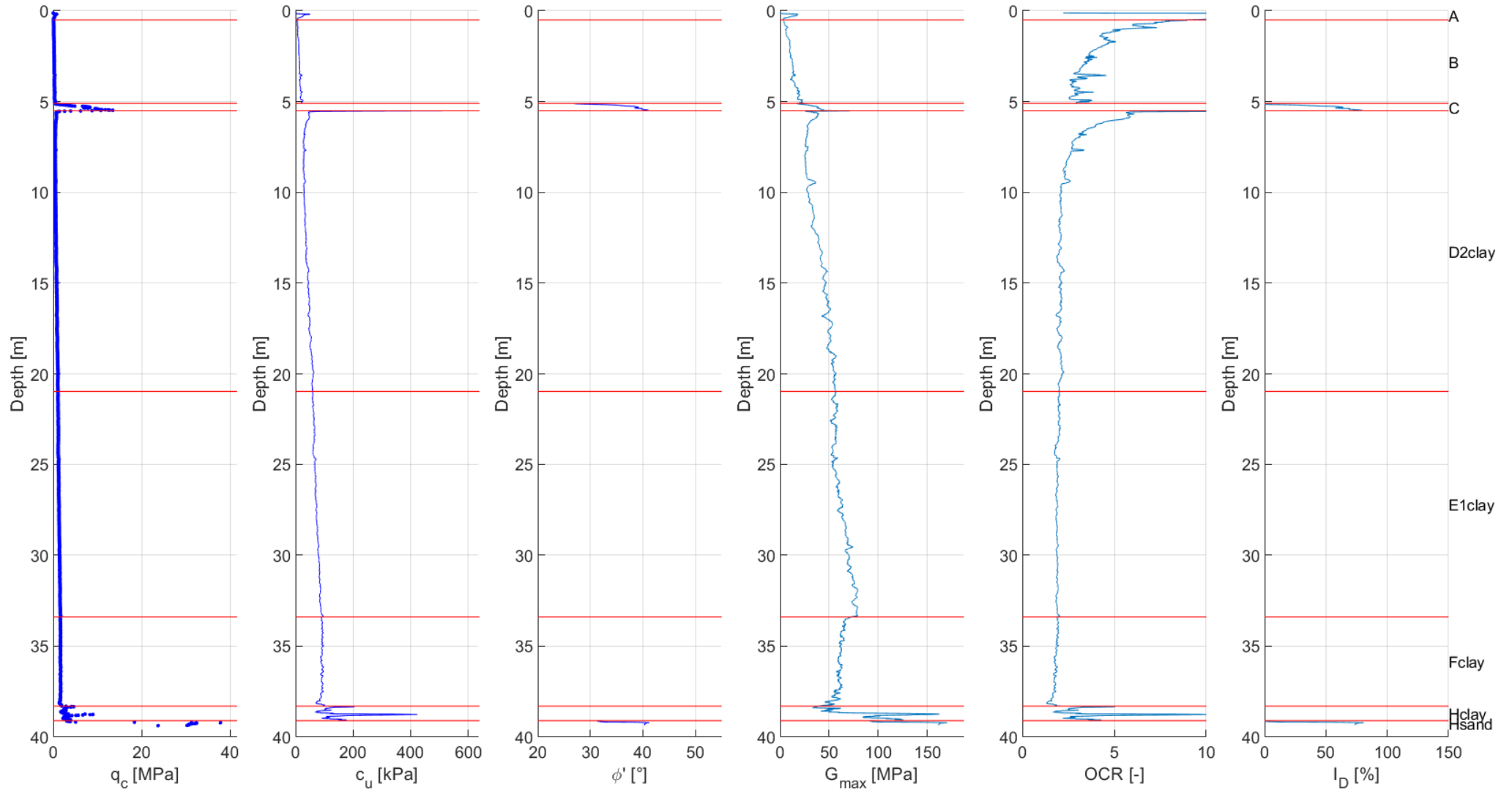
CPT13
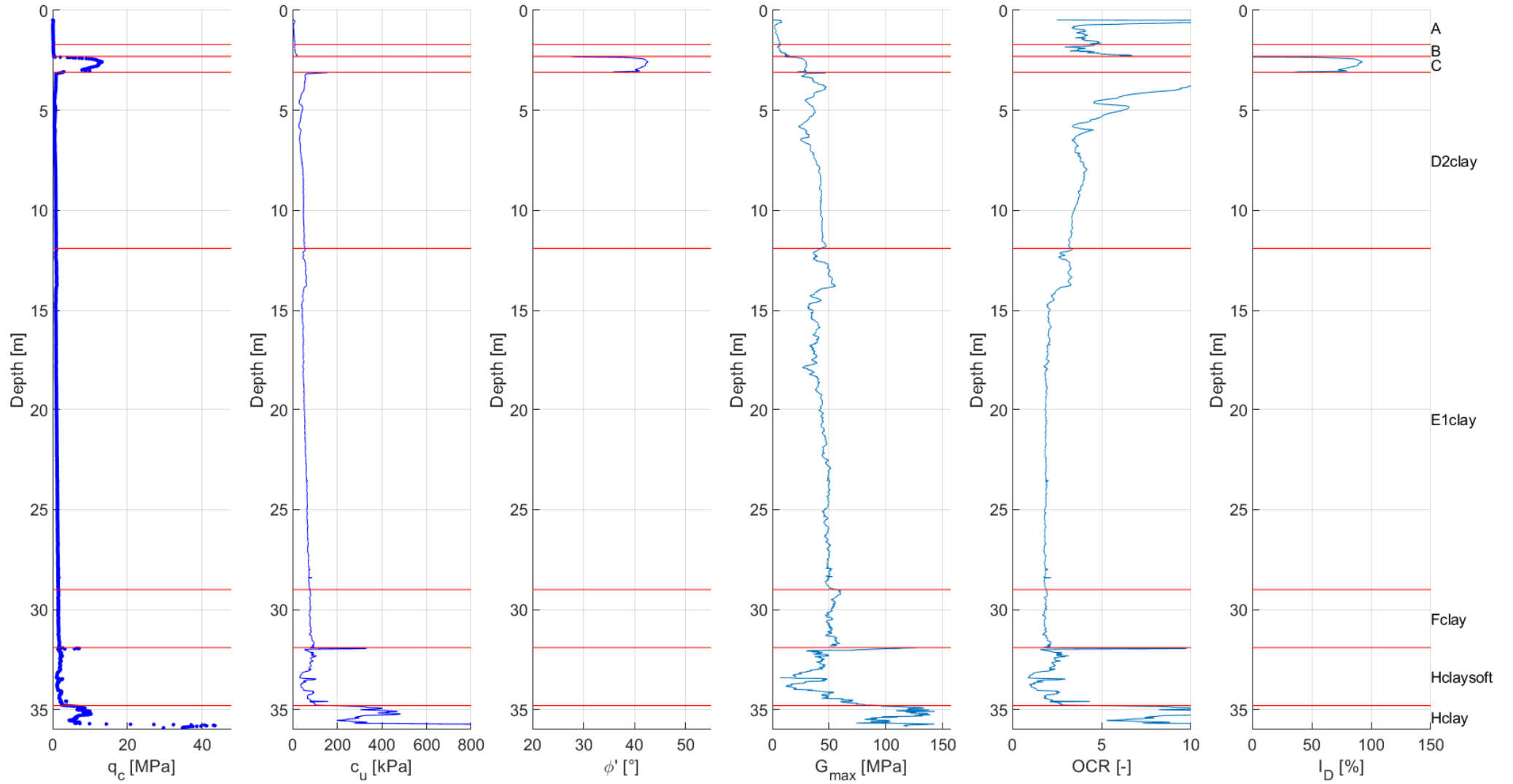
CPT14
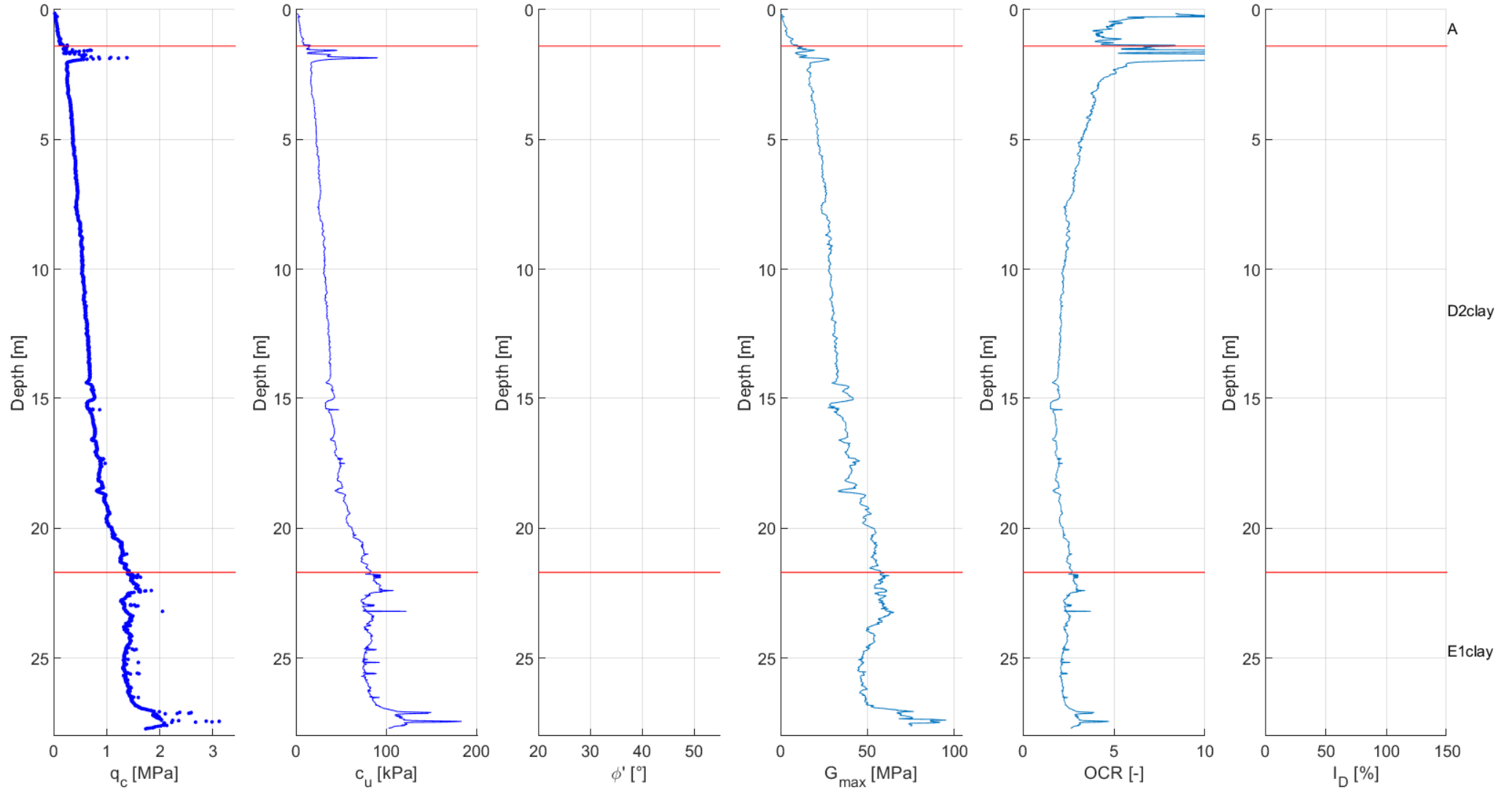
CPT15
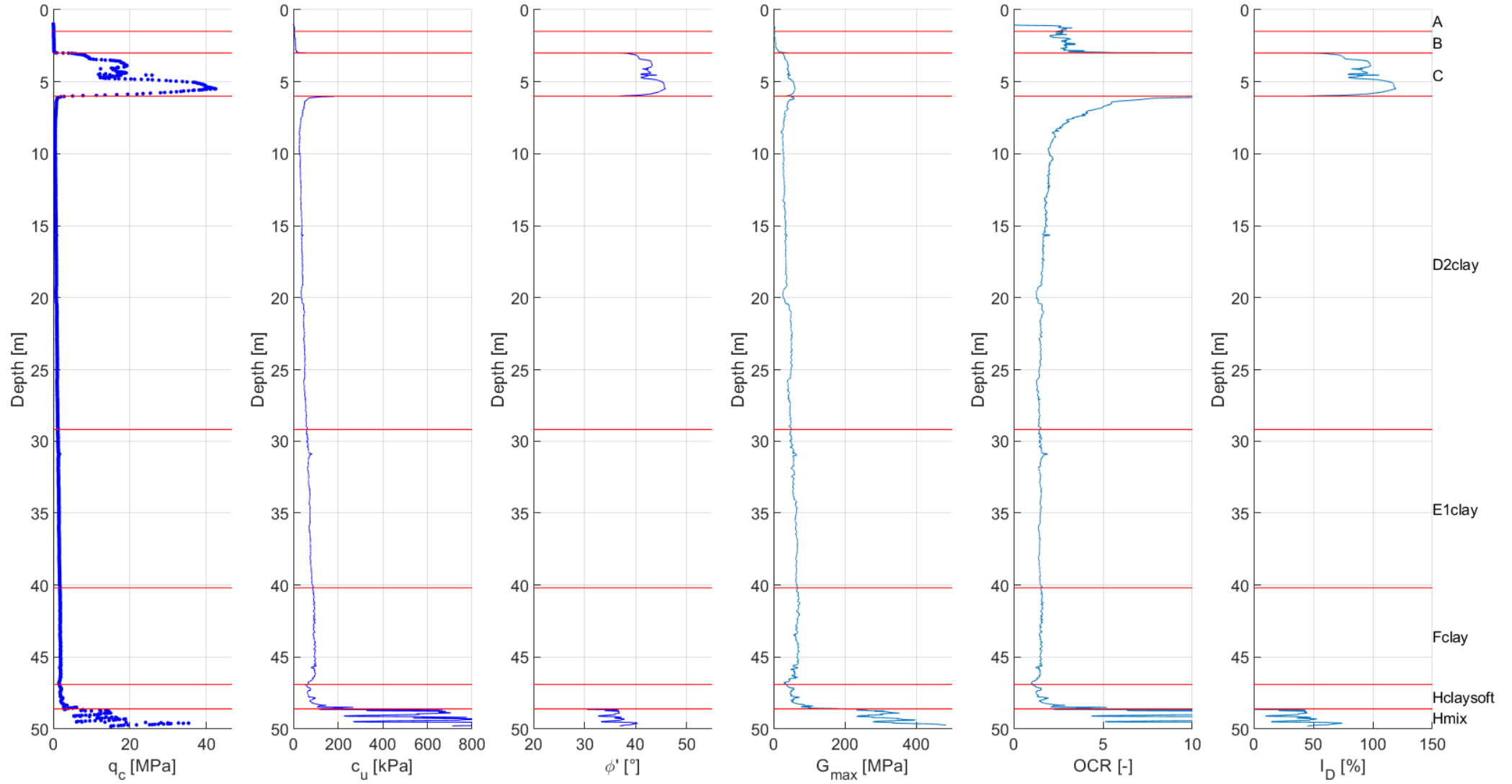
CPT16 /CPT16a
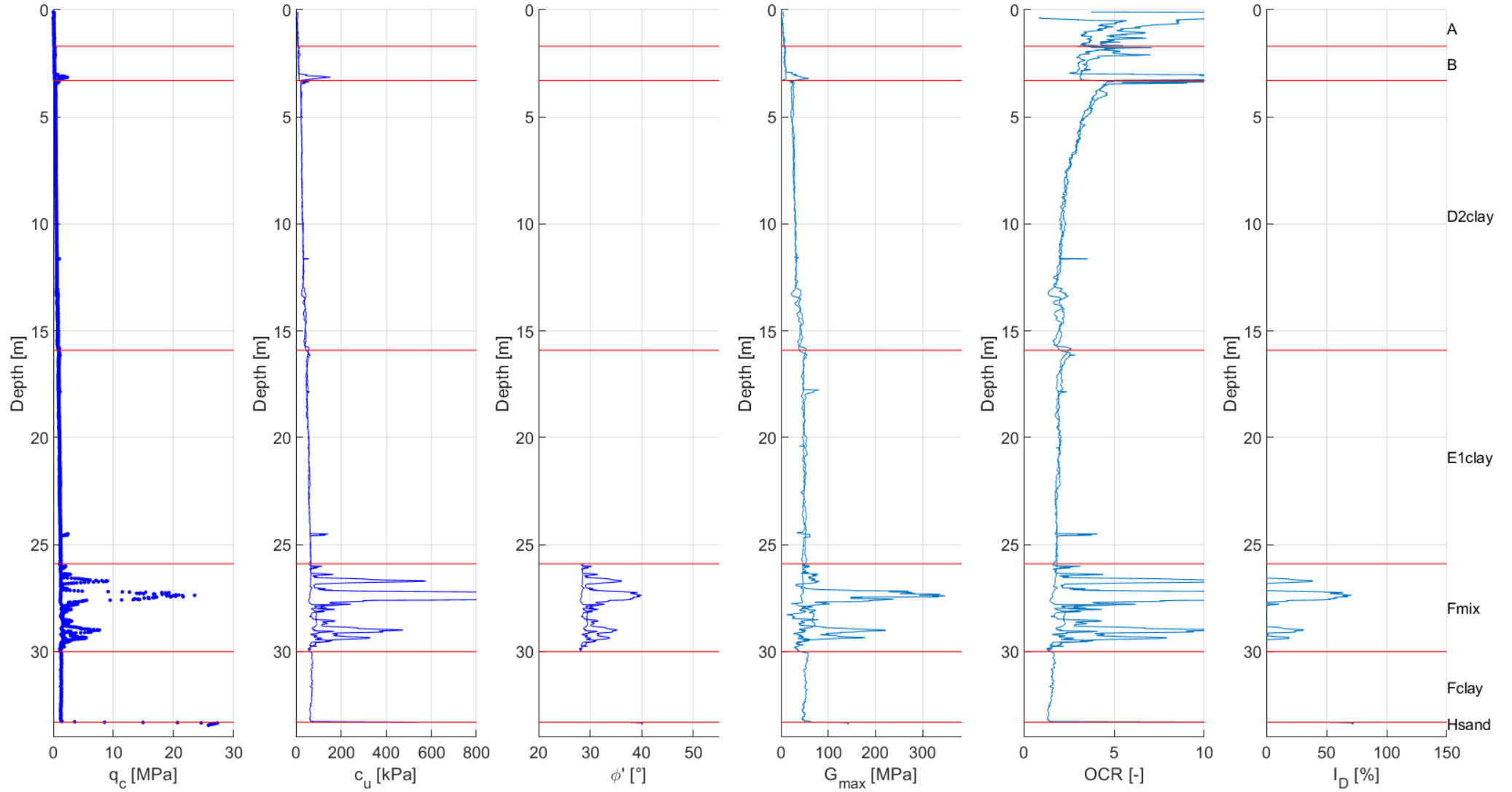
CPT18
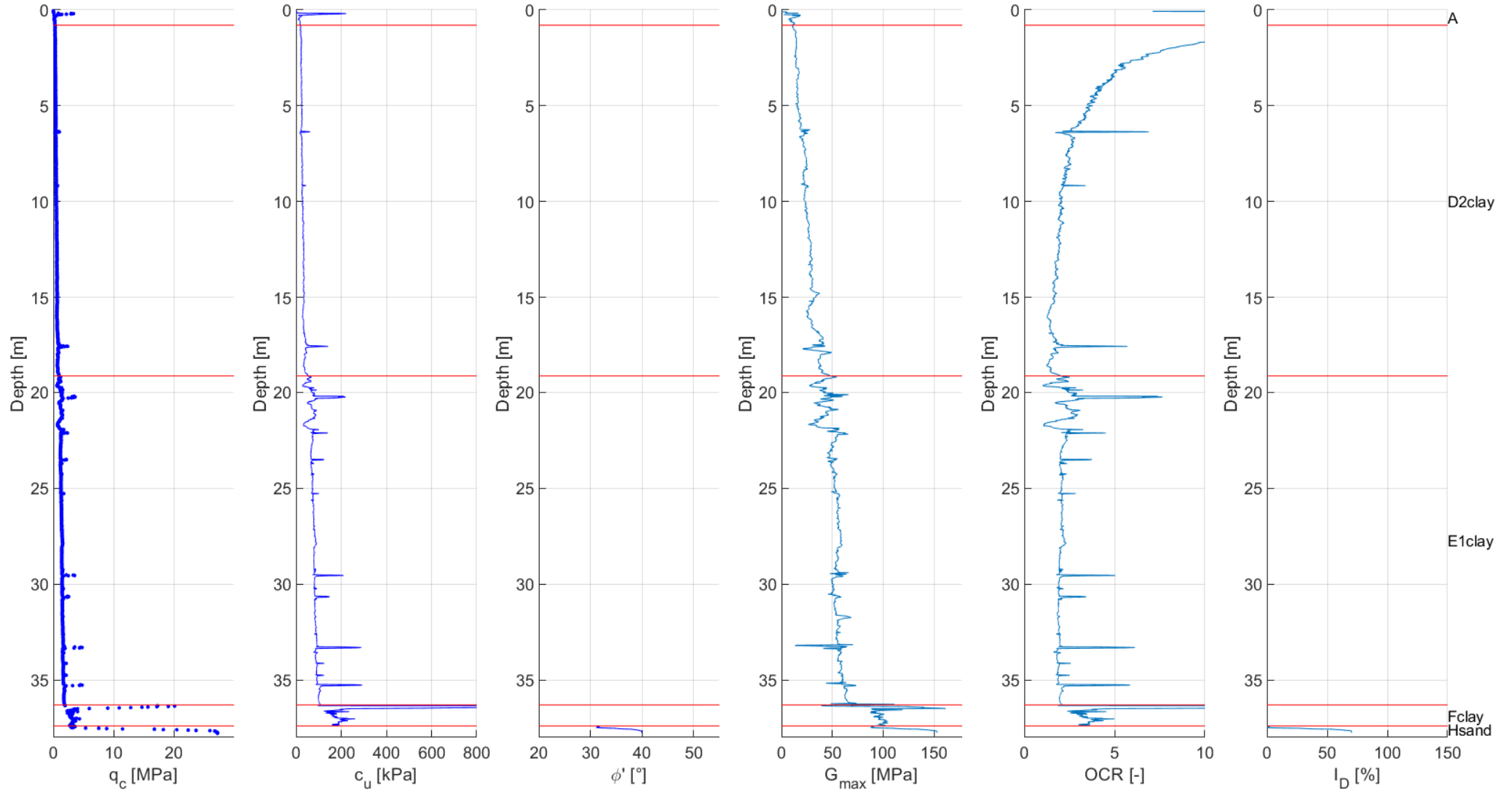
CPT20
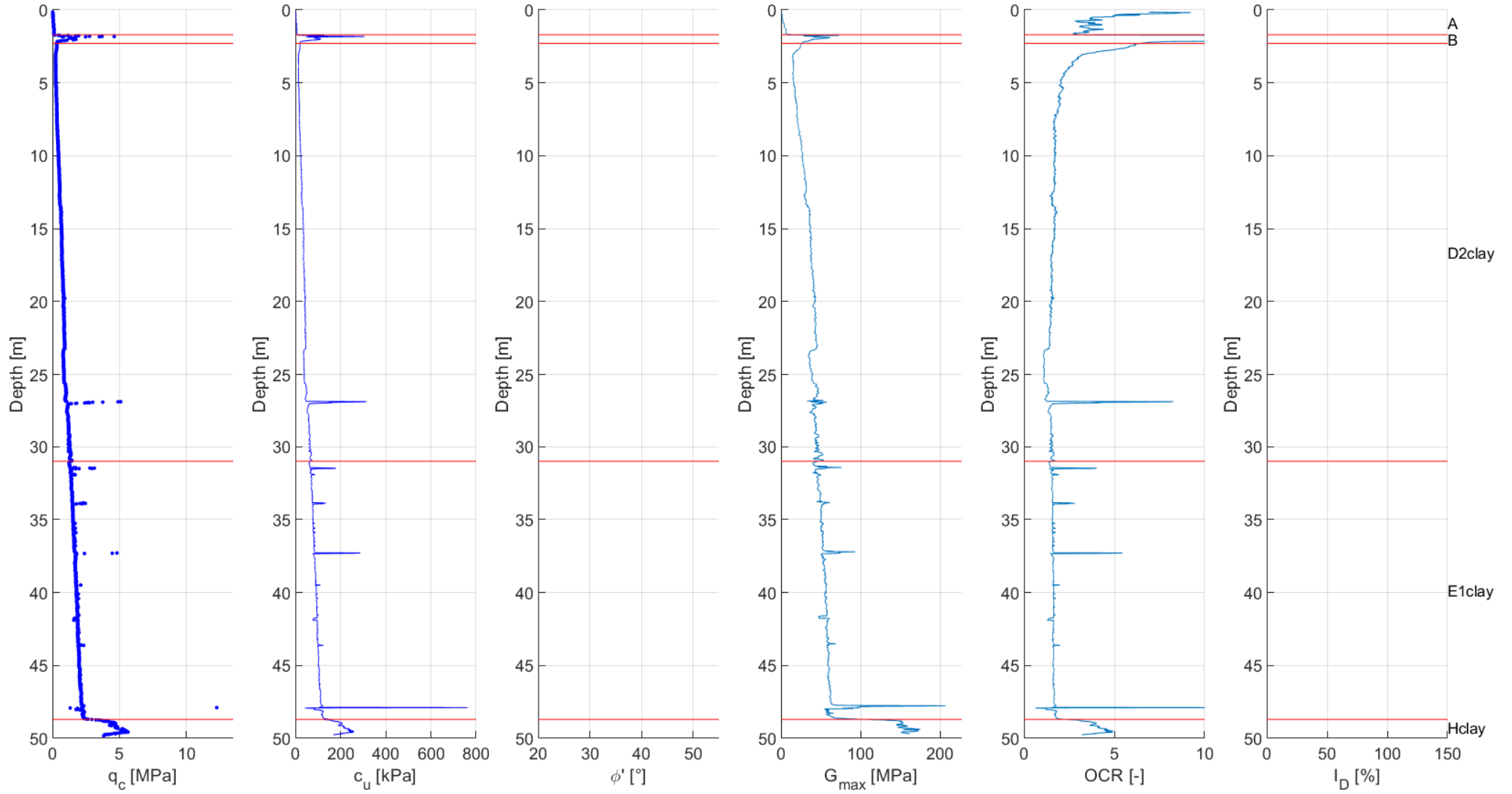
CPT22
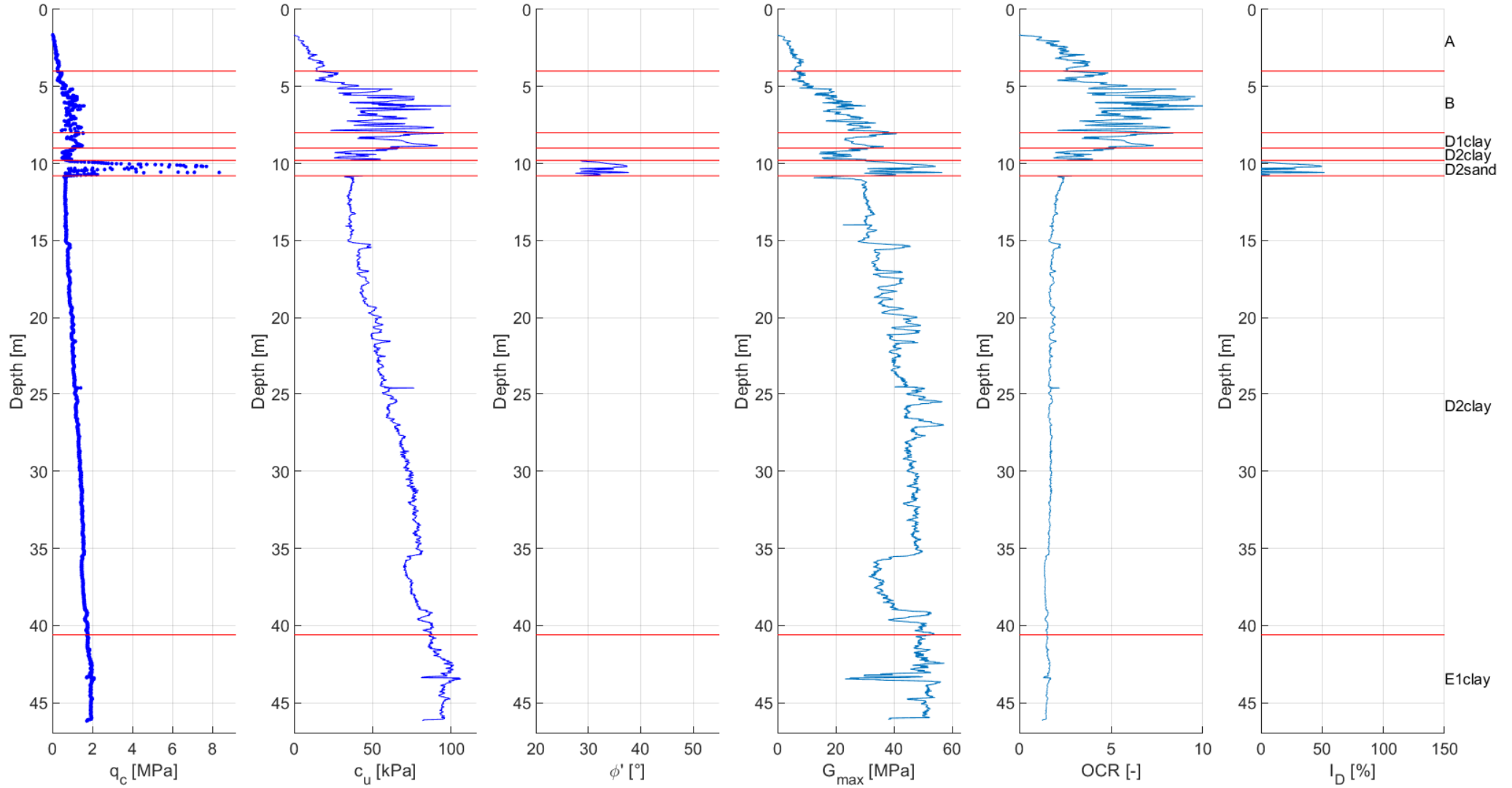
CPT23
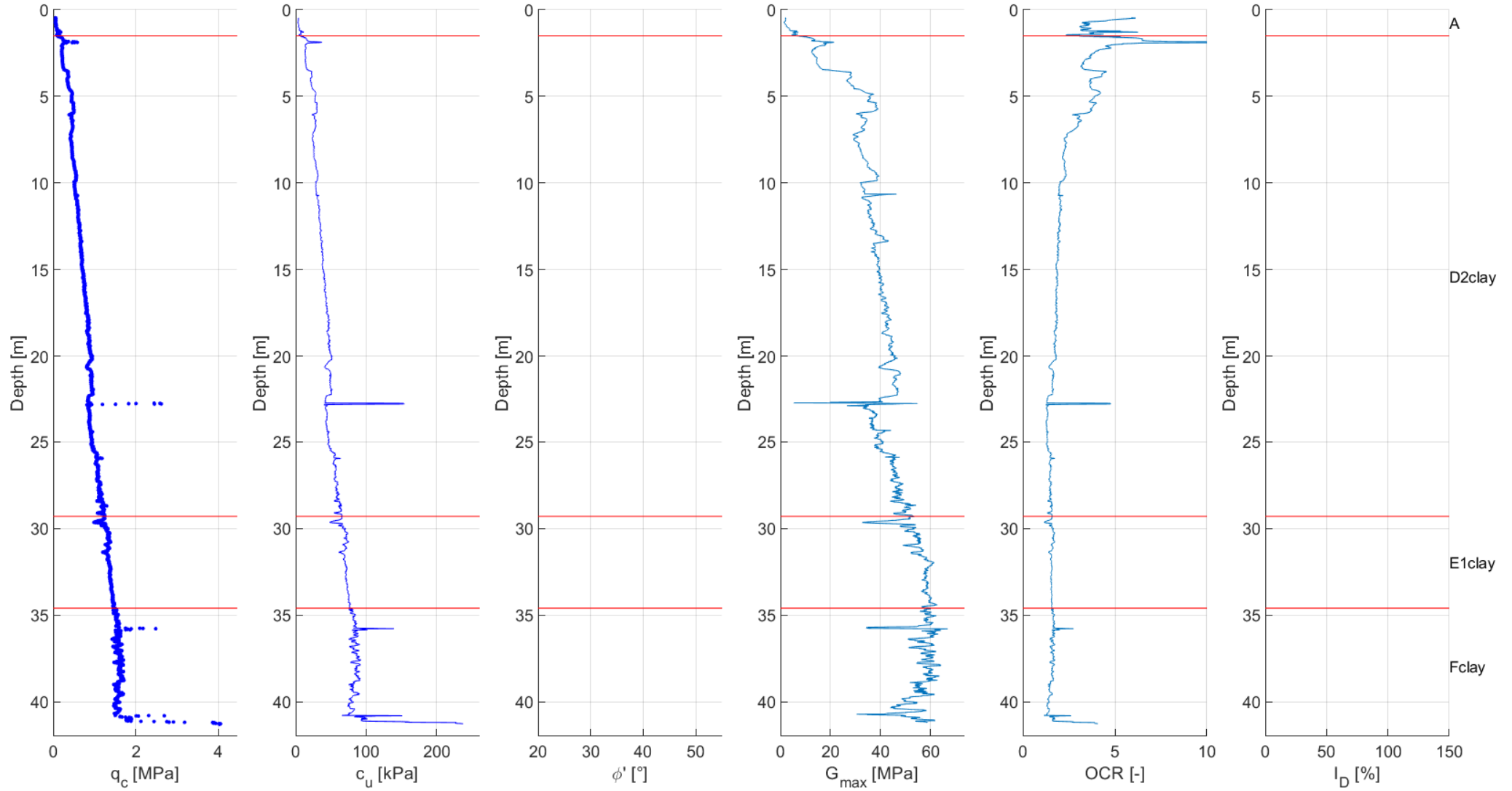
CPT25 /CPT25a /CPT25b
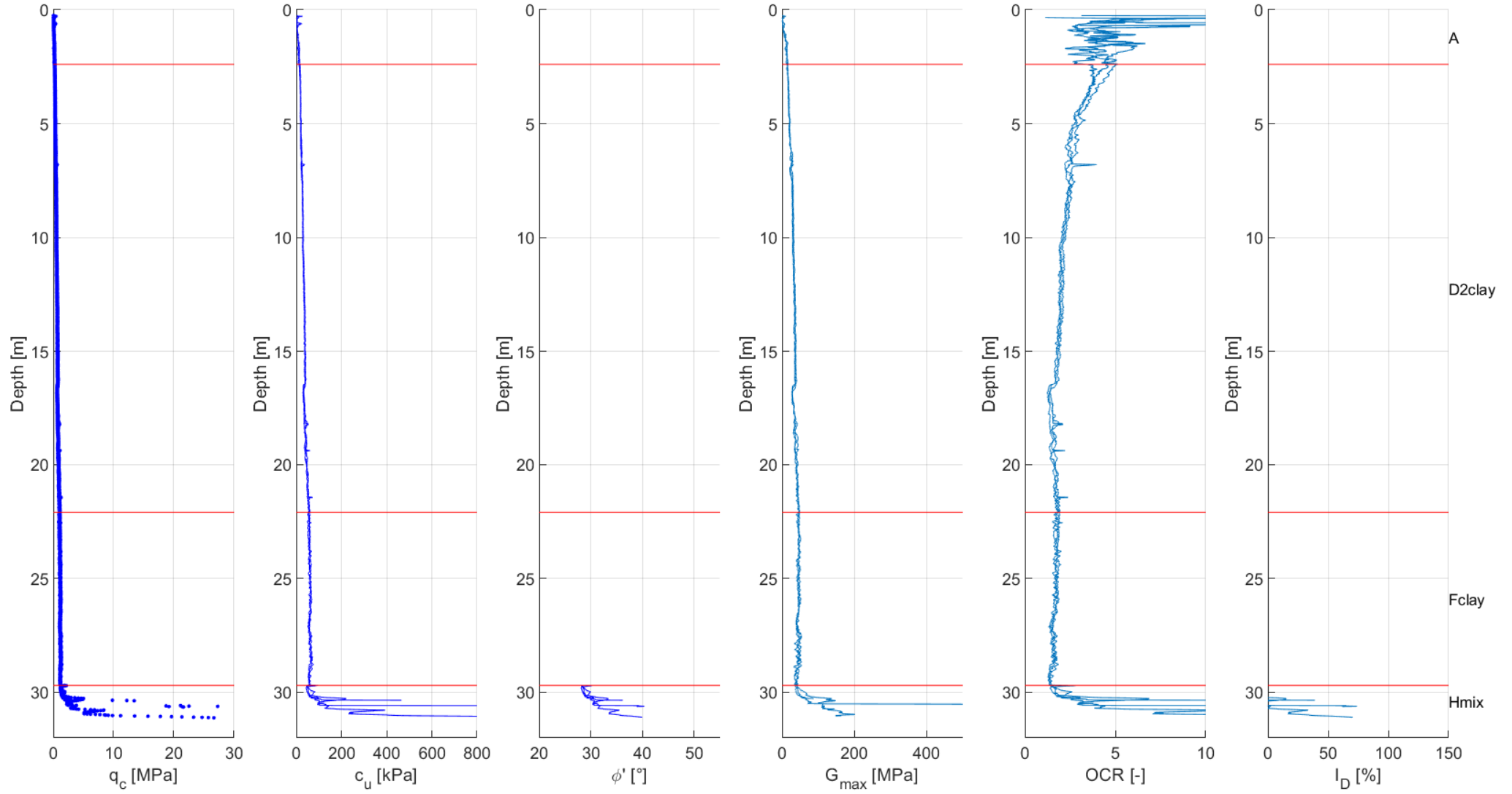
CPT26
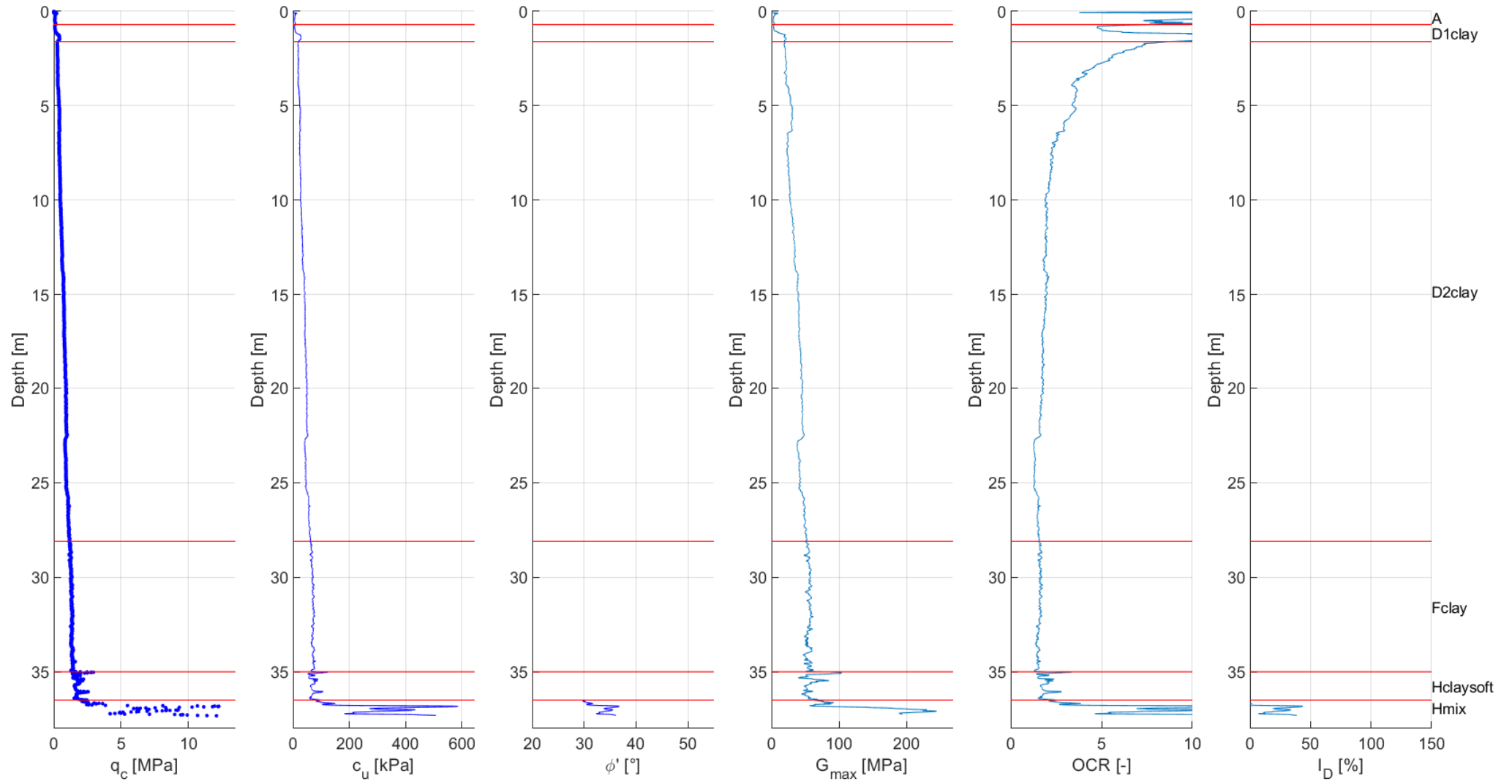
OSS1-BH /OSS$_1$ /OSS$_1$a
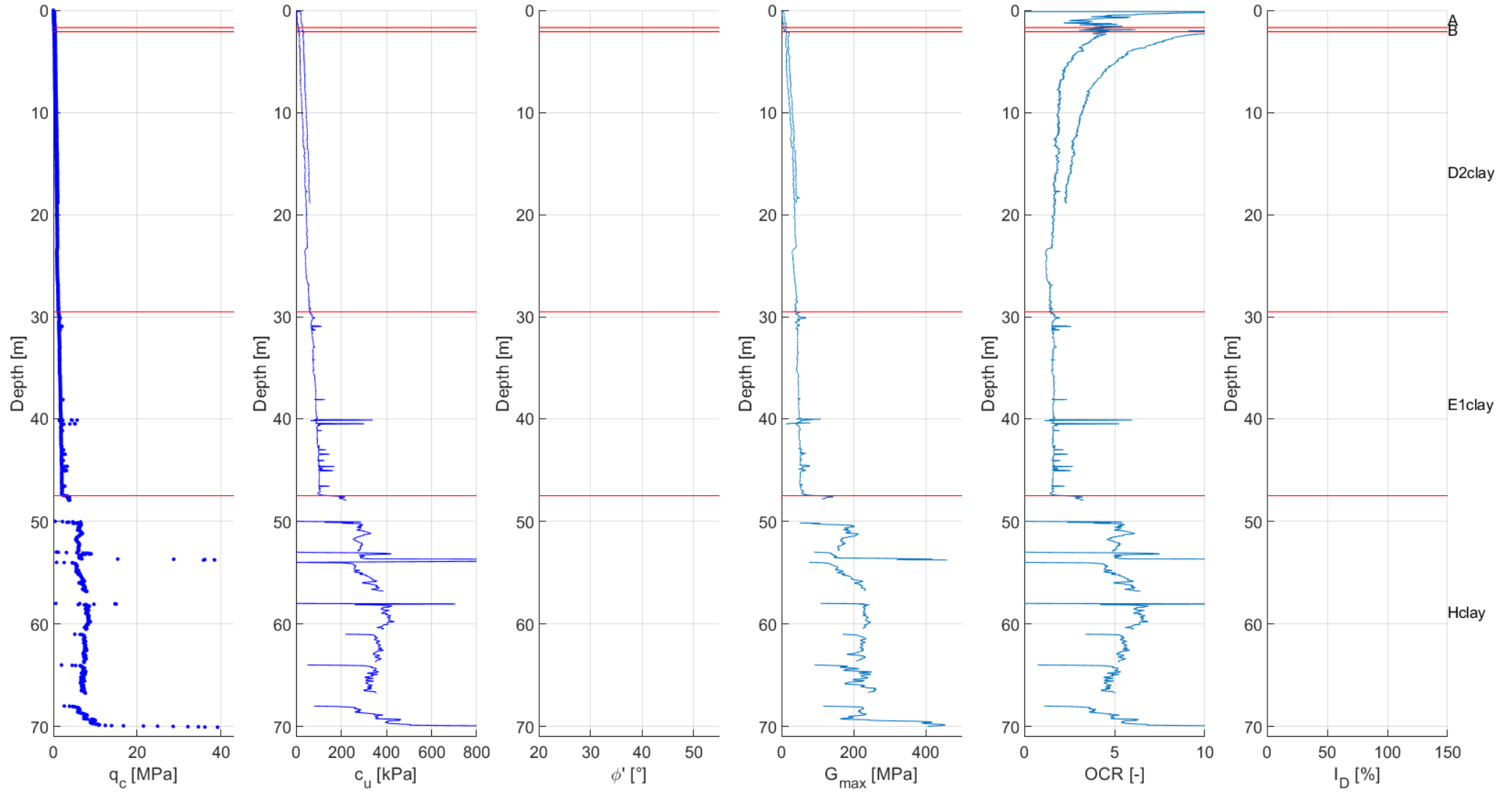
OSS2-BH /OSS$_2$
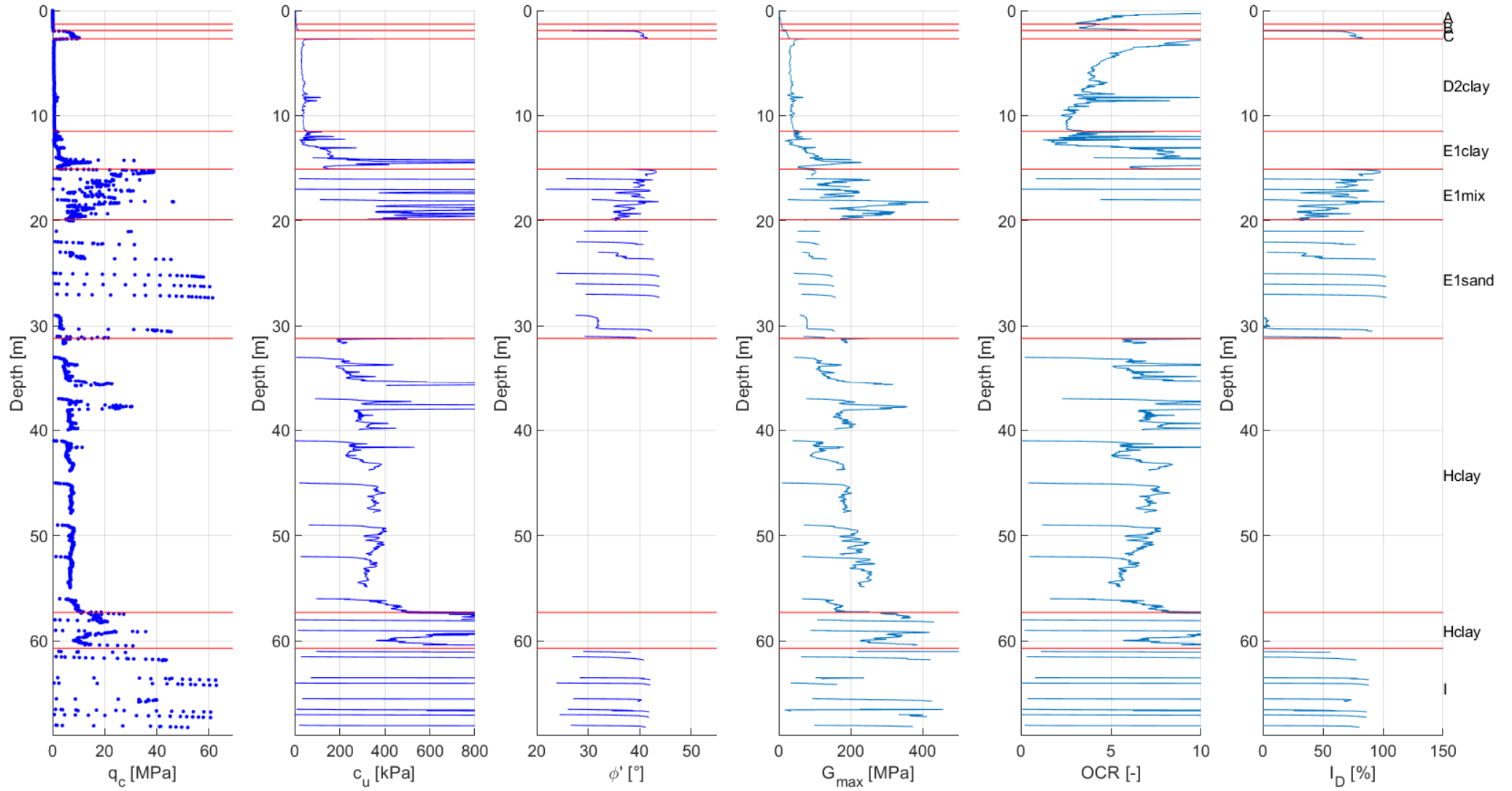
SCPT1 /SCPT1a
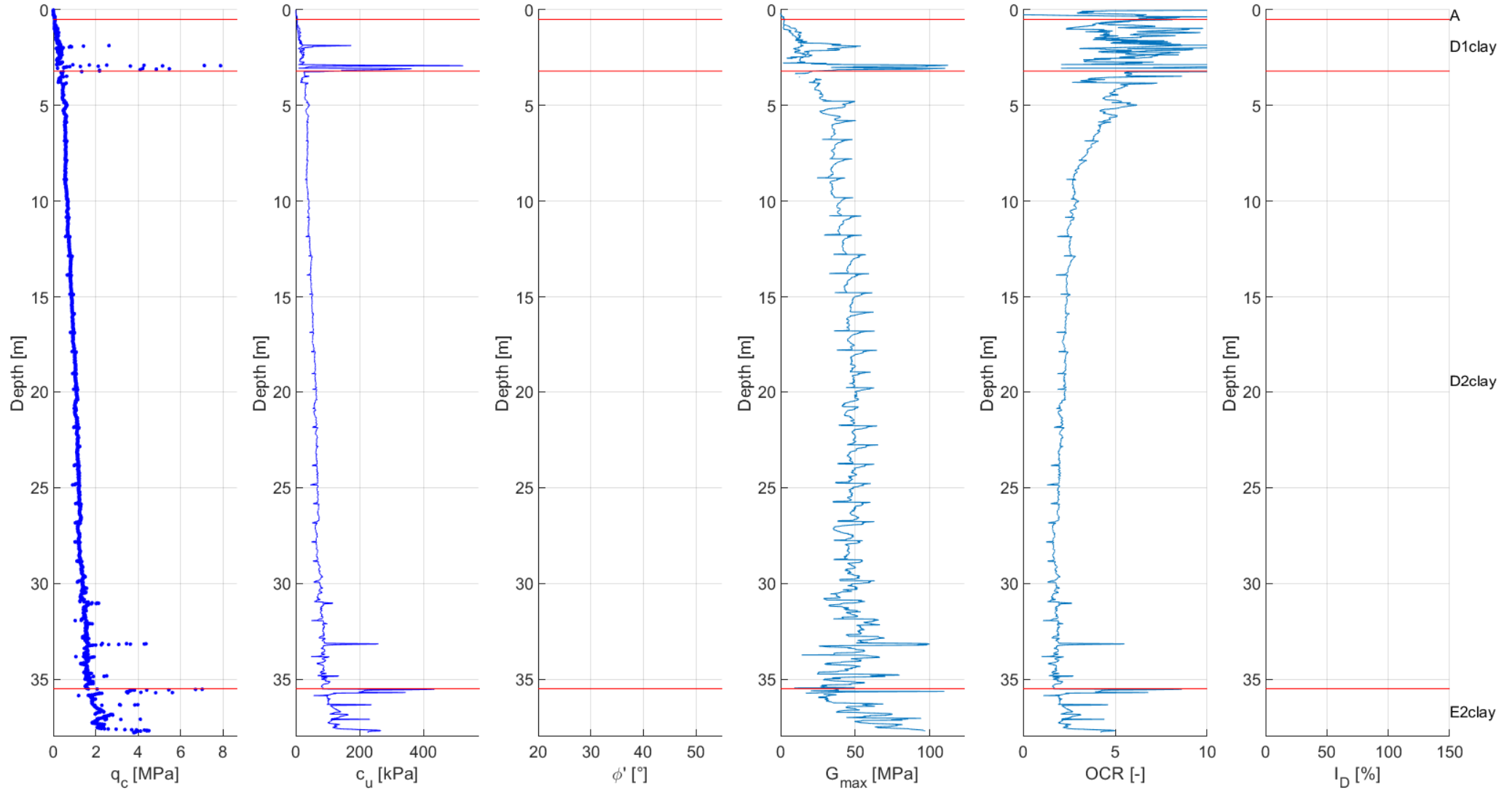
SCPT2
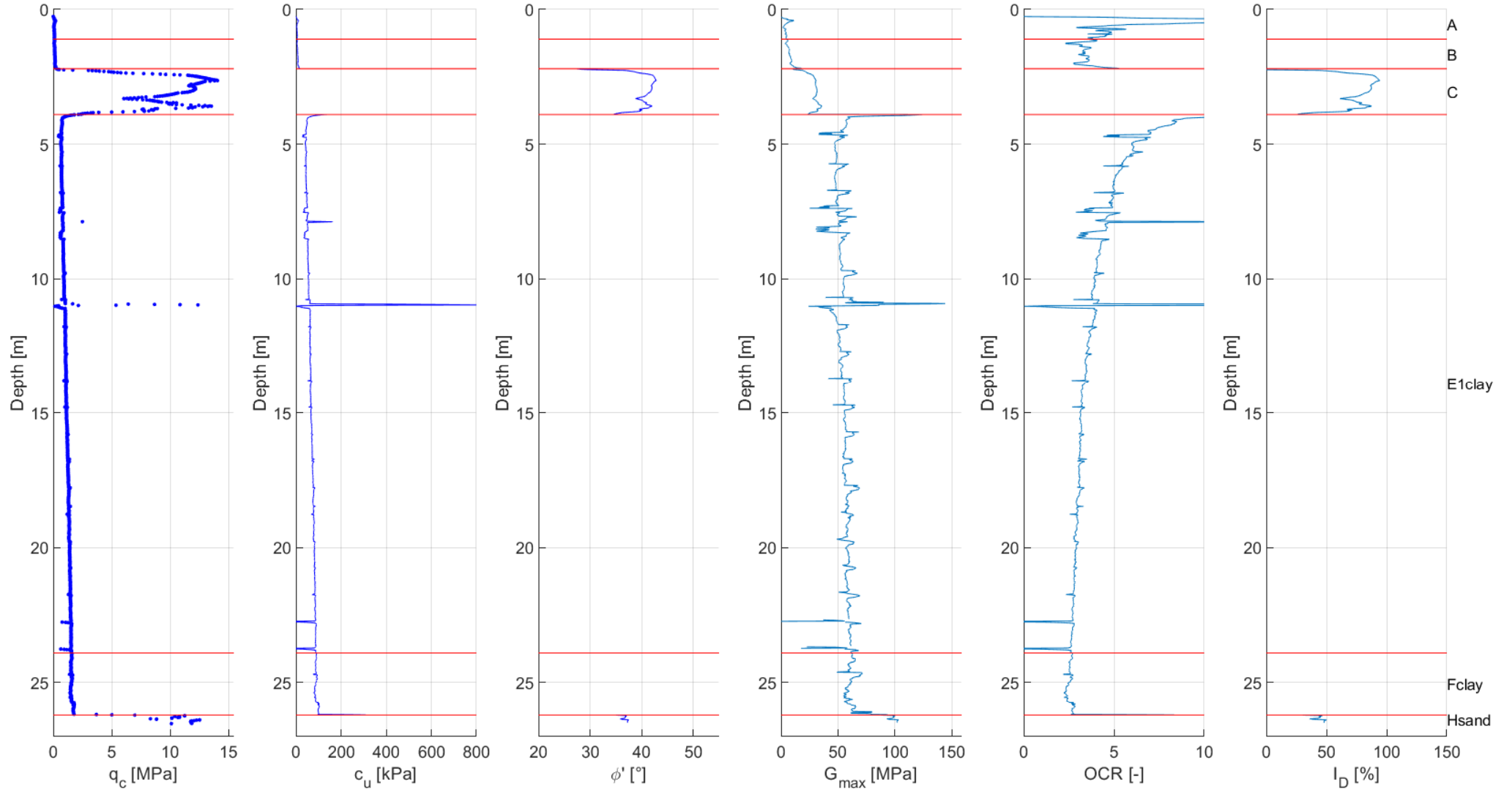
SCPT5
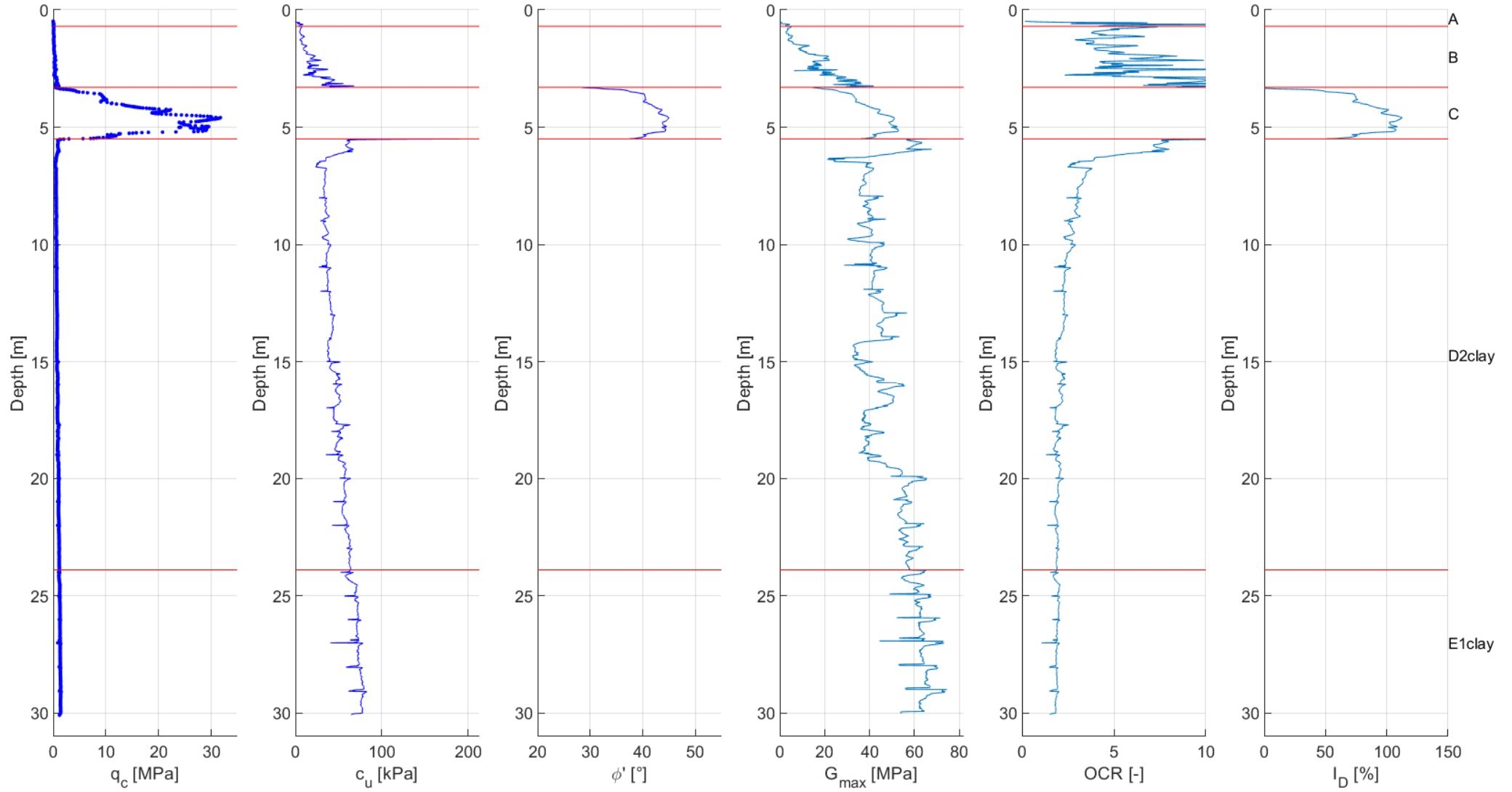
SCPT17
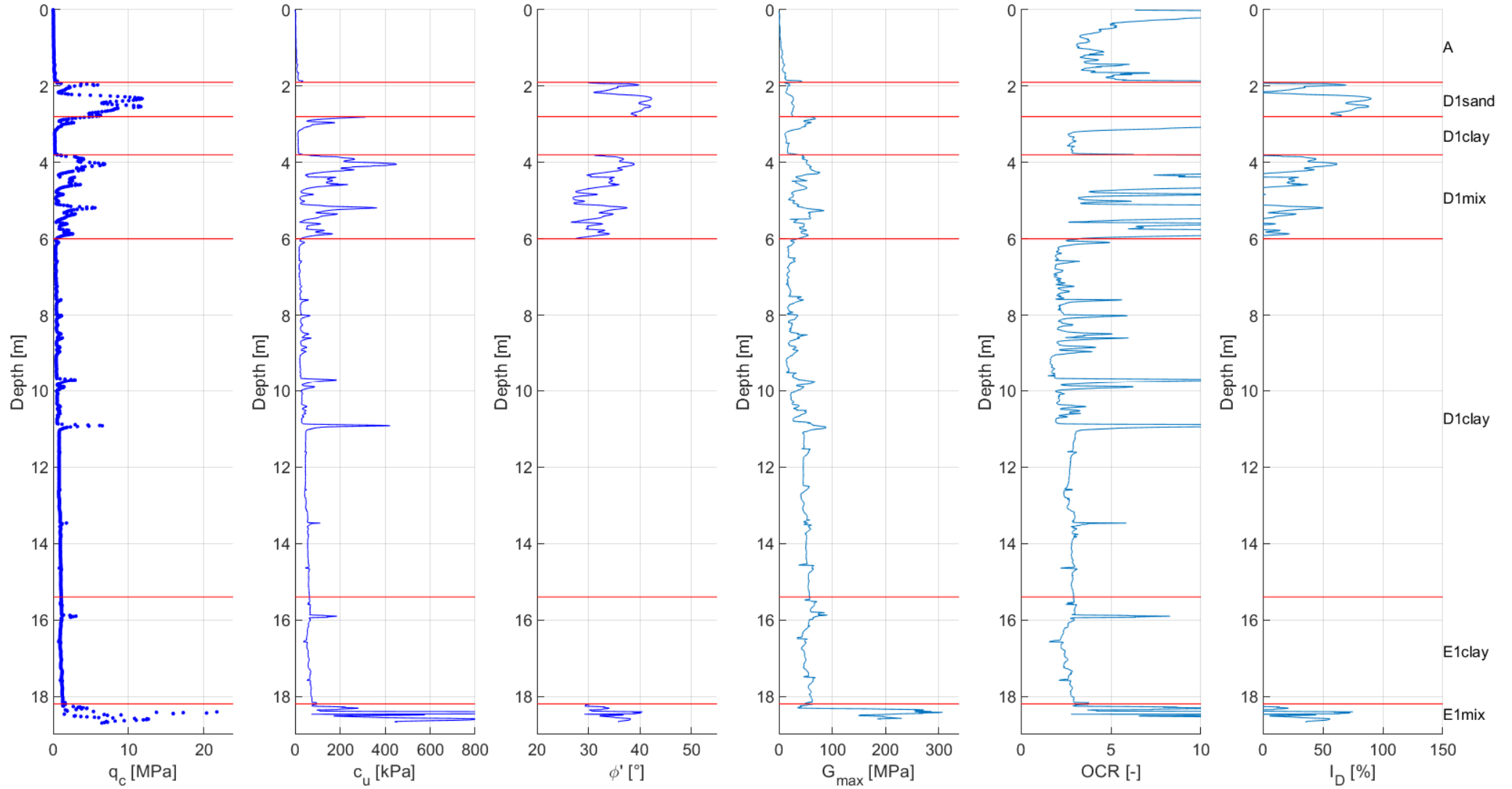
SCPT19
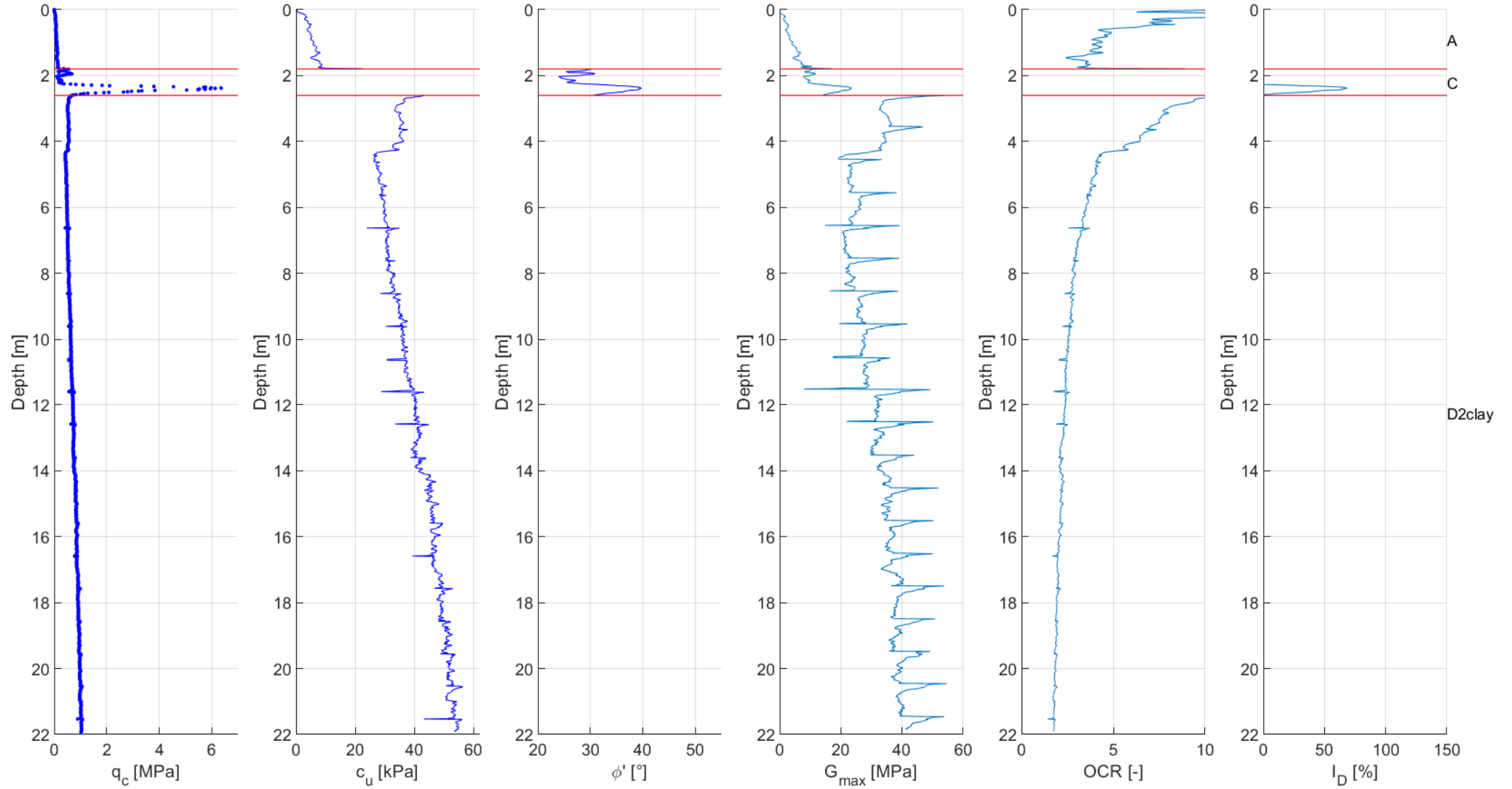
SCPT21
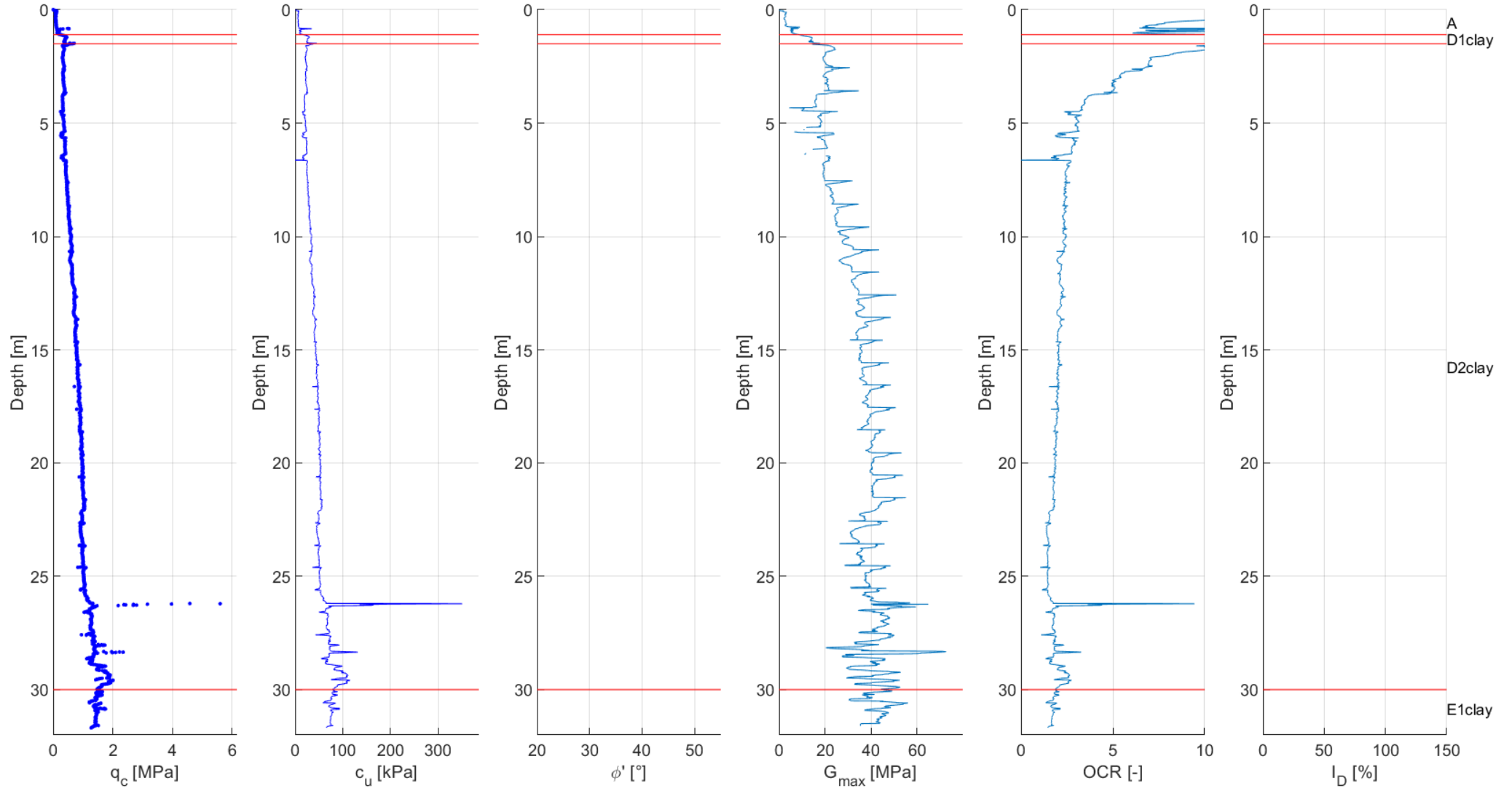
SCPT24
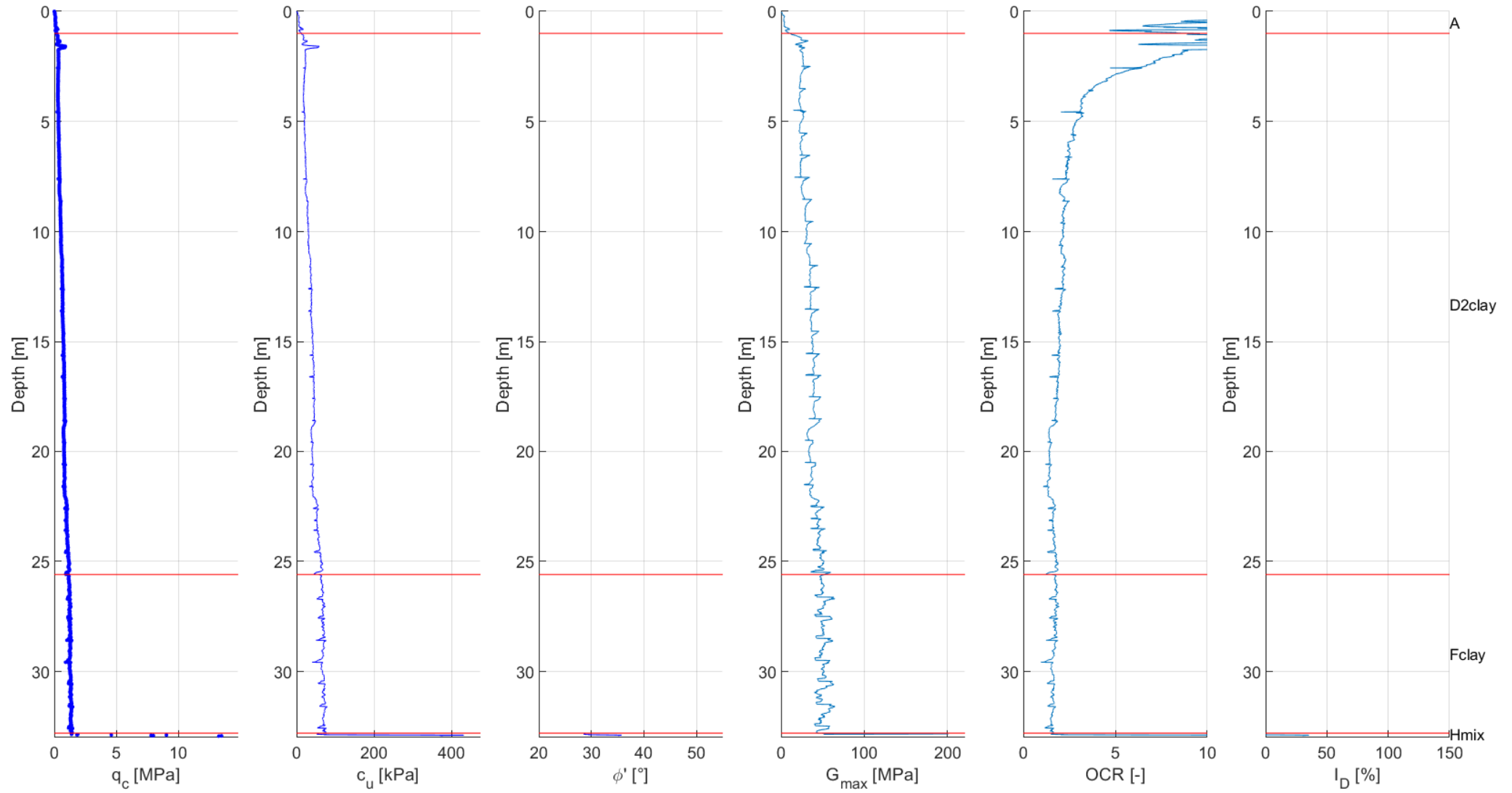
Appendix C   CPT plots per soil unit including properties from laboratory testing

C.1   Measured cone tip resistance and friction ratio
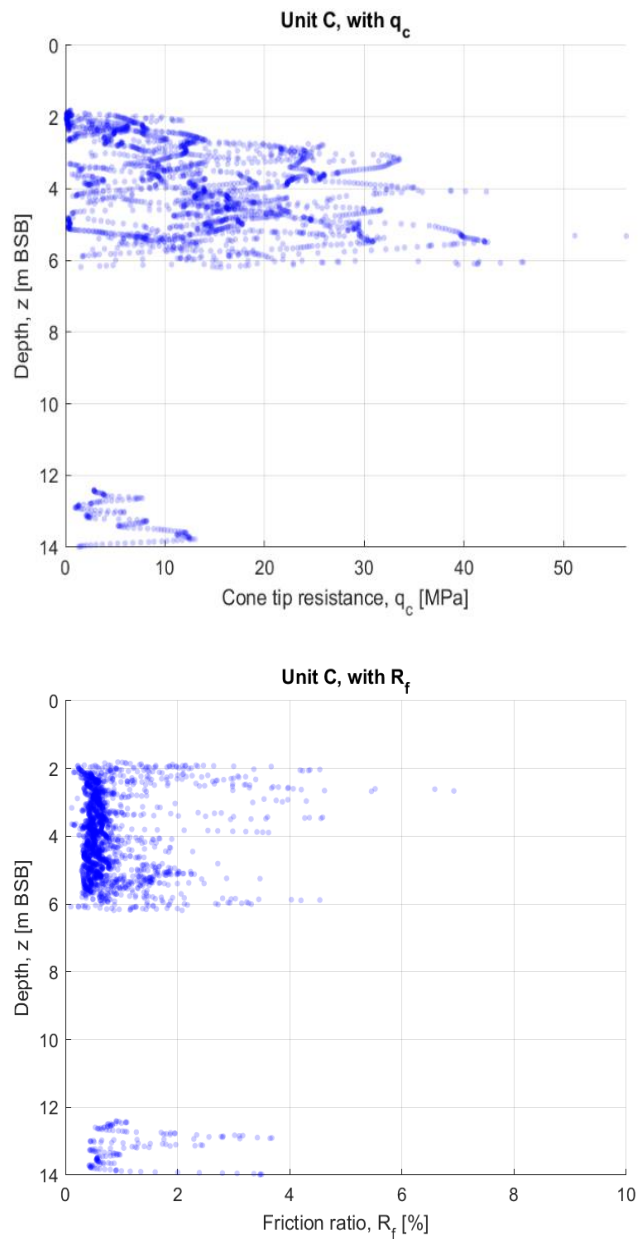
Figure 8.2-1   Range of q_c (upper) and R_f (lower) for geotechnical soil unit C.
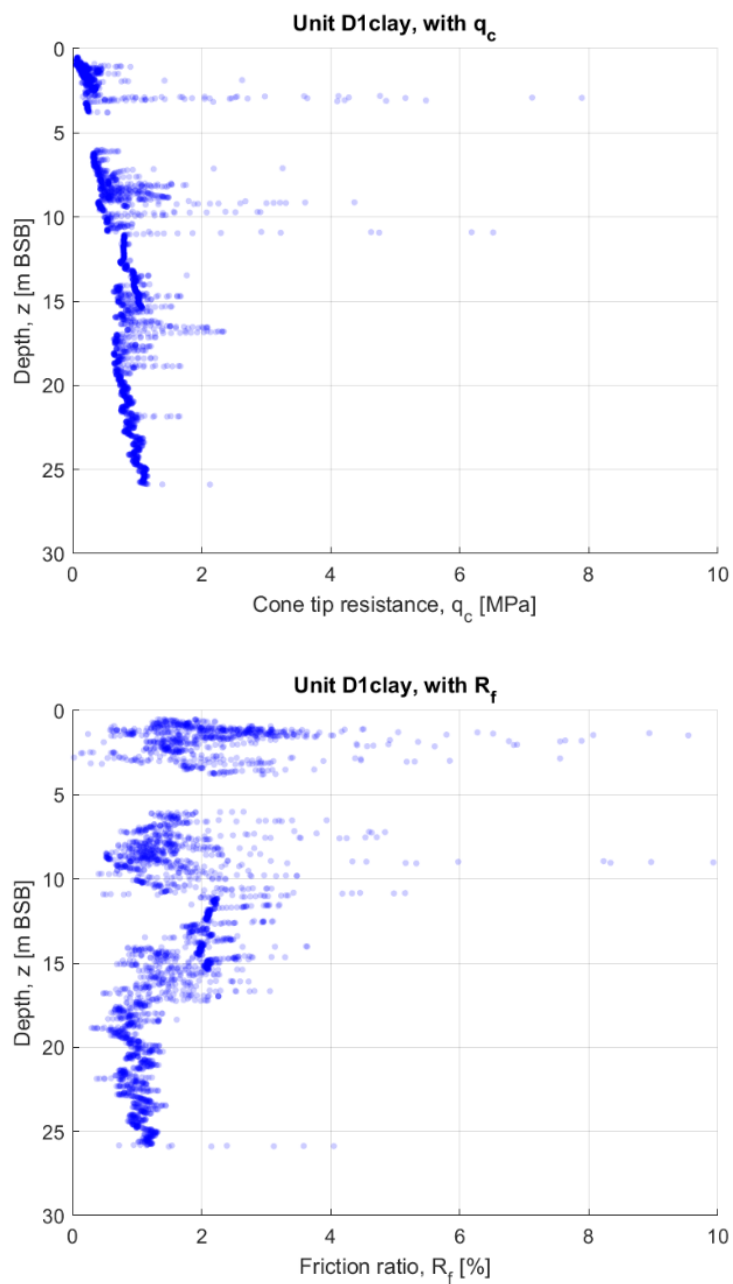
Figure 8.2-2   Range of q_c (upper) and R_f (lower) for geotechnical soil unit D1clay.
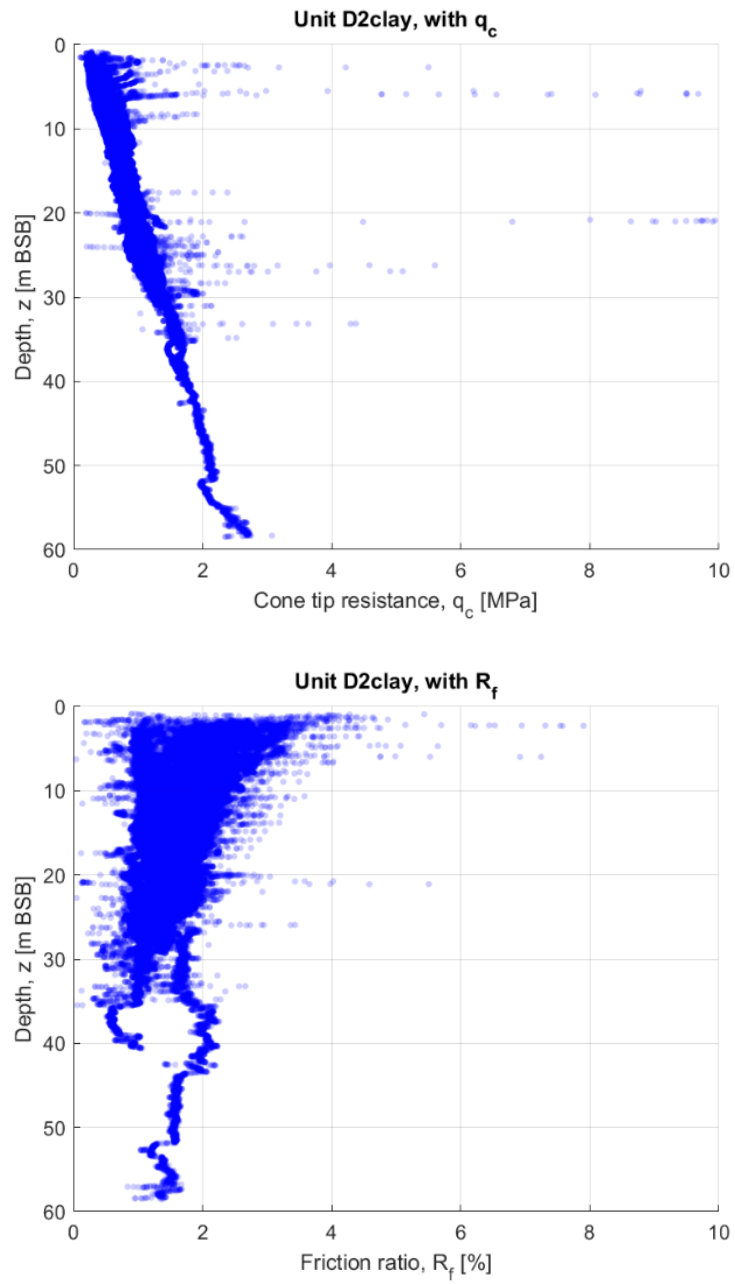
Figure 8.2-3   Range of q_c (upper) and R_f (lower) for geotechnical soil unit D2clay.
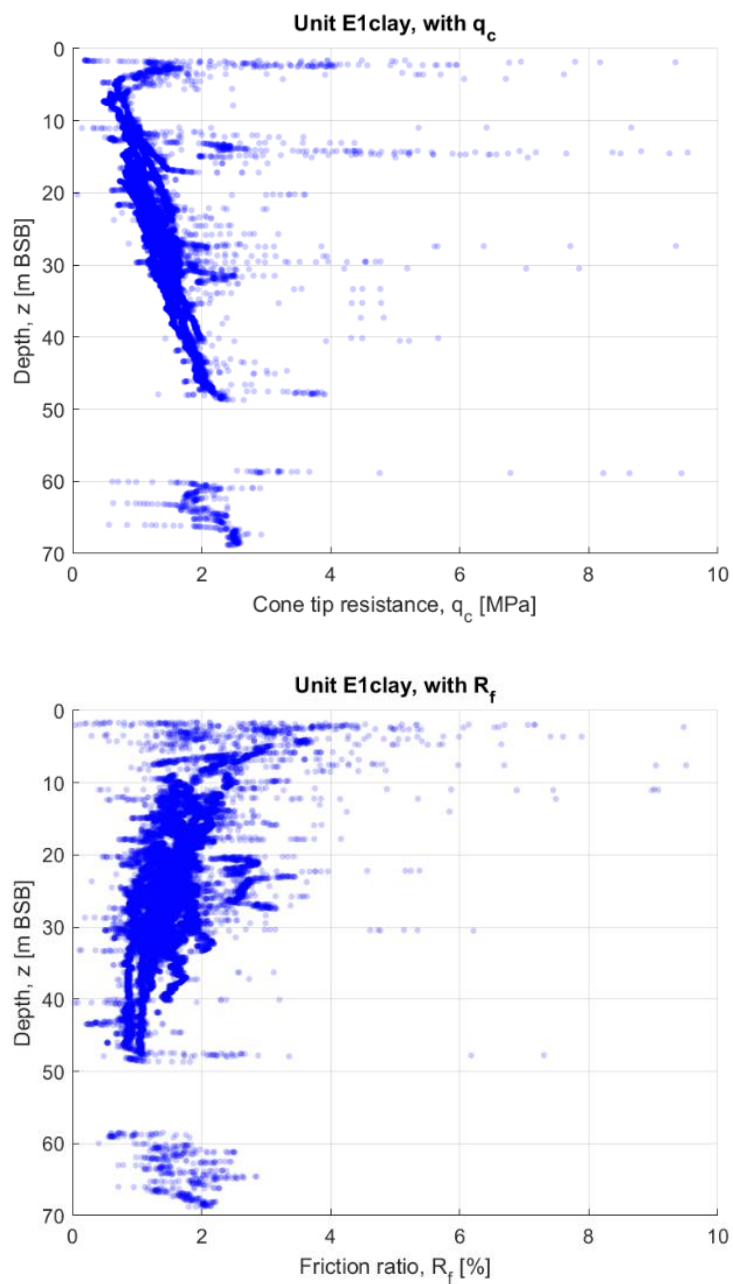
Figure 8.2-4   Range of q_c (upper) and R_f (lower) for geotechnical soil unit E1clay.

Unit E1sand, with q_c

Unit E1sand, with R_f
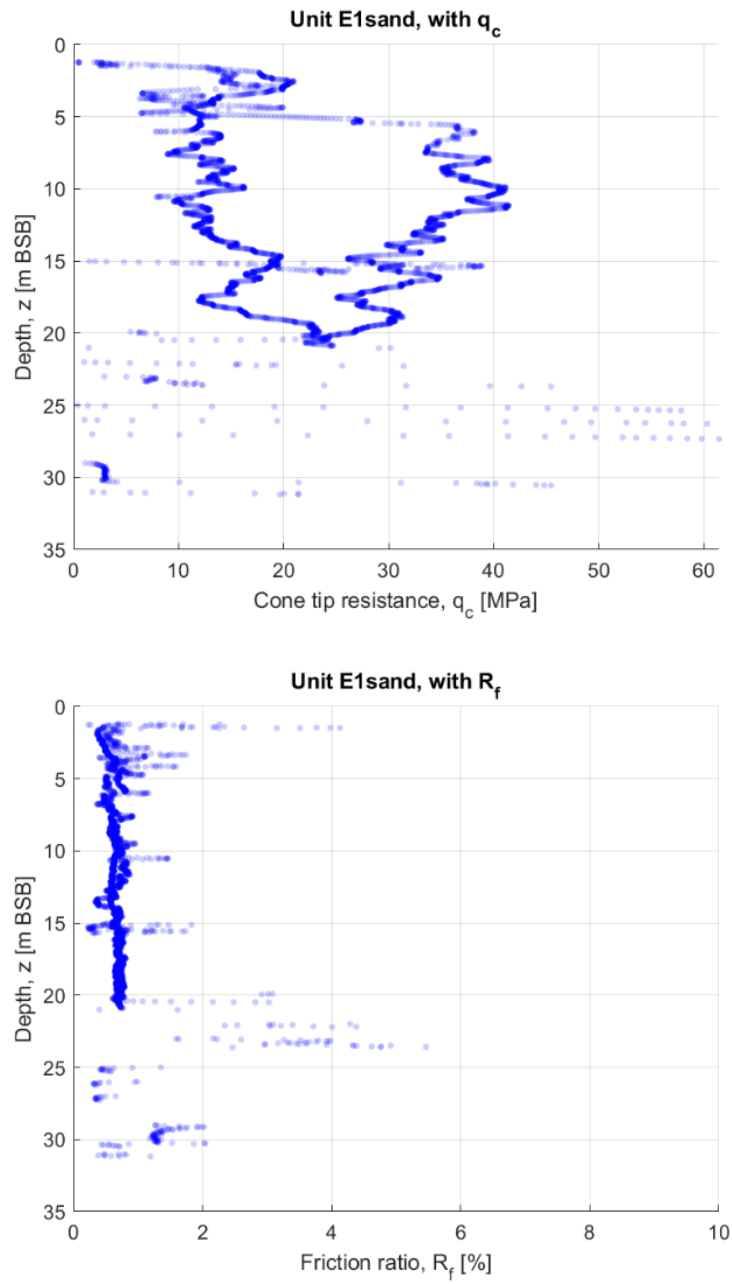
Figure 8.2-5   Range of q_c (upper) and R_f (lower) for geotechnical soil unit E1sand.
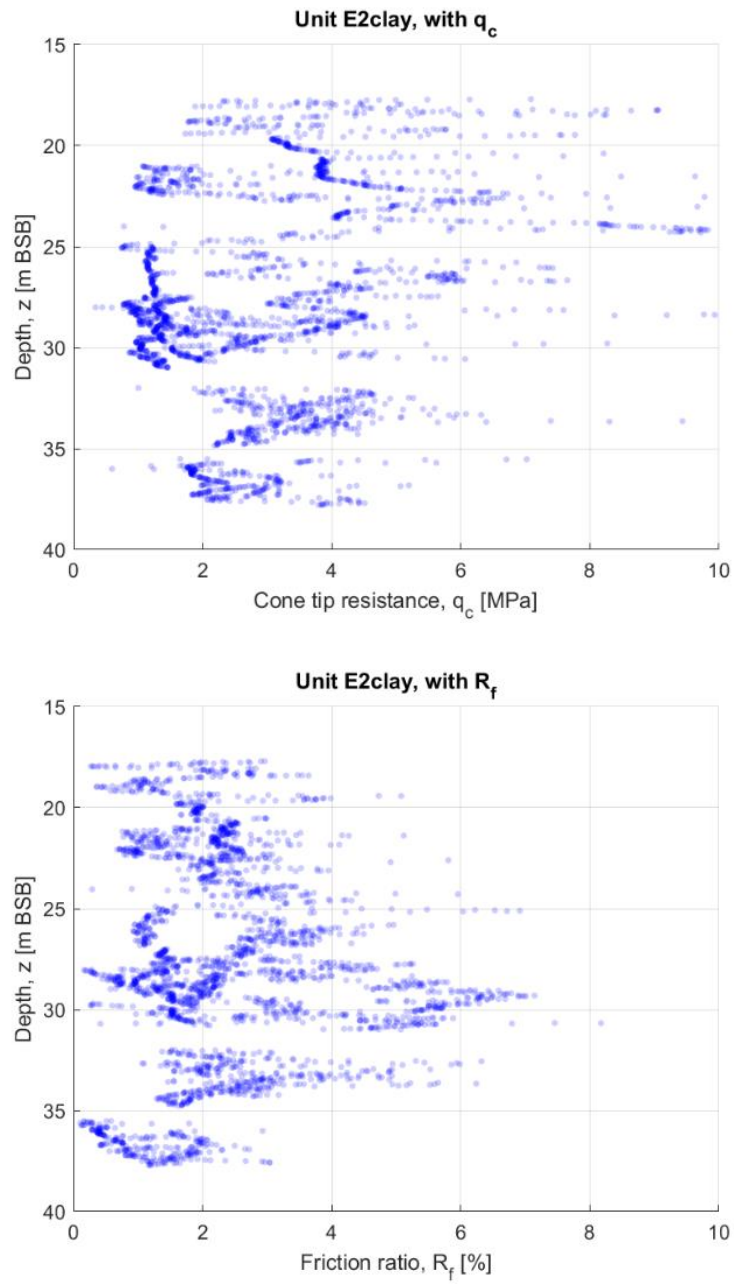
Figure 8.2-6   Range of q_c (upper) and R_f (lower) for geotechnical soil unit E2clay.
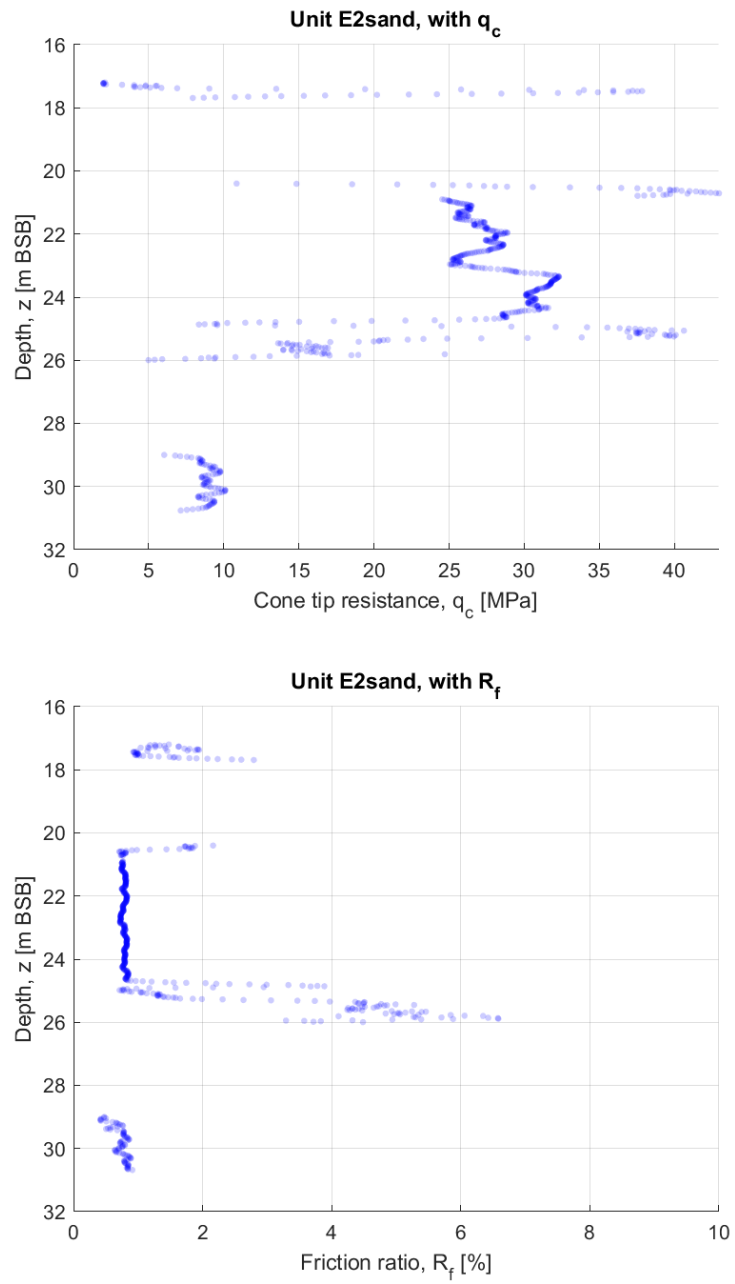
Figure 8.2-7   Range of q_c (upper) and R_f (lower) for geotechnical soil units E2sand.
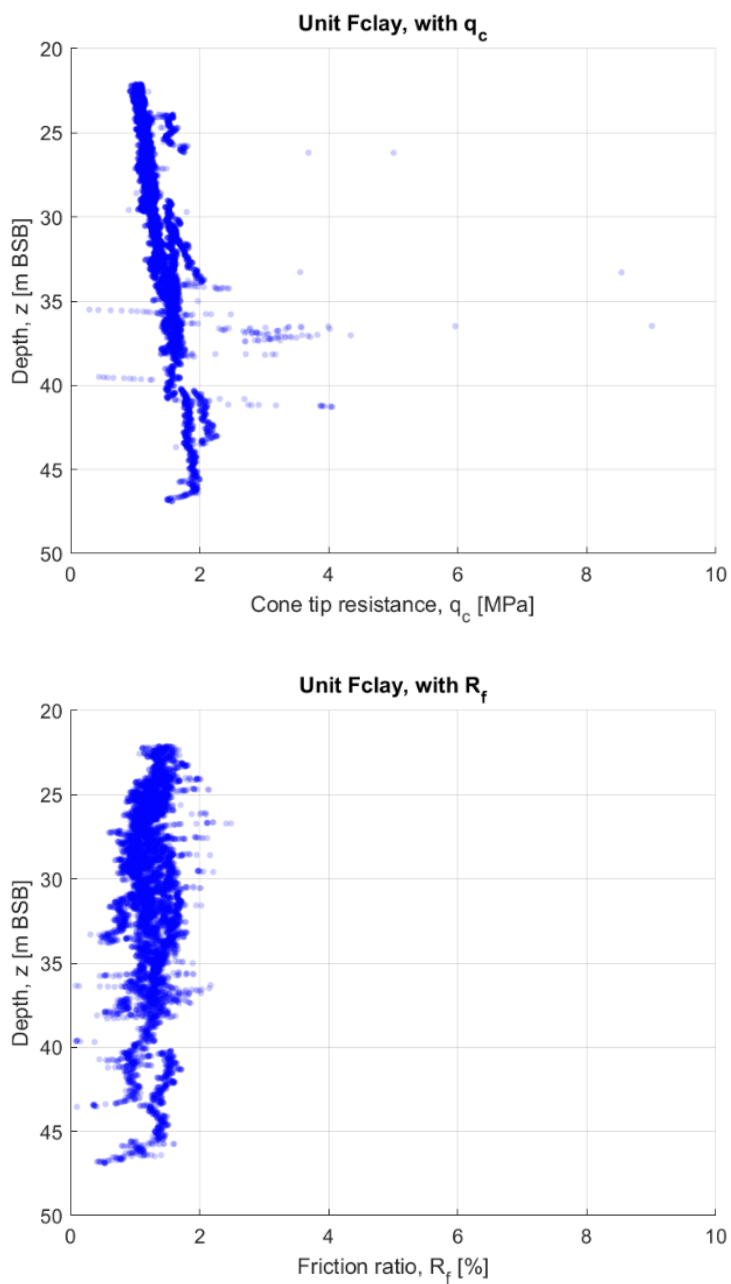
Figure 8.2-8   Range of q_c (upper) and R_f (lower) for geotechnical soil unit Fclay.
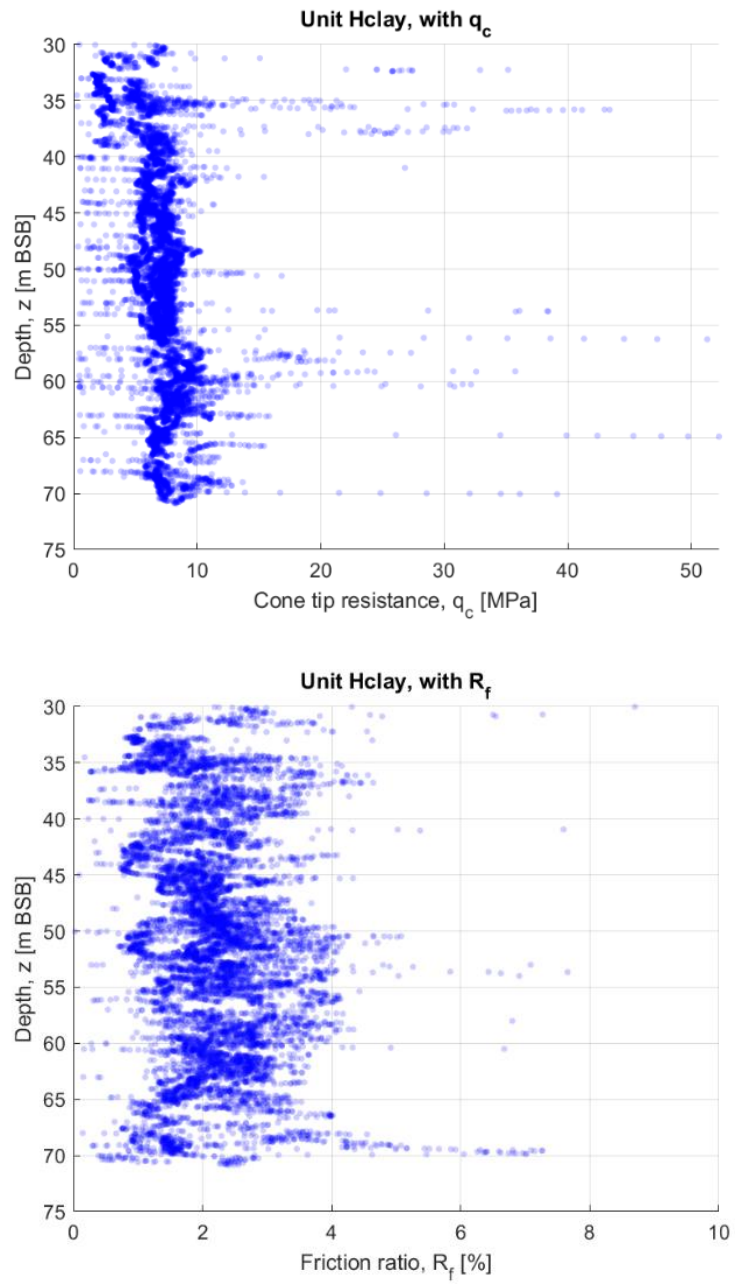
Figure 8.2-9   Range of q_c (upper) and R_f (lower) for geotechnical soil units Hclay

C.2   Overconsolidation ratio
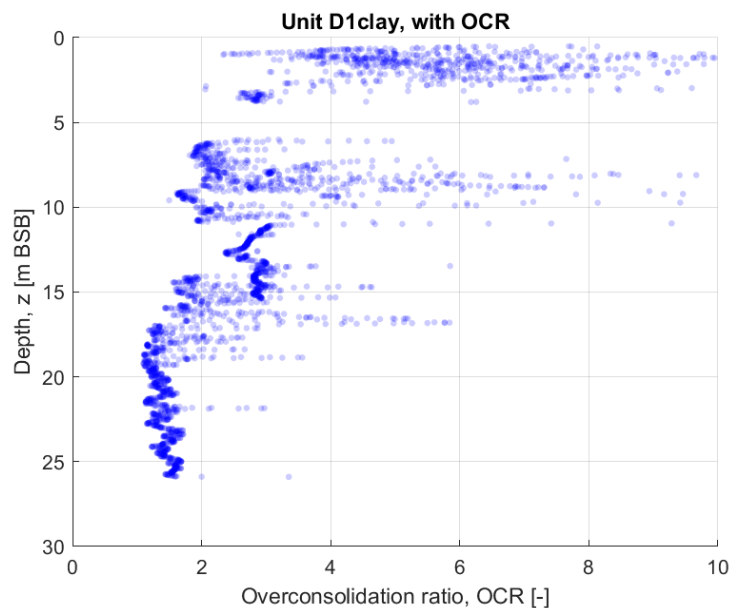
Figure 8.2-10   Range of OCR for geotechnical soil unit D1clay.
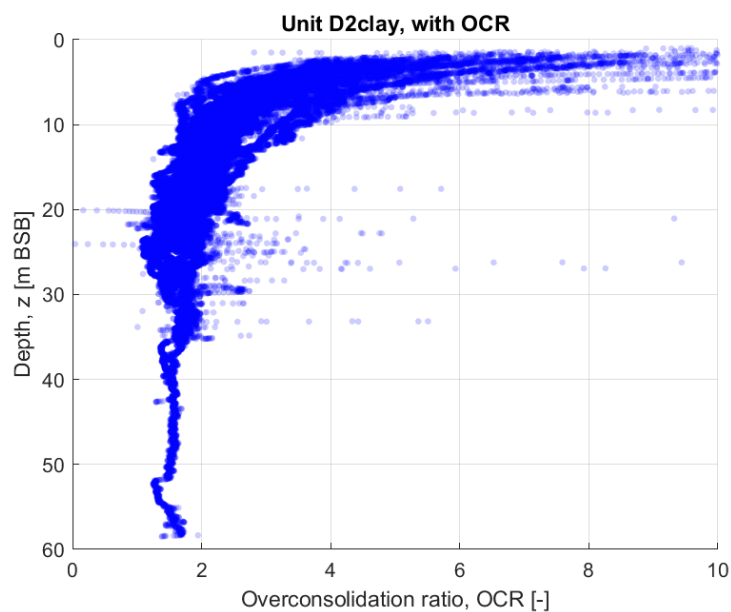
Figure 8.2-11   Range of OCR for geotechnical soil unit D2clay.
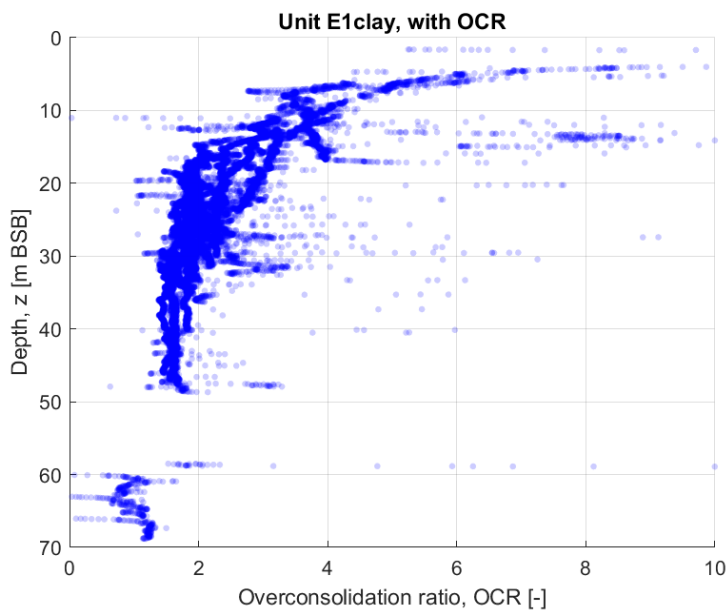
Figure 8.2-12   Range of OCR for geotechnical soil unit E1clay.
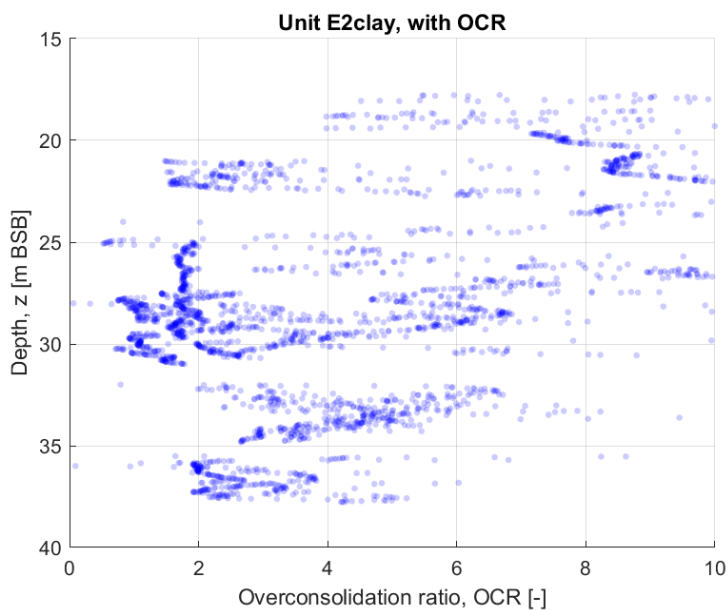
Figure 8.2-13   Range of OCR for geotechnical soil unit E2clay.
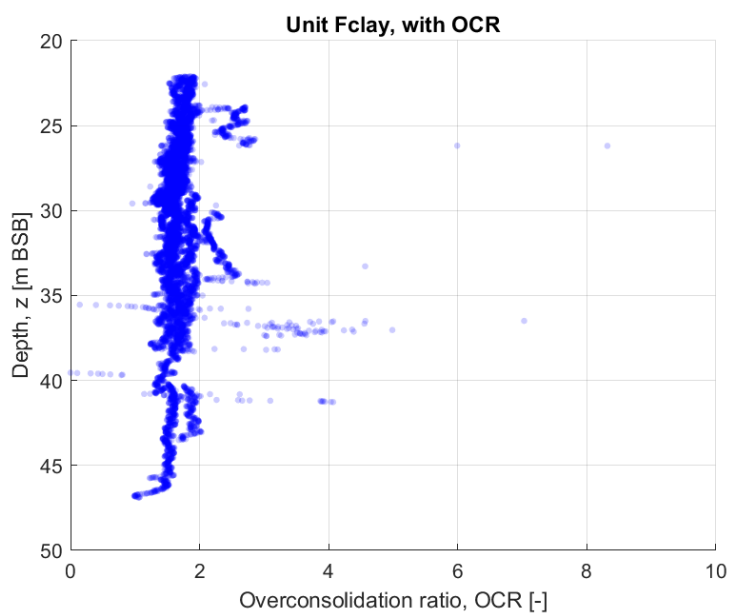
Figure 8.2-14   Range of OCR for geotechnical soil unit Fclay.
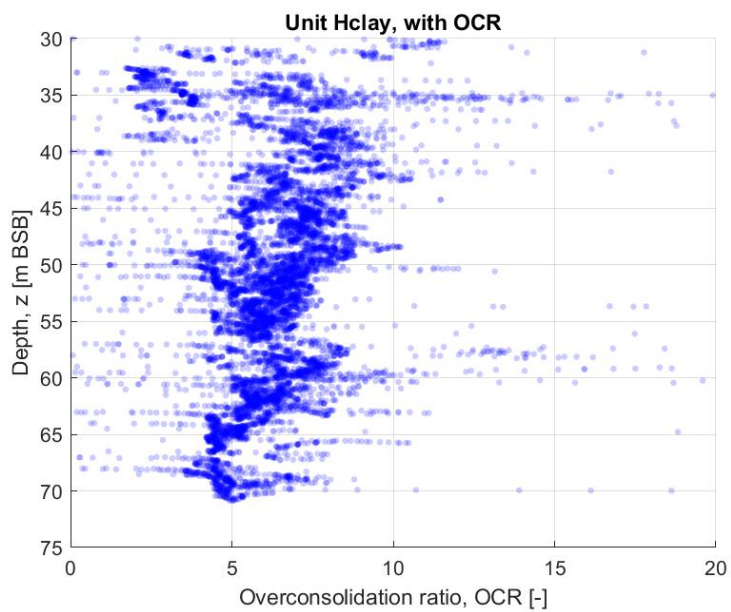
Figure 8.2-15   Range of OCR for geotechnical soil unit Hclay.

C.3   Relative density
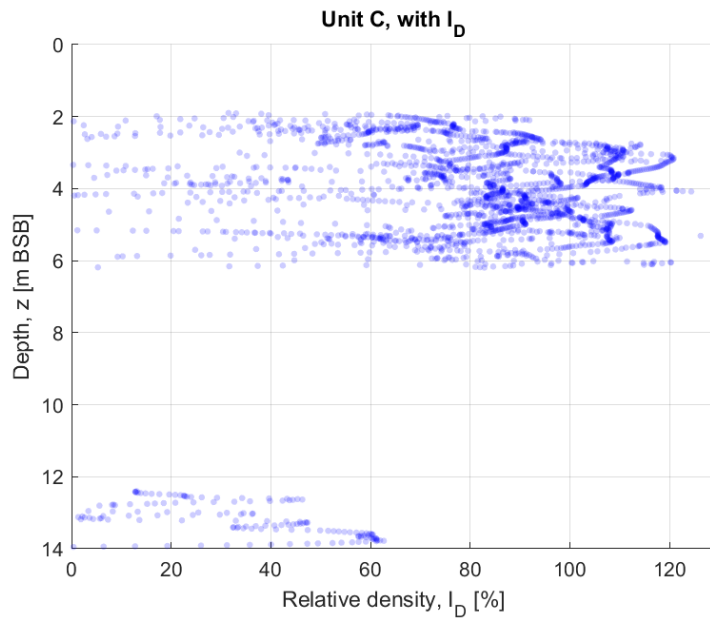
Figure 8.2-16   Range of I_D for geotechnical soil unit C.
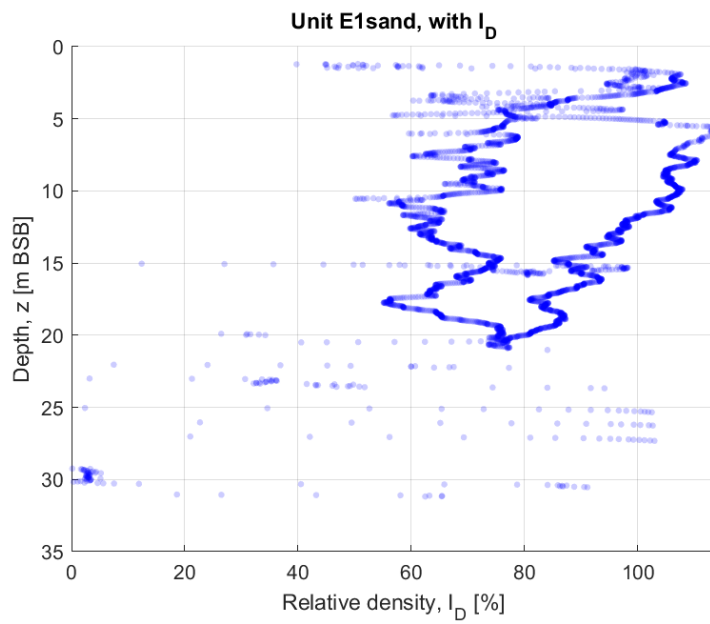
Figure 8.2-17   Range of I_D for geotechnical soil unit E1sand.
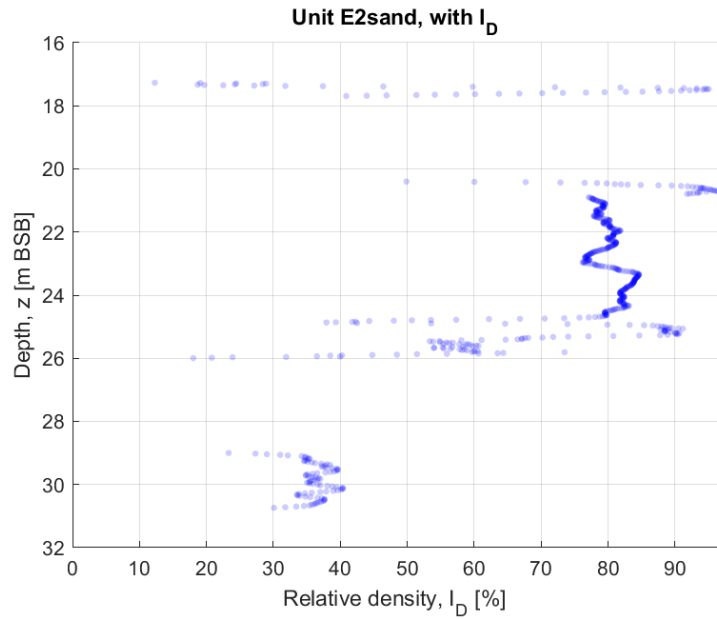
Figure 8.2-18   Range of I_D for geotechnical soil unit E2sand.

C.4   Friction angle
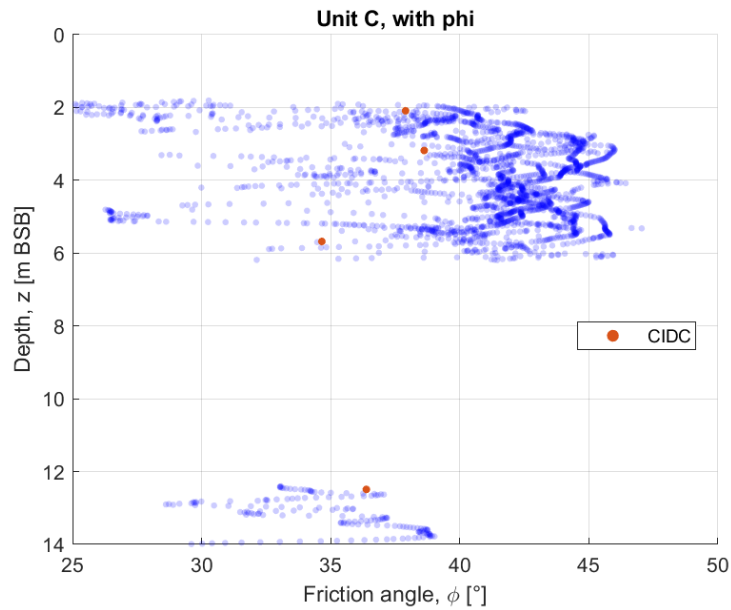
Figure 8.2-19   Range of φ for soil unit C using CPT correlation and laboratory test results (CD – Consolidated Drained triaxial test).
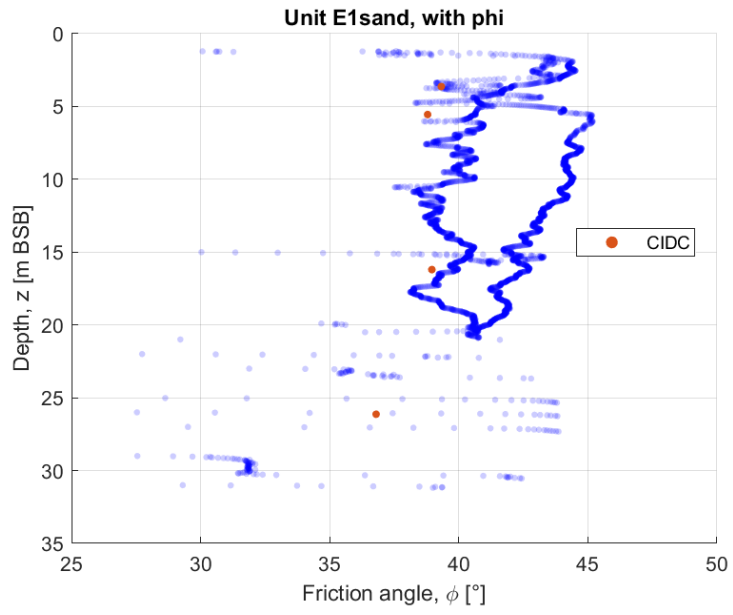
Figure 8.2-20   Range of φ for soil unit E1Sand using CPT correlation and laboratory test results (CD – Consolidated Drained triaxial test).
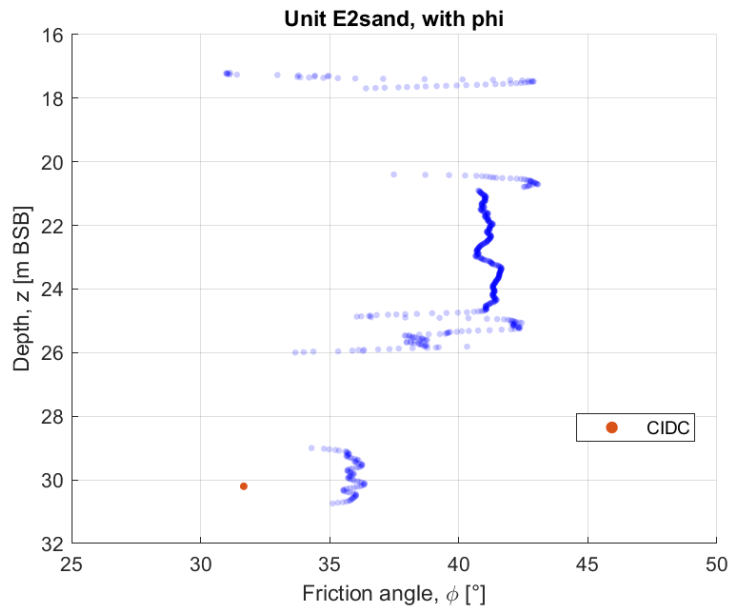
Figure 8.2-21   Range of φ for soil unit E2Sand using CPT correlation and laboratory test results (CD – Consolidated Drained triaxial test).

C.5   Undrained shear strength
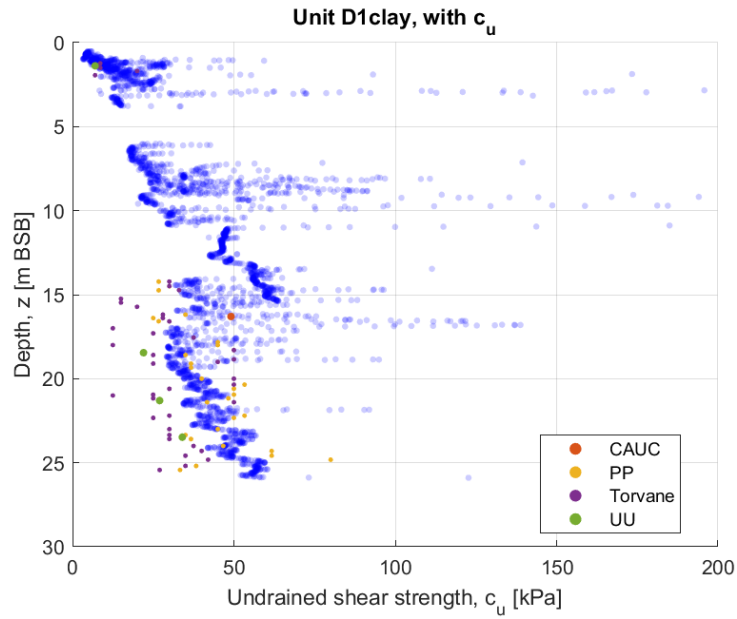
Figure 8.2-22   Range of c_u for the geotechnical soil unit D1clay using CPT correlation and laboratory test results. (CU denotes consolidated [Isotropically or Anisotropically] undrained triaxial tests).
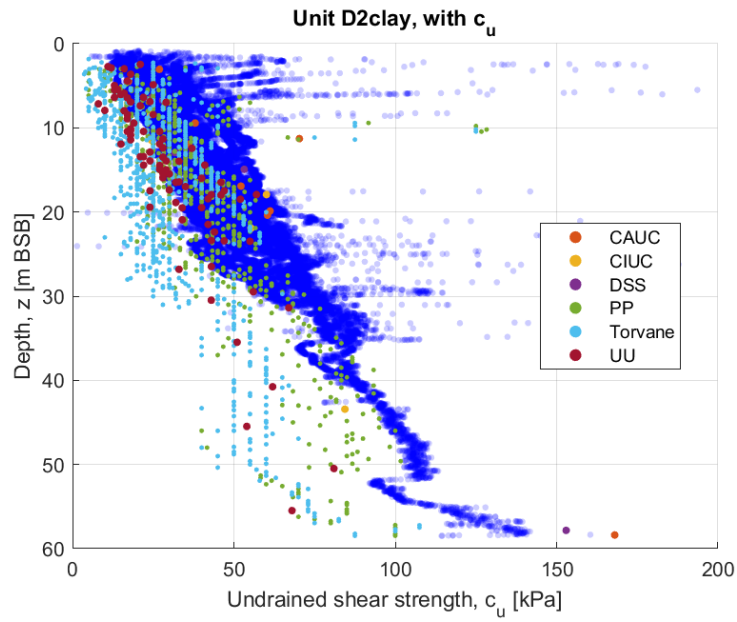
Figure 8.2-23   Range of c_u for the geotechnical soil unit D2clay using CPT correlation and laboratory test results. (CU denotes consolidated [Isotropically or Anisotropically] undrained triaxial tests).
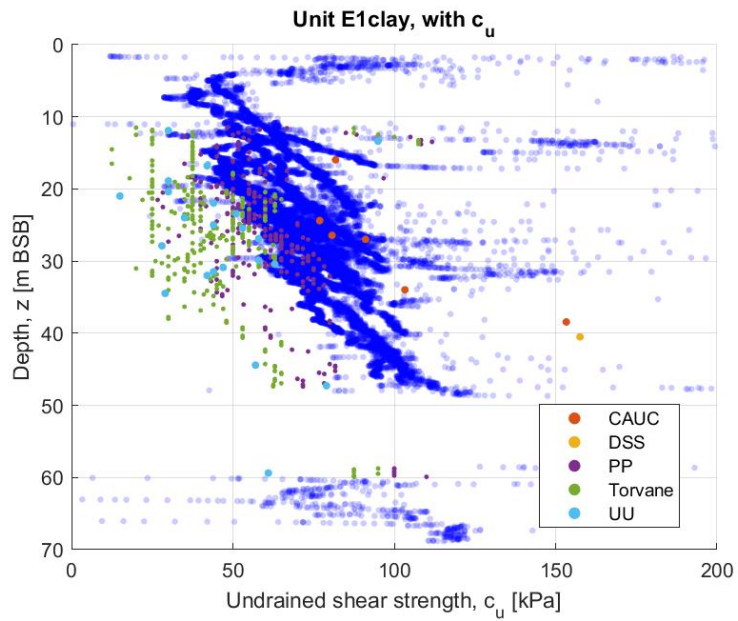
Figure 8.2-24   *Range of c_u for the geotechnical soil unit E1clay using CPT correlation and laboratory test results. (CU denotes consolidated [Isotropically or Anisotropically] undrained triaxial tests).*
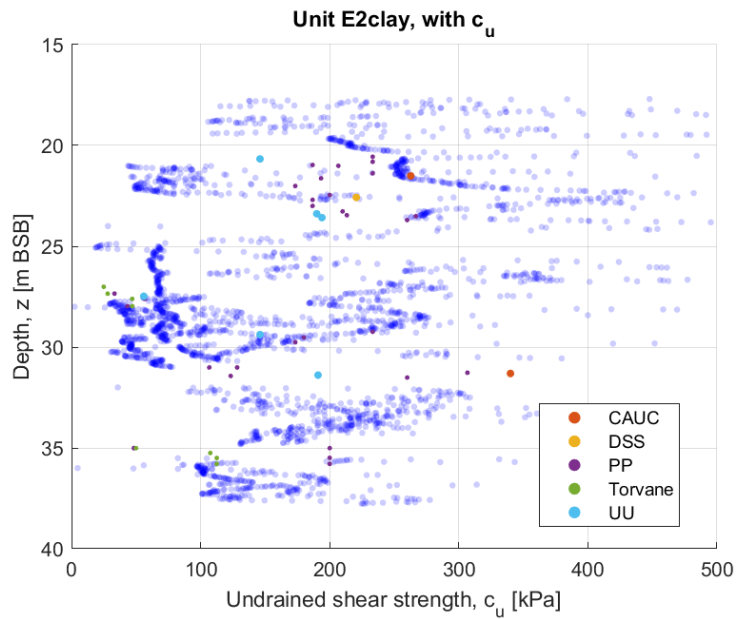
Figure 8.2-25   *Range of c_u for the geotechnical soil unit E2clay using CPT correlation and laboratory test results. (CU denotes consolidated [Isotropically or Anisotropically] undrained triaxial tests).*
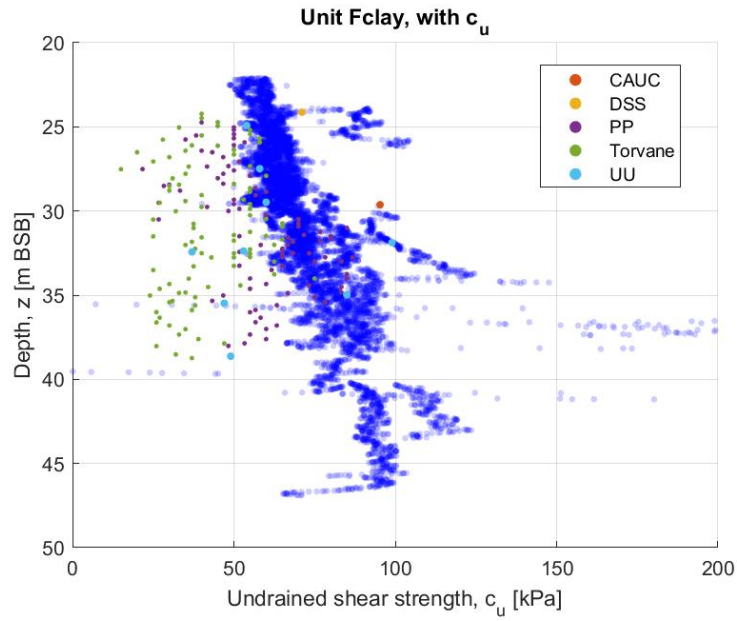
Figure 8.2-26   Range of c_u for the geotechnical soil unit Fclay using CPT correlation and laboratory test results. (CU denotes consolidated [Isotropically or Anisotropically] undrained triaxial tests).
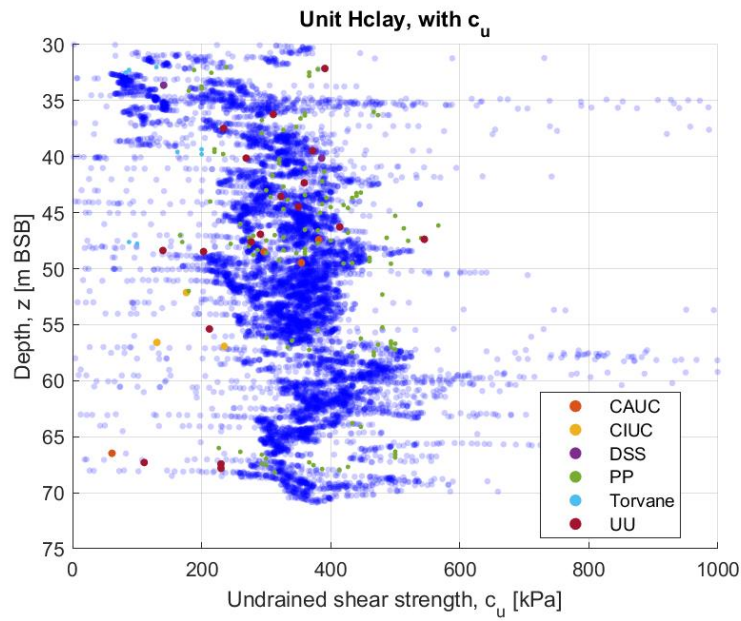
Figure 8.2-27   Range of c_u for the geotechnical soil unit Hclay using CPT correlation and laboratory test results. (CU denotes consolidated [Isotropically or Anisotropically] undrained triaxial tests).

C.6   Ratio between undrained shear strength and depth
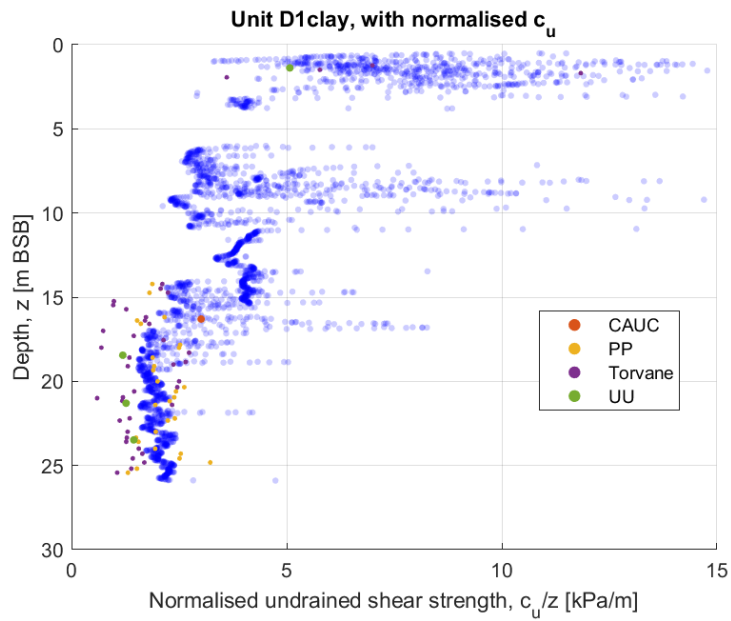
Figure 8.2-28   Range of c_u/z for the geotechnical soil unit D1clay using CPT correlation and laboratory test results. (CU denotes consolidated [Isotropically or Anisotropically] undrained triaxial tests).
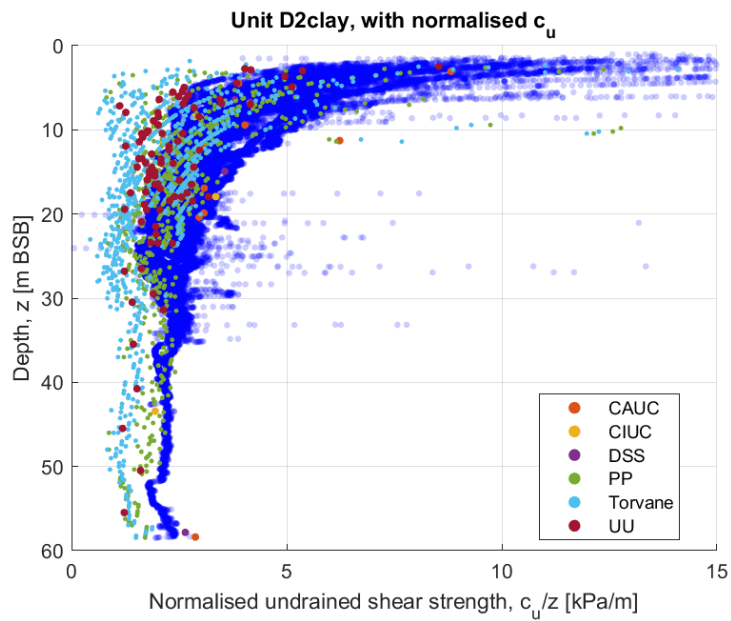
Figure 8.2-29   Range of c_u/z for the geotechnical soil unit D2clay using CPT correlation and laboratory test results. (CU denotes consolidated [Isotropically or Anisotropically] undrained triaxial tests).
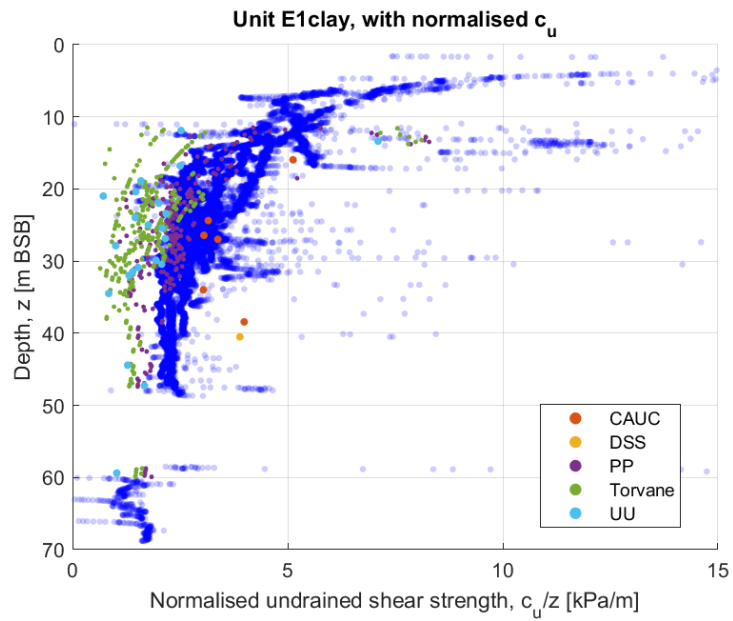
Figure 8.2-30   Range of c_u/z for the geotechnical soil unit E1clay using CPT correlation and laboratory test results. (CU denotes consolidated [Isotropically or Anisotropically] undrained triaxial tests).
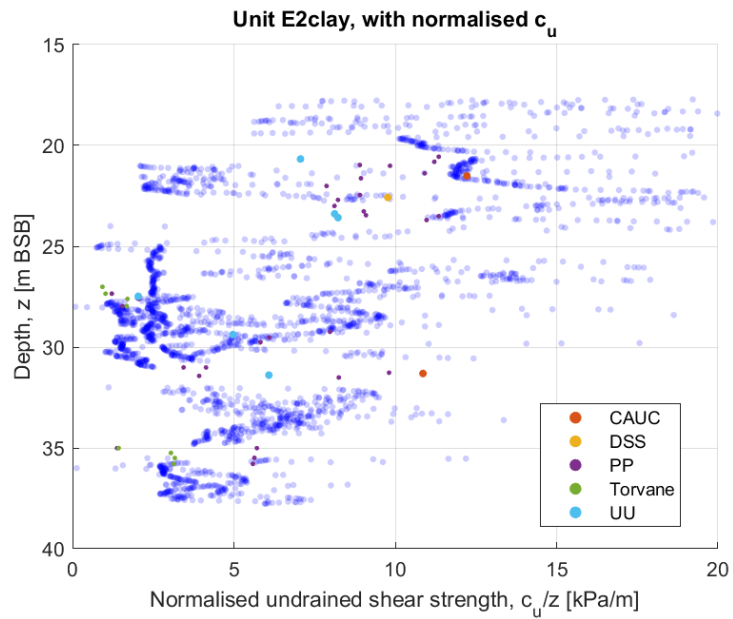
Figure 8.2-31   Range of c_u/z for the geotechnical soil unit E2clay using CPT correlation and laboratory test results. (CU denotes consolidated [Isotropically or Anisotropically] undrained triaxial tests).
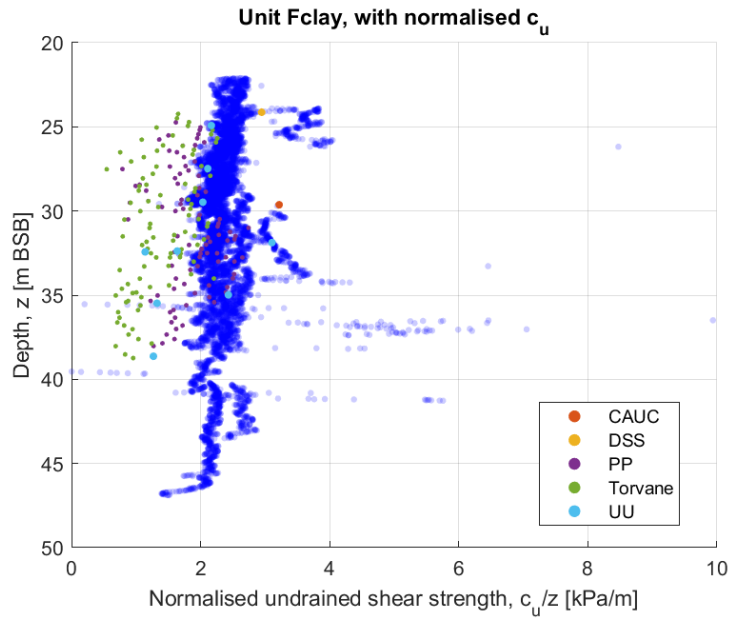
Figure 8.2-32   *Range of c_u/z for the geotechnical soil unit Fclay using CPT correlation and laboratory test results. (CU denotes consolidated [Isotropically or Anisotropically] undrained triaxial tests).*
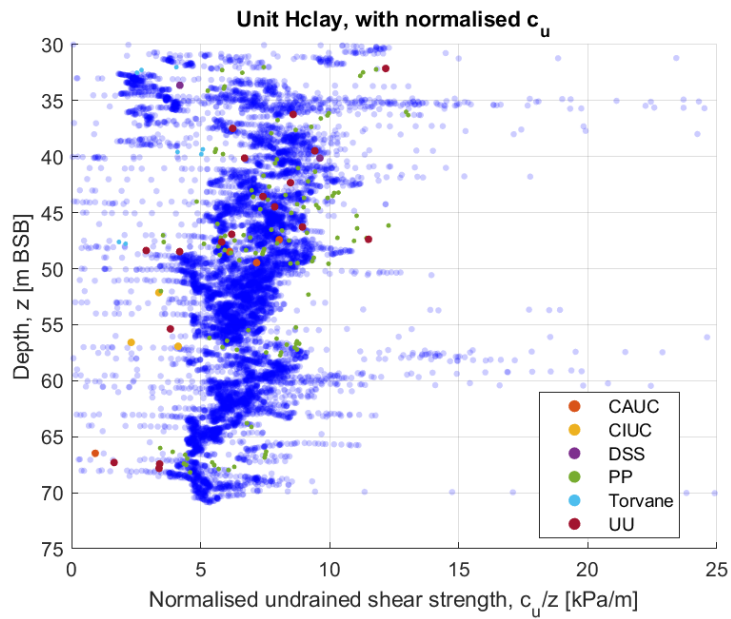
Figure 8.2-33   *Range of c_u/z for the geotechnical soil unit Hclay using CPT correlation and laboratory test results. (CU denotes consolidated [Isotropically or Anisotropically] undrained triaxial tests).*

C.7   Small-strain shear modulus
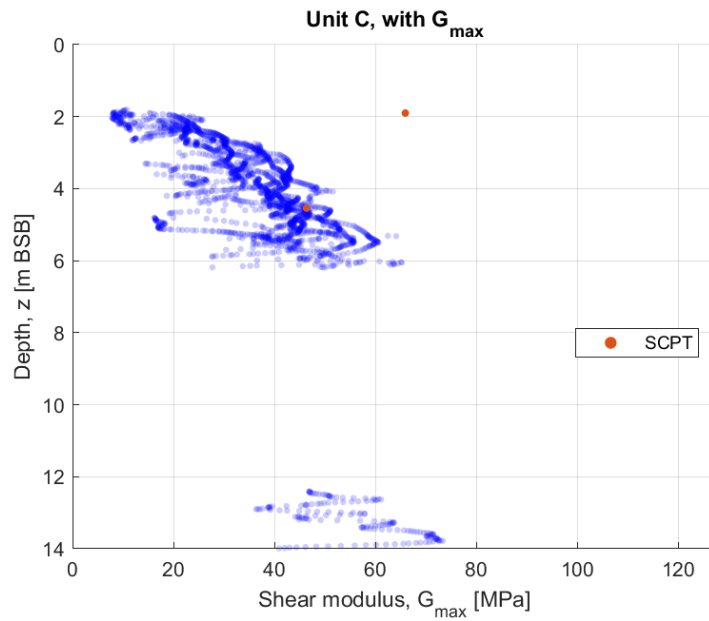
Figure 8.2-34   Range of G_{max} for the geotechnical soil unit C using CPT correlation, SCPT and P-S logging.
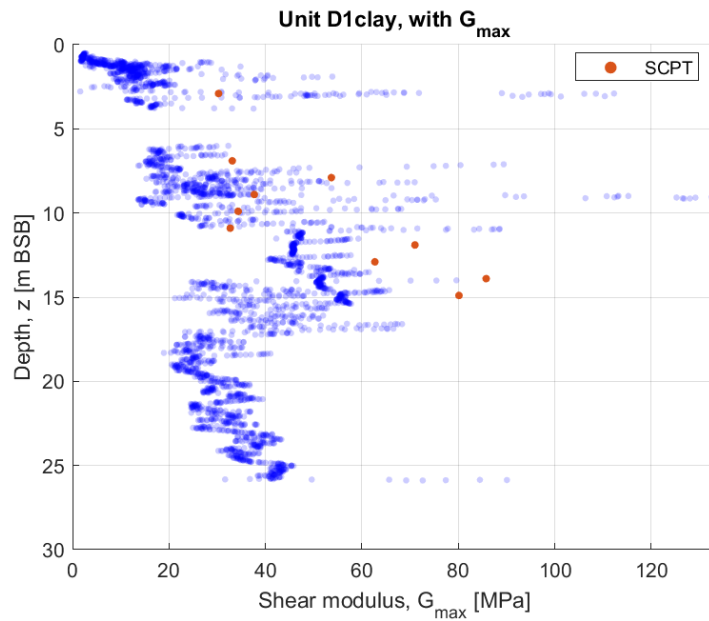
Figure 8.2-35   Range of G_{max} for the geotechnical soil unit D1clay using CPT correlation, SCPT and P-S logging.
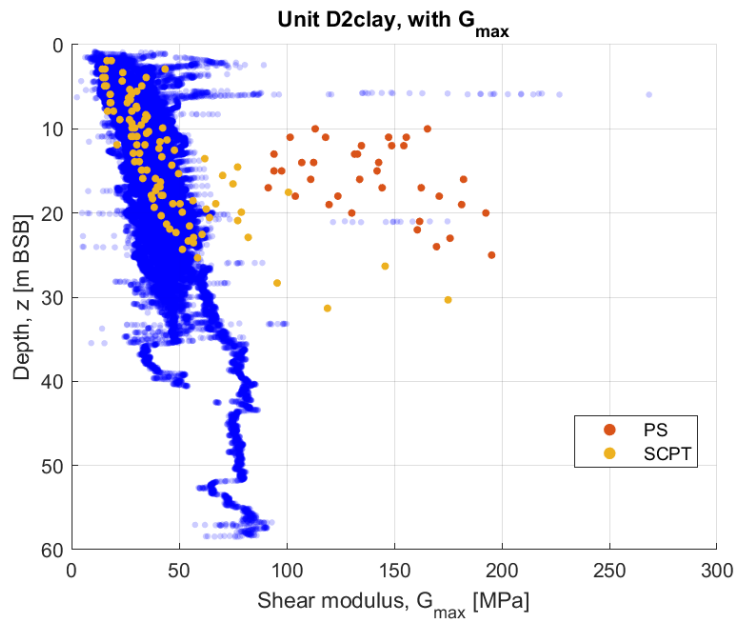
Figure 8.2-36   Range of G_{max} for the geotechnical soil unit D2clay using CPT correlation, SCPT and P-S logging.
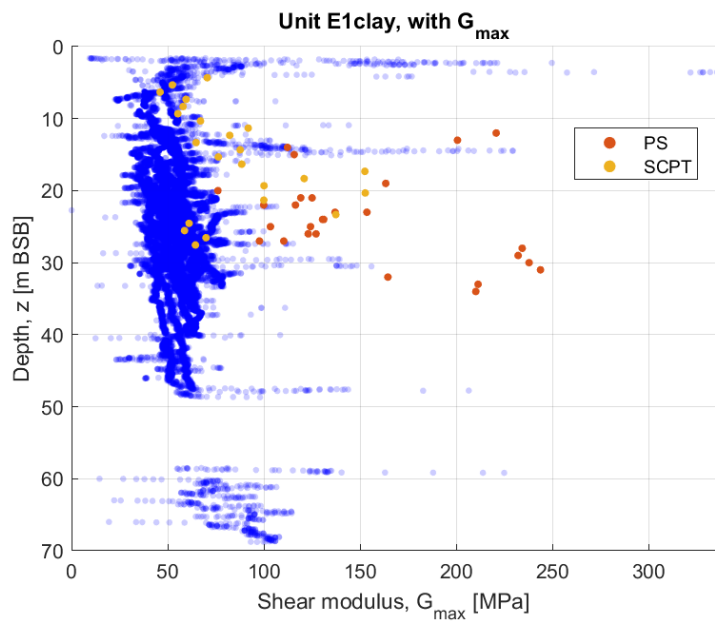
Figure 8.2-37   Range of G_{max} for the geotechnical soil unit E1clay using CPT correlation, SCPT and P-S logging.
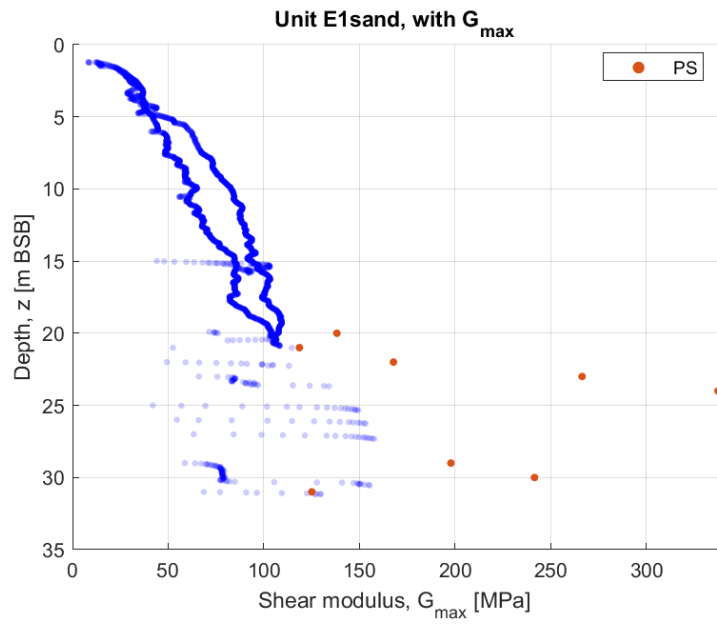
Figure 8.2-38   Range of G_{max} for the geotechnical soil unit E1sand using CPT correlation, SCPT and P-S logging.
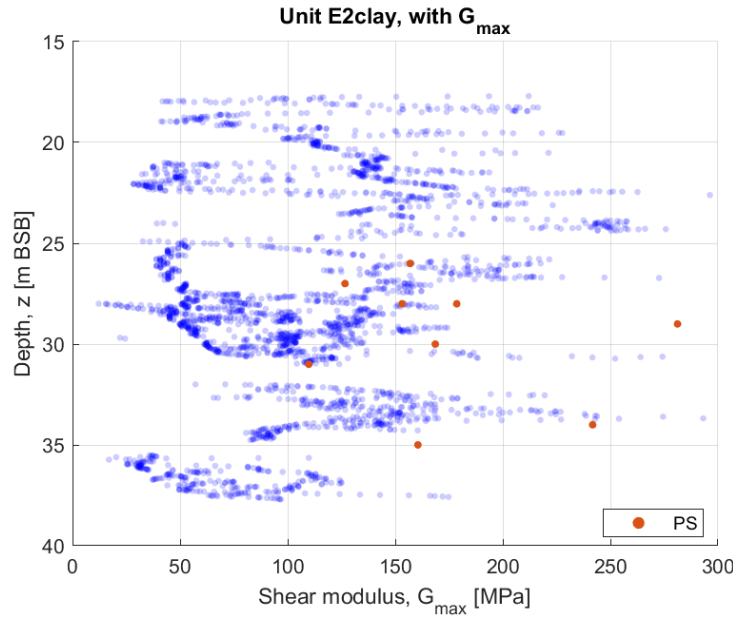
Figure 8.2-39   Range of G_{max} for the geotechnical soil unit E2clay using CPT correlation, SCPT and P-S logging.
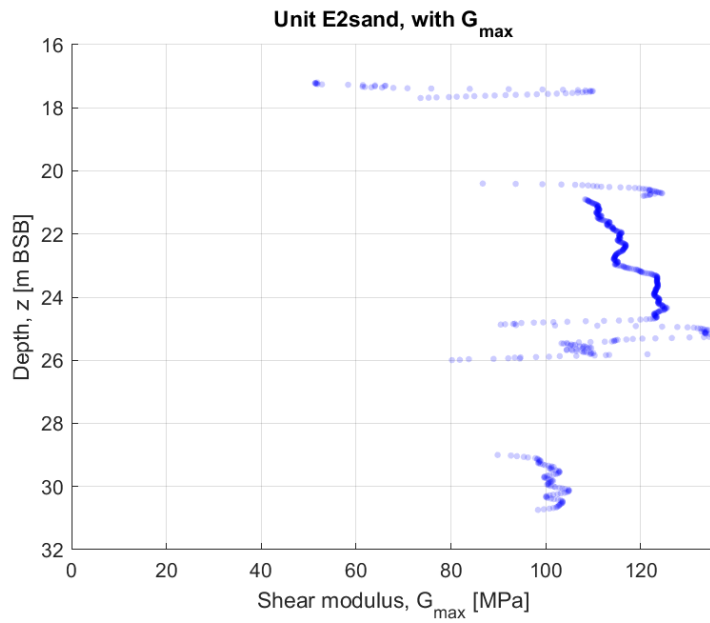
Figure 8.2-40   Range of G_{max} for the geotechnical soil unit E2sand using CPT correlation, SCPT and P-S logging.
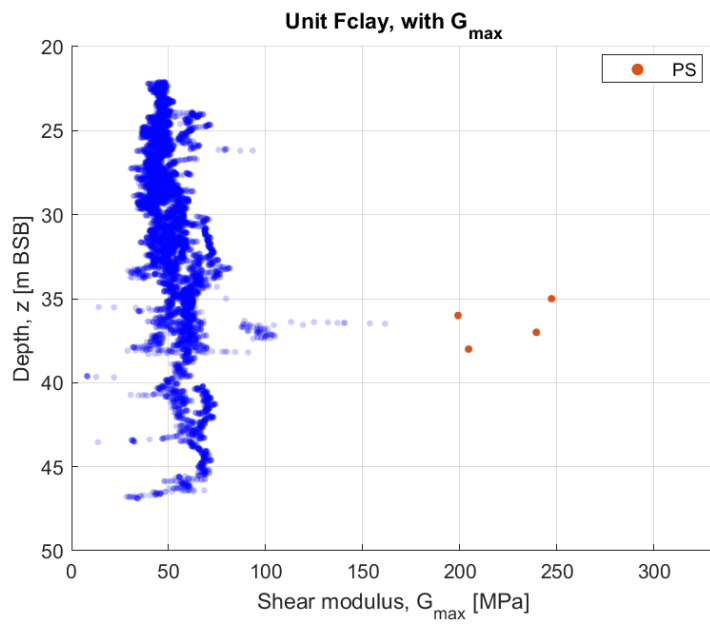
Figure 8.2-41   Range of G_{max} for the geotechnical soil unit Fclay using CPT correlation, SCPT and P-S logging.
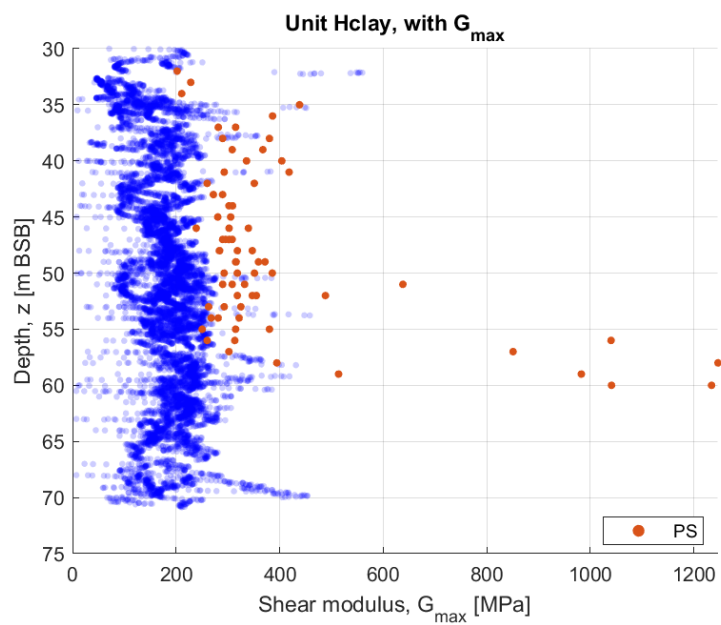
Figure 8.2-42   Range of G_{max} for the geotechnical soil unit Hclay using CPT correlation, SCPT and P-S logging.

Appendix D   Range of soil properties per soil unit

Table 11-1   Classification properties for geotechnical soil unit A, B, C, D1clay, D2clay and E1clay. Values given as Min/Max/Avg(no. of tests).

Soil property	A	B	C	D1clay	D2clay	E1clay
Bulk density [Mg/m^3]	1.52/2/1.85/(29)	1.51/2.1/1.92/(18)	1.78/2.34/2.03/(10)	1.63/2.04/1.89/(12)	1.64/2.31/1.81/(233)	1.77/2.25/1.96/(71)
Dry density [Mg/m^3]	0.85/1.56/1.32/(25)	0.87/1.68/1.38/(4)	1.58/1.69/1.63/(5)	0.98/0.98/0.98/(1)	1/1.79/1.27/(11)	1.62/1.62/1.62/(1)
Particle density [Mg/m^3]	2.63/2.65/2.64/(10)	2.63/2.64/2.64/(3)	2.65/2.65/2.65/(3)	2.65/2.65/2.65/(2)	2.64/2.69/2.66/(28)	2.65/2.66/2.66/(6)
Moisture content [%]	23/63/39.29/(21)	18/74/37.37/(27)	15/51/28/(14)	18/62/34.8/(25)	11/76/44.74/(452)	10/50/30.99/(147)
Plastic limit [%]	14/19/17.14/(7)	26/26/26/(1)	-/-/- (0)	18/20/19/(2)	18/27/23.14/(28)	14/22/18.14/(7)
Liquid limit [%]	29/39/32.86/(7)	48/48/48/(1)	-/-/- (0)	36/45/40.5/(2)	42/67/55.93/(28)	30/54/43.43/(7)
Plasticity index [%]	10/21/15.71/(7)	22/22/22/(1)	-/-/- (0)	18/25/21.5/(2)	23/41/32.79/(28)	16/33/25.29/(7)
Thermal conductivity [W/(mK)]	1.78/1.78/1.78/(1)	1.82/1.82/1.82/(1)	-/-/- (0)	-/-/- (0)	1.06/1.58/1.3/(8)	-/-/- (0)
Organic content [%]	0.84/2.7/1.89/(4)	1.3/1.3/1.3/(1)	5.7/5.7/5.7/(1)	-/-/- (0)	3.9/5.6/5.05/(4)	-/-/- (0)
Acid soluble sulphate [%]	0.09/0.28/0.15/(7)	0.14/0.14/0.14/(1)	0.09/0.09/0.09/(1)	0.06/0.06/0.06/(1)	0.05/0.16/0.09/(7)	-/-/- (0)
Chloride content [mg/L]	3300/6200/4571/(7)	4000/4000/4000/(1)	4500/4500/4500/(1)	4200/4200/4200/(1)	4700/7000/6114/(7)	-/-/- (0)
Carbonate content [%]	1.9/9.5/5.34/(7)	9.5/9.5/9.5/(1)	30/30/30/(1)	12/12/12/(1)	20/32/28/(7)	-/-/- (0)

Table 11-2   Classification properties for geotechnical soil unit E1sand, E2clay, E2sand, Fclay, Hclay, Hclaysoft and Hsand. Values given as Min/Max/Avg(no. of tests).

Soil property	E1sand	E2clay	E2sand	Fclay	Hclay	Hclaysoft	Hsand
Bulk density [Mg/m^3]	1.94/2.4/2.1/(41)	2.03/2.37/2.19/(10)	-/-/- (0)	1.77/2.21/1.89/(29)	1.74/2.16/1.94/(43)	1.86/2.31/2.13/(11)	1.92/2.31/2.05/(13)
Dry density [Mg/m^3]	1.58/2/1.72/(37)	-/-/- (0)	-/-/- (0)	1.95/1.96/1.96/(2)	-/-/- (0)	-/-/- (0)	1.66/1.75/1.7/(5)
Particle density [Mg/m^3]	2.64/2.66/2.66/(6)	2.66/2.67/2.66/(5)	2.66/2.66/2.66/(1)	2.66/2.67/2.67/(3)	2.49/2.68/2.62/(26)	2.63/2.67/2.65/(4)	2.63/2.67/2.64/(11)
Moisture content [%]	10/25/16.07/(15)	11/45/18.45/(60)	22/62/32.5/(4)	18/44/35.95/(60)	4/50/26.54/(279)	11/38/18/(57)	8/38/19.43/(47)
Plastic limit [%]	14/15/14.5/(2)	13/25/15.75/(8)	-/-/- (0)	22/22/22/(3)	15/37/25.04/(27)	12/19/15.25/(4)	13/18/15.33/(3)
Liquid limit [%]	27/34/30.5/(2)	27/53/34.13/(8)	-/-/- (0)	49/53/51.33/(3)	32/73/52.41/(27)	21/47/32.25/(4)	22/28/25/(3)
Plasticity index [%]	13/19/16/(2)	14/28/18.38/(8)	-/-/- (0)	27/31/29.33/(3)	17/38/27.37/(27)	9/28/17/(4)	7/13/9.67/(3)
Thermal conductivity [W/(mK)]	2.41/2.41/2.41/(1)	-/-/- (0)	-/-/- (0)	1.63/1.63/1.63/(1)	1.37/1.38/1.37/(3)	1.74/1.74/1.74/(1)	1.92/2.29/2.1/(2)
Organic content [%]	0.55/0.55/0.55/(1)	2.8/2.8/2.8/(1)	-/-/- (0)	6.5/6.5/6.5/(1)	4.3/12/7.2/(5)	3.6/3.6/3.6/(1)	0.32/7.3/3.81/(2)
Acid soluble sulphate [%]	0.03/0.03/0.03/(1)	0.09/0.09/0.09/(1)	-/-/- (0)	0.04/0.41/0.23/(2)	0.04/0.32/0.18/(5)	0.27/0.27/0.27/(1)	0.02/0.1/0.06/(3)
Chloride content [mg/L]	3200/3200/3200/(1)	1800/1800/1800/(1)	-/-/- (0)	4000/4700/4350/(2)	1300/2400/1880/(5)	1500/1500/1500/(1)	990/2900/2030/(3)
Carbonate content [%]	4.7/4.7/4.7/(1)	9.4/9.4/9.4/(1)	-/-/- (0)	21/28/24.5/(2)	2.8/9.4/5.26/(5)	6.6/6.6/6.6/(1)	0.95/47/17.58/(3)

Table 11-3   Particle size distribution for geotechnical soil unit A, B, C, D1clay, D2clay and E1clay. Values given as Min/Max/Avg(no. of tests).

Soil property	A	B	C	D1clay	D2clay	E1clay
Gravel content [%]	0/3/1/(10)	0/1/1/(3)	0/12/4/(4)	0/1/1/(2)	0/2/0/(28)	0/4/1/(7)
Sand content [%]	35/81/60/(10)	14/89/62/(3)	73/96/89/(4)	27/35/31/(2)	0/17/2/(28)	1/23/10/(7)
Silt content [%]	10/44/23/(10)	8/68/29/(3)	3/7/5/(4)	33/34/34/(2)	33/68/44/(28)	43/50/47/(7)
Clay content [%]	7/34/15/(10)	0/17/8/(3)	0/8/2/(4)	32/38/35/(2)	31/66/53/(28)	28/56/42/(7)
Fines content [%]	18/64/39/(10)	10/85/37/(3)	3/15/7/(4)	65/72/69/(2)	81/100/97/(28)	73/99/89/(7)

Table 11-4   Particle size distribution for geotechnical soil unit E1sand, E2clay, E2sand, Fclay, Hclay, Hclaysoft and Hsand. Values given as Min/Max/Avg(no. of tests).

Soil property	E1sand	E2clay	E2sand	Fclay	Hclay	Hclaysoft	Hsand
Gravel content [%]	0/9/2/(6)	0/9/3/(7)	0/0/0/(1)	0/0/0/(3)	0/7/1/(26)	0/4/2/(4)	0/10/4/(11)
Sand content [%]	31/94/65/(6)	1/39/26/(7)	76/76/76/(1)	1/2/1/(3)	1/50/17/(26)	4/59/37/(4)	13/95/65/(11)
Silt content [%]	6/31/17/(6)	31/49/41/(7)	19/19/19/(1)	39/52/46/(3)	15/67/45/(26)	24/55/38/(4)	3/72/20/(11)
Clay content [%]	0/35/15/(6)	21/50/29/(7)	5/5/5/(1)	46/60/53/(3)	18/76/38/(26)	13/41/24/(4)	0/37/11/(11)
Fines content [%]	6/66/33/(6)	53/99/71/(7)	24/24/24/(1)	98/99/99/(3)	46/99/83/(26)	37/96/61/(4)	3/87/31/(11)

Table 11-5   Strength properties for geotechnical soil unit A, B, C, D1clay, D2clay and E1clay. Values given as Min/Max/Avg(no. of tests).

Soil property	A	B	C	D1clay	D2clay	E1clay
Undrained shear strength, CAU [kPa]	-/-/- (0)	10.6/10.6/10.6/(1)	N.A.	49/49/49/(1)	17/168/59/(9)	77/153/98/(6)
Undrained shear strength, CIU [kPa]	6.4/6.4/6.4/(1)	-/-/- (0)	N.A.	-/-/- (0)	24/84/50/(5)	-/-/- (0)
Undrained shear strength, DSS [kPa]	19/19/19/(1)	-/-/- (0)	N.A.	-/-/- (0)	24/153/58/(5)	158/158/158/(1)
Undrained shear strength, UU [kPa]	11/11/11/(1)	12/16/14/(2)	N.A.	7/34/23/(4)	8/81/30/(88)	15/95/47/(22)
Undrained shear strength, Torvane [kPa]	1/20/8/(32)	6/23/13/(16)	N.A.	7/50/29/(40)	3.6/125/32/(759)	13/108/45/(249)
Undrained shear strength, Pocket penetrometer [kPa]	20/20/20/(1)	15/30/24/(3)	N.A.	25/80/43/(29)	5/128/41/(747)	27/112/60/(248)
Friction angle, CID [°]	N.A.	N.A.	35/39/37/(4)	N.A.	N.A.	N.A.

Table 11-6   Strength properties for geotechnical soil unit E1sand, E2clay, E2sand, Fclay, Hclay, Hclaysoft and Hsand. Values given as Min/Max/Avg(no. of tests).

Soil property	E1sand	E2clay	E2sand	Fclay	Hclay	Hclaysoft	Hsand
Undrained shear strength, CAU [kPa]	N.A.	263/340/301/(2)	N.A.	95/95/95/(1)	61/381/273/(4)	205/205/205/(1)	N.A.
Undrained shear strength, CIU [kPa]	N.A.	-/-/- (0)	N.A.	-/-/- (0)	131/235/181/(3)	-/-/- (0)	N.A.
Undrained shear strength, DSS [kPa]	N.A.	221/221/221/(1)	N.A.	71/71/71/(1)	141/386/264/(2)	154/154/154/(1)	N.A.
Undrained shear strength, UU [kPa]	N.A.	56/194/154/(6)	N.A.	37/99/60/(9)	111/545/292/(18)	89/130/116/(4)	N.A.
Undrained shear strength, Torvane [kPa]	N.A.	25/113/66/(8)	N.A.	15/75/42/(96)	83/200/131/(8)	38/138/86/(17)	N.A.
Undrained shear strength, Pocket penetrometer [kPa]	N.A.	25/307/177/(30)	N.A.	22/87/57/(96)	167/567/364/(115)	58/225/123/(26)	N.A.
Friction angle, CID [°]	37/39/38/(4)	N.A.	32/32/32/(1)	N.A.	N.A.	N.A.	28/35/33/(6)

Table 11-7   Small-strain shear modulus for geotechnical soil unit A, B, C, D1clay, D2clay and E1clay based on SCPT and P-S logging. Values given as Min/Max/Avg(no. of tests).

Test type	A	B	C	D1clay	D2clay	E1clay
P-S logging [MPa]	-/-/- (0)	-/-/- (0)	-/-/- (0)	-/-/- (0)	91/195/139/(36)	76/244/153/(27)
SCPT [MPa]	-/-/- (0)	46/128/80/(3)	30/86/52/(10)	14/175/41/(125)	46/153/83/(23)	-/-/- (0)

Table 11-8   Small-strain shear modulus for geotechnical soil unit E1sand, E2clay, E2sand, Fclay, Hclay, Hclaysoft and Hsand based on SCPT and P-S logging. Values given as Min/Max/Avg(no. of tests).

Test type	E1sand	E2clay	E2sand	Fclay	Hclay	Hclaysoft	Hsand
P-S logging [MPa]	119/337/199/(8)	110/281/175/(9)	-/-/- (0)	199/332/244/(5)	202/638/325/(64)	103/213/157/(9)	129/947/562/(5)
SCPT [MPa]	-/-/- (0)	-/-/- (0)	-/-/- (0)	-/-/- (0)	-/-/- (0)	-/-/- (0)	-/-/- (0)

Appendix E   CPT measurements and soil properties in unit E – Effect of glaciation
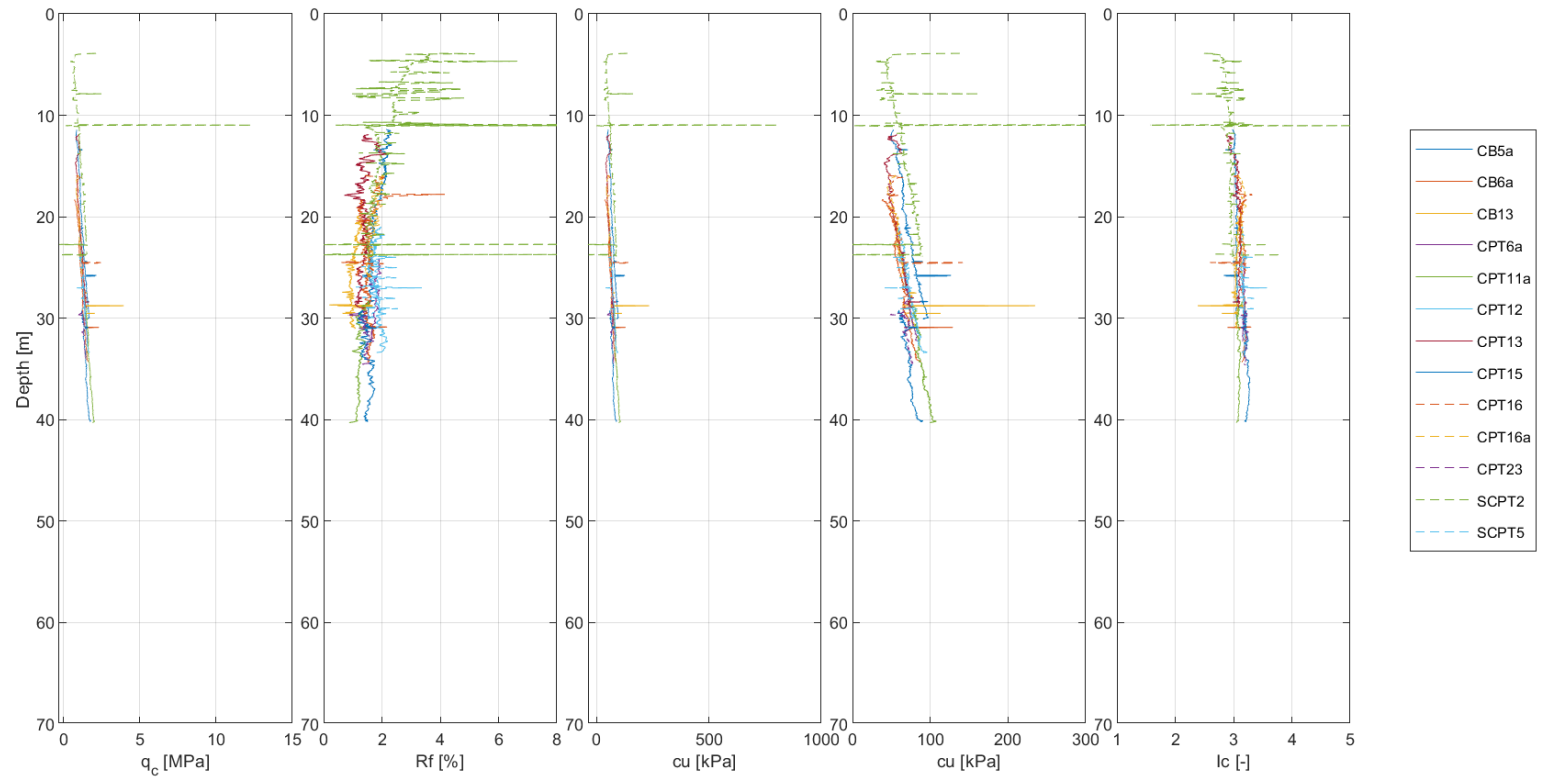
Figure 8.2-43   *CPT measurements and interpreted soil properties for unit E. Data from geotechnical locations for which no glacial impact from Late Weichselian is expected.*
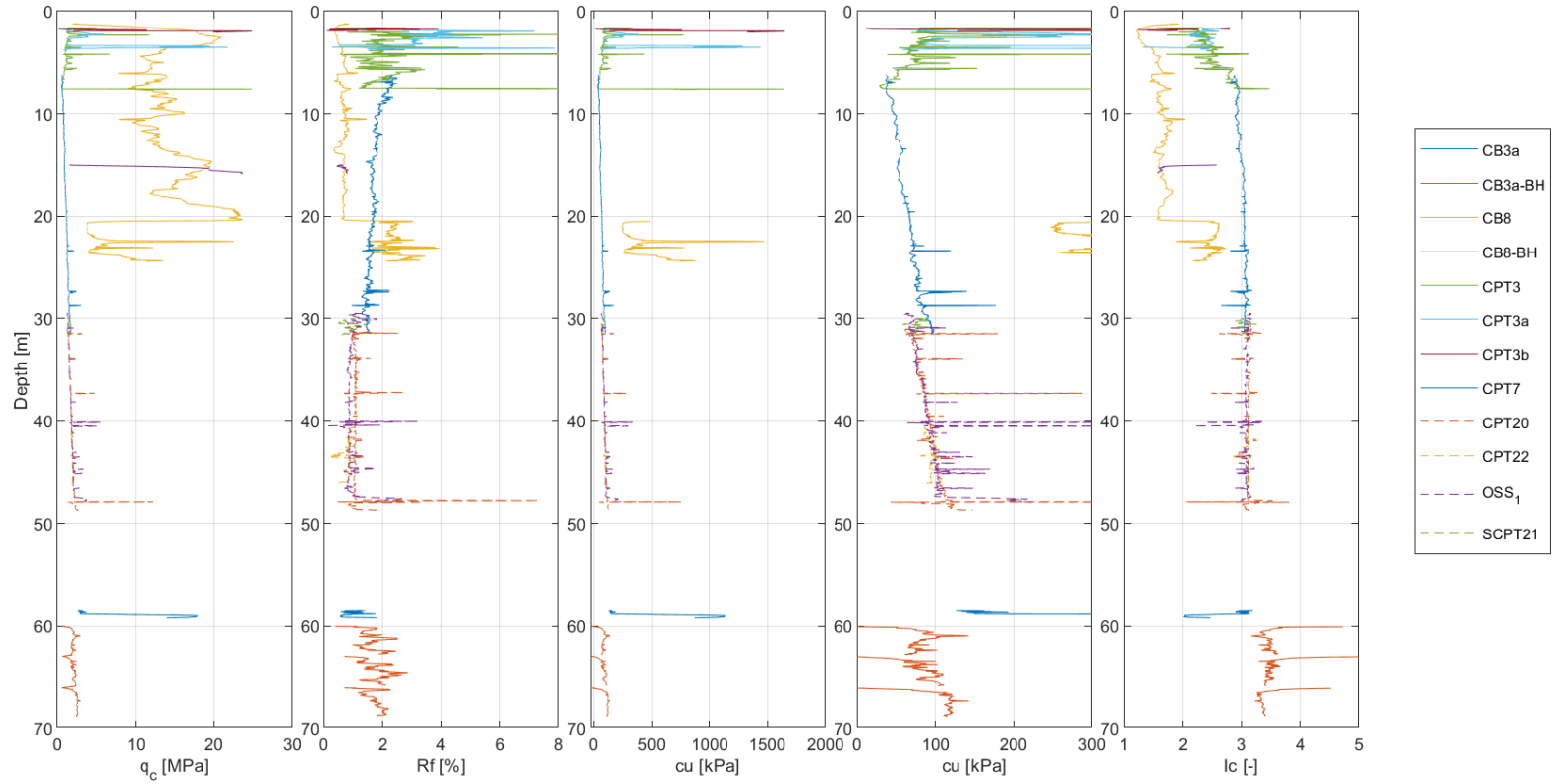
Figure 8.2-44   CPT measurements and interpreted soil properties for unit E. Data from geotechnical locations for which moderate glacial impact from Late Weichselian is expected.
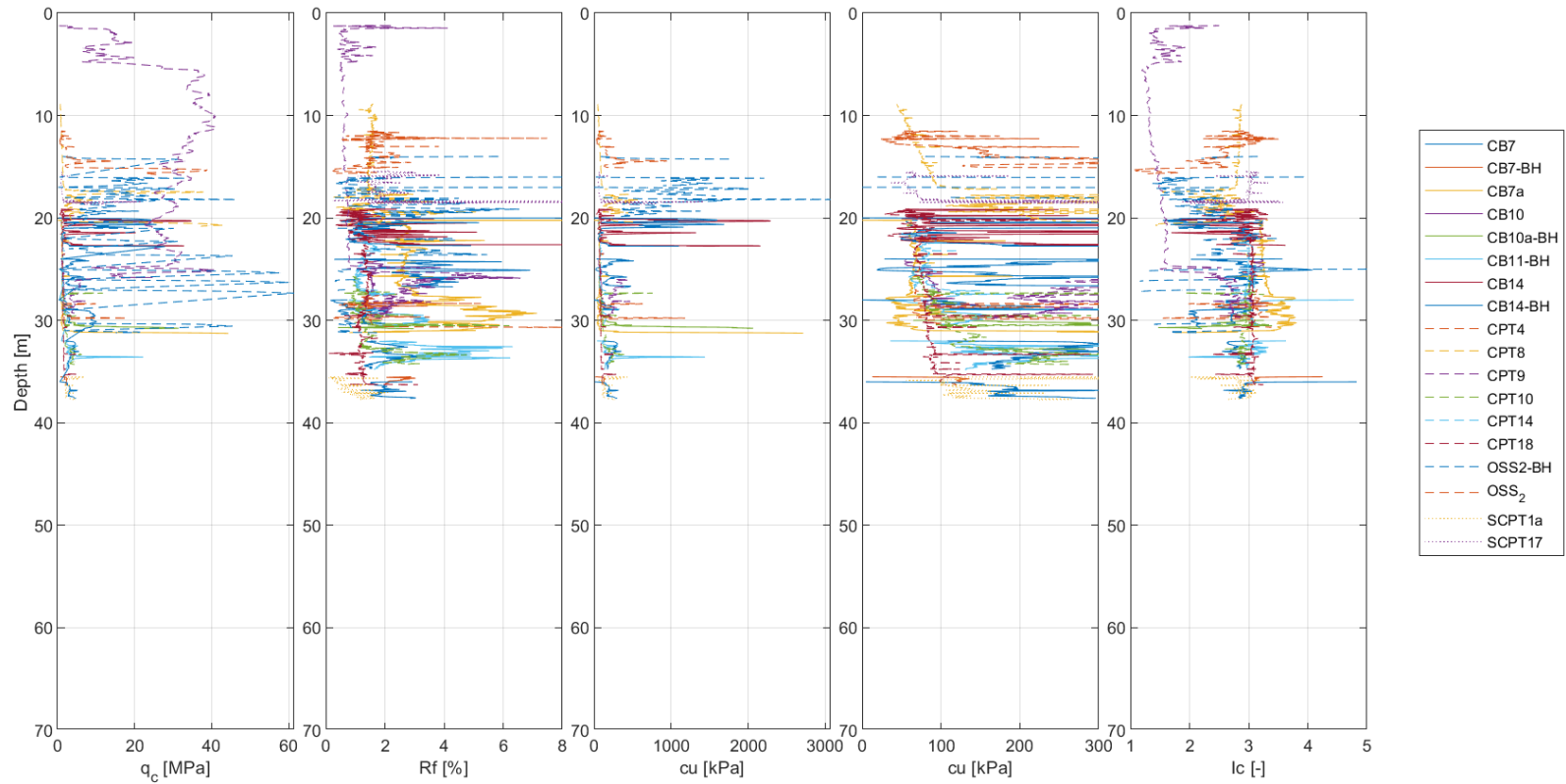
Figure 8.2-45   CPT measurements and interpreted soil properties for unit E. Data from geotechnical locations for which high glacial impact from Late Weichselian is expected.